Online ISSN 2716-9650
Print ISSN 2676-5837

Volume 2, Mar 30, 2020

Journal of
Composites and Compounds

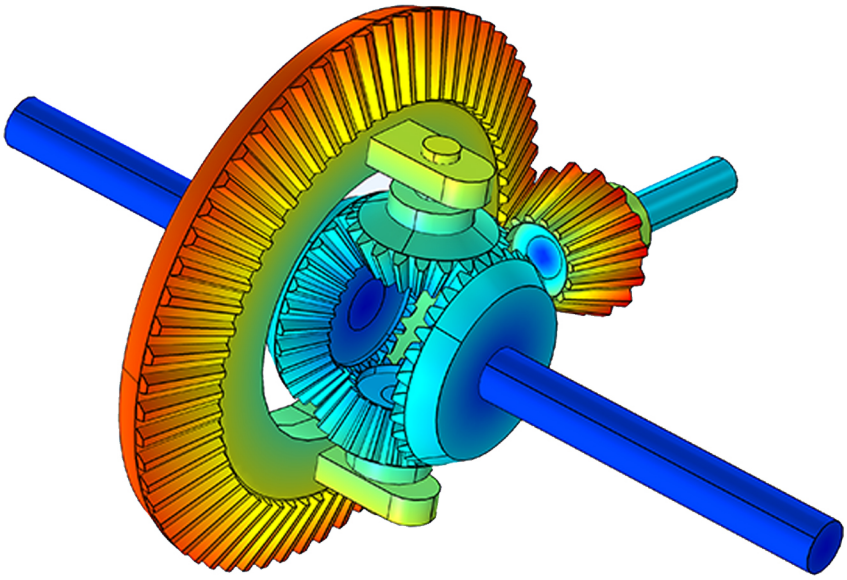

Editor In Chief: F. Sharifianjazi

www.JOURCC.com

Journal of
Composites and Compounds

Online ISSN 2716-9650
Print ISSN 2676-5837
Mar. 30, 2020
Volume 2
No. 2

Available online at www.jourcc.com

Janatabad St., Tehran, Iran

+982144437782

Journal of
Composites and Compounds

Online ISSN 2716-9650
Print ISSN 2676-5837
Mar. 30, 2020
Volume 2
No. 2

Table of contents

Production methods of CNT-reinforced Al matrix composites: A review.....1

Bioactive glass coated zirconia for dental implants: A review.....10

Factors influencing the failure of dental implants: A systematic review.....18

Hydroxyapatite consolidated by zirconia: Applications for dental implant.....26

A review on the Comsol Multiphysics studies of heat transfer in advanced ceramics 35

Production and characterization of PCL (Polycaprolactone) coated TCP/nanoBG composite scaffolds by sponge foam method for orthopedic applications.....44

Photosensitive nanocomposites: environmental and biological applications.....50

Available online at www.jourcc.com

Janatabad St., Tehran, Iran
+982144437782

Available online at www.jourcc.com

Journal homepage: www.JOURCC.com

Journal of Composites and Compounds

Production methods of CNT-reinforced Al matrix composites: A review

Iman Tajzad[a], Ehsan Ghasali[b]*

[a] *Department of Mechanical Engineering, Islamic Azad University, Majlesi Branch, Isfahan, Iran*
[b] *Ceramic Dept., Materials and Energy Research Center, Alborz, Iran*

A B S T R A C T

Carbon nanotubes (CNTs)-reinforced Al composites have attracted attention due to their high specific strength and low density, which makes them suitable for the use in aerospace and automobile industries. In this review, preparation methods of Al/CNTs composites for achieving a homogeneous desperation of the CNT in the Al matrix are summarized. In addition, the effect of processing methods on carbon nanotube distribution and enhancement of mechanical properties such as toughness, wear behavior and hardness of the nanocomposites are reviewed. Improvement of mechanical characteristics was observed by the incorporation of carbon nanotubes into aluminum matrix. The strengthening factors gained by the carbon nanotubes addition are the interface of metal and CNTs and the chemical and structural stability of CNTs.

Peer review under responsibility of jourcc

A R T I C L E I N F O R M A T I O N

Article history:
Received 6 December 2019
Received in revised form 18 December 2019
Accepted 5 February 2020

Keywords:
Metal matrix composites
Nanocomposite
Spark plasma sintering
Mechanical properties
Powder metallurgy

Table of contents

1. Introduction 1
2. Carbon nanotubes (CNTs) 2
3. Metal matrix composites (MMCs) 2
4. Aluminum matrix composites (AMCs) 2
5. Strengthening mechanisms in carbon nanotube-reinforced composites 3
6. CNT-reinforced AMCs processing techniques 4
6.1.Powder metallurgy 4
6.1.1. Ball milling 4
6.1.2. Ultrasonication 4
6.1.3. Application of surfactants 4
6.1.4. Metallization 4
6.1.5. Cold press and sintering 4
6.1.6. Hot extrusion 5
6.1.7. Spark plasma sintering (SPS) 5
6.1.8. Flake powder metallurgy (flake PM) 6
6.2.Friction stir processing (FSP) 6
6.3.Spread dispersion (SD)/ rolling process 7
7. Conclusions and future insights 7

1. Introduction

As composite materials have the capability of developing lightweight materials with tunable properties [1-3] for high-performance applications, they have attracted attention of researchers in recent decades [4-7]. Composite materials are defined as two or more components that are chemically distinct and their interfaces are clearly separated. The matrix can be either metals, ceramics, or polymers [8-11]. The composite materials show high strength and stiffness [14, 15]. The invention of the airplane and the corresponding industry have increased the demand for the development of high strength and lightweight materials [17]. By the enhancement of the stiffness and strength of materials, it is possible to use reduced the dimensions and mass for a particular load bearing application. In aircraft and automobile industry, the reduction of the required size can provide some advantages, including the fuel efficiency improvement and an increase in payload. The increase in the efficiency of fuel consumption of engines is highly desirable due to global oil re-

* *Corresponding author: Ehsan Ghasali; E-mail: ehsan_ghasali@yahoo.com*
https://doi.org/10.29252/jcc.2.1.1

source depletion [19]. As most light metallic materials and alloys cannot offer both high stiffness and strength to a structure, metal matrix composites (MMCs) have been developed in which the metal matrix provides the ductility and strength while the reinforcing component provides the strength and/or stiffness. The reinforcing material can be either particles, whiskers, or fibers of a high stiffness metal or ceramic. Some properties of metal matrix composites such as low thermal expansion coefficient and high thermal conductivity can be achieved, which make them good candidates for applications in the electronic packaging field. Nowadays, MMCs are extensively used in the aerospace and automobile industry [22].

Carbon nanotubes (CNTs) are composed of rolled-up sheets of graphene in cylindrical form often in the nanometer range, which shows remarkable thermal, electrical, and mechanical, characteristics. CNTs exhibit almost one hundred times tensile strength (~150 GPa) and approximately six times elastic modulus (~1 TPa) than do high strength steels depending on their diameter, length, orientation, and chirality [25]. The use of lightweight CNTs as nano-reinforcement for composite materials is highly promising. The aim of using carbon nanotubes is to incorporate their remarkable physical and mechanical properties into the bulk of engineering materials [22, 28]. Carbon nanotubes have been used for the reinforcement of metal, ceramics, and polymer matrices. Among these materials, polymer/CNTs composites have been extensively prepared via interfacial covalent functionalization, solution evaporation having significant energy sonication, repeated stirring, and surfactant-assisted processing. On the other hand, metal/ceramic reinforced with CNT has not been investigated widely. To disperse carbon nanotubes in the matrix uniformly, several synthesis methods have been employed for the production of carbon nanotube/ceramic or metal matrix composites such as hot extrusion, spark plasma hot pressing, sintering (SPS), and in situ synthesis [31].

Carbon nanotubes are also promising reinforcements for aluminum that has recently emerged. The poor dispersion of carbon nanotubes and agglomeration in metallic matrices are major difficulties in achieving the reinforcing effect of CNTs in metallic matrices successfully [23, 32]. Different processing methods have been investigated to solve this problem. In this paper, various preparation methods for CNT-reinforced Al composites have been reviewed.

2. Carbon nanotubes (CNTs)

The most important and abundant element in nature is carbon, and its pure forms are diamond and graphite. CNTs were first discovered by Iijima in 1991 [33], and by the discovery of the fullerenes and graphene, these materials have attracted attention from researchers. The CNT is in the form of a cylinder consisting of rolled-up graphene sheets with a regular hexagon structure, which can have a diameter of several folds smaller than its length. In the structure of an ideal CNT, graphene sheets consisting of hexagonal-structured carbon atoms are rolled up and create a hollow, tube-like structure. Carbon nanotubes are divided into two categories of single-walled carbon nanotube (SWCNT) and multi-walled carbon nanotube (MWCNT) that is based on the number of graphite sheets incorporating in their structure. In the MWCNTs structure, there are a number of concentric tubes of graphene being fitted on each other [34]. The range of MWNTs and SWNTs diameters is between 2 nm to 100 nm and 0.7nm to 2 nm, respectively, but the length of these nanotubes can vary from several millimeters to micrometers [35]. As a result of properties such as remarkable chemical stability, good absorbability, specific surface area, and unique electronic structure, carbon nanotubes are considered as promising materials as catalyst carriers. Moreover, CNT s are reported to have the capability to be utilized as a support for dispersion of functional materials for the improvement of some properties like structure, activity, surface area, and conductivity [36].

As a result of the practical lack of scattering mechanisms, which increase the mobility of the carrier along the tubes, carbon nanotubes exhibit a very high electrical conductivity [37]. Furthermore, through changing the nanotube diameter or helicity, the electronic characteristics of single-walled nanotubes can be altered from semiconductor to metallic behavior or vice versa [38]. Therefore, they are being studied for high-speed electronic applications. In nanocomputing and nanoelectronics usage, CNTs can facilitate heat dissipation due to the high thermal conductivity (about 3000 W/ mK) and are comparable to diamond [39]. Through increasing mechanical integrity and electrical connectivity, CNTs would improve the cycle life in lithium-ion batteries for cellphones and computers. An interesting application of carbon nanotubes is producing light. This is due to the recombination of holes and electrons across the semiconductor gap, resulting in the emission of infrared radiation, which is near to the optical windows related to optical fibers [40].

3. Metal matrix composites (MMCs)

Metal matrix composites (MMC) are composed of a metal matrix and reinforcing components [41, 42]. Reinforcing components are incorporated into the matrix in the form of small fibers, continuous fibers, whiskers, and particles. In the case of MMCs, the reinforcement can be used in the form of particles, small fibers or whiskers, and continuous fibers or sheets [43, 44].

Metal matrix composites that are discontinuously reinforced with particle, whiskers, or short fibers, are of great importance. One reason is the cost of production, which is an essential factor for large volume production. MMCs can be prepared by conventional metallurgical processes, including powder metallurgy [45] or casting [46], and they can be processed by conventional secondary techniques such as extrusion forging [47], and rolling [48]. They can be used in higher temperatures compared to unreinforced metals, and they exhibit improved strength, modulus wear resistance, and thermal stability. They possess relatively isotropic characteristics in comparison with the composites reinforced by fibers [49].

The metal matrix can be different metals such as Cu [50, 51], Ti, Al, Mg, their alloys, and intermetallic compounds. Due to excellent strength, low density, high toughness, and resistance to corrosion, Al alloys, are considered as important materials for aerospace applications [35, 52]. In the automotive, aerospace, and sports industries in where both lightweight and mechanical properties such as high strength and stiffness are desired, carbon nanotube reinforced metals are capable of revolutionizing these industries [53].

4. Aluminum matrix composites (AMCs)

In aluminum Matrix Composites, the matrix is Al or Al alloy, and the reinforcing component is embedded in this metal matrix [54]. This reinforcement is commonly non-metallic and usually a ceramic material like Al_2O_3, SiC, CNTs, and etc. [55-60]. The type of reinforcements and their volume fraction in the matrix alters the properties of AMCs. AMCs have some advantages in comparison with unreinforced materials, including improved stiffness, higher strength, controlled coefficient of thermal expansion, enhanced high-temperature behavior, reduced density, higher abrasion and wear resistance, enhanced electrical properties, and enhanced damping capabilities [61-63].

A significant increase in the elastic modulus of unreinforced Al from 70 GPa to 240GPa can be observed by adding 60 vol. % continuous Al fiber. Moreover, reinforcing pure Al with 60 vol. % alumina fiber can reduce the expansion coefficient (24 ppm/°C to 7 ppm/°C. Also, it has been shown that adding 9 vol% Si and 20 vol.% SiCp to Al has the

potential of having wear resistance comparable to that of grey cast iron [64]. Overall, through the incorporation of suitable reinforcing components with appropriate volume fraction, it is possible to enhance the technological properties of Al and its alloys greatly. Aluminum matrix composites present such superior combination of characteristics that common monolithic materials are not able to compete [65]. Aluminum matrix composites have been utilized in various functional, structural, and non-structural engineering applications owing to their good performance, and environmental and economic advantages [66]. Lower airborne emissions, lower fuel consumption, and less noise is the key advantages of aluminum matrix composites for utilization in the transportation sector. AMCs are becoming inevitable material in the transport industry because of ever-increasing environmental concerns and improved fuel consumption efficiency [67].

Based on the form of reinforcing components aluminum matrix composites can be categorized into four different types: (I) Mono filament-reinforced AMCs (MFAMCs) (II) Continuous fiber-reinforced AMCs (CFAMCs) (III) Whisker-or short fiber-reinforced AMCs (SFAMCs) (IV) (PAMCs) [68]. Particle incorporating in AMCs are generally equiaxed ceramic materials having an aspect ratio smaller than 5 [69]. For structural and wear resistance applications, the amount of ceramic components is less than 30 vol. %, while the volume fraction can reach to 70% for applications in electronic packaging fields. In comparison with other types of AMCs, PAMCs exhibit lower mechanical properties; however, compared to pure Al or Al alloys have better properties. The aspect ratio of reinforcing components is greater than five in SFAMCs, but they are non-continuous. AMCs, including short alumina fibers, is one of the most and first popular Aluminum composites developed to be used in pistons. In CFAMCs, the reinforcing components can be alumina, SiC or carbon continuous fibers having a diameter lower than 20 µm. These continuous fibers can either be braided, woven, or parallel before undergoing the production process of composites [70]. MFAMCs are composites consisting of fibers with a large diameter of 100 to 150 µm that are prepared via chemical vapor deposition (CVD) of B or SiC into a W wire core or carbon fiber. In comparison with multifilaments, monofilaments have lower bending flexibility [71].

Production of aluminum matrix composites at an industrial scale is carried out through two main processes. (1) Liquid state processes, (II) Solid-state processes. Solid-state processes include physical vapor deposition, diffusion bonding, and powder mixing and consolidation (PM processing). In-situ processing, spray deposition, infiltration process, and stir casting are categorized under liquid state processes [64].

A 100% increase in the tensile strength with the incorporation of 10 volume percent of carbon nanotube was first reported by Kuzumaki et al. [72]. Researchers have tried to increase the amount of carbon nanotube up to 6.5 vol.% in Al/CNT composite using the powder metallurgy route [73] and secondary processes such as hot deformation and SPS [74]. The incorporation of 5 vol.% CNT was shown to increase the tensile strength to 129% [75]. In contrast, a reduction of hardness by the incorporation of 5 volume percent was observed by Salas et al. [76] using in a shock-wave consolidation. The reduction of properties is a result of the agglomeration of carbon nanotubes in the Al phase and weak interfacial adhesion of the two phases. Laha et al. [77, 78] studied the effect of adding 10 wt% CNT to aluminum coating through thermal spraying methods, and their results showed that CNTs improved the elastic modulus by 78%, hardness by 72%, and decreased ductility by 46%. The elastic modulus of the sprayed Al/CNT composite coating sintered at 673 K was proposed to increase by 80%, which was reported to be a result of a decrease in porosity and residual stress [79].

5. Strengthening mechanisms in carbon nanotube-reinforced composites

Fibrous reinforcing components such as carbon nanotubes are used to enhance the tensile strength elastic modulus of the matrix. These improvements are a result of the higher strength and stiffness of carbon nanotubes in comparison with the metal matrix. Researchers have tried to understand the mechanisms incorporating in the strengthening of fiber-reinforced composites. The model applied to study CNT composites is the shear lag models [80] related to all conventional composites reinforced with fibers and is presented below:

$$\frac{l_f}{D_f} = \frac{\sigma_f}{2\tau_{mf}} \tag{1}$$

where σ_f is the stress transferred to fibers through the interface of the matrix and the reinforcement and has a relation with the shear stress (τ_{mf}) between the two phases. D_f and l_f are the diameter and length of carbon nanotubes, respectively. The larger aspect ratio of CNTs leads to the larger load transfer to the reinforcement and hence higher reinforcing efficiency is achieved. σ_f equals to the fracture strength of carbon nanotubes for a critical length *lc*. The fracture strength of the composite when $l<l_c$ is calculated by:

$$\sigma_c^{Frac} = V_f \sigma_f^{Frac} \left(\frac{l}{2l_c}\right) + V_m \sigma_m^{Frac} \tag{2}$$

Al/CNT composites synthesized via ball milling and extrusion were shown to follow this relation well [18]. An undesirable reaction that can occur in metal matrix nanotube composites is the formation of carbide at the interface of metal and CNTs. Thus, the shear strength of the formed phase affects transferring the stress to carbon nanotubes. If the applied stress is higher than the shear strength, fiber pulls out occurs due to the carbide layer fracture [81]. The relation derived for the strength in the presence of a carbide interfacial layer by Coleman et al. [82] is given as:

$$\sigma_c = \left(1 + {}^{2b}/_{D}\right)\left[\sigma_{shear}\ {}^{l}/_{D} - \left(1 + {}^{2b}/_{D}\right)\sigma_m\right]V_f + \sigma_m \tag{3}$$

where the interface shear strength is denoted by σ_{shear}. D and b are the diameter of carbon nanotubes and the width of the carbide layer, respectively. It has been reported that the strength measured experimentally (83.1 MPa) is much less than that calculated using this relation (226 MPa). This is a result of different factors that are not taken into account in this model, including the clustering of carbon nanotubes, uniformity of the interfacial carbide phase, and porosity [77]. For example, the carbon nanotube elongated clusters has been observed through the microstructural study of Cu/carbon nanotubes composites synthesized via spark plasma sintering of mechanically alloyed powders post-processed by cold rolling [83].

In the case of Al/CNT, the strengthening mechanisms are proposed to be the generation of dislocations due to the mismatch between thermal expansion of the matrix and reinforcement as well as precipitation hardening through the Orowan looping mechanism. However, these mechanisms have not been observed yet. To achieve the strengths near the theoretical strength, it is important to disperse CNTs uniformly in the matrix [12].

Elastic modulus enhancement is due to the high tensile modulus of carbon nanotubes (350–970 GPa). Most of the models that have also been developed for polymer/carbon nanotubes are applicable for metal matrices [84].

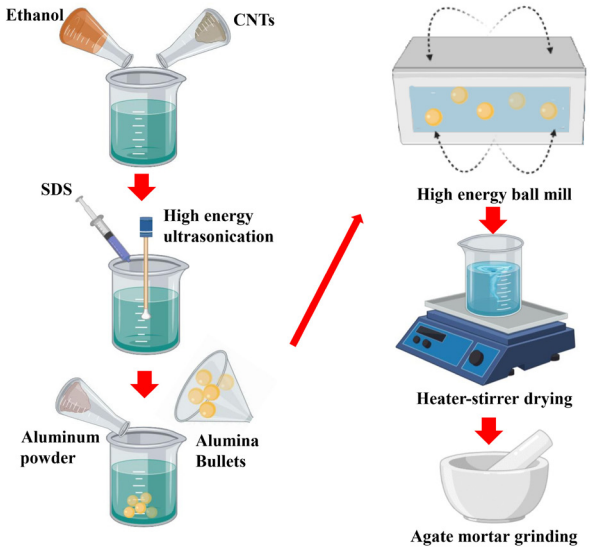

Fig. 1. Dispersion of CNTs in Al through ultrasonication.

6. CNT-reinforced AMCs processing techniques

6.1. Powder metallurgy

One of the widely-used synthesis methods of MMCs is powder metallurgy, which involves cold pressing of powders and subsequent sintering, or hot pressing [85]. Various techniques are used for the preparation of the metal matrix composites in the form of particles or whiskers. The first stage in the preparation of MMCs via powder metallurgy is the blending of particles and the matrix powder to achieve a homogeneous distribution. After blending, the powder mixture is cold-pressed (is called green body) and reaches to 80% of theoretical density. In order to remove the moisture of the powder surface, the prepared green body is degassed in a sealed container. Finally, the compacted powder undergoes sintering process under isostatic or uniaxial pressure to prepare fully compact composites [86]. One of the challenges in preparation of these composites is the dispersion of CNTs in the metal matrix. The improvement of properties could be achieved only when there is a uniformly distribution of CNTs. If such dispersion is not obtained, agglomerated particles and the micro-pores will be formed throughout the microstructure. In order to alleviate this issue, a variety of methods has been developed for the effective dispersion of CNTs in the matrix including ball milling, ultrasonication, application of surfactants, and metallization [24, 87].

6.1.1. Ball milling

In ball milling process, metal powders undergo repeated fracture and welding by several hard balls in the milling container. This method can be used for the dispersion of CNTs in the metallic matrix [88]. The metal powders and CNTs are entrapped between the container wall and balls or balls themselves resulting in the separation of the nanotubes, destruction of the agglomerates, and dispersion of CNTs among the metal particles. The dispersion degree depends significantly on milling time. By the increase of the milling time, the agglomeration is reduced and the metal particles change from round shape to flattened shape in which CNTs are embedded [89].

6.1.2. Ultrasonication

Ultrasonication is a technique in which high frequency ultrasound waves are applied to disperse CNTs in an organic solvents or aqueous surfactants. To reduce the hydrophobicity of CNTs, their surfaces are modified by polymer adsorbates and surfactants to enhance their solubilization in water. Through ultrasonication, the collapse of micro-bubbles produced during the process creates a high local shear stress at the CNT bundles end and when a gap or a gas bubble is formed, surfactants are absorbed on CNTs. The surfactant-coated carbon nanotubes is produced by unzipping process along the longitudinal axis [90]. Fig. 1 illustrates dispersion of CNTs in Al through sonication followed by ball milling process.

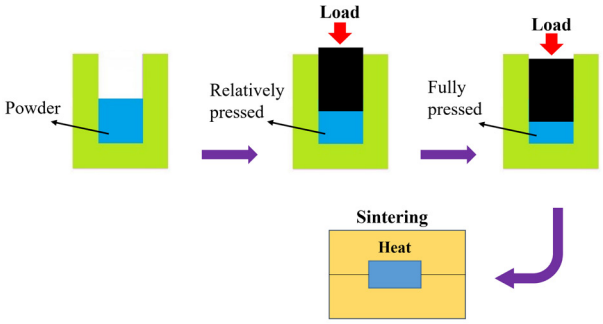

Fig. 2. Schematic illustration of cold pressing and sintering.

6.1.3. Application of surfactants

A way of the surface modification and prevention of agglomeration and rebinding of CNTs is using surfactants. Generally, the surfactants have two parts in their structure: a hydrophobic and a hydrophilic part.

The reactive agents produce steric or electrostatic repulsion between CNTs particles and reduce their surface energy leading to the improvement of the suspensions metastability. According to the head group charges, the surfactants are anionic, cationic, and nonionic or zwitterionic [91].

6.1.4. Metallization

The CNTs surface can be coated with some metals including W, Ni, Mo, Co, and Cu in order to prevent the agglomeration of the reinforcement, enhance the interfacial adhesion between the matrix and the reinforcement, and inhibit the reaction between them [92].

The other important factor affecting the properties of the composites produced by powder metallurgy is the sintering process. The samples can be sintered either above or below the matrix solidus temperature [93]. Different sintering processes employed for the preparation of Al/CNT nanocomposites are described below:

6.1.5. Cold press and sintering

The schematic illustration of cold pressing and sintering is shown in Fig. 2. George et al. [12] prepared Al and CNT powder mixture via ball milling followed by the compaction of the milled powder in a circular die applying120 KN load. The sintering process of the billets was carried out in an N_2 environment. According to the results, the mechanical properties of carbon nanotube reinforced aluminum, e.g. Young's modulus were enhanced [94].

Sivananthan et al. [13] prepared the powder mixture of MWCNT and Al via ball milling with 10 steel balls with a 15 mm diameter for 10 h at room temperature. Then, by applying a pressure under increased temperature, the powder mixture was converted to the green body and sintered for 1 h at 600 °C in an Ar atmosphere. They indicated that the

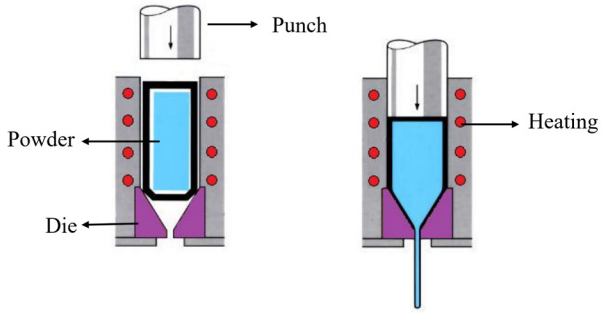

Fig. 3. Schematic illustration of the hot extrusion process.

Al physical properties were improved by the addition of carbon nanotubes. However, the thermal and electrical conductivities decreased by the addition of 0.5 to 3 wt. % carbon nanotubes. The results showed that the incorporation of CNTs does not improve the electrical and thermal conductivities of the Al matrix. Therefore, Al/CNT composites may not be suitable for applications requiring conductive properties, and they might be employed for thermal and electrical resistive applications.

6.1.6. Hot extrusion

Esawi et al. [16] mixed up 5 wt.% carbon nanotubes filler using a ball mill. To consolidate the ball-milled powder mixture, the mixture was cold-compacted and sintered by hot extrusion. The hot extrusion process is illustrated in Fig. 3. They investigated the effect of the carbon nanotubes content on the mechanical characteristics of the nanocomposites. The results revealed that stiffness enhanced up to 23% and tensile strength enhancements up to 50% in comparison with pure Al. In the nanocomposites with 5wt. % carbon nanotube, the formation of the carbide phase was recorded. In the composites with CNT content higher than 2 wt. %, the dispersion of the reinforcement was difficult,

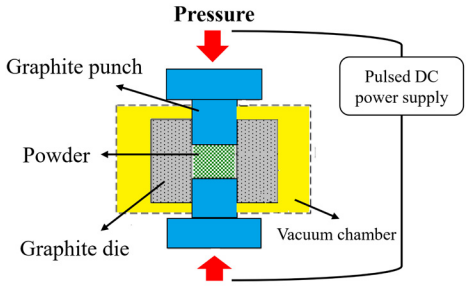

Fig. 4. Schematic illustration of the SPS process.

and hence, the expected enhancement in mechanical characteristics with increasing of the carbon nanotubes content in the matrix was not fully understood.

Choi et al. [18] produced Al/MWNTs composites via ball-milling and hot extrusion. The efficiency of reinforcing by carbon nanotubes follows the discontinuous fibers volume fraction rule in the grain size less than 70 nm. The research asserted that it is possible to produce large-scale Al/CNTs composites with uniaxially aligned carbon nanotubes via a conventional powder metallurgy method. The strengthening efficiency follows the discontinuous fibers volume fraction rule for composites possessing grain sizes of 200 nm and 72 nm, and nanotubes are able to effectively transfer loads.

6.1.7. Spark plasma sintering (SPS)

Kwon et al. [20] synthesized Al/CNTs composites using SPS, followed by hot extrusion. The SPS process is shown schematically in Fig. 4. The results indicated that the tensile strength improved by adding carbon nanotubes to Al without reducing the elongation. They proposed that the existence of carbon nanotubes in the boundary layer influences the mechanical properties, which results in effective stress transfer among CNTs and Al matrix due to the aluminum carbide formation and

Table 1.
Synthesis methods of aluminium/CNTs composites and their properties

Method	CNT content	Density (g/cm^3)	Mechanical properties*	Ref.
Cold press and sintering	2 vol. %	-	**TS:** 138 MPa	[12]
Cold press and sintering	3 wt. %	2.6	**H:** 75.5 HV	[13]
Ball milling and hot extrusion	5 wt. %	-	**TS:** 250 MPa **Indentation modulus:** 74 GPa	[16]
Ball milling and hot extrusion	4 vol. %	-	**TS:** 440 MPa **YS:** 300 MPa	[18]
SPS and hot extrusion	1 vol. %	2.642	**TS:** 207.5 MPa **El:** 21.4 %	[20]
SPS and hot extrusion	5 wt. %	-	**TS:** 174 MPa **YS:** 96 MPa **H:** 50 HV	[21]
SPS and extrusion	2.5 wt. %	2.59	**CS:** 415.3 MPa **H:** 99.1 HV5	[23]
SPS	5 wt. %	2.58	**TS:** 130 MPa	[24]
Flake PM and hot extrusion	2 vol. %	-	**TS:** 440 MPa **E:** 90 GPa	[26]
FSP (4-pass FSP)	1 wt. %	2.733	**TS:** 477 MPa **YS:** 385 MPa **El:** 8%	[27]
FSP	6 vol. %	-	**TS:** 190 MPa **El:** 10 %	[29]
SD	5 wt. %	-	**TS:** 300 MPa	[30]

*TS: Tensile Strength, YS: Yield Strength, CS: Compressive Strength, El: Elongation, E: Young's modulus, H: Hardness

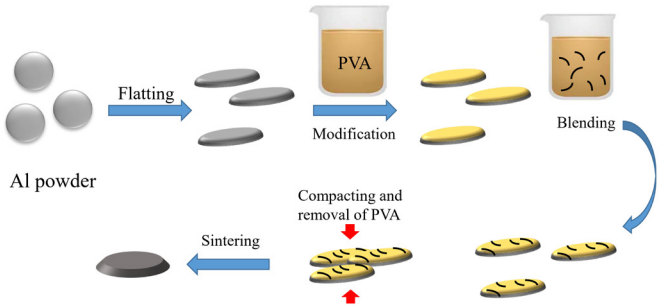

Fig. 5. Schematic illustration of flake PM.

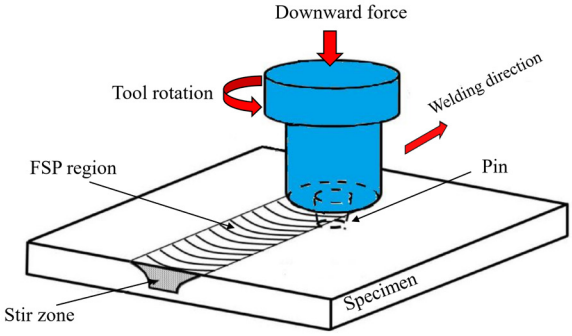

Fig. 6. Schematic illustration of FSP.

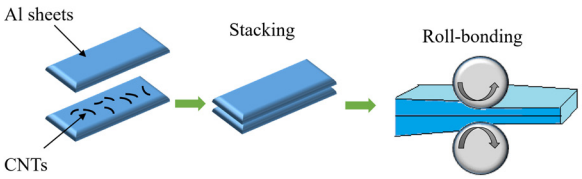

Fig. 7. Schematic illustration of the rolling process.

well-aligned carbon nanotubes along the direction of extrusion.

In another research, 0 to 2 wt. % MWCNTs were added to the Al matrix through the mixing of the reinforcement and matrix powders in a roller mill. The mixture was then sintered by SPS, and subsequent hot extrusion and a fully compact carbon nanotube-reinforced aluminum were achieved. The composite mechanical properties with a low amount of CNTs (0.5 wt. %) at room temperature showed a significant increase in comparison with pure Al without increasing the cost. With increasing the amount of CNTs in the composite, the mechanical properties reduced as a result of the agglomeration of carbon nanotubes and the lack of sufficient bonding at the interface [21].

Wu et al. [24] also employed spark plasma sintering for the preparation of MWNTs- reinforced Al composites containing 0 to 5 wt.% carbon nanotubes. According to the results, thermal conductivity increased by the addition of up to 1 wt. % CNTs compared to the pure Al. Thermal conductivity reached a maximum of 199 W/m/K for the composites containing 0.5 wt.% CNTs. This composition of the Al composites also showed the maximum tensile strength of 130 MPa. They summarized that CNT-reinforced Al composites prepared by SPS method are promising materials for applications requiring high thermal conductivity.

CNTs (2.5 wt.%) and Al powders were ball-milled and consolidated through a spark plasma extrusion (SPE) process by Morsi et al. [23]. The advantages of SPE compared to SPS is the possibility of preparing materials with extended geometries and providing bulk deformation influenced by an electric current which provides unique properties in materials. Because CNTs have strengthening effects in Al and decrease the Al crystal size, aluminum/CNT composites had enhanced compressive strength (10%) and hardness (33%).

6.1.8. Flake powder metallurgy (flake PM)

The steps of flake powder metallurgy route are illustrated in Fig. 5. To disperse carbon nanotubes uniformly in aluminum matrix, the flake powder metallurgy (flake PM) strategy was used by Jiang et al. [26]. To disperse the reinforcement in the matrix uniformly, CNTs were adsorbed onto the surface of aluminum nanoflake through slurry blending and the prepared composite powders were consolidated via hot extrusion. In flake processing, the Al spherical powders changes to nanoflakes, and their surface is modified by polyvinyl alcohol hydrosol; thus, high surface and geometrical compatibilities between aluminum and CNTs powders are achieved. Therefore, the achievement of a homogeneous and less-agglomerated distribution of carbon nanotubes is possible via direct slurry blending. As carbon nanotubes are not exposed to high-energy physical forces such as ball milling, the structural integrity of carbon nanotubes is well maintained in the composite. Therefore, in this study, ductile CNT-reinforced composites with the plasticity of 6% and tensile strength of 435 MPa was produced, which is greater than values obtained from other conventional routes.

Rikhtegar et al. [95] also used the flake PM route for the modification of CNTs dispersion in Al powder. They used short fibers and long fibers of CNTs-COOH with 1.5wt. %CNTs to reinforce and strengthen the Al powders with particle sizes of <20 μm and <45 μm and with a large aspect ratio of 125 and 50, respectively. The influence of different variables of the process, including speed and time of rotation in ball milling, Al nanoflake production, the carboxyl agent, and chemical modification by polyvinyl alcohol on the wall of carbon nanotubes as well as morphological changes of the components were studied.

They reported that in this method, hydrogen bonding is formed between –COOH groups of carbon nanotubes and the –OH groups of PVA, and consequently, a good dispersion of reinforcement in the Al matrix was observed for both short and long carbon nanotubes.

6.2. Friction stir processing (FSP)

Liu et al. [27] applied powder metallurgy and subsequent friction stir processing (FSP) (Fig. 6). Investigation of the microstructure indicated that carbon nanotubes were well dispersed in the Al-based composites. The smaller grain size of aluminum was achieved due to the tendency of carbon nanotubes to be located along grain boundaries. The carbon nanotubes retained their layered structure despite shortening and the formation of Al_4C_3 in the matrix. It was shown that during the FSP process, there was no severe damage to nanotubes. The composites containing 1 wt. % and 3 wt. % nanotubes showed an increase in the yield strength about 23.9% and 45.0%, respectively, compared to pure Al.

In other work, Al/MWCNTs composites with various contents of CNTs were synthesized using friction stir processing. The investigation showed good dispersion of CNTs in the Al matrix through friction stir processing. Hardness and tensile tests indicated that the hardness and

tensile strength of Al/MWCNTs composites slightly increased with the increase of the nanotube content; however, the reduction in elongation was observed. For the specimen containing 6 vol. % CNTs, ultimate tensile strength reached a maximum of 190.2 MPa, which was two times higher than that of pure Al. The ductility of the nanocomposites decreased with the increase of the carbon nanotube content [29].

For homogeneous incorporation of a high volume fraction (>50%) of CNTs in the Al matrix, Izadi et al. [96] used multi-pass FSP. TEM and SEM investigations showed that CNTs were dispersed uniformly after three passes; however, the tubular shape of CNTs was destroyed by the thermo-mechanical cycles. The microhardness of the samples increased significantly compared to non-reinforced samples due to the influence of the reinforcing component on grain refinement and strengthening of the matrix.

Moreover, TEM analysis indicated that after 3 passes, CNTs were mostly transformed into turbostratic and polyaromatic structures along with Al_4C_3. They concluded that two passes preserve the structure of multi-walled CNTs while for uniform distribution of the reinforcement, three passes are required, but the reinforcement stability was not preserved.

6.3. Spread dispersion (SD)/ rolling process

X Liao et al. [30] prepared Al/CNTs composite using a spread dispersion (SD) technique. The SD procedure was the repeated pressing and rolling for the preparation of aluminum/carbon nanotubes nanocomposites. This technique was first utilized by Yasuna et al. [8–11] in 1997. The rolling process is depicted schematically in Fig. 7. This technique consists of the stacking of several metal sheets and the subsequent pressing and rolling in order to bond the layers and produce a bulk form from multilayers.

In this study, the researchers applied this method for the dispersion of carbon nanotubes in the Al matrix. It was reported that ultra-fine grain size about 20 nm was formed, the ductility decreased and tensile strength of the nanocomposites increased by 66% over pure aluminum. This improvement was due to stronger Al/CNT bonding, eliminated porosity, the disappearance of the CNT-free zones, and segregation of clustered CNTs.

Samadzadeh et al. [97] synthesized Al/ MWCNTs composites using the roll bonding process. According to the results, using the solution dispersion route in comparison with the spread route leads to the decrease of Al sheets bond strength. Furthermore, the sheets bond strength reduced by the incorporation of carbon nanotubes at a specific reduction of thickness. At higher thickness reductions, the bond strength improved in the sheet with and without carbon nanotubes, and the increase in the entry temperature enhanced bond strength; however, the increase in bond strength was higher in pure Al compared to the reinforced composites. Different synthesis methods of aluminum/CNTs composites and the effect on their mechanical properties are summarized in Table 1.

7. Conclusions and future insights

In this review, the processing techniques applied for the synthesis of aluminum/CNTs composites and mechanical properties enhancement, including hardness, toughness, and wear resistance, were discussed. According to previous research reports, a very effective factor in the improvement of the mechanical properties of theses Al-based nanocomposites is CNTs distribution in the metal matrix. Therefore, the preparation conditions and methods are required to be optimized in order to have good dispersion of the reinforcement, enhanced interfacial properties between the two phases, reduction of Al matrix cold working, and subsequently less damage to nanotubes. In addition, other existing challenges are carbon nanotube distribution at micro level in the case of bulk manufacturing, the influence of carbon nanotube alignment, uniform dispersion at high concentration of CNTs. Overall, new methods or modifications of conventional methods are required to develop to optimize these factors.

REFERENCES

[1] V.S. Rizi, F. Sharifianjazi, H. Jafarikhorami, N. Parvin, L.S. Fard, M. Irani, A. Esmaeilkhanian, Sol–gel derived SnO_2/Ag_2O ceramic nanocomposite for H_2 gas sensing applications, Materials Research Express 6(11) (2019) 1150g2.

[2] S.A. Delbari, B. Nayebi, E. Ghasali, M. Shokouhimehr, M.S. Asl, Spark plasma sintering of TiN ceramics codoped with SiC and CNT, Ceramics International 45(3) (2019) 3207-3216.

[3] Y. Orooji, M.R. Derakhshandeh, E. Ghasali, M. Alizadeh, M.S. Asl, T. Ebadzadeh, Effects of ZrB_2 reinforcement on microstructure and mechanical properties of a spark plasma sintered mullite-CNT composite, Ceramics International (2019).

[4] E. Asadi, A. Fassadi Chimeh, S. Hosseini, S. Rahimi, B. Sarkhosh, L. Bazli, R. Bashiri, A.H. Vakili Tahmorsati, A Review of Clinical Applications of Graphene Quantum Dot-based Composites, Composites and Compounds 1(1) (2019).

[5] F.S. Jazi, N. Parvin, M. Tahriri, M. Alizadeh, S. Abedini, M. Alizadeh, The relationship between the synthesis and morphology of SnO_2-Ag_2O nanocomposite, Synthesis and Reactivity in Inorganic, Metal-Organic, and Nano-Metal Chemistry 44(5) (2014) 759-764.

[6] F.S. Jazi, N. Parvin, M. Rabiei, M. Tahriri, Z.M. Shabestari, A.R. Azadmehr, Effect of the synthesis route on the grain size and morphology of ZnO/Ag nanocomposite, Journal of Ceramic Processing Research 13(5) (2012) 523-526.

[7] Y. Orooji, A.a. Alizadeh, E. Ghasali, M.R. Derakhshandeh, M. Alizadeh, M.S. Asl, T. Ebadzadeh, Co-reinforcing of mullite-TiN-CNT composites with ZrB_2 and TiB_2 compounds, Ceramics International 45(16) (2019) 20844-20854.

[8] L. Bazli, A. Khavandi, M.A. Boutorabi, M. Karrabi, Morphology and viscoelastic behavior of silicone rubber/EPDM/Cloisite 15A nanocomposites based on Maxwell model, Iranian Polymer Journal 25(11) (2016) 907-918.

[9] L. Bazli, A. Khavandi, M.A. Boutorabi, M. Karrabi, Correlation between viscoelastic behavior and morphology of nanocomposites based on SR/EPDM blends compatibilized by maleic anhydride, Polymer 113 (2017) 156-166.

[10] V. Balouchi, F.S. Jazi, A. Saidi, Developing (W, Ti) C-(Ni, Co) nanocomposite by SHS method, Journal of Ceramic Processing Research 16(5) (2015) 605-608.

[11] A. Moghanian, F. Sharifianjazi, P. Abachi, E. Sadeghi, H. Jafarikhorami, A. Sedghi, Production and properties of Cu/TiO_2 nano-composites, Journal of Alloys and Compounds 698 (2017) 518-524.

[12] R. George, K. Kashyap, R. Rahul, S. Yamdagni, Strengthening in carbon nanotube/aluminium (CNT/Al) composites, Scripta Materialia 53(10) (2005) 1159-1163.

[13] S. Sivananthan, S. Gnanasekaran, J.S.C. Samson, Preparation and Characterization of Aluminium Nanocomposites Based on MWCNT, Applied Mechanics and Materials, Trans Tech Publ, 2014, pp. 30-38.

[14] D. Singla, K. Amulya, Q. Murtaza, CNT reinforced aluminium matrix composite-a review, Materials Today: Proceedings 2(4-5) (2015) 2886-2895.

[15] L. Bazli, M. Siavashi, A. Shiravi, A Review of Carbon nanotube/TiO_2 Composite prepared via Sol-Gel method, Journal of Composites and Compounds 1(1) (2019) 1-12.

[16] A. Esawi, K. Morsi, A. Sayed, M. Taher, S. Lanka, Effect of carbon nanotube (CNT) content on the mechanical properties of CNT-reinforced aluminium composites, Composites Science and Technology 70(16) (2010) 2237-2241.

[17] R. Tenne, Inorganic nanotubes and fullerene-like nanoparticles, Nature Nanotechnology 1(2) (2006) 103-111.

[18] H. Choi, G. Kwon, G. Lee, D. Bae, Reinforcement with carbon nanotubes in aluminum matrix composites, Scripta Materialia 59(3) (2008) 360-363.

[19] S.R. Bakshi, D. Lahiri, A. Agarwal, Carbon nanotube reinforced metal matrix composites-a review, International materials reviews 55(1) (2010) 41-64.

[20] H. Kwon, D.H. Park, J.F. Silvain, A. Kawasaki, Investigation of carbon nanotube reinforced aluminum matrix composite materials, Composites Science and Technology 70(3) (2010) 546-550.

[21] J.-z. Liao, M.-J. Tan, I. Sridhar, Spark plasma sintered multi-wall carbon nanotube reinforced aluminum matrix composites, Materials & Design 31 (2010) S96-S100.

[22] M.F. De Volder, S.H. Tawfick, R.H. Baughman, A.J. Hart, Carbon nanotubes: present and future commercial applications, science 339(6119) (2013) 535-539.

[23] K. Morsi, A. Esawi, S. Lanka, A. Sayed, M. Taher, Spark plasma extrusion (SPE) of ball-milled aluminum and carbon nanotube reinforced aluminum composite powders, Composites Part A: Applied Science and Manufacturing 41(2)

(2010) 322-326.
[24] J. Wu, H. Zhang, Y. Zhang, X. Wang, Mechanical and thermal properties of carbon nanotube/aluminum composites consolidated by spark plasma sintering, Materials & Design 41 (2012) 344-348.
[25] A. Takakura, K. Beppu, T. Nishihara, A. Fukui, T. Kozeki, T. Namazu, Y. Miyauchi, K. Itami, Strength of carbon nanotubes depends on their chemical structures, Nature Communications 10(1) (2019) 3040.
[26] L. Jiang, Z. Li, G. Fan, L. Cao, D. Zhang, The use of flake powder metallurgy to produce carbon nanotube (CNT)/aluminum composites with a homogenous CNT distribution, Carbon 50(5) (2012) 1993-1998.
[27] Z. Liu, B. Xiao, W. Wang, Z. Ma, Singly dispersed carbon nanotube/aluminum composites fabricated by powder metallurgy combined with friction stir processing, Carbon 50(5) (2012) 1843-1852.
[28] M.S. Mustaffa, R.a.S. Azis, N.H. Abdullah, I. Ismail, I.R. Ibrahim, An investigation of microstructural, magnetic and microwave absorption properties of multi-walled carbon nanotubes/$Ni_{0.5}Zn_{0.5}Fe_2O_4$, Scientific Reports 9(1) (2019) 15523.
[29] Q. Liu, L. Ke, F. Liu, C. Huang, L. Xing, Microstructure and mechanical property of multi-walled carbon nanotubes reinforced aluminum matrix composites fabricated by friction stir processing, Materials & Design 45 (2013) 343-348.
[30] J. Liao, M.-J. Tan, A simple approach to prepare Al/CNT composite: Spread–Dispersion (SD) method, Materials Letters 65(17-18) (2011) 2742-2744.
[31] C. Deng, D. Wang, X. Zhang, A. Li, Processing and properties of carbon nanotubes reinforced aluminum composites, Materials Science and engineering: A 444(1-2) (2007) 138-145.
[32] S. Xiang, X. Wang, M. Gupta, K. Wu, X. Hu, M. Zheng, Graphene nanoplatelets induced heterogeneous bimodal structural magnesium matrix composites with enhanced mechanical properties, Scientific Reports 6(1) (2016) 38824.
[33] S. Iijima, Helical microtubules of graphitic carbon, nature 354(6348) (1991) 56.
[34] A.A. Green, M.C. Hersam, Processing and properties of highly enriched double-wall carbon nanotubes, Nature Nanotechnology 4(1) (2009) 64-70.
[35] A.A. White, S.M. Best, I.A. Kinloch, Hydroxyapatite–carbon nanotube composites for biomedical applications: a review, International Journal of Applied Ceramic Technology 4(1) (2007) 1-13.
[36] Z. Spitalsky, D. Tasis, K. Papagelis, C. Galiotis, Carbon nanotube–polymer composites: chemistry, processing, mechanical and electrical properties, Progress in polymer science 35(3) (2010) 357-401.
[37] L. Wang, Z. Yang, Y. Cui, B. Wei, S. Xu, J. Sheng, M. Wang, Y. Zhu, W. Fei, Graphene-copper composite with micro-layered grains and ultrahigh strength, Scientific Reports 7(1) (2017) 41896.
[38] A.V. Krasheninnikov, F. Banhart, Engineering of nanostructured carbon materials with electron or ion beams, Nature Materials 6(10) (2007) 723-733.
[39] L. Zhang, Q. Wei, J. An, L. Ma, K. Zhou, W. Ye, Z. Yu, X. Gan, C.-T. Lin, J. Luo, Construction of 3D interconnected diamond networks in Al-matrix composite for high-efficiency thermal management, Chemical Engineering Journal 380 (2020) 122551.
[40] R.J.M. Palma, J.M.M. Duart, Basic Properties of Low-Dimensional Structures, Nanotechnology for Microelectronics and Photonics, Elsevier, 2017, pp. 81-105.
[41] A. Masoudian, A. Tahaei, A. Shakiba, F. Sharifianjazi, J.A. Mohandesi, Microstructure and mechanical properties of friction stir weld of dissimilar AZ31-O magnesium alloy to 6061-T6 aluminum alloy, Transactions of nonferrous metals society of China 24(5) (2014) 1317-1322.
[42] E. Ghasali, P. Sangpour, A. Jam, H. Rajaei, K. Shirvanimoghaddam, T. Ebadzadeh, Microwave and spark plasma sintering of carbon nanotube and graphene reinforced aluminum matrix composite, Archives of Civil and Mechanical Engineering 18(4) (2018) 1042-1054.
[43] M. Alizadeh, M. Paydar, F.S. Jazi, Structural evaluation and mechanical properties of nanostructured Al/B_4C composite fabricated by ARB process, Composites Part B: Engineering 44(1) (2013) 339-343.
[44] A. Esmaeilkhanian, F. Sharifianjazi, A. Abouchenari, A. Rouhani, N. Parvin, M. Irani, Synthesis and Characterization of Natural Nano-hydroxyapatite Derived from Turkey Femur-Bone Waste, Applied biochemistry and biotechnology (2019) 1-14.
[45] C. Tatar, N. Özdemir, Investigation of thermal conductivity and microstructure of the α-Al_2O_3 particulate reinforced aluminum composites (Al/Al_2O_3-MMC) by powder metallurgy method, Physica B: Condensed Matter 405(3) (2010) 896-899.
[46] S. Naher, D. Brabazon, L. Looney, Computational and experimental analysis of particulate distribution during Al–SiC MMC fabrication, Composites Part A: Applied Science and Manufacturing 38(3) (2007) 719-729.
[47] A. Slipenyuk, V. Kuprin, Y. Milman, J. Spowart, D. Miracle, The effect of matrix to reinforcement particle size ratio (PSR) on the microstructure and mechanical properties of a P/M processed AlCuMn/SiCp MMC, Materials Science and engineering: A 381(1-2) (2004) 165-170.
[48] R. Jamaati, M. Toroghinejad, Microstructure and mechanical properties of Al/Al_2O_3 MMC produced by anodising and cold roll bonding, Materials Science and Technology 27(11) (2011) 1648-1652.
[49] R.N. Yadav, R.K. Porwal, J. Ramkumar, Experimental Modeling of EDMed Aluminum Metal Metrix Composite: A Review, Emerging Trends in Mechanical Engineering, Springer2020, pp. 511-518.
[50] B. Duan, Y. Zhou, D. Wang, Y. Zhao, Effect of CNTs content on the microstructures and properties of CNTs/Cu composite by microwave sintering, Journal of Alloys and Compounds 771 (2019) 498-504.
[51] R. Zheng, N. Li, Z. Zhan, Friction and wear behavior of Cu-La_2O_3 composite sliding against 52100 bearing steel in vacuum, Vacuum 161 (2019) 55-62.
[52] F. Czerwinski, Cerium in aluminum alloys, Journal of Materials Science (2020) 1-49.
[53] Z. Wang, K. Georgarakis, K.S. Nakayama, Y. Li, A.A. Tsarkov, G. Xie, D. Dudina, D.V. Louzguine-Luzgin, A.R. Yavari, Microstructure and mechanical behavior of metallic glass fiber-reinforced Al alloy matrix composites, Scientific Reports 6(1) (2016) 24384.
[54] E. Ghasali, M. Alizadeh, T. Ebadzadeh, A. hossein Pakseresht, A. Rahbari, Investigation on microstructural and mechanical properties of B_4C–aluminum matrix composites prepared by microwave sintering, Journal of Materials Research and Technology 4(4) (2015) 411-415.
[55] A. Masoudian, M. Karbasi, F. SharifianJazi, A. Saidib, Developing Al_2O_3-TiC in-situ nanocomposite by SHS and analyzingtheeffects of Al content and mechanical activation on microstructure, Journal of Ceramic Processing Research 14(4) (2013) 486-491.
[56] E.H. Jazi, R. Esalmi-Farsani, G. Borhani, F.S. Jazi, Synthesis and Characterization of In Situ Al-$Al_{13}Fe_4$-Al_2O_3-TiB_2 Nanocomposite Powder by Mechanical Alloying and Subsequent Heat Treatment, Synthesis and Reactivity in Inorganic, Metal-Organic, and Nano-Metal Chemistry 44(2) (2014) 177-184.
[57] S. Abedini, N. Parvin, P. Ashtari, F. Jazi, Microstructure, strength and CO_2 separation characteristics of α-alumina supported γ-alumina thin film membrane, Advances in Applied Ceramics 112(1) (2013) 17-22.
[58] E. Ghasali, Y. Palizdar, A. Jam, H. Rajaei, T. Ebadzadeh, Effect of Al and Mo addition on phase formation, mechanical and microstructure properties of spark plasma sintered iron alloy, Materials Today Communications 13 (2017) 221-231.
[59] H. Majidian, E. Ghasali, T. Ebadzadeh, M. Razavi, Effect of heating method on microstructure and mechanical properties of zircon reinforced aluminum composites, Materials Research 19(6) (2016) 1443-1448.
[60] D. Gong, L. Jiang, J. Guan, K. Liu, Z. Yu, G. Wu, Stable second phase: The key to high-temperature creep performance of particle reinforced aluminum matrix composite, Materials Science and Engineering: A 770 (2020) 138551.
[61] E. Ghasali, K. Shirvanimoghaddam, M. Alizadeh, T. Ebadzadeh, Ultra-low temperature fabrication of vanadium carbide reinforced aluminum nano composite through spark plasma sintering, Journal of Alloys and Compounds 753 (2018) 433-445.
[62] E. Ghasali, A.H. Pakseresht, M. Agheli, A.H. Marzbanpour, T. Ebadzadeh, WC-Co particles reinforced aluminum matrix by conventional and microwave sintering, Materials Research 18(6) (2015) 1197-1202.
[63] E. Ghasali, K. Shirvanimoghaddam, A.H. Pakseresht, M. Alizadeh, T. Ebadzadeh, Evaluation of microstructure and mechanical properties of Al-TaC composites prepared by spark plasma sintering process, Journal of Alloys and Compounds 705 (2017) 283-289.
[64] M. Surappa, Aluminium matrix composites: Challenges and opportunities, Sadhana 28(1-2) (2003) 319-334.
[65] D.S. Namdeo, G. Subhash, V. Jagadale, Effect of Hybrid Reinforcement on Mechanical Properties of Aluminum Based Matrix Composite, Techno-Societal 2018, Springer2020, pp. 1009-1016.
[66] Q. Liu, F. Wang, X. Qiu, D. An, Z. He, Q. Zhang, Z. Xie, Effects of La and Ce on microstructure and properties of SiC/Al composites, Ceramics International 46(1) (2020) 1232-1235.
[67] M.M. Bastwros, A.M. Esawi, A. Wifi, Friction and wear behavior of Al–CNT composites, Wear 307(1-2) (2013) 164-173.
[68] C. Shao, S. Zhao, X. Wang, Y. Zhu, Z. Zhang, R.O. Ritchie, Architecture of high-strength aluminum–matrix composites processed by a novel microcasting technique, NPG Asia Materials 11(1) (2019) 69.
[69] N. Chawla, V. Ganesh, B. Wunsch, Three-dimensional (3D) microstructure visualization and finite element modeling of the mechanical behavior of SiC particle reinforced aluminum composites, Scripta materialia 51(2) (2004) 161-165.
[70] M. Bazli, H. Ashrafi, A. Jafari, X.-L. Zhao, H. Gholipour, A.V. Oskouei, Effect

of thickness and reinforcement configuration on flexural and impact behaviour of GFRP laminates after exposure to elevated temperatures, Composites Part B: Engineering 157 (2019) 76-99.
[71] K. Shirvanimoghaddam, S.U. Hamim, M.K. Akbari, S.M. Fakhrhoseini, H. Khayyam, A.H. Pakseresht, E. Ghasali, M. Zabet, K.S. Munir, S. Jia, Carbon fiber reinforced metal matrix composites: Fabrication processes and properties, Composites Part A: Applied Science and Manufacturing 92 (2017) 70-96.
[72] T. Kuzumaki, K. Miyazawa, H. Ichinose, K. Ito, Processing of carbon nanotube reinforced aluminum composite, Journal of materials Research 13(9) (1998) 2445-2449.
[73] R. Zhong, H. Cong, P. Hou, Fabrication of nano-Al based composites reinforced by single-walled carbon nanotubes, Carbon 41(4) (2003) 848-851.
[74] A. Maiti, T. Laha, Study of distribution of Carbon nanotube in Al-CNT nanocomposite synthesized via Spark-Plasma sintering, IOP Conference Series: Materials Science and Engineering, IOP Publishing, 2018, p. 012014.
[75] D. Chunfeng, X. ZHANG, M. Yanxia, W. Dezun, Fabrication of aluminum matrix composite reinforced with carbon nanotubes, Rare Metals 26(5) (2007) 450-455.
[76] W. Salas, N. Alba-Baena, L. Murr, Explosive Shock-Wave consolidation of aluminum Powder/Carbon nanotube aggregate mixtures: optical and electron metallography, Metallurgical and Materials Transactions A 38(12) (2007) 2928-2935.
[77] T. Laha, Y. Chen, D. Lahiri, A. Agarwal, Tensile properties of carbon nanotube reinforced aluminum nanocomposite fabricated by plasma spray forming, Composites Part A: Applied Science and Manufacturing 40(5) (2009) 589-594.
[78] T. Laha, Y. Liu, A. Agarwal, Carbon nanotube reinforced aluminum nanocomposite via plasma and high velocity oxy-fuel spray forming, Journal of nanoscience and nanotechnology 7(2) (2007) 515-524.
[79] T. Laha, A. Agarwal, Effect of sintering on thermally sprayed carbon nanotube reinforced aluminum nanocomposite, Materials Science and Engineering: A 480(1-2) (2008) 323-332.
[80] H.J. Ryu, S.I. Cha, S.H. Hong, Generalized shear-lag model for load transfer in SiC/Al metal-matrix composites, Journal of materials research 18(12) (2003) 2851-2858.
[81] J.N. Coleman, U. Khan, W.J. Blau, Y.K. Gun'ko, Small but strong: a review of the mechanical properties of carbon nanotube–polymer composites, Carbon 44(9) (2006) 1624-1652.
[82] J.N. Coleman, M. Cadek, R. Blake, V. Nicolosi, K.P. Ryan, C. Belton, A. Fonseca, J.B. Nagy, Y.K. Gun'ko, W.J. Blau, High performance nanotube-reinforced plastics: Understanding the mechanism of strength increase, Advanced Functional Materials 14(8) (2004) 791-798.
[83] K.T. Kim, S.I. Cha, S.H. Hong, S.H. Hong, Microstructures and tensile behavior of carbon nanotube reinforced Cu matrix nanocomposites, Materials Science and Engineering: A 430(1-2) (2006) 27-33.
[84] M.-F. Yu, O. Lourie, M.J. Dyer, K. Moloni, T.F. Kelly, R.S. Ruoff, Strength and breaking mechanism of multiwalled carbon nanotubes under tensile load, Science 287(5453) (2000) 637-640.
[85] E. Sharifi Sedeh, S. Mirdamadi, F. Sharifianjazi, M. Tahriri, Synthesis and evaluation of mechanical and biological properties of scaffold prepared from Ti and Mg with different volume percent, Synthesis and Reactivity in Inorganic, Metal-Organic, and Nano-Metal Chemistry 45(7) (2015) 1087-1091.
[86] Z.Z. Fang, J.D. Paramore, P. Sun, K.S.R. Chandran, Y. Zhang, Y. Xia, F. Cao, M. Koopman, M. Free, Powder metallurgy of titanium – past, present, and future, International Materials Reviews 63(7) (2018) 407-459.
[87] A. Azarniya, M. Safavi, S. Sovizi, A. Azarniya, B. Chen, H. Madaah Hosseini, S. Ramakrishna, Metallurgical challenges in carbon nanotube-reinforced metal matrix nanocomposites, Metals 7(10) (2017) 384.
[88] V. Yadav, S.P. Harimkar, Microstructure and properties of spark plasma sintered carbon nanotube reinforced aluminum matrix composites, Advanced Engineering Materials 13(12) (2011) 1128-1134.
[89] K. Morsi, A. Esawi, P. Borah, S. Lanka, A. Sayed, Characterization and spark plasma sintering of mechanically milled aluminum-carbon nanotube (CNT) composite powders, Journal of composite materials 44(16) (2010) 1991-2003.
[90] M.S. Strano, V.C. Moore, M.K. Miller, M.J. Allen, E.H. Haroz, C. Kittrell, R.H. Hauge, R. Smalley, The role of surfactant adsorption during ultrasonication in the dispersion of single-walled carbon nanotubes, Journal of nanoscience and nanotechnology 3(1-2) (2003) 81-86.
[91] J.M. Bonard, T. Stora, J.P. Salvetat, F. Maier, T. Stöckli, C. Duschl, L. Forró, W.A. de Heer, A. Châtelain, Purification and size-selection of carbon nanotubes, Advanced Materials 9(10) (1997) 827-831.
[92] R. Cross, B.A. Cola, T. Fisher, X. Xu, K. Gall, S. Graham, A metallization and bonding approach for high performance carbon nanotube thermal interface materials, Nanotechnology 21(44) (2010) 445705.
[93] E. Ghasali, Y. Orooji, H.N. Germi, Investigation on in-situ formed Al_3V-Al-VC nano composite through conventional, microwave and spark plasma sintering, Heliyon 5(5) (2019) e01754.
[94] M. Alizadeh, F. Sharifianjazi, E. Haghshenasjazi, M. Aghakhani, L. Rajabi, Production of nanosized boron oxide powder by high-energy ball milling, Synthesis and Reactivity in Inorganic, Metal-Organic, and Nano-Metal Chemistry 45(1) (2015) 11-14.
[95] F. Rikhtegar, S. Shabestari, H. Saghafian, The homogenizing of carbon nanotube dispersion in aluminium matrix nanocomposite using flake powder metallurgy and ball milling methods, Powder technology 280 (2015) 26-34.
[96] H. Izadi, A.P. Gerlich, Distribution and stability of carbon nanotubes during multi-pass friction stir processing of carbon nanotube/aluminum composites, Carbon 50(12) (2012) 4744-4749.
[97] M. Samadzadeh, M.R. Toroghinejad, The influence of carbon nanotube and roll bonding parameters on the bond strength of Al sheets, Journal of materials engineering and performance 23(5) (2014) 1887-1895.

Available online at www.jourcc.com

Journal homepage: www.JOURCC.com

Journal of Composites and Compounds

Bioactive glass coated zirconia for dental implants: A review

Kaiqiang Zhang[a], Quyet Van Le[b]*

[a] *School of Chemistry and Chemical Engineering, Nanjing University, Nanjing 210023, China*
[b] *Institute of Research and Development, Duy Tan University, Da Nang, 550000, Viet Nam*

ABSTRACT

Nowadays, zirconia has been favored greatly for dental implants; however its disadvantages such as poor mechanical properties and brittleness makes it unsuitable. On the other hand, bioactive glasses coating have been utilized on tougher substrates such as zirconia. Bioactive glass coatings can decrease the healing time and hence accelerate the formation of the bond between bone and implant. Hence, in this study, we introduce the novel zirconia/bioactive glass composites with high mechanical strength and bioactivity to achieve the ideal implant in dentistry. Furthermore, a review of bioactive glass coatings (i.e., 45S5 and 58S) on zirconia as well as surface modification methods (i.e., sol-gel, laser cladding, plasma spraying, etc.) is provided.

Peer review under responsibility of jourcc

ARTICLE INFORMATION

Article history:
Received 11 March 2020
Received in revised form 25 March 2020
Accepted 29 March 2020

Keywords:
Bioactive glass coating
Zirconia
Dental implants
Nanocomposites

Table of contents

1. Introduction 10
2. Zirconia implants 11
3. Bioactive glass in biomedical applications 11
3.1. 45S5 bioglass 11
3.2 58S bioglass 11
4. Bioactive glass coatings 12
4.1. Laser cladding 12
4.2. Sol-gel 13
4.3. Plasma spray 13
4.4. Enameling 14
5. Conclusions and Future insights 14

1. Introduction

In order to replace the missing teeth, oral implants can be considered a preferred option. This procedure was first proposed by Brånemark in the 1960s [1-5]. Many reports have covered the chemical and physical features of these implants including their design factor, surface structure and properties as well as implant microstructure. Moreover, many factors are believed to be important in the implant therapy prediction and clinical consequences.

Implants with good biocompatibility, sufficient corrosion and toughness can be categorized as ideal implants. Other ideal properties can be their great strength and resistance to fracture and wear [6-9]. The biological responses of dental implants as well as their chemical composition are the main properties that are significant in the categorization of these materials. Note that the principles of design of implant should be necessarily based on the material physical features [10].

Building fillers with the more similarity to human teeth is of great importance since current fillers cannot present enough functional and reinforcing impact for dental composites. Although, in the research of monomer structures as well as filler compositions, repair failure can still happen because of reconstruction fracture and the secondary-carriers [11-13].

Ceramics lack the electric current conduction and they can be applied for the production of purification and dissociation membranes of biological fluids in medical equipment. In this regard, they can be suitable to manufacture porous components for dosage drug administration.

* *Corresponding author: Van Le; E-mail: levanquyet@dtu.edu.vn*
https://doi.org/10.29252/jcc.2.1.2

In medical field, they are appropriate to make prosthesis. Ceramics enjoy excellent integration capability with the tissue of human bone that can be considered as a superiority over the implants with metallic nature. Their biological inertness and electrical passivation have made ceramics a promising material for the medical equipment. In comparison with metallic implants, zirconia-based ceramics show minimum ion release and they are biologically inert [14-32].

Modern Ti implant technologies are being introduced owing to possible combination of immunologic and aesthetic aspects of Ti and Ti alloys. Nevertheless, these characteristics should be maintained during the improvement of this technology. To sustain these properties, dental implantology started to apply Zr as a desirable alternative to Ti [29].

Ti and Zr are similar in terms of biocompatibility and osteointegration. However, since Zr is more bioinert than Ti, it is protected more against the attack by different organisms fermentation systems as well as degradation. This can present a minimum release of ion as compared with the metallic implants. It is well understood that the ion released from metallic implants can exert different unwanted effects including inflammatory, toxic, mutagenic and allergic reactions. A decrease in the lifetime and mechanical properties of the metallic implant can be made because of the in vivo corrosion of these implants [33].

The demand for zirconia dental implants is increasing recently. In comparison with the Ti dental implants, their increased esthetic featureowing to similarity to the human tooth color is the main benefit of these implants [34-45]. To enhance the zirconia bioactivity and morphological properties for proliferation, excellent cell attachment and the acceptable differentiation during the surrounded bone cure, many efforts have been made [46, 47].

In terms of advantages, some documents have mentioned that zirconia decreases the risk of explosive reactions in surrounding peri-implant tissues, because it can reduce the biofilm aggregation and bacteria adhesion [32, 36, 48, 49]. On the other hand, titanium is grey and it can be corroded [25, 50]. These two facts about Ti, which surely can influence the appearance and health system, can provide aesthetic disadvantages that cannot be denied [46].Both of the materials would need 3 to 6 months prior to the fixation of complete prosthetic reconstruction [18, 51-56]. This time can be reduced by applying the bioactive glass coating. Furthermore, after implantation, the bone loss rate can be decreased, which is another benefit of these coatings [57-60].

2. Zirconia implants

Zirconia with better optical, aesthetic, mechanical and biological qualifications is a suitable substitute to traditional Ti implant system for oral recovery [61-64]; it is produced by the oxidation of zirconium [25, 27, 65-67]. Zirconium, which is a transition metal [56, 68] with grey-white color [69-73], can be used to make zirconia implant.

Segments of the metal implant can be uncovered by recession of gingiva and the loss of apical bone, which this can disclose a discolored overlying gingiva [74-77]. Thus, it would be possible to use the zirconia ceramics because they enjoy great aesthetic, biological and mechanical characteristics and they lack electrical corrosion. Polyethylene and Ti show more inflammatory reactions than zirconia. Less inflammatory response along with the lack of mutagenicity and toxicity in zirconia, can be considered as the most attractive zirconia properties [58].

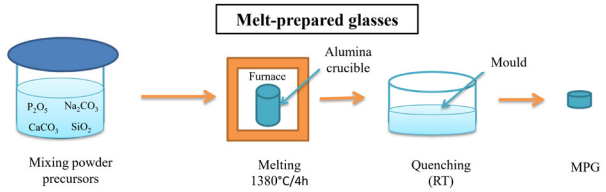

Fig. 1. Schematic of the melting process for preparing bioglass.

3. Bioactive glass in biomedical applications

To regenerate the tissue, many medical approaches have been employed by bioglasses or bioceramics, which are manufactured in various phases and shapes. The capability of reaction with physiological media have been seen to be slower in bioceramics than that of bioactive glasses. This can result in better bonding with alive tissues and the formation of apatite layer. Hence, bioceramics require the special coated layer to improve their biomedical applications [78].

Because of the great bioactivity of BGs, they are one of the best biomaterials for renovation and bone repair. For the first time, they were introduced by Hench's team at the late 1960s [39, 79-81]. Moreover, by combining great mechanical strength and excellent bioactivity of BGs, they can be successfully used as coatings on inert substrates [82]. Reaction with the physiological fluids and the formation of chemical bonding between bones and bioglass can be occurred when bioglasses are implanted in the body [83-87]. A bioactive surface can be considered as important agent to avoid many simultaneous reactions, which take place between the implant and the targeted tissue at the implant surface [82].

Melting process, which starts from carbonates and oxides, is the most important technique of bioactive glass preparation. Then, sol-gel method with the ability of producing bioactive glasses with high bioactivity was introduced. Their increased bioactivity, which is presented by this method, resulted from the microstructural properties and tailored composition. Furthermore, melting approach needs to be processed at higher temperature as compared with the sol-gel methodology, which can limit or avoid the flux addition for sol-gel method [88]. The bioactive glass with its composite coatings can be classified as following categorization according to the coating structure.

3.1. 45S5 bioglass

Ceramic 45S5 BG with 24.5% sodium oxide, 45% silicon dioxides, 24.5% calcium dioxide and 6% phosphorus pentoxide have attracted the attentions of researchers as a biomaterial substance because of its osseointegration capability, bioactive surface and the ability of healing bone damages [89-91]. It can be prepared by melt-cast method with various crystallinity including amorphous and crystalline [92]. A schematic of melting process for producing melt-prepared glasses (MPG) is provided in Fig. 1.

In order to study the impact of bioactive glass 45S5 crystallization on the degradation and constitution of apatite, Plewinski et al. [93], performed XRD analysis on the samples including samples treated by heat and amorphous samples. To guarantee the perfect amorphous sample crystallization, the heat-treatment was continued for 1 hour at 1000 ^{0}C. They found that the apatite layer could be formed on this crystallized bioglass, unlike the amorphous ones, under these conditions.

3.2. 58S bioglass

58S bioactive glass is a great bioactive, biodegradable glass with the capability of bone bonding. Due to these qualifications, this bioactive glass, with 33% calcium oxide, 58% silicon dioxide 9% phosphorus pentoxide, has been favored as scaffold substance [94-97]. The reaction of 58S bioactive glass with physiological fluids occurs after implantation quickly and it makes bond to the tissue of bone. This happens without inflammatory, toxicity and foreign-body reaction. The fast ionic dissolution as well as the hydroxyl-carbonated apatite layer formation was seen after the rapid in-vivo surface reactions. By release of calcium, silicon and phosphorous ions, the gene expression as well as the prolif-

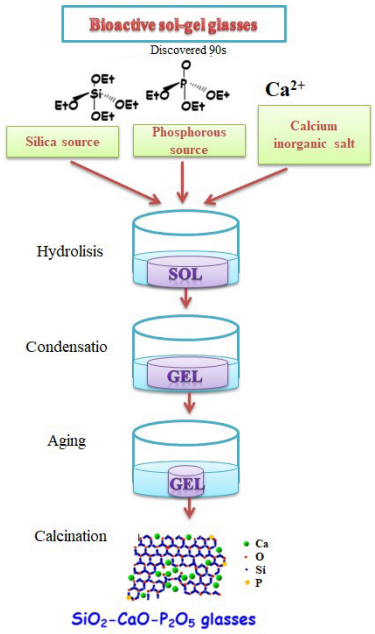

Fig. 2. Schematic illustration of the sol-gel process.

eration of osteoblast takes place to form the bone quickly.

58S-BG, produced by sol-gel approach, was used by Mokhtari et al. [98], to investigate the coatings of Chitosan-58S on nanotube of Titanium dioxide. A schematic illustration of sol-gel derived BGs is shown in Fig. 2. Based on the XRD results, the crystallization process of 58S-BG, which includes calcium silicate, calcium phosphate and Calcium Metasilicate, took place after the calcination at 1100 °C. This was continued by the structure transformation from amorphous to crystalline. Calcium Metasilicate was as the principal crystalline phase in the prepared powder. This demonstrated the intense interaction between osseous tissue and wollastonite.

To improve the bioactivity and mechanical properties of 58S bioglass, Haftbaradaran et al. [99], examined the use of sol-gel prepared 58S bioglass on fabricated-vitallium alloy. Based on the anticipations, the uncoated sample displayed a lower bioactivity as compared with the coated sample.

Faure et al. [100], used an organic acid catalyst to synthesize the 45S5 bioactive glass by a novel sol-gel approach. Instead of the conventional HNO_3 with high concentration, $C_6H_8O_7$ solution with a low concentration can be applied as a catalyst for hydrolysis reaction in the 45S5 bioactive glass preparation. Nevertheless, in this study, the bioactivity of the bioglass seems to be less than sol-gel bioactivity. In fact, sol-gel derived BG grains display extremely rough surfaces with great porosity. This, surely can present excellent exchange surface in physiological medium. Therefore, the sol–gel bioglass exchange surface can be more important than the exchange surface of the produced bioglass by the melting method.

In a study by Bui et al. [101], 58S-BG was prepared via a novel sol-gel technique. In this new approach, a quick transformation process of sol to gel, was conducted by the addition of ammonia solution. Next, the freeze-drying method was applied to dry prepared gel after 6 h. During the *in vitro* evaluations, after 2 days, a clear dense HA layer was formed. This produced layer was as the bioactivity evidence of prepared bioglass.

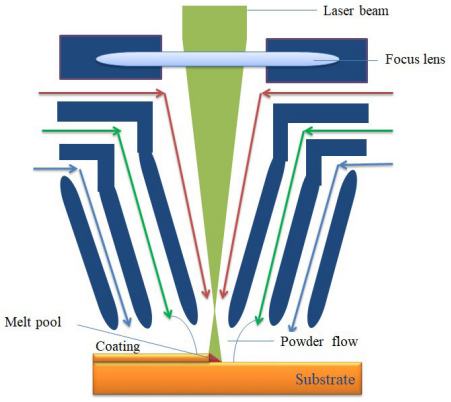

Fig. 3. Laser cladding process schematic for coating.

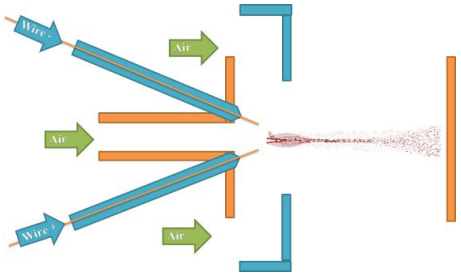

Fig. 4. Plasma spraying technique schematic illustration for deposition of BG coatings.

4. Bioactive glass coating

Considering the investigations by many researchers, bioactive glasses possess potential of many wide applications such as the formation of HCA and bone, but their use as materials for coating, is more attractive than other applications, especially when they are used as an implant. Their mechanical integrity becomes important [102-105] when they are used as coating on tougher substrate [106-108]. The studies about coatings have proved that depending on the approach of coatings and deposition, the main chemical and physical characteristics will change [109-113]. It was understood that chemical properties like long-term stability can also affect the bioactive glass coating performance [82].

Ceramics including $Ca_3(PO_4)_2$, Zr, Al_2O_3 and BGs have gained more attentions recently for medical applications, since ceramic-based prostheses may provide a good opportunity to obtain more effective biomimetic properties [88].

4.1. Laser cladding

Diverse materials can be bonded together by laser cladding technique, which can be defined as a deposition method. The principal of this method is the coating of a substrate by a laser melted powder substance. However, various profiles from this method can be applied. Industrially, a coating can be produced by the powder injection onto the substrate and the melting of it by laser beam [82].

There is a possibility to introduce variability by the operator during the coating preparation. Laser cladding is able to remove them by increasing the products quality, because it can enhance the fabrication process speed automatically (Fig. 3) [39, 114-116].

Great pores interconnectivity in the outer layer of porous layer and the desirable joining quality at the interface of substrate and coating observed by micro-computed tomography in the study by Baino et al.

[114]. They studied the laser cladding fabricated bioactive glass coating. The fabrication process was applied on the ceramic acetabular cups and the coatings can be made in a porous or pore-free form. The desired glass/ceramic joining was confirmed by indentation analysis.

To promote the osteointegration physiologically, a valuable technique is proposed, in which a bioactive coating deposition is applied on the surface of implant to make contact with bone. Baino et al. [117], used two dissimilar approaches (i.e. laser cladding and sponge replication) to produce the porous coatings of bioactive glass on the Al_2O_3-ZrO_2 composite implant. The key for bone binding is the good ability of hydroxyapatite formation. An early evidence of modern porous glass coating biocompatibility and bioactive features was proved in this study.

Laser cladding process, which is believed to be effective in bioactive glass coatings, was applied by Montealegre et al. [118], to coat the bioactive glass on alumina/zirconia composite for orthopedic applications. Besides, for two different BGs, the technology could coat macroporous bioactive glass on alumina/zirconia composite. Moreover, the laser cladding process provides a possibility to achieve dense and homogeneous BG coating. The structure and formulation of the powders of BGs are easily translated to the BG coatings.

4.2. Sol-gel

The wet chemical technique of sol-gel shows high reactivity tobecause of providing a high surface area [119-121]. This high possibility of reactivity, surely provides a low temperature for this process. This means that the process does not need high temperature sintering. Moreover, it does not need high values of pH [122-124].

Sol-gel, as an affordable process, have become favorite technique of coating for glass-ceramic composite or bioactive glass, since it has various benefits i.e. coating layer uniformity, fairly great adhesion power on complex substrate, high composition accommodation [125-127], and desirable purity [128]. This method can be combined with other approaches easily. To fix the bioactive coating on the substrate of ceramic, a high temperature is needed after heat-treatment. Thus, in spite of the convenience of this method, a high temperature can involve the mismatch of the thermal expansion coefficient that can occur between the coating and substrate. This can be continued by the residual stress accumulation on interface or the change of coated glasses composition [129].

The fabrication of a broad bioactive glass range is possible by sol-gel method that has increased the success of this process. Besides, this benefit provides a possibility to make an improvement in cell adhesion and protein absorption, because the sol-gel process can give a high specific surface porous microstructure to the bioactive glass coating.

In vitro behavior of porous zirconia was investigated by Mesquita-Guimarães et al. [130] via MG-63 cells. During the condensation, the optimization of 58S BG coating was followed by changing the number of immersions as well as controlling the sol-gel solution viscosity. In the 423-Z.BG structures, the improvement in the cell proliferation was occurred in the presence of 58S BG bioactive glass. This enhancement, which was continued to maximum level, may reveal that the coating affects the activity of cells positively to make the extracellular matrix.

Araujo et al. [33], used a novel bioactive glass layer including a low ratio of Ca/P on a Zirconia-3% Yttria substrate to prepare the extremely bioactive glass coating. The prepared coatings in this study, had thickness of 345 μm with crack-free surface, which are the representative of great glass/substrate biocompatibility in terms of the matching of expansion coefficient.

In another study, Lin et al. [131], produced mesoporous bioglass (MBGs), which were coated by ZrO_2 using dip-coating method to apply in the engineering process of bone tissue. To remove the excess sols, immersed-samples were centrifuged (30 s and 500 rpm). The results showed desired cell viability and biocompatibility and no cytotoxicity.

The dip-coating method consists of three steps: (i) samples dipping, (ii) withdrawing them and (iii) drying. After immersing the samples in the solution, they should be withdrawn in a constant speed. In order to guarantee the spread of equal thickness all over the substrate surface, it is important to have a steady speed.

The application of the dip-coating technique under extreme conditions as well as surface thickness distribution was studied by Faustino et al. [132] by making some models. The study and optimization of sol- gel method is required, since preparation, curing as well as aging time of sol-gel approaches are time consuming. Moreover, during heat-treatment process, there is the possibility of phase separation. Thus, industrially, these can make limitations in production process.

4.3. Plasma spray

Recently, the deposition of bioactive glass coatings, has been applied by standard spray technique in various studies (Fig. 4). The suspension plasma spray (a modern spray method, SPS) is newly introduced, in which a liquid suspension can be applied as a substitute of a dry powder, as feedstock [133].

Cattini et al. [133], investigated the processing parameters of SPS on mechanical properties, in-vitro condition and microstructure. Micro-size powder suspension was used to produce a bioactive coating. A preliminary screening of processing parameters displayed that the spray distance, the flow rate of H_2 and the inputs of plasma electric power may affect the microstructure. The optimum and suitable hydrogen flow rate, power and spray distance were 7.5 slpm, 36-40 kW and 50-70 mm, respectively, for biomedical applications.

Calvo et al. [134], melt-quenched the powders of 45S5 bioactive glass consisting of 24.5% calcium oxide, 45% silicon dioxide, 6% phosphorus pentoxide and 24.5 % sodium oxide. They investigated the use of atmospheric plasma spraying (PS) on the coatings of 45S5 bioactive glass. They milled the obtained frit via two dissimilar methods including wet and dry milling. To achieve a powder, consisting of porous agglomerates, the primer method was continued by spray drying while the latter should be followed by sieving.

Great surface properties, which can guarantee the effective contact with body fluid and excellent adhesion power to the substrate, was obtained by prepared coatings through atmospheric PS. All of the feed-

Table 1
Various techniques used for bioactive glass coating on zirconia substrates.

Methods	Pros.	Cons.
Plasma spray	A low probability of compromising glass bioactivity, a wide range of coating materials	Weak adhesion between substrate and glass
Laser cladding	The possibility of flat coating on surfaces with curved geometry	Need surface pre-treatment, lack of uniformity
Sol-gel	Multilayer coating, porous microstructure, versatile, large compositional range of bioactive glasses, controlled composition, and homogeneity	Due to the difference in CTE between substrate and coating, post heat treatment introduces internal stress
Enameling	Large range of thickness, versatile, cheap simple	Thermal residual stress, the formation of chemical by-product, metal degradation, glass crystallization, compositional gradient

stocks showed amorphous phase.

Joulia et al. [135], studied the mechanisms of deposition in solution precursor plasma spray (SPPS) and SPS for yttria stabilized zirconia (YSZ). Their investigated the mechanisms of deposition in suspension and solution precursor plasma spraying by studying the characteristics of individual YSZ lamellae and of complete coatings. They found that plasma-spraying using liquid feedstock could be a promising method for depositing finely structured ceramic coatings. Table 1 summerizes various techniques used for bioactive glass coating on zirconia substrates

4.4. Enameling

Enameling is a kind of conventional treatment of surface, with the benefits of facile operation, inexpensive processing system that can provide the optimization possibility via altering the processing parameters [136-138]. Although this technique can involve the glass frit layer fusing, the applied metal substrate for coating can control the introduction of a lower melting frit. The combination of the tailored-composite glass and the enameling method has been proved to be a suitable option for the fabrication process of a bioactive glass layer. This can be done onto a bioinert substrate of metal, which has the great adherence, bioactivity and thermal expansion coefficient.

The enameling approach is facile and affordable, and it is usually used for coating a ceramic or metal by a glass. In this technique, the deposition of a suspension of powder glass or a thin glass layer onto a substrate of metal or ceramic could be followed by glazing the glass by a suitable heat treatment.

In the zirconia, alumina and ceramic composites coating, the enameling by the substrates, which are made by ceramic, has showed more promising results compared to the metal substrates. Moreover, the proper engineering of processing system and glass structure can transfer the surface layer to a coating with functionally graded and enhanced mechanical properties [82].

5. Conclusions and future insights

The bioactive glasses are favored greatly due to their potential for biomedical applications such as improving the bond strength in formation of bone, accelerating healing time, etc. these characteristics have made them good candidates to be used as coating on appropriate substrate such as ZrO_2-based dental implants. This is because of poor mechanical properties and brittleness of zirconia. Thus, the composite of BGs and ZrO_2-based material would be great for biological applications. Hence, a thorough review was performed about these implant composites. It was found that, through coating of BGs on zirconia substrate, reinforcing properties especially in dental implants would be obtained.

Coatings are the advantageous and extensive field for medical applications. Therefore, we can fabricate special coatings to promote the zirconia implants advantages and also decrease the risk factors and possibility of dental implant failure.

REFERENCES

[1] S. Mohammadpour, S. Khorramymehr, Comparing one-and two-piece dental abutments under dynamic loading: A 3-D finite element analysis.

[2] A. TV, SIGN IN/REGISTER, Compendium (2020).

[3] M. Assery, A 22-Year Follow Up of Immediate Implant Placement without Bone Augmentation: A Case Series Study, Journal of Prosthodontics 29(2) (2020) 101-106.

[4] Z.M. Al-Sadah, M.S. AlShakhas, Osseous Integration After Exenteration, in: T.E. Johnson (Ed.), Anophthalmia : The Expert's Guide to Medical and Surgical Management, Springer International Publishing, Cham, 2020, pp. 107-126.

[5] B.R. Chrcanovic, J. Kisch, T. Albrektsson, A. Wennerberg, A retrospective study on clinical and radiological outcomes of oral implants in patients followed up for a minimum of 20 years, Clinical Implant Dentistry and Related Research 20(2) (2018) 199-207.

[6] K.E. Dux, Implantable Materials Update, Clinics in Podiatric Medicine and Surgery 36(4) (2019) 535-542.

[7] S.D. Shah, Implant Strength After Implantoplasty, The Ohio State University, 2019.

[8] M.D. Fahmy, A. Gupta, A. Guentsch, A. Peisker, Materials Used Intraoperatively During Oral and Maxillofacial Surgery Procedures, in: L. Tayebi (Ed.), Applications of Biomedical Engineering in Dentistry, Springer International Publishing, Cham, 2020, pp. 21-42.

[9] R. Das, C. Bhattacharjee, 16 - Titanium-based nanocomposite materials for dental implant systems, in: A.M. Asiri, Inamuddin, A. Mohammad (Eds.), Applications of Nanocomposite Materials in Dentistry, Woodhead Publishing2019, pp. 271-284.

[10] R.B. Osman, M.V. Swain, A critical review of dental implant materials with an emphasis on titanium versus zirconia, Materials 8(3) (2015) 932-958.

[11] J. Wu, X. Xie, H. Zhou, F.R. Tay, M.D. Weir, M.A.S. Melo, T.W. Oates, N. Zhang, Q. Zhang, H.H.K. Xu, Development of a new class of self-healing and therapeutic dental resins, Polymer Degradation and Stability 163 (2019) 87-99.

[12] X. Zhou, X. Huang, M. Li, X. Peng, S. Wang, X. Zhou, L. Cheng, Development and status of resin composite as dental restorative materials, Journal of Applied Polymer Science 136(44) (2019) 48180.

[13] H. Chen, R. Wang, L. Qian, H. Liu, J. Wang, M. Zhu, Surface modification of urchin-like serried hydroxyapatite with sol-gel method and its application in dental composites, Composites Part B: Engineering 182 (2020) 107621.

[14] A. Mzyk, G. Imbir, K. Trembecka-Wójciga, J.M. Lackner, H. Plutecka, E. Jasek-Gajda, J. Kawałko, R. Major, Rolling or Two-Stage Aggregation of Platelets on the Surface of Thin Ceramic Coatings under in Vitro Simulated Blood Flow Conditions, ACS Biomaterials Science & Engineering 6(2) (2020) 898-911.

[15] J. Mallya, N. DuVall, J. Brewster, H. Roberts, Endodontic Access Effect on Full Contour Zirconia and Lithium Disilicate Failure Resistance, Operative Dentistry (2020).

[16] P. Maló, M. Nunes, M. de Araújo Nobre, A. Lopes, A. Ferro, Extramaxillary Zygomatic Implants, in: J. Chow (Ed.), Zygomatic Implants: Optimization and Innovation, Springer International Publishing, Cham, 2020, pp. 87-107.

[17] O. Jung, D. Porchetta, M.-L. Schroeder, M. Klein, N. Wegner, F. Walther, F. Feyerabend, M. Barbeck, A. Kopp, In Vivo Simulation of Magnesium Degradability Using a New Fluid Dynamic Bench Testing Approach, International Journal of Molecular Sciences 20(19) (2019).

[18] N. Shrivastava, H. Barbosa, K. Ali, S.K. Sharma, Materials for Solar Cell Applications: An Overview of TiO2, ZnO, Upconverting Organic and Polymer-Based Solar Cells, in: S.K. Sharma, K. Ali (Eds.), Solar Cells: From Materials to Device Technology, Springer International Publishing, Cham, 2020, pp. 55-78.

[19] A. Kozelskaya, E. Bolbasov, A. Golovkin, A. Mishanin, A. Viknianshchukb, E. Shesterikov, A. Ashrafov, V. Novikov, S. Tverdokhlebov, Modification of the zirconia ceramics by different calcium phosphate coatings: comparative study, arXiv preprint arXiv:1712.00944 (2017).

[20] L. Grima, M. Díaz-Pérez, J. Gil, D. Sola, I.J. Peña, Generation of a Porous Scaffold with a Starting Composition in the CaO–SiO2–MgO–P2O5 System in a Simulated Physiological Environment, Applied Sciences 10(1) (2019).

[21] J.L. Guo, T.C. Piepergerdes, A.G. Mikos, Chapter 6 - Bone graft engineering: Composite scaffolds, in: H. Alghamdi, J. Jansen (Eds.), Dental Implants and Bone Grafts, Woodhead Publishing2020, pp. 159-181.

[22] M. Wöltje, R. Brünler, M. Böbel, S. Ernst, S. Neuss, D. Aibibu, C. Cherif, Functionalization of Silk Fibers by PDGF and Bioceramics for Bone Tissue Regeneration, Coatings 10(1) (2019).

[23] A. Ralls, P. Kumar, M. Misra, P.L. Menezes, Material Design and Surface Engineering for Bio-implants, JOM 72(2) (2020) 684-696.

[24] A. Bharadwaz, A.C. Jayasuriya, Recent trends in the application of widely used natural and synthetic polymer nanocomposites in bone tissue regeneration, Materials Science and Engineering: C 110 (2020) 110698.

[25] S.J. Sadowsky, Has zirconia made a material difference in implant prosthodontics? A review, Dental Materials 36(1) (2020) 1-8.

[26] K.-y. Cheng, V. Gopal, M. McNallan, G. Manivasagam, M.T. Mathew, Enhanced Tribocorrosion Resistance of Hard Ceramic Coated Ti-6Al-4V Alloy for Hip Implant Application: In-Vitro Simulation Study, ACS Biomaterials Science & Engineering 5(9) (2019) 4817-4824.

[27] M. Giri, K. Sabapathy, B. Govindasamy, H. Rajamurugan, Evaluation of insertion torque and surface integrity of zirconia-coated titanium mini screw implants, Journal of the World Federation of Orthodontists 9(1) (2020) 13-17.

[28] D. Faria, S. Madeira, M. Buciumeanu, F.S. Silva, O. Carvalho, Novel laser textured surface designs for improved zirconia implants performance, Materials

Science and Engineering: C 108 (2020) 110390.
[29] Z. Özkurt, E. Kazazoğlu, Zirconia dental implants: a literature review, Journal of oral implantology 37(3) (2011) 367-376.
[30] S. Amtul Haseeb, S.M. Abdul Khader, B. Satish Shenoy, Y.G. Naveen, P. Giridhar Kamath, K.C. Vinaya, Comparative evaluation of stress distribution in bone surrounding implant using different implant biomaterials: A 3DFEA study, Journal of Computational Methods in Sciences and Engineering 19 (2019) 523-532.
[31] E. Kontonasaki, P. Giasimakopoulos, A.E. Rigos, Strength and aging resistance of monolithic zirconia: an update to current knowledge, Japanese Dental Science Review 56(1) (2020) 1-23.
[32] A.W. Suci Dharmayanti, R. Dubey, N.K. Dubey, W.-P. Deng, Chapter 26 - Implant surface modification strategies through antibacterial and bioactive components, in: K. Pal, I. Banerjee, P. Sarkar, D. Kim, W.-P. Deng, N.K. Dubey, K. Majumder (Eds.), Biopolymer-Based Formulations, Elsevier2020, pp. 647-673.
[33] M. Araújo, M. Miola, A. Venturello, G. Baldi, J. Pérez, E. Verné, Glass coatings on zirconia with enhanced bioactivity, Journal of the European Ceramic Society 36(13) (2016) 3201-3210.
[34] N. Kong, A. Chen, W. Yan, H. Zhang, Ceramic implant fracture: A clinical report, The Journal of prosthetic dentistry 122(5) (2019) 425-429.
[35] B. Mansfield, S. Torres, T. Yu, D. Wu, A Review on Additive Manufacturing of Ceramics, ASME 2019 14th International Manufacturing Science and Engineering Conference, American Society of Mechanical Engineers Digital Collection, 2019.
[36] X. He, F.-X. Reichl, S. Milz, B. Michalke, X. Wu, C.M. Sprecher, Y. Yang, M. Gahlert, S. Röhling, H. Kniha, R. Hickel, C. Högg, Titanium and zirconium release from titanium- and zirconia implants in mini pig maxillae and their toxicity in vitro, Dental Materials 36(3) (2020) 402-412.
[37] S. Madeira, A. Barbosa, C.G. Moura, M. Buciumeanu, F.S. Silva, O. Carvalho, Aunps and Agμps-functionalized zirconia surfaces by hybrid laser technology for dental implants, Ceramics International 46(6) (2020) 7109-7121.
[38] M. Koller, E. Steyer, K. Theisen, S. Stagnell, N. Jakse, M. Payer, Two-piece zirconia versus titanium implants after 80 months: Clinical outcomes from a prospective randomized pilot trial, Clinical Oral Implants Research n/a(n/a) (2020).
[39] H. Gul, M. Khan, A.S. Khan, 3 - Bioceramics: types and clinical applications, in: A.S. Khan, A.A. Chaudhry (Eds.), Handbook of Ionic Substituted Hydroxyapatites, Woodhead Publishing2020, pp. 53-83.
[40] Y. Liu, B. Rath, M. Tingart, J. Eschweiler, Role of implants surface modification in osseointegration: A systematic review, Journal of Biomedical Materials Research Part A 108(3) (2020) 470-484.
[41] P. Tidehag, Z. Shen, Digital dentistry calls the change of ceramics and ceramic processes, Advances in Applied Ceramics 118(1-2) (2019) 83-90.
[42] Y.S. Soo, N. Silikas, J. Satterthwaite, Measurement of Fracture Strength of Zirconia Dental Implant Abutments with Internal and External Connections Using Acoustic Emission, Materials 12(12) (2019).
[43] S. Attia, H. Schaaf, T. El Khassawna, D. Malhan, K. Mausbach, H.-P. Howaldt, P. Streckbein, Oral Rehabilitation of Hypodontia Patients Using an Endosseous Dental Implant: Functional and Aesthetic Results, Journal of Clinical Medicine 8(10) (2019).
[44] G. Bryce, N. Diessner, K. Hemmings, N. MacBeth, Solutions for implants placed with prosthetic inconvenience, Dental Update 46(11) (2019) 1003-1014.
[45] M. Uno, Y. Doi, Y. Yokokawa, H. Kawaki, T. Oka, Y. Tamaki, H. Ishigami, Investigating the effectiveness of ceramic materials, particularly zirconium oxide, and the advantages the white metal holds over traditional materials used in dentistry, Impact 2019(2) (2019) 68-70.
[46] F.H. Schünemann, M.E. Galárraga-Vinueza, R. Magini, M. Fredel, F. Silva, J.C. Souza, Y. Zhang, B. Henriques, Zirconia surface modifications for implant dentistry, Materials Science and Engineering: C 98 (2019) 1294-1305.
[47] J. Mesquita-Guimarães, R. Detsch, A.C. Souza, B. Henriques, F.S. Silva, A.R. Boccaccini, O. Carvalho, Cell adhesion evaluation of laser-sintered HAp and 45S5 bioactive glass coatings on micro-textured zirconia surfaces using MC3T3-E1 osteoblast-like cells, Materials Science and Engineering: C 109 (2020) 110492.
[48] S. Hussain, E. Aneggi, S. Briguglio, M. Mattiussi, V. Gelao, I. Cabras, L. Zorzenon, A. Trovarelli, D. Goi, Enhanced ibuprofen removal by heterogeneous-Fenton process over Cu/ZrO_2 and Fe/ZrO_2 catalysts, Journal of Environmental Chemical Engineering 8(1) (2020) 103586.
[49] B. Mjöberg, Is early migration enough to explain late clinical loosening of hip prostheses?, EFORT Open Reviews 5(2) (2020) 113-117.
[50] F.H. Schünemann, M.E. Galárraga-Vinueza, R. Magini, M. Fredel, F. Silva, J.C.M. Souza, Y. Zhang, B. Henriques, Zirconia surface modifications for implant dentistry, Materials Science and Engineering: C 98 (2019) 1294-1305.
[51] A. Roccuzzo, S. Marchese, N. Worsaae, S.S. Jensen, The sandwich osteotomy technique to treat vertical alveolar bone defects prior to implant placement: a systematic review, Clinical Oral Investigations 24(3) (2020) 1073-1089.
[52] M. Chiapasco, G. Tommasato, D. Palombo, M. Del Fabbro, A retrospective 10-year mean follow-up of implants placed in ridges grafted using autogenous mandibular blocks covered with bovine bone mineral and collagen membrane, Clinical Oral Implants Research n/a(n/a) (2020).
[53] E. Askari, I.F. Cengiz, J.L. Alves, B. Henriques, P. Flores, M.C. Fredel, R.L. Reis, J.M. Oliveira, F.S. Silva, J. Mesquita-Guimarães, Micro-CT based finite element modelling and experimental characterization of the compressive mechanical properties of 3-D zirconia scaffolds for bone tissue engineering, Journal of the Mechanical Behavior of Biomedical Materials 102 (2020) 103516.
[54] Y. Cao, T. Shi, C. Jiao, H. Liang, R. Chen, Z. Tian, A. Zou, Y. Yang, Z. Wei, C. Wang, L. Shen, Fabrication and properties of zirconia/hydroxyapatite composite scaffold based on digital light processing, Ceramics International 46(2) (2020) 2300-2308.
[55] V. Lalzawmliana, A. Anand, M. Roy, B. Kundu, S.K. Nandi, Mesoporous bioactive glasses for bone healing and biomolecules delivery, Materials Science and Engineering: C 106 (2020) 110180.
[56] A.-M. Pobloth, M.J. Mersiowsky, L. Kliemt, H. Schell, A. Dienelt, B.M. Pfitzner, R. Burgkart, R. Detsch, D. Wulsten, A.R. Boccaccini, G.N. Duda, Bioactive coating of zirconia toughened alumina ceramic implants improves cancellous osseointegration, Scientific Reports 9(1) (2019) 16692.
[57] A. Kirsten, A. Hausmann, M. Weber, J. Fischer, H. Fischer, Bioactive and thermally compatible glass coating on zirconia dental implants, Journal of dental research 94(2) (2015) 297-303.
[58] M. Roy, A. Pompella, J. Kubacki, A. Piosik, B. Psiuk, J. Klimontko, J. Szade, R.A. Roy, W. Hedzelek, Photofunctionalization of dental zirconia oxide: Surface modification to improve bio-integration preserving crystal stability, Colloids and Surfaces B: Biointerfaces 156 (2017) 194-202.
[59] M.S. Abd-Elwahed, A. Wagih, I.M.R. Najjar, Correlation between micro/nano-structure, mechanical and tribological properties of copper-zirconia nanocomposites, Ceramics International 46(1) (2020) 56-65.
[60] Z. Fattahi, S.A. Sajjadi, A. Babakhani, F. Saba, Ni–Cr matrix composites reinforced with nano- and micron-sized surface-modified zirconia: Synthesis, microstructure and mechanical properties, Journal of Alloys and Compounds 817 (2020) 152755.
[61] A. Katsavochristou, M. Sierraalta, B. Saglik, D. Koumoulis, F. George, M. Razzoog, Implant Angulation Effect on the Fracture Resistance of Monolithic Zirconia Custom Abutments: An In Vitro Study, Journal of Prosthodontics n/a(n/a) (2019).
[62] R. Pilo, M. Folkman, A. Arieli, S. Levartovsky, Marginal Fit and Retention Strength of Zirconia Crowns Cemented by Self-adhesive Resin Cements, Operative Dentistry 43(2) (2018) 151-161.
[63] K.I. Afrashtehfar, M. Del Fabbro, Clinical performance of zirconia implants: A meta-review, The Journal of Prosthetic Dentistry 123(3) (2020) 419-426.
[64] K. Sivaraman, A. Chopra, A.I. Narayan, D. Balakrishnan, Is zirconia a viable alternative to titanium for oral implant? A critical review, Journal of Prosthodontic Research 62(2) (2018) 121-133.
[65] Y. Iinuma, M. Hirota, T. Hayakawa, C. Ohkubo, Surrounding Tissue Response to Surface-Treated Zirconia Implants, Materials 13(1) (2019).
[66] M. AlAmar, F. Alqahtani, The Effect of Different Implant-Abutment Connection Materials on the Fracture Resistance of Zirconia Abutments, Journal of Oral Implantology (2020) 0000-0000.
[67] D.-J. Lee, J.-S. Ryu, M. Shimono, K.-W. Lee, J.-M. Lee, H.-S. Jung, Differential Healing Patterns of Mucosal Seal on Zirconia and Titanium Implant, Frontiers in Physiology 10(796) (2019).
[68] K. Mizuno, A. Torosian, S. Jivraj, Laboratory Fabrication of Full-Arch Implant-Supported Restorations, in: S. Jivraj (Ed.), Graftless Solutions for the Edentulous Patient, Springer International Publishing, Cham, 2018, pp. 261-320.
[69] U. Schepke, M.M.M. Gresnigt, W.R. Browne, S. Abdolahzadeh, J. Nijkamp, M.S. Cune, Phase transformation and fracture load of stock and CAD/CAM-customized zirconia abutments after 1 year of clinical function, Clinical Oral Implants Research 30(6) (2019) 559-569.
[70] E. Schwarzer, S. Holtzhausen, U. Scheithauer, C. Ortmann, T. Oberbach, T. Moritz, A. Michaelis, Process development for additive manufacturing of functionally graded alumina toughened zirconia components intended for medical implant application, Journal of the European Ceramic Society 39(2) (2019) 522-530.
[71] H. Cai, J. Chen, C. Li, J. Wang, Q. Wan, X. Liang, Quantitative discoloration assessment of peri-implant soft tissue around zirconia and other abutments with different colours: A systematic review and meta-analysis, Journal of Dentistry 70 (2018) 110-117.
[72] F. Tabatabaian, Color in Zirconia-Based Restorations and Related Factors: A Literature Review, Journal of Prosthodontics 27(2) (2018) 201-211.
[73] A. Wachtel, T. Zimmermann, M. Sütel, U. Adali, M. Abou-Emara, W.-D.

Müller, S. Mühlemann, A.D. Schwitalla, Bacterial leakage and bending moments of screw-retained, composite-veneered PEEK implant crowns, Journal of the Mechanical Behavior of Biomedical Materials 91 (2019) 32-37.
[74] M. Boniecki, T. Sadowski, P. Gołębiewski, H. Węglarz, A. Piątkowska, M. Romaniec, K. Krzyżak, K. Łosiewicz, Mechanical properties of alumina/zirconia composites, Ceramics International 46(1) (2020) 1033-1039.
[75] Z. Ma, Z. Wang, X. Wang, T. Yu, Effects of laser-assisted grinding on surface integrity of zirconia ceramic, Ceramics International 46(1) (2020) 921-929.
[76] D. Silva-Herzog Rivera, A. Pozos-Guillen, A. Aragón-Piña, B.I. Cerda-Cristerna, D. Masuoka-Ito, L.O. Sánchez-Vargas, Glass coatings to enhance the interfacial bond strength between veneering ceramic and zirconia, Odontology (2020).
[77] M. Ji, J. Xu, M. Chen, M. El Mansori, Enhanced hydrophilicity and tribological behavior of dental zirconia ceramics based on picosecond laser surface texturing, Ceramics International 46(6) (2020) 7161-7169.
[78] S.A. Omar, Y. Castro, J. Ballarre, W.H. Schreiner, A. Durán, S.M. Ceré, Magnesium alloys implants coated with 58S sol-gel bioactive glass to retard first stage corrosion, Corrosion 73(12) (2017) 1448-1460.
[79] M. Abdelraof, M.S. Hasanin, M.M. Farag, H.Y. Ahmed, Green synthesis of bacterial cellulose/bioactive glass nanocomposites: Effect of glass nanoparticles on cellulose yield, biocompatibility and antimicrobial activity, International Journal of Biological Macromolecules 138 (2019) 975-985.
[80] Q. Nawaz, M.A. Ur Rehman, J.A. Roether, L. Yufei, A. Grünewald, R. Detsch, A.R. Boccaccini, Bioactive glass based scaffolds incorporating gelatin/manganese doped mesoporous bioactive glass nanoparticle coating, Ceramics International 45(12) (2019) 14608-14613.
[81] S. Ali, I. Farooq, A.M. Al-Thobity, K.S. Al-Khalifa, K. Alhooshani, S. Sauro, An in-vitro evaluation of fluoride content and enamel remineralization potential of two toothpastes containing different bioactive glasses, Bio-Medical Materials and Engineering 30 (2019) 487-496.
[82] J. Mesquita-Guimarães, B. Henriques, F. Silva, Bioactive glass coatings, Bioactive Glasses, Elsevier2018, pp. 103-118.
[83] S.M. Rabiee, M. Azizian, Effect of zirconia concentration on the growth of nanowires in bioactive glass–ceramic coatings, International Journal of Applied Ceramic Technology 10(1) (2013) 33-39.
[84] S. Ferraris, S. Yamaguchi, N. Barbani, M. Cazzola, C. Cristallini, M. Miola, E. Vernè, S. Spriano, Bioactive materials: In vitro investigation of different mechanisms of hydroxyapatite precipitation, Acta Biomaterialia 102 (2020) 468-480.
[85] J. Massera, 10 - Bioactive glass-ceramics: From macro to nano, in: V. Guarino, M. Iafisco, S. Spriano (Eds.), Nanostructured Biomaterials for Regenerative Medicine, Woodhead Publishing2020, pp. 275-292.
[86] A. Diez-Escudero, M. Espanol, M.-P. Ginebra, Chapter 5 - Synthetic bone graft substitutes: Calcium-based biomaterials, in: H. Alghamdi, J. Jansen (Eds.), Dental Implants and Bone Grafts, Woodhead Publishing2020, pp. 125-157.
[87] M. Manzano, M. Vallet-Regí, Mesoporous Silica Nanoparticles for Drug Delivery, Advanced Functional Materials 30(2) (2020) 1902634.
[88] I. Cacciotti, M. Lombardi, A. Bianco, A. Ravaglioli, L. Montanaro, Sol–gel derived 45S5 bioglass: synthesis, microstructural evolution and thermal behaviour, Journal of Materials Science: Materials in Medicine 23(8) (2012) 1849-1866.
[89] K. Dimitriadis, D. Moschovas, D.U. Tulyaganov, S. Agathopoulos, Development of novel bioactive glass-ceramics in the Na_2O/K_2O-CaO-MgO-SiO_2-P_2O_5-CaF2 system, Journal of Non-Crystalline Solids 533 (2020) 119936.
[90] O. Rojas, M. Prudent, M.E. López, F. Vargas, H. Ageorges, Influence of Atmospheric Plasma Spraying Parameters on Porosity Formation in Coatings Manufactured from 45S5 Bioglass® powder, Journal of Thermal Spray Technology 29(1) (2020) 185-198.
[91] P. Eshghinejad, H. Farnoush, M.S. Bahrami, H.R. Bakhsheshi-Rad, E. Karamian, X.B. Chen, Electrophoretic deposition of bioglass/graphene oxide composite on Ti-alloy implants for improved antibacterial and cytocompatible properties, Materials Technology 35(2) (2020) 69-74.
[92] C. Gao, T. Liu, C. Shuai, S. Peng, Enhancement mechanisms of graphene in nano-58S bioactive glass scaffold: mechanical and biological performance, Scientific reports 4 (2014) 4712.
[93] M. Plewinski, K. Schickle, M. Lindner, A. Kirsten, M. Weber, H. Fischer, The effect of crystallization of bioactive bioglass 45S5 on apatite formation and degradation, Dental Materials 29(12) (2013) 1256-1264.
[94] M. Arango-Ospina, Q. Nawaz, A.R. Boccaccini, 9 - Silicate-based nanoceramics in regenerative medicine, in: V. Guarino, M. Iafisco, S. Spriano (Eds.), Nanostructured Biomaterials for Regenerative Medicine, Woodhead Publishing2020, pp. 255-273.
[95] Q. Yao, H. Liu, X. Lin, L. Ma, X. Zheng, Y. Liu, P. Huang, S. Yu, W. Zhang, M. Lin, L. Dai, Y. Liu, 3D Interpenetrated Graphene Foam/58S Bioactive Glass Scaffolds for Electrical-Stimulation-Assisted Differentiation of Rabbit Mesenchymal Stem Cells to Enhance Bone Regeneration, Journal of Biomedical Nanotechnology 15(3) (2019) 602-611.
[96] A.K. Singh, K. Pramanik, A. Biswas, MgO enables enhanced bioactivity and antimicrobial activity of nano bioglass for bone tissue engineering application, Materials Technology 34(13) (2019) 818-826.
[97] N. Karimi, M. Kharaziha, K. Raeissi, Electrophoretic deposition of chitosan reinforced graphene oxide-hydroxyapatite on the anodized titanium to improve biological and electrochemical characteristics, Materials Science and Engineering: C 98 (2019) 140-152.
[98] H. Mokhtari, Z. Ghasemi, M. Kharaziha, F. Karimzadeh, F. Alihosseini, Chitosan-58S bioactive glass nanocomposite coatings on TiO_2 nanotube: Structural and biological properties, Applied Surface Science 441 (2018) 138-149.
[99] M. Haftbaradaran-Esfahani, M. Ahmadian, A.H. Nassajpour-Esfahani, Fabrication and characterization of porous biomedical Vitallium alloy with 58S bioglass coating prepared by sol-gel method, Applied Surface Science 506 (2020) 144959.
[100] J. Faure, R. Drevet, A. Lemelle, N.B. Jaber, A. Tara, H. El Btaouri, H. Benhayoune, A new sol–gel synthesis of 45S5 bioactive glass using an organic acid as catalyst, Materials Science and Engineering: C 47 (2015) 407-412.
[101] X.V. Bui, T.H. Dang, Bioactive glass 58S prepared using an innovation sol-gel process, Processing and Application of Ceramics 13(1) (2019) 98-103.
[102] G. Kaur, V. Kumar, F. Baino, J.C. Mauro, G. Pickrell, I. Evans, O. Bretcanu, Mechanical properties of bioactive glasses, ceramics, glass-ceramics and composites: State-of-the-art review and future challenges, Materials Science and Engineering: C 104 (2019) 109895.
[103] K.C.R. Kolan, J.A. Semon, A.T. Bindbeutel, D.E. Day, M.C. Leu, Bioprinting with bioactive glass loaded polylactic acid composite and human adipose stem cells, Bioprinting 18 (2020) e00075.
[104] M.N. Gómez-Cerezo, D. Lozano, D. Arcos, M. Vallet-Regí, C. Vaquette, The effect of biomimetic mineralization of 3D-printed mesoporous bioglass scaffolds on physical properties and in vitro osteogenicity, Materials Science and Engineering: C 109 (2020) 110572.
[105] H.A. Abo-Mosallam, E.A. Mahdy, The influence of MgO on the crystallization behaviour and properties of SrO-rich phosphosilicate glasses, Ceramics International (2020).
[106] I. Farooq, S. Ali, S. Husain, E. Khan, R.G. Hill, 17 - Bioactive glasses—structure and applications, in: Z. Khurshid, S. Najeeb, M.S. Zafar, F. Sefat (Eds.), Advanced Dental Biomaterials, Woodhead Publishing2019, pp. 453-476.
[107] M. Chavali, P. Palanisamy, M.P. Nikolova, R.-J. Wu, R. Tadiboyina, P.T.S.R.K. Prasada Rao, Chapter 2 - Inorganic composites in biomedical engineering, in: V. Grumezescu, A.M. Grumezescu (Eds.), Materials for Biomedical Engineering, Elsevier2019, pp. 47-80.
[108] E. Villicaña-Molina, E.A. Aguilar-Reyes, C.A. León-Patiño, R.E. Nuñez-Anita, Preparation of CEL2 glass-ceramic porous scaffolds coated with chitosan microspheres that have a drug delivery function, International Journal of Applied Ceramic Technology 16(5) (2019) 1812-1822.
[109] B. Zhang, J. Huang, R. Narayan, 3 - Nanostructured biomaterials for regenerative medicine: Clinical perspectives, in: V. Guarino, M. Iafisco, S. Spriano (Eds.), Nanostructured Biomaterials for Regenerative Medicine, Woodhead Publishing2020, pp. 47-80.
[110] C. Domínguez-Trujillo, F. Ternero, J.A. Rodríguez-Ortiz, S. Heise, A.R. Boccaccini, J. Lebrato, Y. Torres, Bioactive coatings on porous titanium for biomedical applications, Surface and Coatings Technology 349 (2018) 584-592.
[111] D. Faria, J.M. Pires, A.R. Boccaccini, O. Carvalho, F.S. Silva, J. Mesquita-Guimarães, Development of novel zirconia implant's materials gradated design with improved bioactive surface, Journal of the Mechanical Behavior of Biomedical Materials 94 (2019) 110-125.
[112] S. Mandal, S. Meininger, U. Gbureck, B. Basu, 3D powder printed tetracalcium phosphate scaffold with phytic acid binder: fabrication, microstructure and in situ X-Ray tomography analysis of compressive failure, Journal of Materials Science: Materials in Medicine 29(3) (2018) 29.
[113] M. Ganjali, A. Yazdanpanah, M. Mozafari, Chapter 8 - Laser deposition of nano coatings on biomedical implants, in: A. Barhoum, A.S.H. Makhlouf (Eds.), Emerging Applications of Nanoparticles and Architecture Nanostructures, Elsevier2018, pp. 235-254.
[114] F. Baino, M.A. Montealegre, G. Orlygsson, G. Novajra, C. Vitale-Brovarone, Bioactive glass coatings fabricated by laser cladding on ceramic acetabular cups: A proof-of-concept study, Journal of Materials Science 52(15) (2017) 9115-9128.
[115] Q. Wu, M.L. Mei, X. Wu, S. Shi, Y. Xu, C.H. Chu, Y. Chen, Remineralising effect of 45S5 bioactive glass on artificial caries in dentine, BMC Oral Health 20(1) (2020) 49.
[116] E. Marin, T. Adachi, M. Zanocco, F. Boschetto, A. Rondinella, W. Zhu, S. Somekawa, R. Ashida, R.M. Bock, B.J. McEntire, B.S. Bal, O. Mazda, G. Pezzot-

ti, Enhanced bioactivity of Si3N4 through trench-patterning and back-filling with Bioglass®, Materials Science and Engineering: C 106 (2020) 110278.
[117] F. Baino, J. Minguella-Canela, F. Korkusuz, P. Korkusuz, B. Kankılıç, M.Á. Montealegre, D. los Santos-López, M. Antonia, C. Vitale-Brovarone, In vitro assessment of bioactive glass coatings on alumina/zirconia composite implants for potential use in prosthetic applications, International journal of molecular sciences 20(3) (2019) 722.
[118] M.Á. Montealegre, F. Baino, J.L. Arias, J. Minguella, C. Vitale-Brovarone, M. Marshall, Bioactive glass coatings on Al_2O_3-ZrO_2 composite substrates by laser cladding for orthopaedic applications, International Congress on Applications of Lasers & Electro-Optics, Laser Institute of America, 2013, pp. 43-49.
[119] F. Foroutan, B.A. Kyffin, I. Abrahams, A. Corrias, P. Gupta, E. Velliou, J.C. Knowles, D. Carta, Mesoporous Phosphate-Based Glasses Prepared via Sol–Gel, ACS Biomaterials Science & Engineering (2020).
[120] A. Anand, P. Das, S.K. Nandi, B. Kundu, Development of antibiotic loaded mesoporous bioactive glass and its drug release kinetics, Ceramics International 46(4) (2020) 5477-5483.
[121] F. Iqbal, H. Fatima, 14 - Coating of hydroxyapatite and substituted apatite on dental and orthopedic implants, in: A.S. Khan, A.A. Chaudhry (Eds.), Handbook of Ionic Substituted Hydroxyapatites, Woodhead Publishing2020, pp. 327-353.
[122] A. Nasar, Hydroxyapatite and its coatings in dental implants, Applications of Nanocomposite Materials in Dentistry, Elsevier2019, pp. 145-160.
[123] P. Ning, F. Zhang, L.J. Wang, Y. Zhou, Y.J. Wang, Y.Y. Wu, T. Fu, Sol-gel derived AgMgO films for antibacterial and bioactive surface modification of niobium metal, Materials Chemistry and Physics 243 (2020) 122646.
[124] B. Liu, G.-y. Xiao, C.-z. Chen, Y.-p. Lu, X.-w. Geng, Hopeite and scholzite coatings formation on titanium via wet-chemical conversion with controlled temperature, Surface and Coatings Technology 384 (2020) 125330.
[125] J. Martinez, D. Espericueta, G. Lobo Guerrero Serrano, G. Ortega-Zarzosa, E. Espericueta, A.L. Guerrero Serrano, Stabilization of β-carotene embedded in a silica matrix and study of its physical properties, Materials Research Express (2020).
[126] E.B. Fredj, S. Rousselot, L. Danis, T. Bibienne, M. Gauthier, G. Liang, M. Dollé, Synthesis and characterization of $LiFe_{1-x}Mn_xPO_4$ (x = 0.25, 0.50, 0.75) lithium ion battery cathode synthesized via a melting process, Journal of Energy Storage 27 (2020) 101116.
[127] X. Xu, Y. Pan, L. Ge, Z. Shao, Perovskite Materials in Electrocatalysis, in: N.S. Arul, V.D. Nithya (Eds.), Revolution of Perovskite: Synthesis, Properties and Applications, Springer Singapore, Singapore, 2020, pp. 209-250.
[128] D.S. Raghav, S. Kumari, H.K. Singh, G.D. Varma, Structure, magnetism and electrical transport of sol-gel derived La0.30Pr0.30Ca0.40MnO3: Elucidating consequences of size effect, Journal of Magnetism and Magnetic Materials 497 (2020) 166003.
[129] N.O. Joy-anne, Y. Su, X. Lu, P.-H. Kuo, J. Du, D. Zhu, Bioactive glass coatings on metallic implants for biomedical applications, Bioactive materials 4 (2019) 261-270.
[130] J. Mesquita-Guimarães, L. Ramos, R. Detsch, B. Henriques, M. Fredel, F. Silva, A. Boccaccini, Evaluation of in vitro properties of 3D micro-macro porous zirconia scaffolds coated with 58S bioactive glass using MG-63 osteoblast-like cells, Journal of the European Ceramic Society 39(7) (2019) 2545-2558.
[131] F. Lin, C. Yan, W. Zheng, W. Fan, C. Adam, A. Oloyede, Preparation of mesoporous bioglass coated zirconia scaffold for bone tissue engineering, Advanced Materials Research, Trans Tech Publ, 2012, pp. 209-215.
[132] M. Faustini, B. Louis, P.A. Albouy, M. Kuemmel, D. Grosso, Preparation of sol− gel films by dip-coating in extreme conditions, The Journal of Physical Chemistry C 114(17) (2010) 7637-7645.
[133] A. Cattini, L. Łatka, D. Bellucci, G. Bolelli, A. Sola, L. Lusvarghi, L. Pawłowski, V. Cannillo, Suspension plasma sprayed bioactive glass coatings: Effects of processing on microstructure, mechanical properties and in-vitro behaviour, Surface and Coatings Technology 220 (2013) 52-59.
[134] V.L. Calvo, M.V. Cabedo, E. Bannier, E.C. Recacha, A.R. Boccaccini, L.C. Arias, E.S. Vilches, 45S5 bioactive glass coatings by atmospheric plasma spraying obtained from feedstocks prepared by different routes, Journal of Materials Science 49(23) (2014) 7933-7942.
[135] A. Joulia, G. Bolelli, E. Gualtieri, L. Lusvarghi, S. Valeri, M. Vardelle, S. Rossignol, A. Vardelle, Comparing the deposition mechanisms in suspension plasma spray (SPS) and solution precursor plasma spray (SPPS) deposition of yttria-stabilised zirconia (YSZ), Journal of the European Ceramic Society 34(15) (2014) 3925-3940.
[136] M.R. Syed, M. Khan, F. Sefat, Z. Khurshid, M.S. Zafar, A.S. Khan, Chapter 17 - Bioactive Glass and Glass Fiber Composite: Biomedical/Dental Applications, in: G. Kaur (Ed.), Biomedical, Therapeutic and Clinical Applications of Bioactive Glasses, Woodhead Publishing2019, pp. 467-495.
[137] F. Baino, Chapter 16 - Functionally Graded Bioactive Glass-Derived Scaffolds Mimicking Bone Tissue, in: G. Kaur (Ed.), Biomedical, Therapeutic and Clinical Applications of Bioactive Glasses, Woodhead Publishing2019, pp. 443-466.
[138] J. Chang, Y.L. Zhou, 6 - Surface modification of bioactive glasses, in: H. Ylänen (Ed.), Bioactive Glasses (Second Edition), Woodhead Publishing2018, pp. 119-143.

Available online at www.jourcc.com

Journal homepage: www.JOURCC.com

Journal of Composites and Compounds

Factors influencing the failure of dental implants: A systematic review

Leila Bazli[a], Hiva Nargesi Khoramabadi[b] , Amir Modarresi Chahardehi[c], Hasni Arsad[d], Behzad Malekpouri[e], Mohammadreza Asgari Jazi[f], Negar Azizabadi[g]*

[a] *School of Metallurgy and Materials Engineering, Iran University of Science and Technology, Tehran, Iran*
[b] *Department of Medical Engineering, Payame Noor University (PNU),19395-3697 Alborz, Iran*
[c] *Integrative Medicine Cluster, Advanced Medical and Dental Institute, Universiti Sains Malaysia, Kepala Batas, 13200, Bertam, Pulau Pinang, Malaysia*
[d] *Advanced Medical and Dental Institute, Universiti Sains Malaysia, Bertam, Pulau Pinang 13200, Malaysia*
[e] *Department of Materials Science and Engineering, Sharif University of Technology, Tehran, Iran*
[f] *Department of Dentistry, Islamic Azad University, Isfahan (khorasgan) Branch, Isfahan, Iran*
[g] *Department of Chemistry, Science and Research Branch, IAU, Tehran, Iran*

A B S T R A C T

Currently, dental implants are considered useful alternatives to missing teeth, although they may suffer from failure. In this study, the current scientific literature has been reviewed to highlight the risk factors affecting dental implant failure. Radiotherapy in the neck and head cancers, diabetes, smoking, osteoporosis, and HIV can increase the occurrence of risk factors for the failure of a dental implant. As a result of negative impacts on osseointegration, osteoporosis, smoking, and head, neck radiotherapy causes a higher risk of dental implant failure. The irradiation target volume during radiotherapy is the main cause of implant failure, especially due to the increment of marginal bone resorption. Additionally, the healing of bones around dental implants is negatively affected by heavy smoking due to the reduction of the healing speed. Moreover, diabetic patients have some complications (e.g., delayed wound healing of soft tissues, periodontitis, impaired response to infection, tooth loss, and microvascular disease) affecting therapyial preliminary considerations of dental implant treatment. However, in case of HIV-positive patients, the dental implant failure rate would not increase due to affective factors (e.g., prophylactic antibiotic treatment, the administration of active antiretroviral therapy, and control of the CD^{4+} T lymphocyte counts). Therefore, these patients have no clinical signs of mobility or infection in this treatment and much more attention should be paid to these patients and they should be treated with controlled oral surgical procedures.

Peer review under responsibility of jourcc

A R T I C L E I N F O R M A T I O N

Article history:
Received 14 March 2020
Received in revised form 28 March 2020
Accepted 30 March 2020

Keywords:
Risk factor
Failure
Dental implants
Osseointegration
Diabetes

Table of contents

1. Introduction....18
2. Dental implants....19
3. Failure of dental implants....19
4. Influencing factors on dental implants failure....19
4.1. Diabetes....19
4.2. HIV-positive....20
4.3. Smoking....20
4.4. Radiotherapy....21
4.5. Osteoporosis....21
5. Conclusions and future insights....22

1. Introduction

One of the restorative techniques practiced today for missing teeth replacement is using dental implants [1-5]. Enhancement of implant design, surgical protocols, and surface characteristics suggest implants as a procedure that is secure and highly predictable. The mean success rate and mean survival rate of implants are 89.7 % and 94.6 %, respectively, after more than 10 years [6].

For patients who suffer from tooth loss, dental implants are a widely utilized option that provides esthetic and functional resolution [7]. However, the associated factors leading to early implant failure have not been

* *Corresponding author: Hiva Nargesi Khoramabadi; E-mail: Hiva.nargesi@yahoo.com*
https://doi.org/10.29252/jcc.2.1.3

documented well. Moreover, it is required to determine the factors that affect the osseointegration establishment to minimize implant failures and maximize the predictability of the procedure [8].

The initial osseointegration and prolonged stability determine success in implant dentistry. Long-term implant stability depends on various factors, including periodontal pathogenic bacteria, implant macrodesign and microdesign, susceptibility to periodontal diseases, and patient systemic factors [9].

Successful osseointegration after placement is the initial factor influencing implant survival [10-15]. Treatment outcome may be affected adversely by any change in this biological process. by restoring and placing an implant into function, bone remodeling would be considered as a critical aspect of implant survival in terms of response to the functional demands placed on the supporting bone and implant restoration. Certain risk factors can be evaluated by the critical dependence on bone metabolism for implant survival [6].

In this study, the major problems and factors associated with dental implant failure as well as high-risk patients whose diseases affect dental implant survival are reviewed.

2. Dental implants

Since Brånemark introduced oral implants in the 1960s, they have been a reliable and optimal restoration option for missing teeth [16-20]. Regarding esthetics function, mastication, and speech function, dental implants are considered as effective oral rehabilitation [21].

There are substantial documented reports about chemical and physical characteristics of implant materials and factors influencing the prognosis of implant therapy and the clinical outcome [9, 22-29].

Implant dentistry includes a prosthetic procedure having a surgical protocol [30, 31]. It must be planned prior to the therapy so that an optimal prosthetic construct is obtained. The bone quality and quantity in different locations [32] and the size of prosthesis affect the position and number of implants required to support prosthesis [33].

Osseointegration provides a stable, long-lasting, and firm connection between the implant and surrounding bone tissue, which is necessary for implant survival. The absence of osseointegration would result in biological failure leading to consequent implant failure [34].

The long-term survival and highly desirable outcomes of dental implant therapy are reported widely in various studies; however, the duration of treatment could be decreased in patients with systemic conditions or a compromised medical status [35]. Additionally, there are a few documents regarding the influence of general health conditions on implant failure rates [34].

3. Failure of dental implants

Mechanical removal of the mobile implant, due to the absence of osseointegration, is the definition of implant failure outcome [36-39].

To obtain the best patient outcomes, dental clinicians should pay attention to the contraindications, precautions, and indications of treatment on a daily basis. Treatment indications generally are considered when patients initially face a complaint or problem. Subsequently, the contraindications and precautions must be considered as balancing elements of the informed consent process and decision-making. The seriousness of special treatment as well as the cases, cause a specific treatment to be inadvisable due to the harm, or serious negative outcome that makes precautions and contraindications be taken into account. Precautions indicate the ability to inhibit or mitigate the adverse impact [40].

Failure at the early stages is caused mostly by the initial phase disruption in which fibrous scar tissue is produced between the surrounding bone and the implant surface. However, failures at later stages are associated with multiple factors such as the prosthetic rehabilitation and microbial environment [34].

Although early failure is prevalent, the successful outcome of implantation after prosthetic loading has been mostly addressed, which limits our understanding of the mechanisms and causes of preloading failures. Sex, age, tobacco use, implant localization, and dimensions, bone volume and quality, systemic diseases, and immune factors, are attributed to early implant failure among other variables [41].

4. Influencing factors on dental implants failure

Although implant treatment is highly successful and predictable, some risk factors may reduce the success rates leading to a higher risk for implant failure for individuals [34]. The outcome for implant restoration is influenced by various conditions such as surgery-related factors (surgical design or surgeon's skill), risk factors related to the patients (systemic habits or diseases, like smoking), and design of implant (shape, surface, or length texture). Researchers have recently concentrated on risk factors related to the patients for the failure of the dental implant due to the considerable advancements in surgical techniques and materials science [35].

A person who has a distinctive mental or physical feature compared to individuals of the same age is considered as a medically compromised patient (MCP). These patients may face a higher medical risk due to the presence of more interactions between implant surgery and their disease [42-48]. Therefore, these patients are required to fill in a medical questionnaire and do some exhaustive medical examination before implant placement, which will be helpful for the estimation of the patient's risk and determination of the specific measures that should be adopted. To define the patient's risk, the system adopted by McCarthy and Malamed and the one proposed by the American Society of Anesthesiologists in 1941 to the dental patient were employed [49].

Buser et al. [35] reported that heavy smoking habits, severe diabetes, and being exposed to irradiation before implantation or after that have led to a significant rise in risks of failure in dental implants. Based on research reports, these conditions could affect the implant survival negatively by interfering with the process of tissue healing or by reducing the susceptibility of patients to other diseases. Fig. 1 the most important risk factors in dental implants.

4.1. Diabetes

Diabetes is a chronic metabolic malfunction that causes hyperglycemia, leading to several complications resulting from macro- and mi-

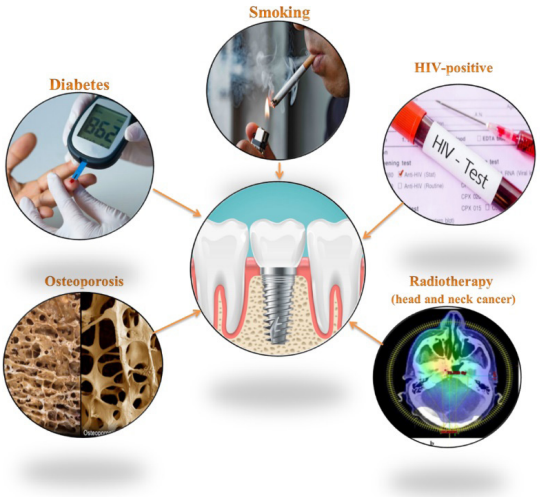

Fig. 1. Factors affecting dental implants.

croangiopathy [50-54]. Diabetes increases tooth loss and frequency of periodontitis, delays wound healing and disrupts the response to infection [46, 55-57]. According to statistics, more than 150 million people were affected by diabetes worldwide in 1980, and the number raised up to 350 million by 2008. Based on recent investigations, oral rehabilitation by dental implant treatment provides diabetic patients with indirect benefits. Patients avoid food that needs more effort to masticate patients after tooth loss, leading to malnutrition with poor metabolic control. The advantages of dental rehabilitation are the improvement of nutrition and metabolic control for patients [6].

In order to make appropriate decisions and refine the therapy procedure for optimizing the outcomes, surgeons should recognize situations that would create higher complication risk for the patient [6].

According to Halimi et al. [58], diabetic patients, particularly type 2 patients, are often elderly people whose dental status usually makes implant specialists ask their physician about the possible contraindications due to diabetes's status. As known, the risk of dental loss and periodontal disease in patients with diabetes (both types of 1 and 2) is high. According to a few studies, success rates of diabetic and non-diabetic subjects are almost equivalent to each other in this case. This result implies good glycemic control, strict oral hygiene, and the expertise of the odontologist at the time of implantation, which requires close collaboration among the different involving health actors.

Juncar et al. [59], performed mandible histological study in patients having type 2 diabetes mellitus for implant rehabilitation. Based on the results, diabetes mellitus is the main factor influencing the metabolic activity of various tissues. In the case of rehabilitation based on prosthetic restorations supported on dental implants, its effect on the jaw bones should be emphasized. The obtained results demonstrated a lower degree of mineralization in the bone, a higher cellular density in the diabetic bone, and the existence of diabetic angiopathy in the mandible taken from the patients.

Almehmadi et al. [60] analyzed population awareness in terms of the effects of diabetes on dental implant therapy in Jeddah, Saudi Arabia. According to the results, diabetes mellitus (DM) causes some problems. These complications that affect dental implant therapy adversely include impaired response to infections, microvascular disease, and delayed wound healing. The main goal of this study was the investigation of the population awareness about the DM impact on dental implant treatment. Based on the study, the awareness level about the relation between diabetes and oral hygiene in dental implant therapy was satisfying. On the other hand, the knowledge about diabetes effects on dental implants is less than adequate, and most of the respondents believed that the only factor that helps dental implant therapy is controlled diabetes.

4.2. HIV-positive

The acquired immunodeficiency syndrome (AIDS) results from infection with HIV leading to increased rates of morbidity and mortality. The infection impairs the immune system, particularly CD^{4+} T-cells, leading to host resistance reduction against various pathogens [61-63]. Moreover, several investigations have proposed a relation between HIV/AIDS and increased risk of complications in oral surgical procedures [42, 64-68]. Such complications may adversely affect implant survival and, consequently, contributing to failures [34].

Elective treatments and procedures are employed for HIV-infected individuals with adequate immune status. However, some factors have been introduced for distinguishing these patients from the general population including age (the majority of them are over 40 years old), chronic inflammation, the need for regular medication, a greater need for medical care, long-term complications of Highly Active Antiretroviral Therapy (HAART), and an increased prevalence of comorbidities [69].

Lemos et al. [34] investigated dental implants' survival in HIV-infected patients. Totally, 328 and 493 implants were placed in 135 normal and 169 HIV-positive patients. The follow-up was done in the mean duration of 47.9 months. Success rates and mean survival at the patient level were reported to be 93.81% and 94.76%, respectively. The average marginal bone loss was 0.99 mm at the implant level and 0.83 mm at the patient level; these rates were 90.37% and 94.53% at the implant level. Therefore, for patients with normal CD4+ cell counts and controlled risk factors, placing dental implants is a suitable way for rehabilitation.

Ata-Ali et al. [69] studied the impact of HIV infection on dental implant osseointegration. They reported that HIV infection does not accelerate the failure rate of the dental implant. The main contributing factors are controlling the CD^{4+} T lymphocyte counts, managing highly active antiretroviral therapy, and prophylactic antibiotic treatment. 38 and 135 implants were placed in 24 normal and 56 HIV-positive patients. Among HIV-positive patients, a single dental implant osseointegration loss was recorded. No clinical signs of infection or mobility were shown in implants, and periotest values revealed a progressive decrease.

Vidal et al. [70] investigated bone augmentation of dental implants in HIV-positive cases under HAART. Based on the results, as long as CD^{4+} T lymphocytes count and plasmatic HIV viral load of the patients are considered as the parameters indicating immune stability, HIV-infected patients who are under control and undergo HAART can be candidates for implant rehabilitation. Maintaining function and esthetics, a long-term stability of hard and soft tissues can be achieved. Nevertheless, more evidence and controlled clinical trials are required to prepare conclusive data for the medical and dental teams.

Escoda et al. [71] studied nine participants and 57 implants. The average age of the patients was 42 years (IQR of ~13 years), and the average follow-up period was 77.5 months. The implant survival and success rates were about 98 % and 68%, respectively. Satisfactory results were achieved in HIV-positive patients with regard to oral rehabilitation with dental implants. Strict maintenance programs have to be implemented to decrease the remarkably high incidence of peri-implant diseases.

4.3. Smoking

Another factor influencing peri-implant bone loss and dental implant survival is smoking [12, 42, 72-76]. According to various studies, smoking has a negative effect on osseointegration [77-83] and its dose-related impact [84].

Among more than 4000 potentially harmful constituents of tobacco products, nicotine is the most important substance [86-90]. Nicotine contributes to the pathogenesis of numerous diseases, mediates the smoking hemodynamic effects, and is the main chemical component causing tobacco addiction. Smokers have a higher number of missing teeth compared to non-smokers. Moreover, gingival recession, attachment loss, and moderate to severe periodontitis are more prevalent in smokers in comparison with non-smokers, revealing their poorer periodontal health [91].

The process of peri-implant bone healing is undermined by cigarette smoking [72, 80, 92-94]. The proliferation of precursor cells that is important for bone healing is inhibited by smoking, which delays the healing process of normal bones. Toxins, including nicotine, hydrogen cyanide, aldehydes, benzenes, nitrosamines, and carbon monoxide, have been reported to affect bone healing processes [95-99].

The effect of cigarette smoking on the early stages of osseointegration in dental implants was studied by Bezerra Ferreira et al. [95]. No osseointegration was observed in two micro-implants placed in smokers, while the newly formed bone (mainly in the non-smokers) indicated early stages of maturation. In addition, around few implants retrieved from smokers marginal bone loss, fibrous tissue and gap were presented. Based on the histometric evaluation, the mean bone to-implant contact (BIC) % increased from 25.9 ± 9.1 for smokers to 39.8 ± 14.2 for non-

smokers. Initial bone tissue response around implant surface topographies that are sandblasted and acid-etched is adversely influenced by cigarette smoking.

D'haese et al. [84] studied smoking habits effect on implant placement outcome using mucosally supported stereolithographic surgical instructions. The dental implant placement accuracy was significantly different among smokers and nonsmokers. In comparison with nonsmokers, supporting mucosal tissues was thicker in smokers, which could explain inaccuracy resulting from reduced stability of the surgical guide or the scanning prosthesis.

Shenava et al. [85] investigated the relation between bone healing process around dental implants and smoking. They reported that smoking had a remarkable influence on implant survival, and smokers should be aware of the negative effects of tobacco. While the amount of tobacco does not exhibit a major impact, the habit duration plays a significant role in implant failure.

Sun et al. [100] reported the effect of heavy smoking on dental implants placed in posterior mandibles of male patients. They placed the dental implants into the partially edentulous posterior mandibles of 16 nonsmokers and 16 heavy smokers. For both smokers and non-smokers, an initial decrease in the implant stability quotient (ISQ) was observed from the ISQ obtained immediately after surgery and after 2 weeks started to increase. By reducing the healing rate, bone healing around dental implants is negatively affected by heavy smoking. The results demonstrated the importance of selecting the right time for applying the implant loading in heavy smokers. Additionally, heavy smoking accelerated the marginal bone loss and the consequent development of dental pockets.

Omran et al. [101] studied the survival short endosseous dental implants rate. It was concluded that the survival time was in the range of 6 to 141 months, with an average time of 47.3 months. The short implants' survival rate was achieved to be 95.77% revealing that it was not statistically remarkable compared to regular implants. Short implants with a high survival rate can be predictably placed for rehabilitation, and the survival rate of these implants is adversely affected by smoking.

4.4. Radiotherapy

More than 550,000 cases of head and neck cancer are recorded annually worldwide. Its survival rate is 50% over 5 years and it is the sixth common cancer site. The survival rate of this cancer has not changed in the past few decades. However, some evidence shows a decrease in mortality rates over the last 20 years. A combination of radiotherapy and surgery are treatment modalities. Radiotherapy may cause a reduction of bone-healing capacity, soft tissues, and fibrosis of blood vessels, xerostomia, irradiation caries, and oral mucositis, and surgery may result in anatomical alterations [102].

Patients having oral cancer are treated by a combination of ablative surgery and radiotherapy. Following radical surgery, the oral rehabilitation of a patient is required. Surgical resection and radiotherapy lead to hard and soft tissue defects in most patients, which results in esthetic deformity and functional disabilities [21].

Because dental implants are placed in the bone that is usually in the irradiation field, implant therapy in oral cancer patients is a challenging issue and leads to an increase in implant failure in irradiated bone [103]. The reason is partly due to progressive fibrosis of soft tissue and vessels caused by radiotherapy, which results in healing capacity decline. Furthermore, the osseointegration of implants is hindered by radiations (osteoradionecrosis) by decreasing bone vascularity [21].

Based on the results obtained by Granstrom et al. [104], irradiated points are prone to tissue necrosis and, consequently, implants loss. Complications such as fungal infections, periodontal disease, and dental caries can be caused by a decreased salivary flow rate in irradiated patients. Cao and Weischer [105], studied the efficiency of dental implants in 27 patients who suffered from oral carcinoma and undergone radiotherapy. Compared to non-irradiated patients, a considerably lower implant survival rate was observed in irradiated patients after approximately two years of follow-up [106].

Claudy et al. [107] studied the effect of time-interval after radiotherapy on the failure of dental implants. They proposed that a minimum waiting period of 6 months after radiotherapy before placing dental implants is not suitable, while the duration over 12 months may be advantageous to healing periods. To install dental implants, clinicians should wait longer than a year after radiotherapy. Higher pooled relative risk (RR) of failure was obtained in patients who installed dental implants in 6 to 12 months post-radiotherapy.

Ettl et al. [108] investigated the effect of neck and head cancer radiotherapy on implant rehabilitation. Results proved that rehabilitation of implant prosthetic in patients suffering from the neck, and head cancer is feasible at a calculable risk. Implant success rates obtained from Albrektsson criteria are greatly lower compared to non-tumor patients. The main causes for failure of the implant, especially for accelerated marginal bone resorption are implant placement in the target area of the irradiation and xerostomia. Placing dental implants outside the target area showed a promising prognosis comparable to those implanted in non-irradiated patients. Implant prosthetic rehabilitation enhances patients' functional quality of life, social integration, and self-confidence in terms of irritation by dry mouth, eating, swallowing, and/or speaking.

Chen et al. [35] investigated different risk factors such as osteoporosis, diabetes, radiotherapy, and smoking for the failure of a dental implant. The analysis supported the insight that radiotherapy and smoking are considered as higher risks of failure in dental implants. They suggested that smoking or radiotherapy before or after implant placement might result in about 35% or 70% higher risk of failure of a dental implant, respectively.

Korfage et al. [109] studied overdentures in patients with oral cancer during 14 years of follow-up. Implant-retained mandibular overdentures showed that oral functioning and prosthetic rehabilitation did not relate to type or number of implants, stage or primary site of the tumor, or the type of reconstruction. Inflammation was not observed in the peri-implant mucosa over time. The number of lost implants was higher in radiotherapy-treated patients (8.5%) compared to the untreated ones (0.5%). Compared to non-treated patients, problems in oral functioning was more in patients who had been radiotherapy-treated, and less satisfaction was reported. Fewer problems were reported in oral functioning by patients having an implant-retained mandibular overdenture in comparison with patients without an overdenture. Since peri-implant health was reasonable in patients with mandibular overdentures and oral functioning enhanced significantly, the initial placement of an implant should be considered as a routine procedure in the surgical planning implemented for patients suffering from oral cancer.

Patients with oral cancer who had been treated by radiotherapy and surgery were studied by Pompa et al. [21] in terms of survival of dental implants. Results showed that the location and position of the implants had an effect on implant loss. Furthermore, radiotherapy considerably influenced implant survival. When the implant was loaded at least 6 months after placement, considerably better outcomes were observed. According to the study, the best chance of implant stability, osseointegration, and, consequently, effective dental rehabilitation can be achieved by a delayed loading protocol.

4.5. Osteoporosis

A very common skeletal disease in human is osteoporosis, which is determined by the low density of bone tissues [110-115]. A constant reduction in bone quantity and volume results from imbalances in bone

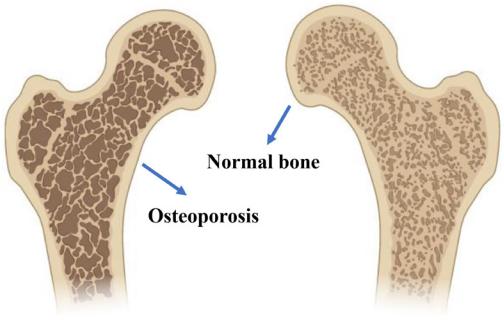

Fig. 2. Comparison of normal bone and osteoporosis.

remodeling [116]. Fig. 2 depicts the normal bone and osteoporosis.

Osteoporosis that is highly prevalent in the aged population has detrimental impacts on dental implant therapy; the low bone mineral density and alveolar ridge atrophy, resulting from osteoporosis can deteriorate bone quality and quantity in implant location [35].

According to the latest estimations, osteoporosis is expected to influence 200 million women around the world, among which two-thirds aged 90 years, two-fifths aged 80, one-fifth aged 70, and one-tenth aged 60 [117]. Primary osteoporosis is senile and postmenopausal. Senile osteoporosis appears at older ages and is caused by a reduction in bone mass, while postmenopausal osteoporosis occurrs due to bone loss acceleration caused by low levels of oestrogen [116].

Apart from the surgical procedure and properties of the implant, osseointegration can be affected by patient dependent variables altering the bone quantity and quality. Hence, osteoporosis that causes the reduction of the bone mass and strength, decreases in the regenerative capacity of bone, and changes in the microstructure that is regarded as a risk factor for dental implants. Nevertheless, there is no strong evidence that shows differences in the survival of patients with osteoporosis and healthy individuals. Thus, the disease could not be considered as a contraindication for placing implants. Unfortunately, the use of bisphosphonates (BP), especially parenteral BPs, which is the most commonly utilized pharmacologic agents for osteoporosis treatment, leads to the acceleration of problems related to implant osseointegration [117].

Niedermaier et al. [118] also evaluated survival rates of implant-supported dentures in osteoporosis patients for up to 7 years. Although the results showed a higher level of implant failure in osteoporosis patients during 7 years of followed up, the researchers investigated only seven patients with such conditions. They mentioned that two of the failures were related to a patient who was being treated with oral bisphosphonates. However, the relation between the use of bisphosphonates and implant failure is still controversial.

Alsaadi et al. [119], studied the influence of systemic and local factors on the failures in oral implant, up to abutment connection. A positive relation between osteoporosis and osseointegrated implant failure was reported, and also higher implant failure rates were observed in patients who smoke, patients with lower bone quality, patients with implants placed in the posterior region, and individual suffering from Crohn's disease, and the ones with short and wide implants.

Liu et al. [120] reported that the combined use of silicon and gallium improve osseointegration of the dental implant in osteoporosis patients. Based on the study, gallium could directly augment bone mass, inhibit bone calcium release, and prevent bone osteolysis. Bone anabolic effects are seen in silicon that acts as a necessary modulator in bone formation. They proposed that their hypothesis could be beneficial to osteoporotic patients by improving the success rate of dental implants.

5. Conclusions and future insights

In the present study, the impact of different risk factors including osteoporosis, diabetes, smoking, radiotherapy in head and neck on dental implant failure has been reviewed. Due to the adverse influence on osseointegration, osteoporosis, radiotherapy, and smoking are considered as higher risk factors for dental implant failure. Additionally, taking some drugs such as bisphosphonates that are used for osteoporosis treatment can cause some complications in osseointegration. Heavy smoking has an adverse impact on the healing of bone surrounding dental implants through the reduction of healing speed. In addition, the target area of radiotherapy is susceptible to marginal bone resorption leading to implant failure. However, diabetes has lower risk factors (i.e., complications compromise the healing of soft tissues, periodontitis, tooth loss, delayed wound healing, and impaired response to infection, etc.). Overall, additional insight for implementing dental implants through controlled and predictable treatment procedures should be provided for clinical dentists.

Coatings are of great importance in medical applications and offer various advantages in extensive fields. Hence, a special coating can be developed to reduce the possibility, and risk factors contributing to dental implant failure such as osteoporosis, radiotherapy, smoking, etc. that are influenced by some external factors including chemical materials, radio waves, and effective drugs. Considering the lack of individual risk-isolated research with high quality in terms of osteoporosis and diabetes, there is a need for further well-designed investigations, with precise control of confounding parameters in future studies.

REFERENCES

[1] H. Mously, B. Badeeb, N. Bahbishi, W. Mzain, G. Naguib, M. Hamed, Knowledge and attitude toward replacing missing teeth with dental implants among the Saudi population, journal of orthodontic science 9(1) (2020) 5-5.

[2] A. Solderer, A. Al-Jazrawi, P. Sahrmann, R. Jung, T. Attin, P.R. Schmidlin, Removal of failed dental implants revisited: Questions and answers, Clinical and Experimental Dental Research 5(6) (2019) 712-724.

[3] M. Roy, L. Loutan, G. Garavaglia, D. Hashim, Removal of osseointegrated dental implants: a systematic review of explantation techniques, Clinical Oral Investigations 24(1) (2020) 47-60.

[4] C. Machuca, M.V. Vettore, P.G. Robinson, How peoples' ratings of dental implant treatment change over time?, Quality of Life Research (2020).

[5] P. Vasamsetty, T. Pss, D. Kukkala, M. Singamshetty, S. Gajula, 3D printing in dentistry – Exploring the new horizons, Materials Today: Proceedings (2020).

[6] H. Naujokat, B. Kunzendorf, J. Wiltfang, Dental implants and diabetes mellitus—a systematic review, International journal of implant dentistry 2(1) (2016) 5.

[7] N. Pranno, G. La Monaca, A. Polimeni, M.S. Sarto, D. Uccelletti, E. Bruni, M.P. Cristalli, D. Cavallini, I. Vozza, Antibacterial Activity against Staphylococcus Aureus of Titanium Surfaces Coated with Graphene Nanoplatelets to Prevent Peri-Implant Diseases. An In-Vitro Pilot Study, International Journal of Environmental Research and Public Health 17(5) (2020) 1568.

[8] M.V. Olmedo-Gaya, F.J. Manzano-Moreno, E. Cañaveral-Cavero, J. de Dios Luna-del Castillo, M. Vallecillo-Capilla, Risk factors associated with early implant failure: A 5-year retrospective clinical study, The Journal of prosthetic dentistry 115(2) (2016) 150-155.

[9] J. Yazdani, E. Ahmadian, S. Sharifi, S. Shahi, S.M. Dizaj, A short view on nanohydroxyapatite as coating of dental implants, Biomedicine & Pharmacotherapy 105 (2018) 553-557.

[10] X.-y. Qi, L. Sui, W.-q. Liu, Dental Implant and Oral Diseases, in: Q. Yuan (Ed.), Dental Implant Treatment in Medically Compromised Patients, Springer International Publishing, Cham, 2020, pp. 185-209.

[11] G.C. Boven, H.J.A. Meijer, A. Vissink, G.M. Raghoebar, Maxillary implant overdentures retained by use of bars or locator attachments: 1-year findings from a randomized controlled trial, Journal of Prosthodontic Research 64(1) (2020) 26-33.

[12] A. Bezdjian, Z. Verzani, H.G.X.M. Thomeer, B. Willie, S.J. Daniel, Smoking as a risk factor for spontaneous bone anchored hearing implant extrusion: A case report and review of literature, Otolaryngology Case Reports 14 (2020) 100140.

[13] J.-J. Kim, J.-H. Lee, J.C. Kim, J.-B. Lee, I.-S.L. Yeo, Biological Responses to the Transitional Area of Dental Implants: Material- and Structure-Dependent Responses of Peri-Implant Tissue to Abutments, Materials 13(1) (2019) 72.
[14] A. Alghamdi, K. Al-Motari, C. Sundar, J.A. Jansen, H. Alghamdi, Chapter 2 - Dental implants treatment: Clinical indications, in: H. Alghamdi, J. Jansen (Eds.), Dental Implants and Bone Grafts, Woodhead Publishing2020, pp. 23-42.
[15] M. Hou, R.S.B. Lee, Z. Du, S.M. Hamlet, C. Vaquette, S. Ivanovski, The influence of high-dose systemic zoledronate administration on osseointegration of implants with different surface topography, Journal of Periodontal Research 54(6) (2019) 633-643.
[16] S. Mohammadpour, S. Khorramymehr, Comparing one-and two-piece dental abutments under dynamic loading: A 3-D finite element analysis.
[17] A. TV, SIGN IN/REGISTER, Compendium (2020).
[18] M. Assery, A 22-Year Follow Up of Immediate Implant Placement without Bone Augmentation: A Case Series Study, Journal of Prosthodontics 29(2) (2020) 101-106.
[19] Z.M. Al-Sadah, M.S. AlShakhas, Osseous Integration After Exenteration, in: T.E. Johnson (Ed.), Anophthalmia : The Expert's Guide to Medical and Surgical Management, Springer International Publishing, Cham, 2020, pp. 107-126.
[20] B.R. Chrcanovic, J. Kisch, T. Albrektsson, A. Wennerberg, A retrospective study on clinical and radiological outcomes of oral implants in patients followed up for a minimum of 20 years, Clinical Implant Dentistry and Related Research 20(2) (2018) 199-207.
[21] G. Pompa, M. Saccucci, G. Di Carlo, E. Brauner, V. Valentini, S. Di Carlo, T. Gentile, G. Guarino, A. Polimeni, Survival of dental implants in patients with oral cancer treated by surgery and radiotherapy: a retrospective study, BMC Oral Health 15(1) (2015) 5.
[22] X. Wen, R. Liu, G. Li, M. Deng, L. Liu, X.-T. Zeng, X. Nie, History of periodontitis as a risk factor for long-term survival of dental implants: a meta-analysis, Int J Oral Maxillofac Implants 29(6) (2014) 1271-80.
[23] Z. Goudarzi, N. Parvin, F. Sharifianjazi, Formation of hydroxyapatite on surface of SiO2– P2O5–CaO–SrO–ZnO bioactive glass synthesized through sol-gel route, Ceramics International 45(15) (2019) 19323-19330.
[24] M.S.N. Shahrbabak, F. Sharifianjazi, D. Rahban, A. Salimi, A Comparative Investigation on Bioactivity and Antibacterial Properties of Sol-Gel Derived 58S Bioactive Glass Substituted by Ag and Zn, Silicon 11(6) (2019) 2741-2751.
[25] S. Rahimi, F. SharifianJazi, A. Esmaeilkhanian, M. Moradi, A.H. Safi Samghabadi, Effect of SiO_2 content on Y-TZP/Al_2O_3 ceramic-nanocomposite properties as potential dental applications, Ceramics International (2020).
[26] A.R. Rouhani, A.H. Esmaeil-Khanian, F. Davar, S. Hasani, The effect of agarose content on the morphology, phase evolution, and magnetic properties of $CoFe_2O_4$ nanoparticles prepared by sol-gel autocombustion method, International Journal of Applied Ceramic Technology 15(3) (2018) 758-765.
[27] M. Alizadeh, M.H. Paydar, F. Sharifian Jazi, Structural evaluation and mechanical properties of nanostructured Al/B4C composite fabricated by ARB process, Composites Part B: Engineering 44(1) (2013) 339-343.
[28] K. Shirvanimoghaddam, S.U. Hamim, M. Karbalaei Akbari, S.M. Fakhrhoseini, H. Khayyam, A.H. Pakseresht, E. Ghasali, M. Zabet, K.S. Munir, S. Jia, J.P. Davim, M. Naebe, Carbon fiber reinforced metal matrix composites: Fabrication processes and properties, Composites Part A: Applied Science and Manufacturing 92 (2017) 70-96.
[29] M. Shahedi Asl, I. Farahbakhsh, B. Nayebi, Characteristics of multi-walled carbon nanotube toughened ZrB2–SiC ceramic composite prepared by hot pressing, Ceramics International 42(1, Part B) (2016) 1950-1958.
[30] A. Klinge, D. Khalil, B. Klinge, B. Lund, A. Naimi-Akbar, S. Tranaeus, M. Hultin, Prophylactic antibiotics for staged bone augmentation in implant dentistry, Acta Odontologica Scandinavica 78(1) (2020) 64-73.
[31] R. Lieber, N. Pandis, C.M. Faggion Jr, Reporting and handling of incomplete outcome data in implant dentistry: A survey of randomized clinical trials, Journal of Clinical Periodontology 47(2) (2020) 257-266.
[32] A. Esmaeilkhanian, F. Sharifianjazi, A. Abouchenari, A. Rouhani, N. Parvin, M. Irani, Synthesis and Characterization of Natural Nano-hydroxyapatite Derived from Turkey Femur-Bone Waste, Applied Biochemistry and Biotechnology 189(3) (2019) 919-932.
[33] J. Carpentieri, G. Greenstein, J. Cavallaro, Hierarchy of restorative space required for different types of dental implant prostheses, The Journal of the American Dental Association 150(8) (2019) 695-706.
[34] C.A.A. Lemos, F.R. Verri, R.S. Cruz, J.F. Santiago Júnior, L.P. Faverani, E.P. Pellizzer, Survival of dental implants placed in HIV-positive patients: a systematic review, International Journal of Oral and Maxillofacial Surgery 47(10) (2018) 1336-1342.
[35] H. Chen, N. Liu, X. Xu, X. Qu, E. Lu, Smoking, radiotherapy, diabetes and osteoporosis as risk factors for dental implant failure: a meta-analysis, PloS one 8(8) (2013).
[36] E. Madeley, The use of MRFA as an adjunct to conventional clinical examination following peri-implantitis treatment. A 12 month follow-up, Trinity College Dublin, 2020.
[37] F. Rodríguez Sánchez, C. Rodríguez Andrés, I. Arteagoitia, Which antibiotic regimen prevents implant failure or infection after dental implant surgery? A systematic review and meta-analysis, Journal of Cranio-Maxillofacial Surgery 46(4) (2018) 722-736.
[38] A. Puisys, M. Schlee, T. Linkevicius, P. Petrakakis, A. Tjaden, Photo-activated implants: a triple-blinded, split-mouth, randomized controlled clinical trial on the resistance to removal torque at various healing intervals, Clinical Oral Investigations (2019).
[39] S. Sprio, L. Preti, M. Montesi, S. Panseri, A. Adamiano, A. Vandini, N.M. Pugno, A. Tampieri, Surface Phenomena Enhancing the Antibacterial and Osteogenic Ability of Nanocrystalline Hydroxyapatite, Activated by Multiple-Ion Doping, ACS Biomaterials Science & Engineering 5(11) (2019) 5947-5959.
[40] A.S. Kullar, C.S. Miller, Are There Contraindications for Placing Dental Implants?, Dental Clinics 63(3) (2019) 345-362.
[41] A. Monje, G. Alcoforado, M. Padial-Molina, F. Suarez, G.H. Lin, H.L. Wang, Generalized aggressive periodontitis as a risk factor for dental implant failure: A systematic review and meta-analysis, Journal of periodontology 85(10) (2014) 1398-1407.
[42] Y. Huang, P. Gong, The Role of Substance Abuse in Dental Implant Treatment, in: Q. Yuan (Ed.), Dental Implant Treatment in Medically Compromised Patients, Springer International Publishing, Cham, 2020, pp. 21-35.
[43] T.V. Sparrow, D.W. Dodington, J.L. Yumol, P.C. Fritz, W.E. Ward, Higher intakes of flavonoids are associated with lower salivary IL-1β and maintenance of periodontal health 3–4 years after scaling and root planing, Journal of Clinical Periodontology n/a(n/a) (2020).
[44] X.-b. Duan, K. Doi, Q. Yuan, S.-w. Zhang, Other Conditions Affecting Dental Implant Treatment, in: Q. Yuan (Ed.), Dental Implant Treatment in Medically Compromised Patients, Springer International Publishing, Cham, 2020, pp. 211-253.
[45] C. Hsiao, H. Qing, Drug-Induced Disorders and Dental Implant Treatment, in: Q. Yuan (Ed.), Dental Implant Treatment in Medically Compromised Patients, Springer International Publishing, Cham, 2020, pp. 149-183.
[46] Y.-s. Wu, Y. Wang, Q. Yuan, Dental Implant Treatment for Diabetic Patients, in: Q. Yuan (Ed.), Dental Implant Treatment in Medically Compromised Patients, Springer International Publishing, Cham, 2020, pp. 103-127.
[47] J. Collen, C. Lettieri, E. Wickwire, A. Holley, Obstructive sleep apnea and cardiovascular disease, a story of confounders!, Sleep and Breathing (2020).
[48] C.R. Ellis, G.G. Jackson, When to Refer Patients for Left Atrial Appendage Closure, Cardiac Electrophysiology Clinics 12(1) (2020) 29-37.
[49] R. Gómez-de Diego, Indications and contraindications of dental implants in medically compromised patients: update, Medicina oral, patologia oral y cirugia bucal 19(5) (2014) e483.
[50] E. van Duinkerken, A.M.A. Brands, Neurocognitive Functioning in Type 1 and Type 2 Diabetes Mellitus, in: A.M. Delamater, D.G. Marrero (Eds.), Behavioral Diabetes: Social Ecological Perspectives for Pediatric and Adult Populations, Springer International Publishing, Cham, 2020, pp. 365-380.
[51] J. Dissemond, Peripheral Occlusive Arterial Disease, in: G. Plewig, L. French, T. Ruzicka, R. Kaufmann, M. Hertl (Eds.), Braun-Falco´s Dermatology, Springer Berlin Heidelberg, Berlin, Heidelberg, 2020, pp. 1-10.
[52] M. Karvani, P. Simos, S. Stavrakaki, D. Kapoukranidou, Neurocognitive impairment in type 2 diabetes mellitus, Hormones 18(4) (2019) 523-534.
[53] G. Sharma, M.U. Ashhar, V. Aeri, D.P. Katare, Development and characterization of late-stage diabetes mellitus and -associated vascular complications, Life Sciences 216 (2019) 295-304.
[54] S. Kolahian, V. Leiss, B. Nürnberg, Diabetic lung disease: fact or fiction?, Reviews in Endocrine and Metabolic Disorders 20(3) (2019) 303-319.
[55] D. Cabanillas-Balsera, J. Martín-González, P. Montero-Miralles, B. Sánchez-Domínguez, M.C. Jiménez-Sánchez, J.J. Segura-Egea, Association between diabetes and nonretention of root filled teeth: a systematic review and meta-analysis, International Endodontic Journal 52(3) (2019) 297-306.
[56] V. Nagendrababu, J.J. Segura-Egea, A.F. Fouad, S.J. Pulikkotil, P.M.H. Dummer, Association between diabetes and the outcome of root canal treatment in adults: an umbrella review, International Endodontic Journal n/a(n/a) (2019).
[57] A. Ghadiri-Anari, N. Hazar, M. Jalili Sadrabad, S. Kharazmi, K. Kheirollahi, A. Mohiti, N. Namiranian, Comparing the frequency of some oral lesions in prediabetic and healthy individuals: Is there any difference?, International Journal of Preventive Medicine 10(1) (2019) 177-177.

[58] S. Halimi, J.P. Brun, Peut-on poser des implants dentaires chez les patients diabétiques ?, Médecine des Maladies Métaboliques 12(4) (2018) 333-339.
[59] D. Popa, R.I. Juncar, M. Juncar, Histological Analysis of the Mandible in Patients with Type 2 Diabetes Mellitus for Implant-Prosthetic Rehabilitation. A Pilot Case-Control Study, American Scientific Research Journal for Engineering, Technology, and Sciences (ASRJETS) 61(1) (2019) 54-60.
[60] A.H. Almehmadi, Awareness of population regarding the effects of diabetes on dental implant treatment in Jeddah, Saudi Arabia, Heliyon 5(9) (2019) e02407.
[61] P. Barrionuevo, G.H. Giambartolomei, Inhibition of antigen presentation by Brucella: many more than many ways, Microbes and Infection 21(3) (2019) 136-142.
[62] Y. Suzuki, The immune system utilizes two distinct effector mechanisms of T cells depending on two different life cycle stages of a single pathogen, Toxoplasma gondii, to control its cerebral infection, Parasitology International 76 (2020) 102030.
[63] K.B. Arnold, G.L. Szeto, G. Alter, D.J. Irvine, D.A. Lauffenburger, CD4<-sup>+</sup> T cell–dependent and CD4⁺ T cell–independent cytokine-chemokine network changes in the immune responses of HIV-infected individuals, Science Signaling 8(399) (2015) ra104.
[64] M.T. Goupil, C. Niekrash, Surgical complications in dentistry, Clinical Dentistry Reviewed 4(1) (2020) 3.
[65] D. Lauritano, G. Moreo, L. Oberti, A. Lucchese, D. Di Stasio, M. Conese, F. Carinci, Oral Manifestations in HIV-Positive Children: A Systematic Review, Pathogens 9(2) (2020) 88.
[66] L.T. Odono, C.M. Brady, M. Urata, 1.14 - Mandible Fractures, in: A.H. Dorafshar, E.D. Rodriguez, P.N. Manson (Eds.), Facial Trauma Surgery, Content Repository Only!, London, 2020, pp. 168-185.
[67] A. Bonito, L. Palton, D. Shugars, K. Lohr, J. Nelson, J. Bader, A. Jackman, Management of dental patients who are HIV-positive: complications, (2019).
[68] M.C. Sloniak, S.R.B. Todero, L.A. Lyra, E.B. Fontana, P.S. Batista, A.A.S. de Lima, Dental extraction in patients with HIV/AIDS: report of two cases, RSBO 16(1) (2019) 51-56.
[69] J. Ata-Ali, F. Ata-Ali, N. Di-Benedetto, L. Bagán, J.-V. Bagán, Does HIV infection have an impact upon dental implant osseointegration? A systematic review, Medicina oral, patologia oral y cirugia bucal 20(3) (2015) e347.
[70] F. Vidal, R. Vidal, J. Bochnia, R.C. de Souza, L.S. Gonçalves, Dental implants and bone augmentation in HIV-infected patients under HAART: Case report and review of the literature, Special Care in Dentistry 37(3) (2017) 150-155.
[71] C. Gay-Escoda, D. Pérez-Álvarez, O. Camps-Font, R. Figueiredo, Long-term outcomes of oral rehabilitation with dental implants in HIV-positive patients: A retrospective case series, Medicina oral, patologia oral y cirugia bucal 21(3) (2016) e385.
[72] R. Naseri, J. Yaghini, A. Feizi, Levels of smoking and dental implants failure: A systematic review and meta-analysis, Journal of Clinical Periodontology n/a(n/a) (2020).
[73] S.Ş. Güven, F. Cabbar, N. Güler, Local and systemic factors associated with marginal bone loss around dental implants: a retrospective clinical study, Quintessence International 51(2) (2020).
[74] F. Zuffetti, L. Testarelli, P. Bertani, S. Vassilopoulos, T. Testori, R. Guarnieri, A Retrospective Multicenter Study on Short Implants With a Laser-Microgrooved Collar (≤7.5 mm) in Posterior Edentulous Areas: Radiographic and Clinical Results up to 3 to 5 Years, Journal of Oral and Maxillofacial Surgery 78(2) (2020) 217-227.
[75] S. Attia, C. Narberhaus, H. Schaaf, P. Streckbein, J. Pons-Kühnemann, C. Schmitt, F.W. Neukam, H.-P. Howaldt, S. Böttger, Long-Term Influence of Platelet-Rich Plasma (PRP) on Dental Implants after Maxillary Augmentation: Implant Survival and Success Rates, Journal of Clinical Medicine 9(2) (2020) 391.
[76] S. Uppala, A.S. Parihar, V. Modipalle, L. Manual, V.M. Oommen, P. Karadiguddi, P. Gupta, Crestal bone loss around dental implants after implantation of Tricalcium phosphate and Platelet-Rich Plasma: A comparative study, Journal of Family Medicine and Primary Care 9(1) (2020) 229.
[77] J.V.d.S. Canellas, R.C. da Costa, R.C. Breves, G.P. de Oliveira, C.M.d.S. Figueredo, R.G. Fischer, A.A. Thole, P.J.D.A. Medeiros, F.G. Ritto, Tomographic and histomorphometric evaluation of socket healing after tooth extraction using leukocyte- and platelet-rich fibrin: A randomized, single-blind, controlled clinical trial, Journal of Cranio-Maxillofacial Surgery 48(1) (2020) 24-32.
[78] L. Van Doorne, L. De Kock, A. De Moor, R. Shtino, E. Bronkhorst, G. Meijer, H. De Bruyn, Flaplessly placed 2.4-mm mini-implants for maxillary overdentures: a prospective multicentre clinical cohort study, International Journal of Oral and Maxillofacial Surgery 49(3) (2020) 384-391.
[79] A. Truschnegg, P. Rugani, B. Kirnbauer, L. Kqiku, N. Jakse, R. Kirmeier, Long-term Follow-up for Apical Microsurgery of Teeth with Core and Post Restorations, Journal of Endodontics 46(2) (2020) 178-183.
[80] X.-f. Zheng, A.-c. Mo, Immune System-Related Diseases and Dental Implant Treatment, in: Q. Yuan (Ed.), Dental Implant Treatment in Medically Compromised Patients, Springer International Publishing, Cham, 2020, pp. 129-147.
[81] D. Zhao, Q.-c. Xiong, S. Ono, Y. Ninomiya, M. Takechi, Organ Diseases and Dental Implant Treatment, in: Q. Yuan (Ed.), Dental Implant Treatment in Medically Compromised Patients, Springer International Publishing, Cham, 2020, pp. 37-72.
[82] A. Parihar, S. Madhuri, R. Devanna, G. Sharma, R. Singh, K. Shetty, Assessment of failure rate of dental implants in medically compromised patients, Journal of Family Medicine and Primary Care 9(2) (2020) 883-885.
[83] J. Nazeer, R. Singh, P. Suri, C. Mouneshkumar, S. Bhardwaj, M. Iqubal, D. , Evaluation of marginal bone loss around dental implants in cigarette smokers and nonsmokers. A comparative study, Journal of Family Medicine and Primary Care 9(2) (2020) 729-734.
[84] J. D'Haese, H. De Bruyn, Effect of Smoking Habits on Accuracy of Implant Placement Using Mucosally Supported Stereolithographic Surgical Guides, Clinical Implant Dentistry and Related Research 15(3) (2013) 402-411.
[85] S. Shenava, P. Singh, C.S. Babu, V. Kumar, B. Jyoti, S. Sharma, Co-relation between smoking and bone healing around dental impants: A clinical study, Journal of International Oral Health 8(2) (2016) 199.
[86] J.D. Chetwood, P. Garg, P. Finch, M. Gordon, Systematic review: the etiology of esophageal squamous cell carcinoma in low-income settings, Expert Review of Gastroenterology & Hepatology 13(1) (2019) 71-88.
[87] I.E. Williams, D.R. Betterton, P.T. Davis, T.P. Ronaldson, Transporter-Mediated Delivery of Small Molecule Drugs to the Brain: A Critical Mechanism That Can Advance Therapeutic Development for Ischemic Stroke, Pharmaceutics 12(2) (2020).
[88] E.G. Xu, W.H. Richardot, S. Li, L. Buruaem, H.-H. Wei, N.G. Dodder, S.F. Schick, T. Novotny, D. Schlenk, R.M. Gersberg, E. Hoh, Assessing Toxicity and in Vitro Bioactivity of Smoked Cigarette Leachate Using Cell-Based Assays and Chemical Analysis, Chemical Research in Toxicology 32(8) (2019) 1670-1679.
[89] H.A. Alhazmi, A. Khalid, S. Sultana, S.I. Abdelwahab, W. Ahsan, M.E. Oraiby, M.A. Bratty, Determination of Phytocomponents of Twenty-one Varieties of Smokeless Tobacco using Gas Chromatography-Mass Spectroscopy (GC-MS), South African Journal of Chemistry 72 (2019) 47-54.
[90] D.H. Nguyen, Y.-C. Liao, Y.-S. Ho, L.-C. Chen, H.-W. Chang, T.-C. Cheng, D. Liu, W.-R. Lee, S.-C. Shen, C.-H. Wu, S.-H. Tu, The α9 Nicotinic Acetylcholine Receptor Mediates Nicotine-Induced PD-L1 Expression and Regulates Melanoma Cell Proliferation and Migration, Cancers 11(12) (2019).
[91] B.R. Chrcanovic, T. Albrektsson, A. Wennerberg, Smoking and dental implants: A systematic review and meta-analysis, Journal of Dentistry 43(5) (2015) 487-498.
[92] J. Meyle, P. Casado, I. Fourmousis, P. Kumar, M. Quirynen, G.E. Salvi, General genetic and acquired risk factors, and prevalence of peri-implant diseases – Consensus report of working group 1, International Dental Journal 69(S2) (2019) 3-6.
[93] F.V. Ribeiro, S.P. Pimentel, M.G. Corrêa, J.P. Bortoli, M.R. Messora, M.Z. Casati, Resveratrol reverses the negative effect of smoking on peri-implant repair in the tibia of rats, Clinical Oral Implants Research 30(1) (2019) 1-10.
[94] L. Xiang, Y.-q. Chen, Q. Yuan, Medically Compromised Patients: A Biological and Social Challenge, in: Q. Yuan (Ed.), Dental Implant Treatment in Medically Compromised Patients, Springer International Publishing, Cham, 2020, pp. 11-20.
[95] J.D. Bezerra Ferreira, J.A. Rodrigues, A. Piattelli, G. Iezzi, S.A. Gehrke, J.A. Shibli, The effect of cigarette smoking on early osseointegration of dental implants: a prospective controlled study, Clinical Oral Implants Research 27(9) (2016) 1123-1128.
[96] J.M.d. Campos, A.J. Prati, F.R. Cirano, S.P. Pimentel, G.P. Pastore, V.G. Pecorari, F.V. Ribeiro, M.Z. Casati, R.C.V. Casarin, Smoking Modulates Gene Expression of Type I Collagen, Bone Sialoprotein, and Osteocalcin in Human Alveolar Bone, Journal of Oral and Maxillofacial Surgery 73(11) (2015) 2123-2131.
[97] K. Hemani, D. Ganapathy, V. Ramanathan, Factors contributing to peri-implantitis-A practitioner's perspective, Drug Invention Today 12(5) (2019).
[98] G. Iezzi, A. Piattelli, A. Scarano, M. Degidi, J.A. Shibli, C. Mangano, V. Perrotti, Histological Evaluation of Early and Immediately Loaded Implants Retrieved from Human Jaws, in: M. Peñarrocha-Diago, U. Covani, L. Cuadrado (Eds.), Atlas of Immediate Dental Implant Loading, Springer International Publishing, Cham, 2019, pp. 29-47.
[99] L. Romito, Perioperative Management of the Tobacco User, in: E.M. Ferneini, J.D. Bennett (Eds.), Perioperative Assessment of the Maxillofacial Surgery Patient: Problem-based Patient Management, Springer International Publishing, Cham, 2018, pp. 345-358.

[100] C. Sun, J. Zhao, C. Jianghao, T. Hong, Effect of heavy smoking on dental implants placed in male patients posterior mandibles: A prospective clinical study, Journal of Oral Implantology 42(6) (2016) 477-483.
[101] M.T.A. Omran, D.D. Miley, D.E. McLeod, M.N. Garcia, Retrospective Assessment of Survival Rate for Short Endosseous Dental Implants, Implant Dentistry 24(2) (2015) 185-191.
[102] B. Shugaa-Addin, H.-M. Al-Shamiri, S. Al-Maweri, B. Tarakji, The effect of radiotherapy on survival of dental implants in head and neck cancer patients, Journal of clinical and experimental dentistry 8(2) (2016) e194.
[103] M. Mancha de la Plata, L.N. Gías, P.M. Díez, M. Muñoz-Guerra, R. González-García, G.-Y.C. Lee, S. Castrejón-Castrejón, F.J. Rodríguez-Campo, Osseointegrated Implant Rehabilitation of Irradiated Oral Cancer Patients, Journal of Oral and Maxillofacial Surgery 70(5) (2012) 1052-1063.
[104] G. Granström, M. Jacobsson, A. Tjellström, Titanium implants in irradiated tissue: benefits from hyperbaric oxygen, International Journal of Oral & Maxillofacial Implants 7(1) (1992).
[105] C. Yingguang, T. Weischer, Comparison of maxillary implant-supported prosthesis in irradiated and non-irradiated patients, Journal of Huazhong University of Science and Technology [Medical Sciences] 23(2) (2003) 209-212.
[106] F. Javed, K. Al-Hezaimi, A. Al-Rasheed, K. Almas, G.E. Romanos, Implant survival rate after oral cancer therapy: A review, Oral Oncology 46(12) (2010) 854-859.
[107] M.P. Claudy, S.A.Q. Miguens Jr, R.K. Celeste, R. Camara Parente, P.A.G. Hernandez, A.N. da Silva Jr, Time Interval after Radiotherapy and Dental Implant Failure: Systematic Review of Observational Studies and Meta-Analysis, Clinical Implant Dentistry and Related Research 17(2) (2015) 402-411.
[108] T. Ettl, J. Weindler, M. Gosau, S. Müller, M. Hautmann, F. Zeman, M. Koller, D. Papavasileiou, R. Bürgers, O. Driemel, I. Schneider, C. Klingelhöffer, J. Meier, U. Wahlmann, T.E. Reichert, Impact of radiotherapy on implant-based prosthetic rehabilitation in patients with head and neck cancer: A prospective observational study on implant survival and quality of life—Preliminary results, Journal of Cranio-Maxillofacial Surgery 44(9) (2016) 1453-1462.
[109] A. Korfage, G.M. Raghoebar, J.J.R.H. Slater, J.L.N. Roodenburg, M.J.H. Witjes, A. Vissink, H. Reintsema, Overdentures on primary mandibular implants in patients with oral cancer: a follow-up study over 14 years, British Journal of Oral and Maxillofacial Surgery 52(9) (2014) 798-805.
[110] I. Macías, N. Alcorta-Sevillano, I.C. Rodríguez, A. Infante, Osteoporosis and the Potential of Cell-Based Therapeutic Strategies, International Journal of Molecular Sciences 21(5) (2020).
[111] Y.-c. Guo, Q. Yuan, Bone Diseases and Dental Implant Treatment, in: Q. Yuan (Ed.), Dental Implant Treatment in Medically Compromised Patients, Springer International Publishing, Cham, 2020, pp. 73-101.
[112] Y. Zhou, C. Xu, W. Zhu, H. He, L. Zhang, B. Tang, Y. Zeng, Q. Tian, H.-W. Deng, Long Noncoding RNA Analyses for Osteoporosis Risk in Caucasian Women, Calcified Tissue International 105(2) (2019) 183-192.
[113] T. Gupta, N. Das, S. Imran, The Prevention and Therapy of Osteoporosis: A Review on Emerging Trends from Hormonal Therapy to Synthetic Drugs to Plant-Based Bioactives, Journal of Dietary Supplements 16(6) (2019) 699-713.
[114] N.N. Younes, Genome-Wide Association Study (Gwas) To Uncover Genetic Risk Factors Associated With Low Bone Mineral Density And Osteoporosis In Qatar Population, 2019.
[115] P. Locantore, V. Del Gatto, S. Gelli, R.M. Paragliola, A. Pontecorvi, The Interplay between Immune System and Microbiota in Osteoporosis, Mediators of Inflammation 2020 (2020).
[116] F.C.F.L. de Medeiros, G.A.H. Kudo, B.G. Leme, P.P. Saraiva, F.R. Verri, H.M. Honório, E.P. Pellizzer, J.F. Santiago Junior, Dental implants in patients with osteoporosis: a systematic review with meta-analysis, International Journal of Oral and Maxillofacial Surgery 47(4) (2018) 480-491.
[117] A.Y. Alqutaibi, I.A.-E. Radi, No Clear Evidence Regarding the Effect of Osteoporosis on Dental Implant Failure, Journal of Evidence Based Dental Practice 16(2) (2016) 124-126.
[118] R. Niedermaier, F. Stelzle, M. Riemann, W. Bolz, P. Schuh, H. Wachtel, Implant-Supported Immediately Loaded Fixed Full-Arch Dentures: Evaluation of Implant Survival Rates in a Case Cohort of up to 7 Years, Clinical Implant Dentistry and Related Research 19(1) (2017) 4-19.
[119] G. Alsaadi, M. Quirynen, A. Komárek, D. Van Steenberghe, Impact of local and systemic factors on the incidence of oral implant failures, up to abutment connection, Journal of Clinical Periodontology 34(7) (2007) 610-617.
[120] J. Liu, Z. Wu, H. He, K. Cai, H. Zhang, L. Xu, Gallium and silicon synergistically promote osseointegration of dental implant in patients with osteoporosis, Medical Hypotheses 103 (2017) 35-38.

Available online at www.jourcc.com

Journal homepage: www.JOURCC.com

Journal of Composites and Compounds

Hydroxyapatite consolidated by zirconia: Applications for dental implant

*Fariborz Sharifianjazi[a], Amir Hossein Pakseresht[b], Mehdi Shahedi Asl[c], Amirhossein Esmaeilkhanian[a], Hiva Nargesi Khoramabadi[d], Ho Won Jang[e], Mohammadreza Shokouhimehr[e]**

[a] Department of Materials and Metallurgical Engineering, Amirkabir University of Technology, Tehran 15875-4413, Iran
[b] Coating Department, Centre for Functional and Surface Functionalized Glass, Alexander Dubcek University of Trencin, Trencin 91150 Slovakia
[c] Department of Mechanical Engineering, University of Mohaghegh Ardabili, Ardabil, Iran
[d] Department of Medical Engineering, Payame Noor University (PNU), Alborz 19395-3697, Iran
[e] Department of Materials Science and Engineering, Seoul National University, Seoul 08826, Republic of Korea

A B S T R A C T

Zirconia has garnered significant attention as a new ceramic material for dental implant due to its excellent biocompatibility, strength, and promoting the oral rehabilitation with high aesthetic, biological and mechanical properties. It also expedites the amelioration of bone minerals surface by its bio-integrative ingredients which are naturally close to ceramic intrinsic of bone. Alternatively, hydroxyapatite (HAp) has prevalently been used in dental implant due to its high biocompatibility. However, it generally shows weak strength and mechanical properties. Consequently, incorporating zirconia and HAp produces appropriate composites for dental implant having improved physiochemical properties. This review provides discussions addressing the methodologies and exemplars for the designed composites used in dental implant applications. The representative methods for surface modification of zirconia incorporating HAp (i.e. sol-gel, hot isostatic pressing, plasma spraying, electrophoretic deposition, etc.) is highlighted. The advantages, disadvantages, biocompatibility, strength, and osseointergration and biointegration properties of the presented composites are explored.

Peer review under responsibility of jourcc

A R T I C L E I N F O R M A T I O N

Article history:
Received 5 March 2020
Received in revised form 17 March 2020
Accepted 27 March 2020

Keywords:
Hydroxyapatite
Zirconia
Dental implant
Biocompatibility
Coating
Ceramic composite

Table of contents

1. Introduction 26
2. Dental implant 27
3. Choosing an appropriate implant 28
4. HAp-Zirconia nanocomposite 28
5. HAp-coated Zirconia 29
5.1. Hot isostatic pressing method 29
5.2. Pulsed laser deposition coating technique 29
5.3. Sol-gel technique 30
5.4. Plasma spraying technique 30
5.5. Electrophoretic deposition 31
5.6. Sputter coating method 31
6. Conclusions and future insights 31

1. Introduction

Dental composites have been confirmed as safe component for filling rotted teeth, principally because of their superior aesthetics and biocompatibility [1-5]. They are typically composed of resin matrix and inorganic fillers [6-8]. Although considerable investigations have been carried out to improve the monomer structures and filler formulations, secondary caries and rebuild fractures of dental composites are the major reasons to repair failure. The accessible fillers cannot present expected strengthening and useful impact in dental composites. Thus, more endeavors have been made to produce fillers providing similar function and structure to the natural human teeth [9].

* *Corresponding author: Mohammadreza Shokouhimehr; E-mail: mrsh2@snu.ac.kr*
https://doi.org/10.29252/jcc.2.1.4

Recently various materials have been utilized in the field of hard tissue engineering [10-12], e.g. hydroxyapatite (HAp) [13], bioactive glasses, bio-ceramics [14], bio-scaffolds [15, 16], etc. Among them, HAp has crystallographic and chemical similarity to human bone tissues, therefore, has extensively been utilized for bone-related issues. It contains calcium phosphate possessing chemical formula of $[Ca_{10}(PO_4)_6(OH)_2]$ [17-19].

In addition, HAp is very well-known biocompatible substitution for the essential mineral constituents of skeletal bones that can be utilized as orthopedic surgeries and tooth implant [20, 21]. HAp is considered to be extremely bioactive, osteoconductive, biocompatible, non-toxic, non-immunogenic, and non-inflammatory [22, 23]. The measurement of alkaline phosphatase activity has indicated that naturally isolated HAp can to be utilized for progression of both cell proliferation and differentiation [17]. Therefore, various chemical routes have been introduced for HAp synthesis including hydrothermal, sol-gel, mechano-chemical, precipitation, and polymer-assisted methods. HAp can also be fabricated from bio-waste or natural resources including clam shell [24], bovine [25], camel bones [26], corals [27], cuttlefish [28], and fish bone [17, 29].

It is noteworthy that the HAp coating application is one of the most promising surface modification method applied for dental implant. The HAp-coated implants have been widely utilized in dental applications due to their great biocompatibility with epithelium, and bone and connective tissues. A thin layer of HAp is used to coat the dental implant surface, which has been generally observed to be effective for the osseointegration process, load stress distribution, healing time to bone, bone implant contact, and bone crest repair [30]. Moreover, the HAp coating can improve the mechanical properties of the substrates; in particular, the surface biocompatibility and maintaining the load-bearing capacity. For example, the histology study and mechanical interface characteristics of HAp coated titanium and commercially pure (CP) titanium, revealed that the HAp coating enhances the mean interface stability of bead-blasted CP titanium system with no coating five to eight times [30]. HAp coated implant can also interact with the surrounding biologic environments. For dental materials, the importance of HAp coatings, due to their developed integration of osseous tissues, has been also improved for implant surfaces. These materials can play a role in the sources of phosphate and calcium in the enamel minerals in supersaturation state. Furthermore, they can protect the outer dental enamel caries lesion by mineralization system [30].

This review focuses on the effect of HAp incorporation either in the form of coating or composite incorporated zirconia. It discusses zirconia implant, nanocomposites, and surface modification techniques to enhance the bio-integration and osseointegration treatment of zirconia-based implant [31].

2. Dental implant

Implant dentistry is a prosthetic effort via a surgical procedure [32, 33]. In order to achieve an ideal prosthetic construct, precise plan should be taken into consideration prior to the beginning of treatment. The position of implant requires protected prosthesis. It can be affected by the implant size, volume, and the quantity and quality of bone provided at various sites [34].

Another parameter that requires to be integrated in to therapeutic deliberations is the measurement of accessible horizontal and vertical space for prosthesis adaption. Various reports have indicated the functional and aesthetic success of this therapy for up to six years of long-term follow-up [34]. In the field of dental implant, handful materials such as pure Ti and some of its alloys, zirconia, and tantalum have been found as appropriate implant materials up to now. The indication of osseointegrated implant in the bone is not closely discoverable mobility. Moreover, osseointegration should be protected during the lifetime of the implant owing to its effectiveness [31].

Biointegration has been described a sort of the interconnection between the recipient tissue and a biomaterial at the microscopic measurement. This connection among implant and tissue is a region of interaction or a specified boundary between the corresponding tissue and biomaterial [35]. Osseointegration is the presence of highly proximity between the supporting bone and the implant without including fibrous tissue or collagen. However, continuity of the implant to bone with no intervening space is known as biointegration. In fact, the ceramic-based implant chemical degradation should occur in the biointegration process for development of bone generation as well as integration of the ceramic implant around the bone. The nature or mechanism of both operations are not entirely understood so far, and their superiority over each other is not recognized very well. There is similarity between both interfaces are natural teeth clinical alkalosis. Although the ceramic has been coated on metallic implants primly enhance a bio-integrated interface, the interface stability is lower as a result of its degradation with time in long term [31] (Fig. 1).

In the past decades, the development of nanocomposites has opened new prospect in different fields to obtain materials with enhanced physical and mechanical properties [36, 37]. Because the nano-HAp has greater surface area and higher reactivity as a biomaterial compared with

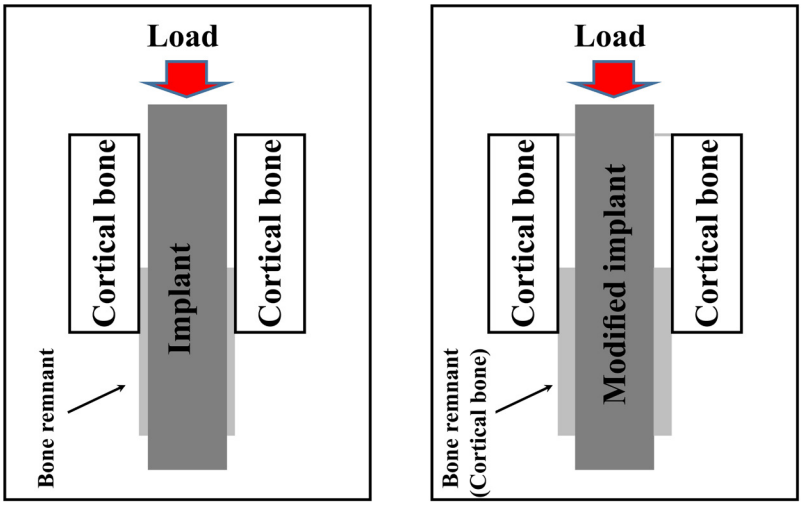

Fig. 1. Schematic illustration of implant vs. surface modified implant

its bulk counterpart, it can provide significant characteristics in several medicinal fields, in particular, dental implant. The effect of HAp incorporation as coating materials in dental implants have been hopeful for futures applications. It can result in formation of chemical bond with bone and lead to reinforced biological and biointegration fixation [31].

3. Choosing an appropriate implant

Fabrication of dental implant is highly utilized with Titanium and titanium alloys due to corrosion resistance and high strength [38]. However, novel implant technologies are being improved, due to aesthetic compatibility and potential immunologic with titanium implant. Meanwhile, ZrO_2 implant is considered as an alternative to Ti-based implant in dental implantology. ZrO_2 has shown to be more effective as implant material [39, 40].

Zirconia (ZrO_2) is oxide form of a gray white, lustrous, strong transition metal named Zirconium (Zr) [41, 42], and has emerged as an alternative to common Titanium based implant for oral rehabilitation with higher aesthetic, biological, optical and mechanical properties [39]. In addition, Zirconia is very interesting because of its potential osseointegration and having other superior properties such as white color and translucency that mimics the natural teeth. It is radiopaque same as Ti and can be observed under radiography. Compared to Ti, bacterial colonization around ZrO_2 is seemed to be lower. Some investigates have indicated that zirconia has higher biocompatibility in comparison with Ti, as the latter fabricates corrosion products at the implant site [43].

Although many studies have been performed for titanium implant compared to zirconia in the past decades, high-strength zirconia ceramics have attracted a great attention as new materials for dental implant. This ceramic indicates minimal ion diffusion compared to metallic implants (i.e. Titanium), which mentioned to be inert in human body. Due to its biocompatibility, mechanical properties and tooth-like color, zirconia have become a superior dental implant material. Surface topography and material composition of a biomaterial in osseointegration act a fundamental role. One of the main agents in the surface of implant is their quality that effects healing of wounds at the implant placement and afterward influences osseointegration. Thus, different physical and chemical modifications of surfaces have been advanced to promote osseous healing [44].

The clinical application of zirconia dental implants is restricted owing to difficult modifications of surface. In addition, implant with smooth surfaces are disadvantageous for osseointegration due to weak tissues interaction [44]. Because bone consists of ceramic phase, a ceramic system with proper mechanical properties, which provides the mineral growth on its surface can be called the right biointegrative material. The zirconia implants with modified topography were investigated and their biointegration by laser modification, UV modification and methodologies like surface modifications were explored [45].

4. HAp-zirconia nanocomposite

Matsumoto et al. [46] studied a composite of HAp-incorporated zirconia having micro porous structure. Their results showed that the produced composite material possessed strength in the range of bio-cortical bone strength with high tissue and cell affinities by combining HAp and ZrO_2. It was found that by changing the molding pressure and raw materials particle size, control the quality of surface is feasible, proposing this material as a good candidate for bone restoration. Izquierdo et al. [47] deposited HAp /ZrO_2 composites on Ti-21Nb-15Ta-6Zr alloy through pulsed layer deposition and investigated their electrochemical properties. Results showed that the presentation of HAp/zirconia layers avoids the interaction of the biomaterial with active molecules and the subsequent reduction oxidation and enhances interaction between bone tissue and implant. The HAp–ZrO_2 coating modifies the Ti alloys electrochemical features in Ringer solutions. The prepared film had good bioactivity through generating an appetite layer similar to bone material and can be offered as a promising material for orthopedic and dental implants. The produced ZrO_2/HAp composite film indicates excellent surface roughness and energy and significant wettability compared to Zr substrate.

Bulut, et al. [48] investigated biocompatibility of HAp-zirconia and HAp-alumina composites and a ternary component of commercial inert glass. Results showed the great mechanical properties of the HAp-ZrO_2 composites as well as the development of bioactive properties. According to the obtained results, the ternary composites can be mentioned as promising materials for bone-related issues.

Buciumeanu et al. [35] deposited composite layers of bioactive zirconia on zirconia structures and investigated their tribological properties. The layer of bioactive zirconia composite (zirconia containing 10 vol. % of β-TCP or 10 vol. % of HAp) was successfully provided by press-sinter method on zirconia substrate. Their results showed that zirconia composites had a great potential to be utilized as a biomaterial in dental implants with a layer of the bioactive zirconia composite, due to great mechanical properties and developing bond between the implant and living tissue. The advantage of bioactive zirconia composite layer is that it is a suitable substitute to coatings on zirconia substrate due to decreasing the possibility of implant failure and the interfacial residual stresses.

Leong et al. [49] prepared nanocomposites of HAp/yttria stabilized zirconia (YSZ) under for dental materials. HAp/YSZ nanocomposites were obtained by wet ball milling and sintering pressureless and also under pressure using nitrogen gas. However, HAp decomposition was found to take place in the samples regardless of the sintering methods. In spite of the sintering techniques that investigated, relative density of 99.5% without identifiable HAp decomposition was attained only with the hot isostatic sintering technique.

Carvalho et al. [50] functionalized zirconia surface by HAp using hybrid laser method for applications in dentistry. Their results showed that the improvement of novel procedures for promotion of the implant biointegration and its long-term retention is challenging. The procedure attempts to mimic the natural bone material. By altering atmosphere and energy density, textured surface could be designed. Moreover, high volume of sintered and maintained bioactive material was produced when the process was carried out with low scan speed and high laser power.

Gergely et al. [51] studied microstructural and mechanical properties of ZrO_2/HAp nanocomposites obtained by spark plasma sintering (SPS). To prevent the reaction between ZrO_2 and nHAp and decomposition of nHA, the SPS method was carried out at short dwelling time (5 min) and low temperatures. It was shown that the mechanical and microstructural characteristics of the composites were strongly dependent on SPS technique specialties.

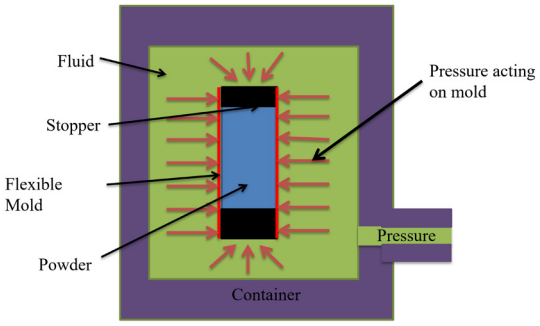

Fig. 2. Schematic of HIP method.

5. HAp-coated zirconia

Nowadays, many studies have focused on corrosion [52] and coating [53], especially importance of ceramic coatings as dental implant to enhance osseointegration. Different forms of ceramic coatings have been utilized on implants for dentistry over the last 15 years including inert ceramics such as zirconium and aluminum oxides and bioactive ceramics including bioglasses and calcium phosphates. Coatings can be porous or dense depending on their production procedure with a thickness ranging from 1 to 100 µm. Various ceramic coating methods in dental implants include sol-gel [54-56], hot isostatic pressing (HIP), plasma spraying [57-59], electrophoretic deposition [60], sputter-deposition and pulsed laser deposition [61].

5.1. Hot isostatic pressing method

In HIP, isostatic temperature and pressure are applied simultaneously. Contrary to hot pressing, a uniform pressure is exerted in different directions (Fig. 2). HIP is used to create metals and ceramics, such as high-density ceramics and composites, components with complex shapes and it is utilized for the solid phase bonding of different or similar materials. The sample is in a gaseous medium and undergoes heat treatment accompanied by a high pressure for consolidation. One of the significant benefits of HIP is the high flexibility in specimen shape.

There are many reports concentrating on pressure sintering techniques including hot pressing (HP) and HIP to maintain the ZrO_2 and HAp phases during sintering process and decrease the sintering temperature. Moreover, pressure sintering techniques are argumentative methods with diverge conclusions and studies regarding the phase stability of the phases. Although an enhancement in reactivity are anticipated because of enhanced contact areas between diffused ZrO_2 particles and HAp matrix, there is a common agreement that the composite is significantly constant particularly after HIP. Indeed, in the composites obtained by hot pressing, a partial reaction between zirconia and HAp occurred, although, much fewer than what observed in sintering in air yet. Hence, the sintering environment can be a major factor influencing the ZrO_2 and HAp thermal stability in the composites [30]. Leong et al. [62] synthesized HAp/zirconia composites and investigated HAp decomposition for the application as dental materials. Their results indicated that HIP of HAp/ZrO_2 could greatly inhibit HAp decomposition and the highest relative density was achieved compared to other techniques.

Ergun et al. [63] prepared composites of HAp/zirconia using HIP and studied their phase stability. According to the results, phase stability of ZrO_2 and HAp in hot isostatically pressed composites was indicated. Higher ZrO_2 contents and lower sintering temperatures led to lower density in air-sintered specimens. The amount of air in the environment of sintering affects the reactivity between HAp and ZrO_2. To achieve phase stability and fully-dense HAp/ZrO_2 composites, HIP would be a suitable technique.

Lim et al. [64] studied sintering of HAp incorporated zirconia using different methods including HIP, solid-state reaction, conventional sintering and microwave sintering. They proposed that HIP revealed more satisfying results compared to other methods. Furthermore, nano structured material can be processed by alternative techniques and show better results.

5.2. Pulsed laser deposition coating technique

Laser texturing methods has been widely investigated to modify materials surface for various applications. This method is a hopeful method to progress the direct sintering of HAp on ZrO_2 substrates in order to produce appropriate coatings. It is known that mechanical interlocking produced through laser texturing is able to enhance the stability of the coating interfaces, therefore preventing delamination of coating during the implants insertion [65].

Mesquita-Guimarães et al. [65] sintered HAp coatings and 45S5 bioactive glass on micro-textured ZrO_2 via laser and evaluated osteoblasts-like cell adhesion. In vitro test indicated that, compared to flat surfaces, the squared textured pattern possessed bioactive coating and 100 µm width grooves provided an increase of 90% of cell viability after incubation for 48 hours. Hence, they showed that laser sintering is an attractive and fast method for HAp coatings.

Carmen Trincă et al. [66] studied the electrochemical properties of a novel biodegradable FeMnSi alloy coated by HAp-zirconia through pulsed laser deposition (PLD) method. Their results showed that the corrosion resistance enhanced significantly for alloys coated with HAp-ZrO_2 in comparison with uncoated sample.

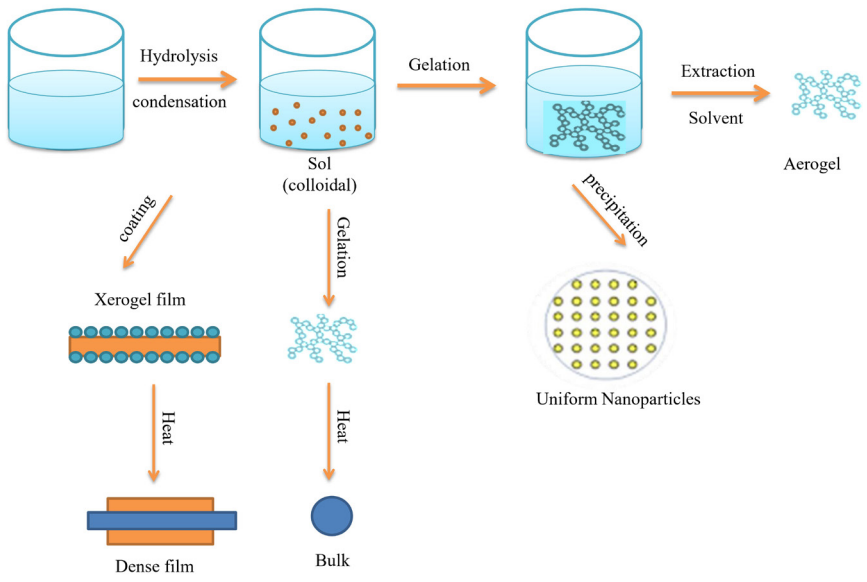

Fig. 3. Schematic illustration of sol-gel technique.

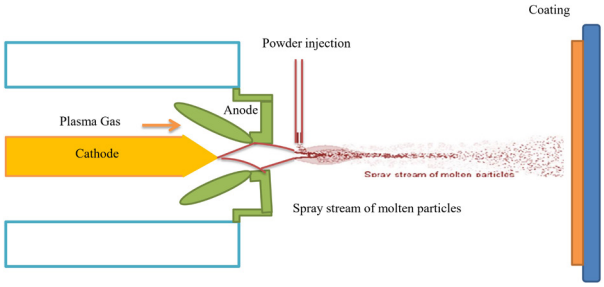

Fig. 4. Plasma spraying technique schematic illustration.

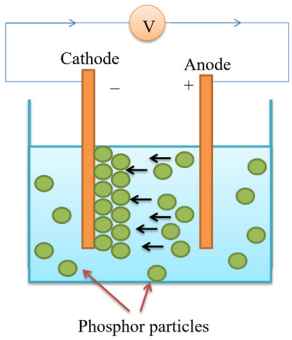

Fig. 5. Electrophoretic deposition process schematic.

Hybrid laser method was employed by Carvalho et al. [50] to functionalize zirconia surfaces by HAp for dental applications. The textures that were generated by Nd:YAG laser were produced to promote the mechanical interlocking of HAp particles, hence reinforcing its incorporation to surface of ZrO_2. For optimization of the textured pattern of ZrO_2 surface, various laser parameters were tested. Hybrid laser process was proposed to have the potential for modification and functionalization of zirconia surfaces.

5.3. Sol-gel technique

The sol–gel procedure is a wet chemical technique in which high temperatures or pH values are not required [55, 67-70] (Fig. 3). Significant reactivity owing to the large surface area of dried gels leads to a low procedure temperature [71, 72]. In addition, this technique can promote chemical homogeneity by providing a molecular mixing precursor solution. Due to its intrinsic benefits over other processes, nowadays, the sol–gel process has been highly utilized for fabricating of ceramics. The process permits the provision of a homogeneous combination of YSZ and HAp nanoparticles.

Vasconcelos et al. [73] studied the microstructure of HAp-ZrO_2 nanocrystalline composites prepared by sol–gel method. Their results showed that optimizing processing parameters could produce HAp-ZrO_2 nano-crystalline composites. The modified sol–gel process could produce a water vapor atmosphere during sintering which could control the HAp thermal stability and provide a high intergranular dispersion of ZrO_2 phase in the HAp matrix [73].

Salehi, et al. [74] studied Properties and fabrication of sol–gel isolated HAp/ ZrO_2 composites nanopowders by different yttria contents. Homogeneous composites of HAp/yttria-stabilized zirconia (HAp–YSZ) nanopowders were produced by the sol–gel technique. Due to ion exchange of zirconium and calcium between zirconia and HAp, the HAp unit cell volume enhanced in the composites. The existence of ZrO_2 nanoparticles between the HAp particles inhibited the HAp grain growth and also the inhibition of the ZrO_2 grain growth was resulted from yttrium ions segregation at the grain boundaries.

In Bollino et al. [75] research, biphasic composition of HAp and the surface modification with a tricalcium phosphate (TCP) was carried out

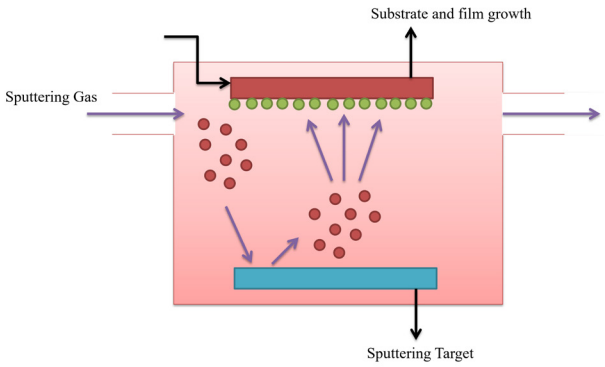

Fig. 6. Schematic of sputter coating method.

on a zirconia substrate by utilizing a sol–gel technique. The microstructure of the conclusive HAp/TCP coatings was found to be related on the sort of zirconia substrate. The heat treatment temperatures of coating on dense and porous zirconia substrates were 750 °C and 1350 °C, respectively. In the case of dense substrate, a thick layer of nano HAp was formed, but cracking and agglomeration were observed.

Catauro et al. [76] studied thermal and morphological characterization of the composites of HAp incorporated zirconia for biomedical applications, obtained through sol-gel method. According to the obtained results, the crystallization of Zr in the tetragonal phase occurred due to existence of HAp in the composite. Moreover, by increasing the Zr content in the composites the degree of amorphization increased.

Jin et al. [77] applied biocompatible and bioactive calcium phosphate layer on zirconia surface. HAp/ZrO_2 composites were prepared by the sol-gel technique and heat-treated at various temperatures in order to modify their chemical structure. They indicated that all materials are bioactive, consequently they can generate a HAp layer on their surfaces. Furthermore, biocompatibility enhanced with heating temperature, while the amount of HAp did not affect it significantly. On the other hand, bioactivity improved with both heat-treatment temperature and the HAp content.

Buciumeanu et al. [35] coated zirconia by zirconia/HAp composite and studied its tribological properties. Their results showed that press and sinter technique on YSZ substrates could significantly influence the performance of composite layer of bioactive zirconia. According to the results, by adding bioactive materials, the tribological characteristics and the friction coefficient were not influenced. The focus of this novel procedure on zirconia substrate was on the application of bioactive zirconia composite layer. Since there is a gradual change between the substrate and composite layer, it seems to be a suitable replacement for coatings due to reduction in interfacial residual stresses and hence it is less prone to failure.

5.4. Plasma spraying technique

One of the promising techniques of preparing coatings with special microstructural characteristics is solution precursor plasma spraying (SPPS) method (Fig. 4). Various studies have reported about SPPS method that promotes the HAp coatings. It is possible to achieve higher contents of HAp in coating with changing spraying parameters e.g. spraying distance [78, 79]. Different substrates including mild steel has been coated by HAp using air plasma spray technique [80, 81].

Hasan et al. [82] studied the mechanical properties of HAp coatings on Zr using plasma spray technique. ZrO_2/HAp composite coating on Zr by plasma spraying illustrated that compared to pure zirconia, the incorporation of HAp in ZrO_2 enhanced biological properties, whereas its biocompatibility is preserved. On the other hand, plasma sprayed

Table 1.

Various techniques used for coating HAp on ZrO_2 substrates.

Method	Coating thickness	Advantages	Disadvantages
Electrophoretic deposition	0.1–2 mm	Control of coating thickness/ morphology, low cost, rapid deposition, simple setup, uniform coating thickness, suitable for complex shaped substrate	Decomposition of HAp during sintering stages, appearance of crack in coating, high sintering temperature requirement
Sputter	0.5–3 μm	High adhesion, dense and uniform coating on flat surface	Produces amorphous coating, low deposition rate, line of sight technique, costly, time-consuming
plasma spraying	<20 μm	Quick bone healing, less possibility of coating degradation, high deposition rate, low cost	Unable to form complete crystalline coating, relatively weak adhesion, non-uniformity in coating density, phase change and grain growth of the material because of high temperature, change of HAp structure during coating
Sol-gel	50–400 nm	Very thin and high purity coatings, low processing temperature, high corrosion resistance, suitable for complex shaped substrate, uniformity in coating	Expensive raw materials, high permeability, difficult to control porosity, requirement of posttreatment (curing), Appearance of edge cracking
Pulsed laser deposition coating	0.05–5 μm	Control of deposition factors, amorphous and crystalline coatings, suitable for porous, dense coating	Line of sight technique, requirement of pretreatment of surface, lack of uniformity, expensive, low deposition rate
HIP	0.2–2.0 mm	Good temperature controlling, dimensional limitation, dense coating, no shape	Reaction of encapsulation material with HAp coating, incompatibility of thermal expansion coefficient, costly, requirement of high temperature, unable to coat complex shaped substrate

coatings suffer from residual stress and lack of uniformity in coatings on complex-shaped Zr implants.

5.5. Electrophoretic deposition

Electrophoretic deposition is a coating method, in which through the influence of an external electric field colloidal particulates migrate and are deposited on an electrode (Fig. 5). Ceramic coatings are able to be produced by this technique and the method has the capability to be used for complex objects coating due to being cost-effective and flexible. This approach allows controlling of the microstructure, thickness and composition of coatings hence electrophoretic deposition is a useful method especially in the HAp deposition [30].

Sandhyarani et al. [83] fabricated nanostructured ZrO_2/HAp coating on zirconium and studied in-vitro performance of manufactured composites. HAp particles were dragged into the evacuation channels, during the film growth step, then by electrophoretic deposition process entrapped into the oxide film. Due to residing of Ca (generating from HAp melting) in Zr sites, zirconia is stabilized. After immersing in SBF for 8 days, apatite layer similar to bone was formed on all surfaces of ZrO_2/HAp films showing their considerably increased in-vitro bioactivity. The cell adhesion test results indicated that the human osteosarcoma cells on the surface of ZrO_2/HAp film could propagate, append and adhere very well [84].

Sakthiabirami et al. [85] coated a composite of glass/zinc-HAp on glass-infiltrated zirconia to tailor interfacial interaction. The surface stabilization of HAp (Ca^{+2} cations) was done by chemical adsorption of non-dissociated 2-propanol and monochloroacetic acid (MCAA) molecules through Cl^- followed by protons dissociation, leading to negatively charged HAp particles.

Drdlik et al. [86] used electrophoretic deposition to prepare HAp/ZrO_2 microfiber with controlled fracture and microporosity properties. Vickers hardness and elastic modulus of composites enhanced with dispersions milling time prior to electrophoretic deposition and were reduced with the ZrO_2 microfibers amount in the coatings, which is related to the density of composites. As a result of tougher β-TCP phase, finer microstructure, and the existence of orientated microfibers of zirconia, fracture toughness of the composites increased significantly compared to pure HAp.

Farnoush et al. [87] prepared HA/YSZ nanocomposite coatings on Ti–6Al–4 V substrate using electrophoretic deposition and studied the stability of suspension and its effect on bonding electrochemical behavior and bonding strength. According to the obtained results, incorporation of 20 wt. % YSZ resulted in the reduction of corrosion rate of coated specimens, whereas linear polarization resistance and corrosion potential increased.

5.6. Sputter coating method

Sputter coating technique is a kind of vapor deposition technique, in which high energy particles are ejected from a target and bombard a substance and is appropriate for thin coatings. For elimination of the substance from the target with negative charge, a gas plasma including xenon, krypton, neon and, argon is used and then the particles are deposited on the substrate (Fig. 6) [30].

Kong et al. [88] used magnetron sputtering for the preparation of HAp-zirconia coatings on Ti6Al4V. They proposed that the porous surface of the deposited coating is suitable for conduction of bone tissue growth. The bonding strength decreased by increasing HAp content and the residual stress reduced by appropriate increasing of HAp contents.

Ozeki et al. [89] fabricated thin films of HAp on zirconia using a sputtering technique. During hydrothermal treatment, the recrystallization of coated films occurred to decrease dissolution. After the films recrystallized under the hydrothermal treatment, bone formation area on the coating for both the Ti and ZrO_2 substrates increased. This value was reported to be higher for the ZrO_2 substrate. Table 1 summarizes the applied methods to prepare HAp-coated ZrO_2 for potential dental implant.

6. Conclusions and future insights

Although hydroxyapatite (HAp) is highly biocompatible, it has low mechanical properties. Instead, zirconia exhibits bioactivity, biocompatibility, and good mechanical and aesthetic properties enhancing the quality of the dental implants. Thus, HAp incorporated in zirconia provide high stability and protection in long time promoting integration of the dental implants. These composites are promising novel bone restorative materials having properties similar to human bone. Furthermore, the surface modification of zirconia composites can be obtained by different types of HAp coatings. Therefore, these materials can be considered as

alternatives to conventional counterparts in dentistry such as titanium and its alloys due to their advantages in dental implant applications.

REFERENCES

[1] G. Rajan, R. Raju, S. Jinachandran, P. Farrar, J. Xi, B.G. Prusty, Polymerisation Shrinkage Profiling of Dental Composites using Optical Fibre Sensing and their Correlation with Degree of Conversion and Curing Rate, Scientific Reports 9(1) (2019) 3162.

[2] K. Cho, G. Wang, Raju, J. Fang, G. Rajan, M.H. Stenzel, P. Farrar, B.G. Prusty, Selective Atomic-Level Etching on Short S-Glass Fibres to Control Interfacial Properties for Restorative Dental Composites, Scientific Reports 9(1) (2019) 3851.

[3] A.A. Pérez-Mondragón, C.E. Cuevas-Suárez, J.A. González-López, N. Trejo-Carbajal, M. Meléndez-Rodríguez, A.M. Herrera-González, Preparation and evaluation of a BisGMA-free dental composite resin based on a novel trimethacrylate monomer, Dental Materials (2020).

[4] Y. Boussès, N. Brulat-Bouchard, P.-O. Bouchard, H. Abouelleil, Y. Tillier, Theoretical prediction of dental composites yield stress and flexural modulus based on filler volume ratio, Dental Materials 36(1) (2020) 97-107.

[5] S.V. Palagummi, T. Hong, Z. Wang, C.K. Moon, M.Y.M. Chiang, Resin viscosity determines the condition for a valid exposure reciprocity law in dental composites, Dental Materials 36(2) (2020) 310-319.

[6] A.P. Fugolin, D. Sundfeld, J.L. Ferracane, C.S. Pfeifer, Toughening of Dental Composites with Thiourethane-Modified Filler Interfaces, Scientific Reports 9(1) (2019) 2286.

[7] E. Habib, R. Wang, J. Zhu, Dental Nanocomposites, Advances in Nanostructured Composites: Volume 1: Carbon Nanotube and Graphene Composites (2019) 114.

[8] S.-N. Zhao, D.-L. Yang, D. Wang, Y. Pu, Y. Le, J.-X. Wang, J.-F. Chen, Design and efficient fabrication of micro-sized clusters of hydroxyapatite nanorods for dental resin composites, Journal of Materials Science 54(5) (2019) 3878-3892.

[9] L. Bohner, M. Hanisch, J. Kleinheinz, S. Jung, Dental implants in growing patients: a systematic review, British Journal of Oral and Maxillofacial Surgery 57(5) (2019) 397-406.

[10] A.-D. Draghici, C. Busuioc, A. Mocanu, A.-I. Nicoara, F. Iordache, S.-I. Jinga, Composite scaffolds based on calcium phosphates and barium titanate obtained through bacterial cellulose templated synthesis, Materials Science and Engineering: C 110 (2020) 110704.

[11] P. Kumar, M. Saini, B.S. Dehiya, A. Umar, A. Sindhu, H. Mohammed, Y. Al-Hadeethi, Z. Guo, Fabrication and in-vitro biocompatibility of freeze-dried CTS-nHA and CTS-nBG scaffolds for bone regeneration applications, International Journal of Biological Macromolecules 149 (2020) 1-10.

[12] Y. Chen, P. Han, A. Dehghan-Manshadi, D. Kent, S. Ehtemam-Haghighi, C. Jowers, M. Bermingham, T. Li, J. Cooper-White, M.S. Dargusch, Sintering and biocompatibility of blended elemental Ti-xNb alloys, Journal of the Mechanical Behavior of Biomedical Materials 104 (2020) 103691.

[13] A. Shahbaz, M. Esmaeilian, R. NasrAzadani, K. Gavanji, The Effect of MgF_2 Addition on the Mechanical Properties of Hydroxyapatite Synthesized via Powder Metallurgy, Composites and Compounds 1(1) (2019).

[14] E. Asadi, A. Fassadi Chimeh, S. Hosseini, S. Rahimi, B. Sarkhosh, L. Bazli, R. Bashiri, A.H. Vakili Tahmorsati, A Review of Clinical Applications of Graphene Quantum Dot-based Composites, Composites and Compounds 1(1) (2019).

[15] Z.-K. Cui, S. Kim, J.J. Baljon, B.M. Wu, T. Aghaloo, M. Lee, Microporous methacrylated glycol chitosan-montmorillonite nanocomposite hydrogel for bone tissue engineering, Nature Communications 10(1) (2019) 3523.

[16] Y. Wang, N. Sun, Y. Zhang, B. Zhao, Z. Zhang, X. Zhou, Y. Zhou, H. Liu, Y. Zhang, J. Liu, Enhanced osteogenic proliferation and differentiation of human adipose-derived stem cells on a porous n-HA/PGS-M composite scaffold, Scientific Reports 9(1) (2019) 7960.

[17] A. Esmaeilkhanian, F. Sharifianjazi, A. Abouchenari, A. Rouhani, N. Parvin, M. Irani, Synthesis and characterization of natural nano-hydroxyapatite derived from turkey femur-bone waste, Applied biochemistry and biotechnology 189(3) (2019) 919-932.

[18] J. Soares da Silva, T.R. Machado, T.A. Martins, M. Assis, C.C. Foggi, N.G. Macedo, H. Beltrán-Mir, E. Cordoncillo, J. Andrés, E. Longo, α-$AgVO_3$ Decorated by Hydroxyapatite ($Ca_{10}(PO4)_6(OH)_2$): Tuning Its Photoluminescence Emissions and Bactericidal Activity, Inorganic Chemistry 58(9) (2019) 5900-5913.

[19] X. Guo, D. Li, Synthesis of Hydroxyapatite Containing some Trace Amounts Elements in Simulated Body Fluids, Iranian Journal of Chemistry and Chemical Engineering (IJCCE) 38(1) (2019) 83-91.

[20] M. Mansoorianfar, M. Mansourianfar, M. Fathi, S. Bonakdar, M. Ebrahimi, E.M. Zahrani, A. Hojjati-Najafabadi, D. Li, Surface modification of orthopedic implants by optimized fluorine-substituted hydroxyapatite coating: Enhancing corrosion behavior and cell function, Ceramics International 46(2) (2020) 2139-2146.

[21] A. Veiga, F. Castro, C.C. Reis, A. Sousa, A.L. Oliveira, F. Rocha, Hydroxyapatite/sericin composites: A simple synthesis route under near-physiological conditions of temperature and pH and preliminary study of the effect of sericin on the biomineralization process, Materials Science and Engineering: C 108 (2020) 110400.

[22] K. Wongsawichai, A. Kingkaew, A. Pariyaisut, S. Khondee, Porous Hydroxyapatite/Chitosan/Carboxymethyl Cellulose Scaffolds with Tunable Microstructures for Bone Tissue Engineering, Key Engineering Materials 819 (2019) 9-14.

[23] C.Y. Goh, S.S. Lim, K.Y. Tshai, A.W.Z.Z. El Azab, H.-S. Loh, Fabrication and in vitro biocompatibility of sodium tripolyphosphate-crosslinked chitosan–hydroxyapatite scaffolds for bone regeneration, Journal of Materials Science 54(4) (2019) 3403-3420.

[24] Gunawarman, J. Affi, Y. Yetri, Ilhamdi, D. Juliadmi, N.F. Nuswantoro, H. Fajri, A. Ahli, R. Gundini, H. Nur, Synthesis and characterization of calcium precursor for hydroxyapatite synthesis from blood clam shell (Anadara antiquata) using planetary ball mill process, IOP Conference Series: Materials Science and Engineering 602 (2019) 012072.

[25] P. Galindo-Moreno, M. Padial-Molina, L. Lopez-Chaichio, L. Gutiérrez-Garrido, N. Martín-Morales, F. O'Valle, Algae-derived hydroxyapatite behavior as bone biomaterial in comparison to anorganic bovine bone. a split-mouth clinical, radiological and histologic randomized study in humans, Clinical Oral Implants Research n/a(n/a) (2020).

[26] H.L. Jaber, A.S. Hammood, N. Parvin, Synthesis and characterization of hydroxyapatite powder from natural Camelus bone, Journal of the Australian Ceramic Society 54(1) (2018) 1-10.

[27] S.M.B. Nabavi, M.R. Shushizadeh, A. Behfar, M.G. Ashrafi, Persian Gulf Corals: A New Hydroxyapatite Bioceramics in Medicine, International Journal of Pharmaceutical and Phytopharmacological Research (eIJPPR) 7(5) (2017) 59-64.

[28] N. Lagopati, S. Agathopoulos, Hydroxyapatite Scaffolds Produced from Cuttlefish Bone via Hydrothermal Transformation for Application in Tissue Engineering and Drug Delivery Systems, in: A.H. Choi, B. Ben-Nissan (Eds.), Marine-Derived Biomaterials for Tissue Engineering Applications, Springer Singapore, Singapore, 2019, pp. 179-205.

[29] A. Pal, S. Paul, A.R. Choudhury, V.K. Balla, M. Das, A. Sinha, Synthesis of hydroxyapatite from Lates calcarifer fish bone for biomedical applications, Materials Letters 203 (2017) 89-92.

[30] A. Nasar, Hydroxyapatite and its coatings in dental implants, Applications of Nanocomposite Materials in Dentistry, Elsevier (2019), pp. 145-160.

[31] J. Yazdani, E. Ahmadian, S. Sharifi, S. Shahi, S.M. Dizaj, A short view on nanohydroxyapatite as coating of dental implants, Biomedicine & Pharmacotherapy 105 (2018) 553-557.

[32] A. Klinge, D. Khalil, B. Klinge, B. Lund, A. Naimi-Akbar, S. Tranaeus, M. Hultin, Prophylactic antibiotics for staged bone augmentation in implant dentistry, Acta Odontologica Scandinavica 78(1) (2020) 64-73.

[33] R. Lieber, N. Pandis, C.M. Faggion Jr, Reporting and handling of incomplete outcome data in implant dentistry: A survey of randomized clinical trials, Journal of Clinical Periodontology 47(2) (2020) 257-266.

[34] J. Carpentieri, G. Greenstein, J. Cavallaro, Hierarchy of restorative space required for different types of dental implant prostheses, The Journal of the American Dental Association 150(8) (2019) 695-706.

[35] M. Buciumeanu, D. Faria, J. Mesquita-Guimarães, F. Silva, Tribological characterization of bioactive zirconia composite layers on zirconia structures, Ceramics International 44(15) (2018) 18663-18671.

[36] A. Paksheresht, H.A. Baghbaderani, R. Yazdani-Rad, Role of different fractions of nano-size SiC and milling time on the microstructure and mechanical properties of Al–SiC nanocomposites, Transactions of the Indian Institute of Metals 69(5) (2016) 1007-1014.

[37] M.D. Chermahini, M. Rahimipour, A. Paksheresht, Microstructure and magnetic properties of nanostructured Fe–Co powders prepared by series of milling and annealing treatments, Advanced Powder Technology 25(1) (2014) 462-466.

[38] K. Shirvanimoghaddam, E. Ghasali, A. Paksheresht, S. Derakhshandeh, M. Alizadeh, T. Ebadzadeh, M. Naebe, Super hard carbon microtubes derived from natural cotton for development of high performance titanium composites, Journal of Alloys and Compounds 775 (2019) 601-616.

[39] Z. Özkurt, E. Kazazoğlu, Zirconia dental implants: a literature review, Journal of oral implantology 37(3) (2011) 367-376.

[40] S. Rahimi, F. SharifianJazi, A. Esmaeilkhanian, M. Moradi, A.H. Safi Samghabadi, Effect of SiO_2 content on Y-TZP/Al_2O_3 ceramic-nanocomposite properties as potential dental applications, Ceramics International (2020).

[41] M. Nejati, M. Rahimipour, I. Mobasherpour, A. Paksheresht, Microstructural

analysis and thermal shock behavior of plasma sprayed ceria-stabilized zirconia thermal barrier coatings with micro and nano Al_2O_3 as a third layer, Surface and Coatings Technology 282 (2015) 129-138.
[42] N. Pourmohammadie Vafa, B. Nayebi, M. Shahedi Asl, M. Jaberi Zamharir, M. Ghassemi Kakroudi, Reactive hot pressing of ZrB_2-based composites with changes in ZrO_2/SiC ratio and sintering conditions. Part II: Mechanical behavior, Ceramics International 42(2, Part A) (2016) 2724-2733.
[43] A. Apratim, P. Eachempati, K.K.K. Salian, V. Singh, S. Chhabra, S. Shah, Zirconia in dental implantology: A review, Journal of International Society of Preventive & Community Dentistry 5(3) (2015) 147.
[44] A. Hafezeqoran, R. Koodaryan, Effect of zirconia dental implant surfaces on bone integration: a systematic review and meta-analysis, BioMed research international 2017 (2017).
[45] S.P. Victor, C.K.S. Pillai, C.P. Sharma, 1 - Biointegration: an introduction, in: C.P. Sharma (Ed.), Biointegration of Medical Implant Materials (Second Edition), Woodhead Publishing (2020), pp. 1-16.
[46] T.J. Matsumoto, S.-H. An, T. Ishimoto, T. Nakano, T. Matsumoto, S. Imazato, Zirconia–hydroxyapatite composite material with micro porous structure, Dental materials 27(11) (2011) e205-e212.
[47] J. Izquierdo, G. Bolat, N. Cimpoesu, L.C. Trinca, D. Mareci, R.M. Souto, Electrochemical characterization of pulsed layer deposited hydroxyapatite-zirconia layers on Ti-21Nb-15Ta-6Zr alloy for biomedical application, Applied Surface Science 385 (2016) 368-378.
[48] B. Bulut, Z. Erkmen, E. Kayali, Biocompatibility of Hydroxyapatite-Alumina and Hydroxyapatite-Zirconia Composite including Commercial Inert Glass (CIG) as a Ternary Component, J. Ceram. Sci. Tech 7(03) (2016) 263-276.
[49] C. Leong, A. Muchtar, C. Tan, M. Razali, N.F. Amat, Sintering of hydroxyapatite/yttria stabilized zirconia nanocomposites under nitrogen gas for dental materials, Advances in Materials Science and Engineering 2014 (2014).
[50] O. Carvalho, F. Sousa, S. Madeira, F. Silva, G. Miranda, HAp-functionalized zirconia surfaces via hybrid laser process for dental applications, Optics & Laser Technology 106 (2018) 157-167.
[51] G. Gergely, F.C. Sahin, G. Göller, O. Yücel, C. Balázsi, Microstructural and mechanical investigation of hydroxyapatite–zirconia nanocomposites prepared by spark plasma sintering, Journal of the European Ceramic Society 33(12) (2013) 2313-2319.
[52] V.T. Targhi, H. Omidvar, S.M.M. Hadavi, F. Sharifianjazi, Microstructure and hot corrosion behavior of hot dip siliconized coating on Ni-base superalloy IN-738LC, Materials Research Express (2020).
[53] M. Barekat, R.S. Razavi, F. Sharifianjazi, Synthesis and the surface resistivity of carbon black pigment on black silicone thermal control coating, Synthesis and Reactivity in Inorganic, Metal-Organic, and Nano-Metal Chemistry 45(4) (2015) 502-506.
[54] L. Bazli, M. Siavashi, A. Shiravi, A Review of Carbon Nanotube/TiO_2 Composite Prepared via Sol-Gel Method, Composites and Compounds 1(1) (2019).
[55] A.R. Rouhani, A.H. Esmaeil-Khanian, F. Davar, S. Hasani, The effect of agarose content on the morphology, phase evolution, and magnetic properties of $CoFe_2O_4$ nanoparticles prepared by sol-gel autocombustion method, International Journal of Applied Ceramic Technology 15(3) (2018) 758-765.
[56] V. Salimian Rizi, F. Sharifianjazi, H. Jafarikhorami, N. Parvin, L. Saei Fard, M. Irani, A. Esmaeilkhanian, Sol–gel derived SnO_2/Ag_2O ceramic nanocomposite for H2 gas sensing applications, Materials Research Express 6(11) (2019) 1150g2.
[57] A.H. Paksereshtt, Microstructural Investigation of BaTiO3 Plasma Sprayed Coating Deposited by Splash and Disk-Like Splats, Journal of Environmental Friendly Materials 2(1) (2018) 1-6.
[58] M. Heydari, M.R. Vaezi, A.A. Behnamghader, A.H. Paksereshtt, M. Sarmast, Hydroxyapatite/silica Nanopowders Deposition on Ti Substrate by Plasma Spray Method, Advanced Ceramics Progress 3(4) (2017) 21-24.
[59] A. Jam, S.M.R. Derakhshandeh, H. Rajaei, A.H. Paksereshtt, Evaluation of microstructure and electrochemical behavior of dual-layer NiCrAlY/mullite plasma sprayed coating on high silicon cast iron alloy, Ceramics International 43(16) (2017) 14146-14155.
[60] H. Salimkhani, P. Palmeh, A.B. Khiabani, E. Hashemi, S. Matinpour, H. Salimkhani, M.S. Asl, Electrophoretic deposition of spherical carbonyl iron particles on carbon fibers as a microwave absorbent composite, Surfaces and Interfaces 5 (2016) 1-7.
[61] R.B. Osman, M.V. Swain, A critical review of dental implant materials with an emphasis on titanium versus zirconia, Materials 8(3) (2015) 932-958.
[62] C. Leong, K. Lim, A. Muchtar, N. Yahaya, Decomposition of hydroxyapatite in hydroxyapatite/zirconia composites for dental applications, Advanced Materials Research, Trans Tech Publ, 2013, pp. 1664-1668.
[63] C. Ergun, Enhanced phase stability in hydroxylapatite/zirconia composites with hot isostatic pressing, Ceramics International 37(3) (2011) 935-942.
[64] K.F. Lim, M. Andanastuti, R. Mustaffa, C.Y. Tan, Sintering of HA/Zirconia composite for biomedical and dental applications: A Review, Advanced Materials Research, Trans Tech Publ, 2013, pp. 290-295.
[65] J. Mesquita-Guimarães, R. Detsch, A. Souza, B. Henriques, F. Silva, A. Boccaccini, O. Carvalho, Cell adhesion evaluation of laser-sintered HAp and 45S5 bioactive glass coatings on micro-textured zirconia surfaces using MC3T3-E1 osteoblasts-like cells, Materials Science and Engineering: C (2019) 110492.
[66] N. Cimpoeşu, L.C. Trincă, G. Dascălu, S. Stanciu, S.O. Gurlui, D. Mareci, Electrochemical characterization of a new biodegradable FeMnSi alloy coated with hydroxyapatite-zirconia by PLD technique, Journal of Chemistry 2016 (2016).
[67] F. Sharifianjazi, N. Parvin, M. Tahriri, Synthesis and characteristics of sol-gel bioactive SiO_2-P_2O_5-CaO-Ag_2O glasses, Journal of Non-Crystalline Solids 476 (2017) 108-113.
[68] F. Sharifianjazi, N. Parvin, M. Tahriri, Formation of apatite nano-needles on novel gel derived SiO_2-P_2O_5-CaO-SrO-Ag_2O bioactive glasses, Ceramics International 43(17) (2017) 15214-15220.
[69] Z. Goudarzi, N. Parvin, F. Sharifianjazi, Formation of hydroxyapatite on surface of SiO_2– P_2O_5–CaO–SrO–ZnO bioactive glass synthesized through sol-gel route, Ceramics International 45(15) (2019) 19323-19330.
[70] M.S.N. Shahrbabak, F. Sharifianjazi, D. Rahban, A. Salimi, A Comparative Investigation on Bioactivity and Antibacterial Properties of Sol-Gel Derived 58S Bioactive Glass Substituted by Ag and Zn, Silicon 11(6) (2019) 2741-2751.
[71] F.S. Jazi, N. Parvin, M. Tahriri, M. Alizadeh, S. Abedini, M. Alizadeh, The relationship between the synthesis and morphology of SnO_2-Ag_2O nanocomposite, Synthesis and Reactivity in Inorganic, Metal-Organic, and Nano-Metal Chemistry 44(5) (2014) 759-764.
[72] S. Abedini, N. Parvin, P. Ashtari, F. Jazi, Microstructure, strength and CO_2 separation characteristics of α-alumina supported γ-alumina thin film membrane, Advances in Applied Ceramics 112(1) (2013) 17-22.
[73] H. Vasconcelos, M. Barreto, Tailoring the microstructure of sol–gel derived hydroxyapatite/zirconia nanocrystalline composites, Nanoscale Res Lett 6(1) (2011) 1-5.
[74] S. Salehi, M. Fathi, Fabrication and characterization of sol–gel derived hydroxyapatite/zirconia composite nanopowders with various yttria contents, Ceramics International 36(5) (2010) 1659-1667.
[75] F. Bollino, E. Armenia, E. Tranquillo, Zirconia/hydroxyapatite composites synthesized via Sol-Gel: Influence of hydroxyapatite content and heating on their biological properties, Materials 10(7) (2017) 757.
[76] M. Catauro, F. Bollino, E. Tranquillo, R. Tuffi, A. Dell'Era, S.V. Ciprioti, Morphological and thermal characterization of zirconia/hydroxyapatite composites prepared via sol-gel for biomedical applications, Ceramics International 45(2) (2019) 2835-2845.
[77] S.D. Jin, S.C. Um, J.K. Lee, Surface Modification of Zirconia Substrate by Calcium Phosphate Particles Using Sol–Gel Method, Journal of nanoscience and nanotechnology 15(8) (2015) 5946-5950.
[78] R.T. Candidato Jr, P. Sokołowski, L. Pawłowski, G. Lecomte-Nana, C. Constantinescu, A. Denoirjean, Development of hydroxyapatite coatings by solution precursor plasma spray process and their microstructural characterization, Surface and Coatings Technology 318 (2017) 39-49.
[79] A. Paksereshtt, M. Rahimipour, M. Vaezi, M. Salehi, Effect of plasma spray parameters on the microstructure anddielectric properties of barium titanate coating, DENT 18 (2014) 21.
[80] A.H. Paksereshtt, M.R. Rahimipour, M.R. Vaezi, M. Salehi, Effect of morphology and non-bounded interface on dielectric properties of plasma sprayed $BaTiO_3$ coating, Journal of advanced materials and processing (journal of materials science) 2(4) (2014) 25-32.
[81] A. Paksereshtt, M. Rahimipour, M. Vaezi, M. Salehi, Thermal plasma spheroidization and spray deposition of barium titanate powder and characterization of the plasma sprayable powder, Materials Chemistry and Physics 173 (2016) 395-403.
[82] M.F. Hasan, J. Wang, C. Berndt, Evaluation of the mechanical properties of plasma sprayed hydroxyapatite coatings, Applied surface science 303 (2014) 155-162.
[83] A. Rafieerad, A. Bushroa, B. Nasiri-Tabrizi, S. Baradaran, S. Shahtalebi, S. Khanahmadi, M. Afshar-Mohajer, J. Vadivelu, F. Yusof, W. Basirun, In-vitro bioassay of electrophoretically deposited hydroxyapatite–zirconia nanocomposite coating on Ti–6Al–7Nb implant, Advances in Applied Ceramics 116(6) (2017) 293-306.
[84] M. Sandhyarani, N. Rameshbabu, K. Venkateswarlu, Fabrication, characterization and in-vitro evaluation of nanostructured zirconia/hydroxyapatite composite film on zirconium, Surface and Coatings Technology 238 (2014) 58-67.

[85] K. Sakthiabirami, J.W. Kim, J.H. Kang, K.J. Jang, G.J. Oh, J.G. Fisher, K.D. Yun, H.P. Lim, S.W. Park, Tailoring interfacial interaction through glass fusion in glass/zinc-hydroxyapatite composite coatings on glass-infiltrated zirconia, Ceramics International 44(14) (2018) 16181-16190.
[86] D. Drdlik, M. Slama, H. Hadraba, J. Cihlar, Hydroxyapatite/zirconia-microfibre composites with controlled microporosity and fracture properties prepared by electrophoretic deposition, Ceramics International 41(9) (2015) 11202-11212.
[87] H. Farnoush, Z. Rezaei, Effect of suspension stability on bonding strength and electrochemical behavior of electrophoretically deposited HA–YSZ nanostructured composite coatings, Ceramics International 43(15) (2017) 11885-11897.
[88] D.-j. Kong, D. Long, Y.-z. Wu, C.-z. Zhou, Mechanical properties of hydroxyapatite-zirconia coatings prepared by magnetron sputtering, Transactions of Nonferrous Metals Society of China 22(1) (2012) 104-110.
[89] K. Ozeki, T. Goto, H. Aoki, T. Masuzawa, Fabrication of hydroxyapatite thin films on zirconia using a sputtering technique, Bio-medical materials and engineering 24(5) (2014) 1793-1802.

Available online at www.jourcc.com

Journal homepage: www.JOURCC.com

Journal of Composites and Compounds

A review on the Comsol Multiphysics studies of heat transfer in advanced ceramics

Mohammad Vajdi[a], *Farhad Sadegh Moghanlou*[a]*, *Fariborz Sharifianjazi*[b]

Mehdi Shahedi Asl[a]*, *Mohammadreza Shokouhimehr*[c]

[a] *Department of Mechanical Engineering, University of Mohaghegh Ardabili, Ardabil, Iran*

[b] *Department of Materials and Metallurgical Engineering, Amirkabir University of Technology, PO Box 15875-4413, Tehran, Iran*

[c] *Department of Materials Science and Engineering, Research Institute of Advanced Materials, Seoul National University, Seoul 08826, Republic of Korea*

A B S T R A C T

Numerical simulation is a powerful tool to predict the physical behavior of the designed devices. This method provides detailed information about the investigated phenomenon for each point of the device, which is generally challenging by experiments. Comsol Multiphysics can be utilized in a wide range of engineering fields. This software employs the finite element method (FEM) to solve the physical governing equations. Due to the importance of the heat transfer in advanced ceramics and the potential of the numerical methods to solve the related problems, the present article aims to provide a comprehensive review of the performed numerical research works using Comsol Multiphysics.

Peer review under responsibility of jourcc

A R T I C L E I N F O R M A T I O N

Article history:

Received 5 March 2020

Received in revised form 25 March 2020

Accepted 30 March 2020

Keywords:

Advanced ceramics

Numerical simulation

Comsol Multiphysics

Heat transfer

Table of contents

1. Introduction 35
2. Laser drilling 36
3. Heat exchangers 37
4. Solar energy receivers 37
5. Sintering processes 38
6. Turbine blades 41
7. Cutting tools 41
8. Summary 42

1. Introduction

Thermal systems are generally designed based on three objectives: enhancing system thermal efficiency [1–3], ensuring safety, and increasing service lifespan [4]. Selecting suitable working conditions, and the choice of materials, *e.g.* thermal systems, engine design, tool manufacturing, electronic devices, and biomechanics instruments are the important designing parameters [5, 6]. Advanced ceramics with interesting thermomechanical properties are proven promising materials for the harsh condition applications of high temperatures or corrosive media. These materials have wide applications in aerospace, thermal systems, automotive technology, and manufacturing processes [7–10]. Ceramics are generally brittle and this is problematic in the case of impact or thermal shock. This issue needs to be considered with all aspects to avoid undesirable problems. Obtaining detail information about the physical characteristics of a designed device is a problematic issue, and in some cases, it seems to be impossible. Numerical simulation is a reliable method that provides detailed information at any point of the investigated case. The ability of the numerical methods has been verified in various fields of engineering, including biomechanics [11], energy [12–14], optics [15] micro, and nanotechnology [16, 17].

Comsol Multiphysics, as a commercial software package, provides a user-friendly environment to investigate a wide range of physical phenomena. The various embedded modules cover a wide range of physical

* *Corresponding author: F. Sadegh Moghanlou; E-mail: f_moghanlou@uma.ac.ir and M. Shahedi Asl; E-mail: shahedi@uma.ac.ir*

https://doi.org/10.29252/jcc.2.1.5

Table 1.
Temperature-dependent thermal properties of some advanced ceramics.

Material	ZrB_2	TiB_2 [25–27]	TiC
Heat capacity (J/Kg.K)	$0.704+2.52\times10^{-5}\times T-80.2\times T^{-1}$ [28]	$976+0.21\times(T-273)-426\times10^{-0.008\times(T-273)}$	803+5.744×10^{-2} T - 5.427×10^{-5} T^2 - 23.685×10^6/T^2 [29]
Density (Kg/m^3)	6080 [30]	$77.3+(8270\times10^{-0.002\times(T-273)})\times(410+(T-273))^{-1}$	4930 [31]
Thermal conductivity (W/m.K)	$60.316+0.0041\times T$ [30]	$(0.0431T+10.05)\times10^{-8}$	9.8×10^{-3} T + 23.994 [32]

analyses. The physical governing equations are designed to be solved using the finite element method. Numerous researches using Comsol have shown its ability to provide reliable results.

The present review article explores the heat transfer aspect of advanced ceramics using Comsol Multiphysics. By employing this software, it is possible to combine different active or passive methods to enhance heat transfer in thermal devices. In the active methods, external energy serves to increase the heat transfer rate. In the passive methods, variation in geometry or properties of applied materials augments the heat transfer [18, 19]. This review describes numerical simulations by Comsol Multiphysics covering various fields of heat exchangers, cutting tools, solar and energy systems, optical and manufacturing processes. The governing equations for each application are introduced and the results of the numerical simulation are presented.

2. Laser drilling

Among the various methods of fabrications, laser drilling of ceramics offers several advantages such as fast manufacturing rate, precise production, easy handling, high productivity, and low cost [20,21]. In this method, a high-intensity beam is concentrated on the subjected point to melt and vaporize the applied materials [22]. The transfer process in the heat-affected zone is an essential parameter since improper temperature distribution and consequent thermal stresses may cause damage to the products [23, 24]. Local excessive thermal stress in the heating zone may result in surface and subsurface cracks. The detail information about the cutting process is needed to achieve a precise final product. Numerical simulations give detailed information about the heat transfer mechanism, temperature distribution, and phase change during ablation. It is also possible to insert the solid mechanic equations to acquire resulted thermal stresses, elastic and plastic strains, and the points capable of cracks formation.

The governing equations about the laser drilling process are as follow:

Time-dependent energy conversion equation:

$$\rho C_p \frac{\partial T}{\partial t} = \nabla.(k\nabla T)+Q \quad (1)$$

where ρ (kg/m^3) is density, C_p (J/kg.K) is heat capacity, and k (W/m.K) represents thermal conductivity. Q (W/m^3) belongs to the heat source inside the computational domain.

In numerical simulations, finding suitable temperature-dependent properties is very important. Some of the temperature-dependent thermal properties of several advanced ceramics are given in Table 1.

To simulate the thermal stresses and strains, the following equations are needed:

$$\{\sigma\} = \frac{E\{\alpha\}\Delta T}{1-\nu} \quad (2)$$

where $\{\sigma\}$ (Pa) is thermal stress, $E\{\alpha\}$ (Pa) represents Young's modulus, ΔT (ºC) denotes temperature difference, and ν is Poisson's ratio.

The thermal strain vector is defined as:

$$\{\varepsilon^{th}\} = \{\alpha\}\Delta T \quad (3)$$

The heating effect of the applied laser can be used as a boundary source or boundary heat flux. The commonly used laser power is as [24]:

$$P_s = P_0 \exp(-\frac{r^2}{w_0^2}) \quad (4)$$

where P_s is the intensity of applied laser power (W/m^2), P_0 is the peak power value, r (m) is the radial distance from the beam center, and the w_0 (W/m^2) belongs to the radius, in which the amplitude is 1/e^2.

The heat transfer to the surrounding occurs via all boundaries. Two mechanisms of convection and radiation dissipate the heat from the hot surfaces to the ambient. The convective heat transfer is introduced as Newton cooling law:

$$q_c = h.A.\Delta T \quad (5)$$

where q_c (W) denotes convective heat transfer, A (m^2) is the heat transfer area, and ΔT (ºC) is the temperature difference between the hot surface and ambient fluid. The radiation heat loss is as:

$$q_r = \varepsilon\sigma A(T_w^4 - T_{sur}^4) \quad (6)$$

where q_r (W) is radiative heat transfer to the surroundings, ε is the emissivity factor, and σ ($5.6704\times10^{-8}(\frac{W}{m^2K^4})$) is Steffen-Boltzmann constant.

Bharatish et al. [24] evaluated the thermal residual stresses during the laser drilling of a workpiece made of alumina (Al_2O_3). Some factors, *e.g.* laser power, frequency, hole diameter, and the scanning speed, were investigated. A series of time-dependent numerical simulations were performed to obtain the temperature distribution and predict the ther-

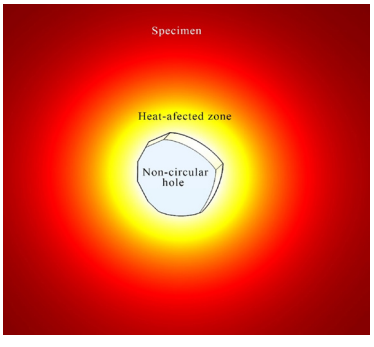

Fig. 1. Schematic of the heat-affected zone in the laser-drilled hole.

mal stresses. The governing equations of transient heat transfer as well as stress-strain equations were solved using Comsol Multiphysics software. The results of simulations were used as validation for Raman thermal residual stresses. The captured scanning probe microscopy (SEM) images also confirmed that the cracks occurred at the heat-affected zone. The schematic of the hole and heat affected zone is shown in Fig. 1. Note that the laser-drilled hole is not circular.

Jia et al. [33] performed some experiments to investigate the micro-hole drilling in an Al_2O_3 ceramic. They used combined laser pulses of a millisecond, assisted a nanosecond (ns) pulse train, and reported that the used energy for drilling was decreased by order of magnitude. They simulated the drilling process using Comsol Multiphysics and showed that the elliptical keyhole ablated by nanosecond pulse train did not affect the circularity of the obtained hole.

Samant et al. [34] proposed a mathematical model to predict machined depth in laser cutting of silicon nitride (Si_3N_4) ceramic. They solved the heat transfer equation to obtain temperature distribution and considered the decomposition of the sample, evaporation because of high heat fluxes, and recoil pressure provoked expulsion of molten material. They reported a reasonable agreement between experimental data and presented a model for most of the cases. The discrepancy, in some cases, was attributed to errors in the measurement of experimental samples depth.

The machining of magnesia (MgO) using pulsed Nd: YAG laser was simulated by Samant and Dahotre [35]. A mathematical model was proposed and the governing equations were solved using Comsol Multiphysics and finally, the results were compared with the experimental data.

The laser drilling of SiC ceramics was investigated by Samant et al. [36]. They claimed that the model is capable of providing required drilling pulses for a given depth of the sample. They also predicted the maximum needed recoil pressure for the melt pool during the drilling.

Wang et al. [37] reviewed the laser drilling of ceramics and referred to some researches performed using Ansys and Comsol. They concluded that the numerical simulations provide important parameters that are involved in the fabrication of high-quality products during the laser drilling of ceramics.

3. Heat exchangers

The application of ceramics as heat exchanger material has attracted more attention in media with high temperatures. Large deformations, oxidation danger, and metallurgical problems confine the application of metals at media with high temperatures or corrosive behavior [38, 39]. Ceramics generally have lower thermal conductivities compared to metals; however, some groups of ceramics such as ZrB_2, TiB_2, SiC, Si_3N_4, AlN, and BeO show astonishing thermal conductivities. The application of these materials in the cooling of thermals systems, especially electrical processors, and optic systems have shown attractive heat transfer enhancement. An exploded view of AlN-made micro heat exchanger is shown in Fig. 2.

Fend et al. [41] performed some computations to simulate a gas/gas heat exchanger made of SiC at high working temperatures. They solved the continuity and momentum equations for fluid flows and the energy equation for both solid domain and fluid flow. The obtained results of the numerical simulation were in reasonable agreement with experimental data. Nekahi et al. [42] investigated the heat transfer and thermal effectiveness of a micro heat exchanger made of TiB_2–SiC ceramic. The governing equations of fluid flow and heat transfer were discretized by the Galerkin method and solved using Comsol Multiphysics software. They compared their results by a micro heat exchanger made of alumina. They reported a 15.5% heat transfer enhancement using TiB_2–SiC ceramic instead of Al_2O_3. This enhancement was attributed to the higher thermal conductivity of TiB_2–SiC compared to Al_2O_3.

The governing equations for the simulation of single-phase (no phase change) heat exchangers are as follow:

Mass conservation equation for fluids:

$$\frac{\partial \rho}{\partial t} + \nabla.(\rho V) = 0 \tag{7}$$

Momentum equation for fluid flow:

$$\frac{\partial V}{\partial t} + v.\nabla V = -\nabla P + \nabla.(\mu(\nabla V + (\nabla V)^T) - \frac{2}{3}\mu(\nabla V)I \tag{8}$$

Energy conservation equation for the ceramic part:

$$\rho C_p \frac{\partial T}{\partial t} = \nabla.(k\nabla T) + Q \tag{9}$$

Energy conservation equation for fluid flow:

$$\rho C_p (\frac{\partial T}{\partial t} + (V.\nabla)T) = \nabla.(k\nabla T) + Q \tag{10}$$

Vajdi et al. [43] investigated a microchannel heat sink made by ZrB_2 numerically. A conjugate heat transfer of solid domain and flow field was considered for simulation, and the governing equations were solved numerically by finite element method. They reported that at the high heat flux of 3.6 MW/m^2, the maximum temperature did not exceed 360 K. Fattahi et al. [40] simulated the fluid flow and heat transfer in a micro heat exchanger made of AlN. Aluminum nitride has attractive properties such as remarkable thermal conductivity, high melting point, and astonishing elastic modulus [44, 45]. As a result of the higher thermal conductivity of AlN compared to Al_2O_3, 59% enhancement in the heat transfer was obtained.

4. Solar energy receivers

Ceramics are an inevitable part of energy harvesting systems nowadays. The thermoelectric refrigerators and generators [46, 47], and photovoltaic systems [48] benefit from the exclusive properties of ceramics. The application of ceramics in solar systems attracts more attention when the high-temperature conditions such as concentrated solar collectors and solar furnaces are encountered. Numerical methods can provide the temperature distribution at each point of the solar system. The obtained temperature gradients can be employed to evaluate consequent thermal stresses.

Ren et al. [49] carried out numerical simulations using Comsol on heat transfer of SiC made ceramic foam in a solar receiver. A schematic of a ceramic foam solar receiver is shown in Fig. 3. Parameters such as thermal conductivity effect, radiation distribution, and the time-dependent response of the proposed receiver were investigated. They found that the thicker the receiver dimension, the higher the efficiency of the system. However, they reported that thickening the receiver structure would increase the production costs. They also concluded that to avoid thermal stress based damages, the standard deviation must be adjusted to the highest possible value.

Wang et al. [50] investigated the thermal radiation in a solar receiver made of SiC. They solved the governing equations for both ceramics and fluid domains. They indicated the Nusselt number counter maps for involved parameters such as solid-fluid thermal conductivity ratio and conduction-radiation parameters. Fend et al. [51] investigated the thermal performance of a honeycomb structure used in a solar tower. Silicon carbide was considered as the material, and two numerical models of single-channel and porous medium were investigated. An experimental set-up was made and used as validation for the numerical results. A good agreement between experimental results and numerical simulation showed the capability of the proposed models.

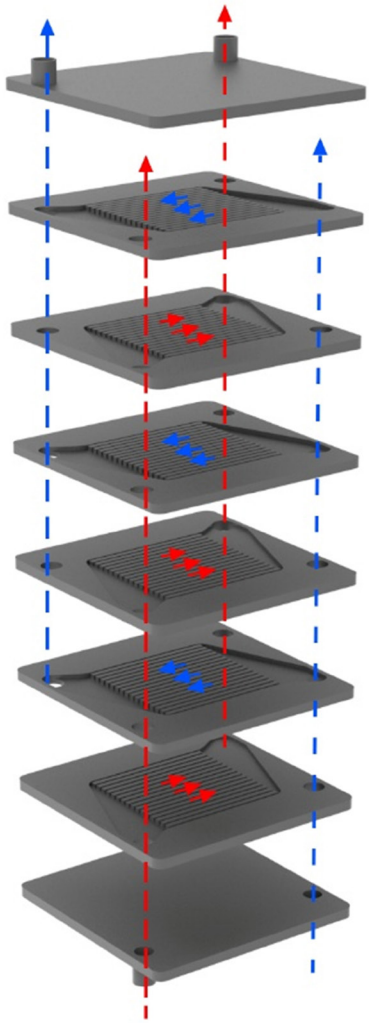

Fig. 2. The exploded view of AlN-made micro heat exchanger. Reproduced with permission [40].

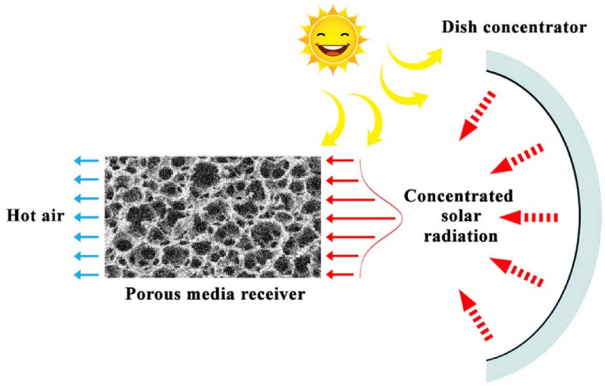

Fig. 3. Scheme of a ceramic foam solar receiver.

5. Sintering processes

Heat transfer during the pressureless sintering of ceramics with low thermal conductivity was simulated by Comsol Multiphysics [52]. The sintered sample was a cylinder heated by convection and conduction mechanisms from a heat source located nearby. The schematic of the sample and furnace used by Salamon et al. [52] is shown in Fig. 4. They reported that the final product was not fully dense, and 14% porosity was obtained with no cracks. The heating rate was in the order of hundreds per minute, and the simulations showed that by considering only the conduction and convection heating mechanisms, the maximum temperature did not exceed 1200 ºC during the sintering. The authors stated that radiation heat transfer is dominant in the rapid sintering of ceramics.

Wei et al. [53] studied the spark plasma sintering (SPS) of ZrC by Comsol Multiphysics. They obtained experimental data of the sintering process and used them to validate the numerical simulations. The 3D sample and die were modeled in a 2D axisymmetric domain to reduce the simulation time. The sample fabricated by the spark plasma sintering showed higher relative density compared to the one obtained by hot pressing (HP). The proposed numerical method could predict the grain size and the consequent relative density, as shown in Fig. 5. Temperature distribution in the sample, die, and punches is given in Fig. 6, which shows the place of maximum temperature at the punches.

Wei et al. [54] studied the capability of SPS in producing net-shaped samples such as ring-shaped or annular ones made of ultrahigh temperature ceramics (UHTCs), which are more complex compared to a solid cylinder or disk. Particular types of graphite die were introduced to consolidate the ZrC powder in the desired shape, as shown in Fig. 7. The numerical simulation by Comsol was used to predict the porosity of an as-sintered annular sample verified by experimental results (Fig. 8). Von Mises stress distribution at different time steps was also obtained. The results showed that stress value at the specimen/mandrel interface was greater than that at the die/specimen interface.

Numerical simulation of heat transfer during SPS of different UHTCs was also investigated. Heat transfer mechanism and temperature distribution during the consolidating of the ZrB_2 powder were studied by Sakkaki et al. [55]. The studied sample was a disk, and heat generation inside the sample was modeled by the Joule heating effect. Since ZrB_2 is electrically conductive, they compared their results with the study of Pavia et al. [56], who modeled the SPS of Al_2O_3 as an electrical insulator

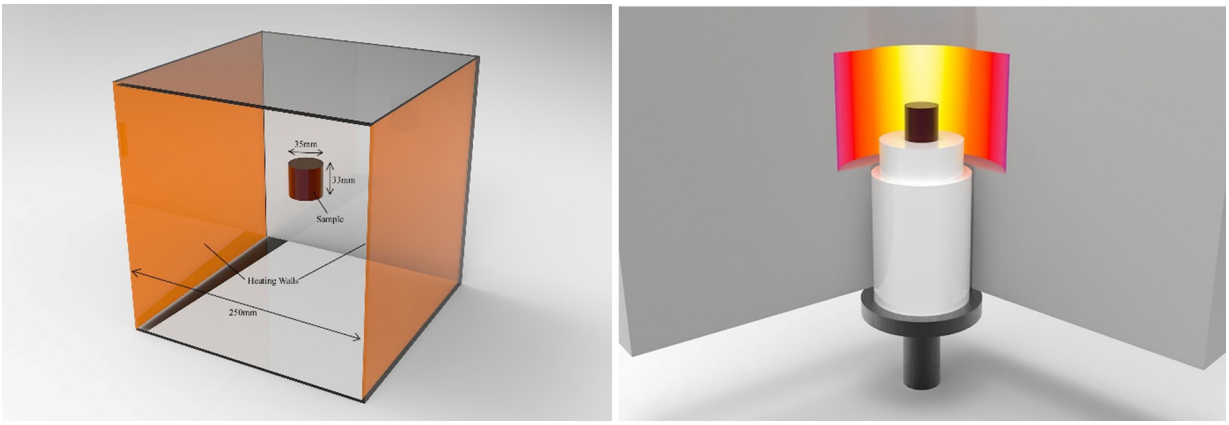

Fig. 4. Schematic of the sample and the furnace used by Salamon et al. Reproduced with permission [52].

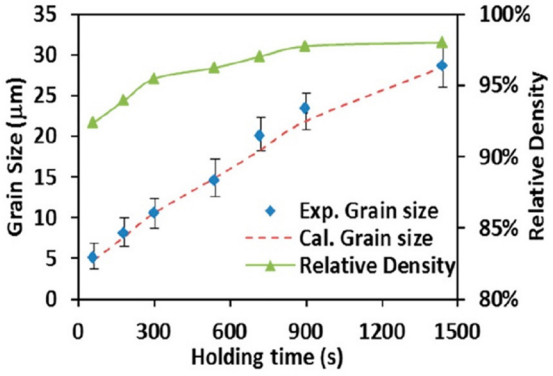

Fig. 5. Numerical simulation validation based on grain size and relative density of ZrC sample. Reproduced with permission [53].

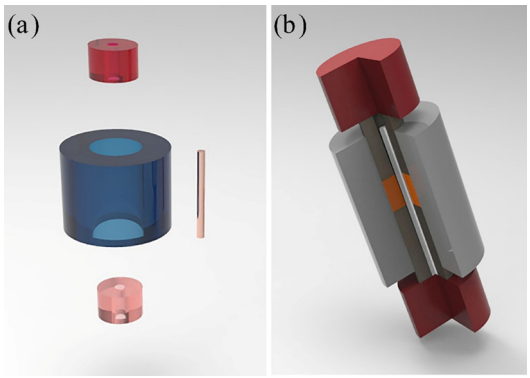

Fig. 7. (a) Exploded view, and (b) assembled form of the schematic of the SPS facility for a ring-shaped sample sintering according to the ref [54].Reproduced with permission [53].

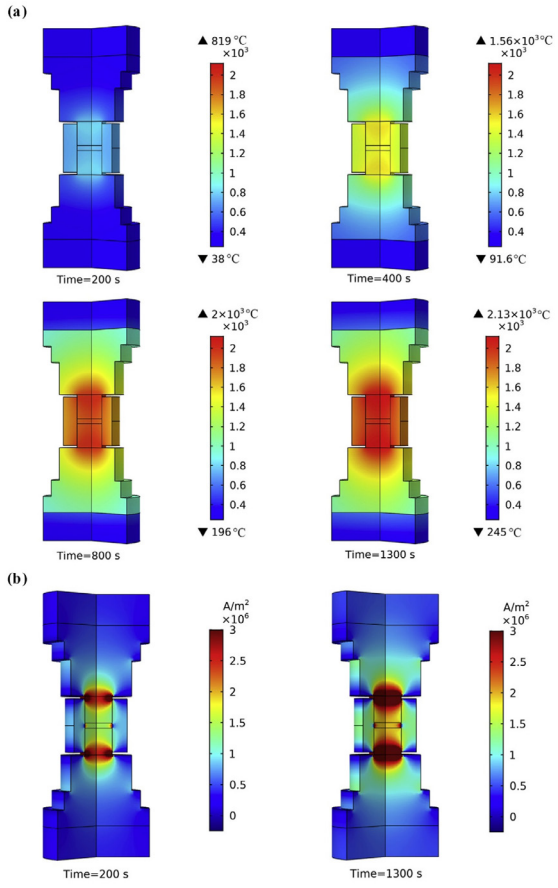

Fig. 9. (a) Temperature contour, and (b) current density contour during SPS of ZrB2. Reproduced with permission [55].

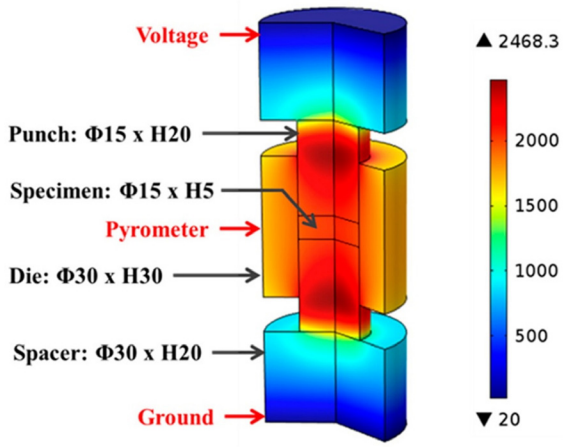

Fig. 6. Temperature (ºC) distribution in the SPS facility and ZrC sample. Reproduced with permission [53].

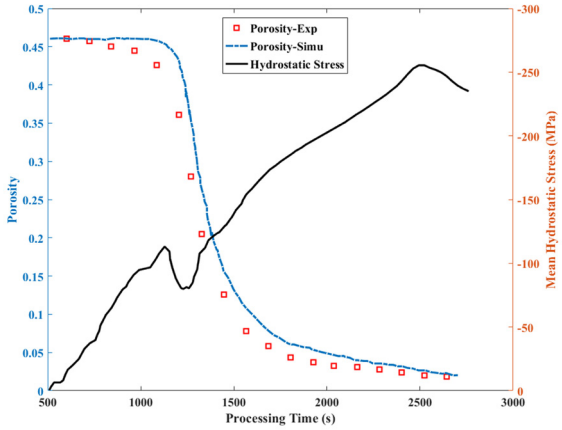

Fig. 8. Comparison of numerical and experimental results of SPS modeling of ZrC. Reproduced with permission [54].

ceramic.

Two sets of governing equations, i.e. electric charge, and energy conservation equations were solved to find the temperature and electric current distribution.

The direct electric (DC) Maxwell's equation is as [57]:

$$\nabla J = \nabla(\sigma E) = \nabla(-\sigma \nabla U) = 0 \tag{11}$$

Where $J(A/m^2)$, $E(V/m)$, $U(V)$ and $\sigma(S/m)$ are responsible for the electric current density, the electric field, the electric potential, and the electrical conductivity of the used materials, respectively.

Concerning the symmetrical shape of the simulated domain, Sakkaki et al. [55] used the axisymmetric form of governing equations. They used the energy conservation equation in the cylindrical form introduced as:

$$\rho C_p \frac{\partial T}{\partial t} = \frac{1}{r}\frac{\partial}{\partial r}\left(rk_r \frac{\partial T}{\partial r}\right) + \frac{1}{z}\frac{\partial}{\partial z}\left(rk_z \frac{\partial T}{\partial z}\right) + q_i \tag{12}$$

where k_r and k_z belong to the thermal conductivity in r and z directions, respectively. The heat generation as a result of Joule heating is shown by q_i which is defined as:

$$q_i = J.E \tag{13}$$

They also used the cylindrical form of the electric current equation as:

$$\frac{1}{r}\frac{\partial(ri_r)}{\partial r} + \frac{\partial i_z}{\partial z} = 0 \tag{14}$$

where i_r and i_z indicate the electrical current densities per volume in the r and z directions, respectively.

They used root–mean–square (RMS) voltage as [56]:

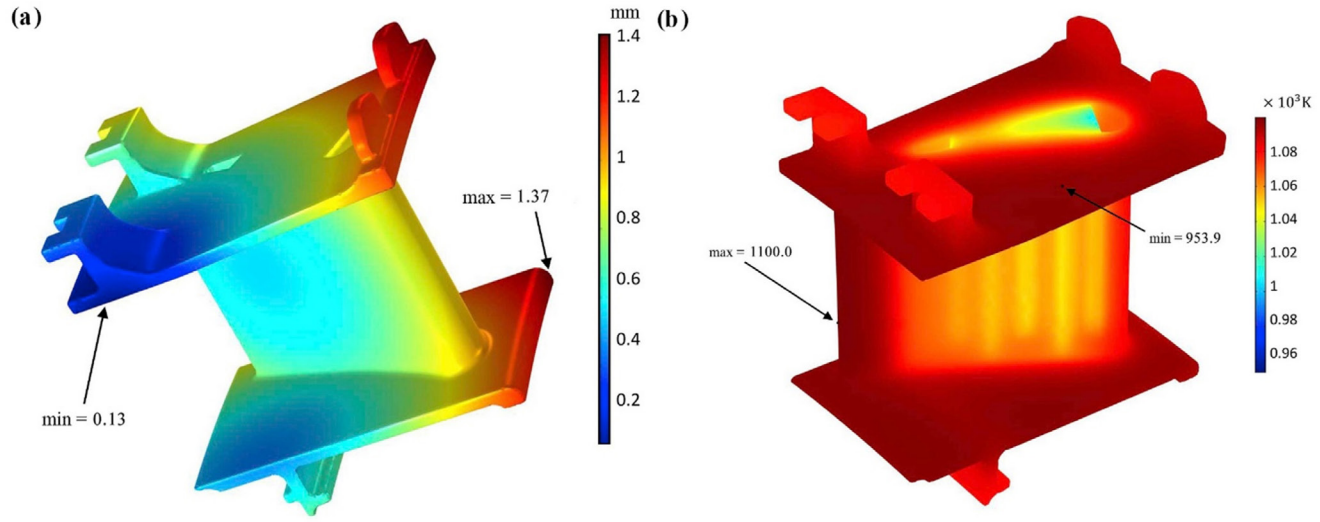

Fig. 10. (a) Displacement, and (b) temperature contours of a gas turbine stator blade made of ZrB_2 ultra high temperature ceramic. Reproduced with permission [60].

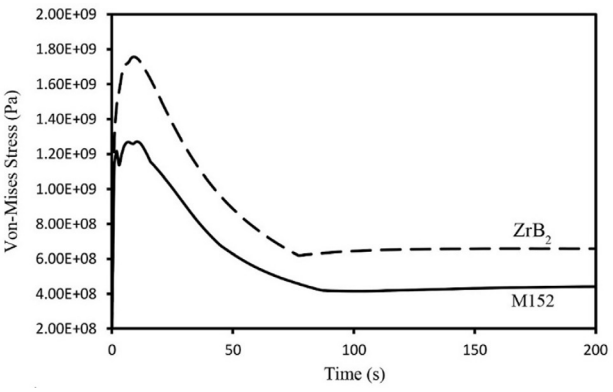

Fig. 11. Von-Mises stress vs. time for gas turbine stator blades made of ZrB_2 ceramic and M152 superalloy. Reproduced with permission [60].

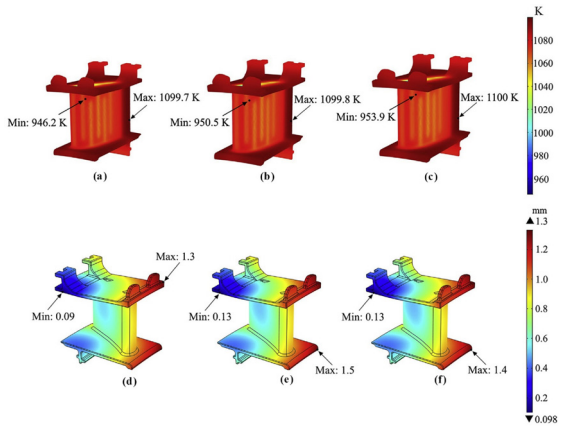

Fig. 12. Temperature contours of turbine stator blades made of (a) HfB_2, (b) TiB2, and (c) ZrB2. Displacement contours of the turbine stator blades made of (d) HfB_2, (e) TiB_2, and (f) ZrB_2 UHTCs. Reproduced with permission [61].

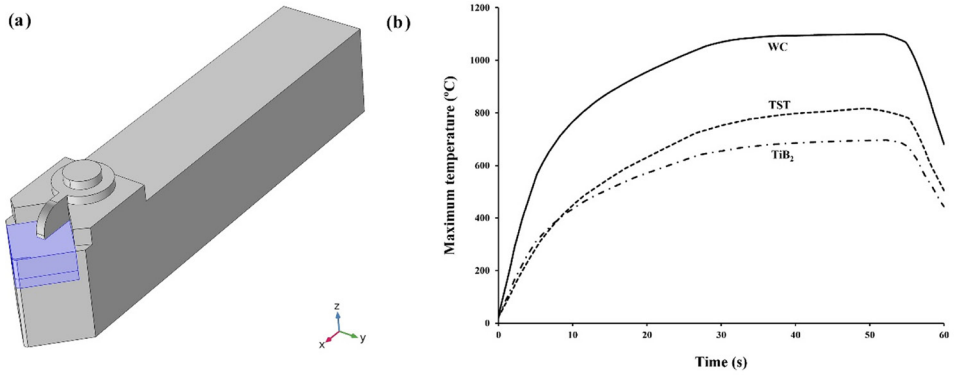

Fig. 13. (a) Cutting tool model in Comsol, and (b) obtained maximum temperature vs. time for different ceramics. Reproduced with permission [62].

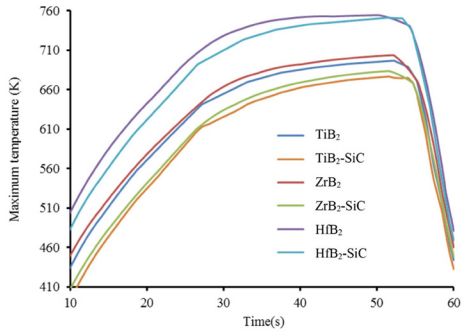

Fig. 14. Effect of SiC addition on the maximum temperature of diboride made cutting tools. Reproduced with permission [63].

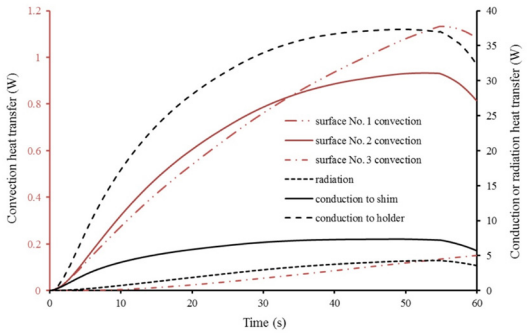

Fig. 15. The portion of different heat transfer mechanisms in heat dissipation from the HfB_2 made cutting tool. Reproduced with permission [63].

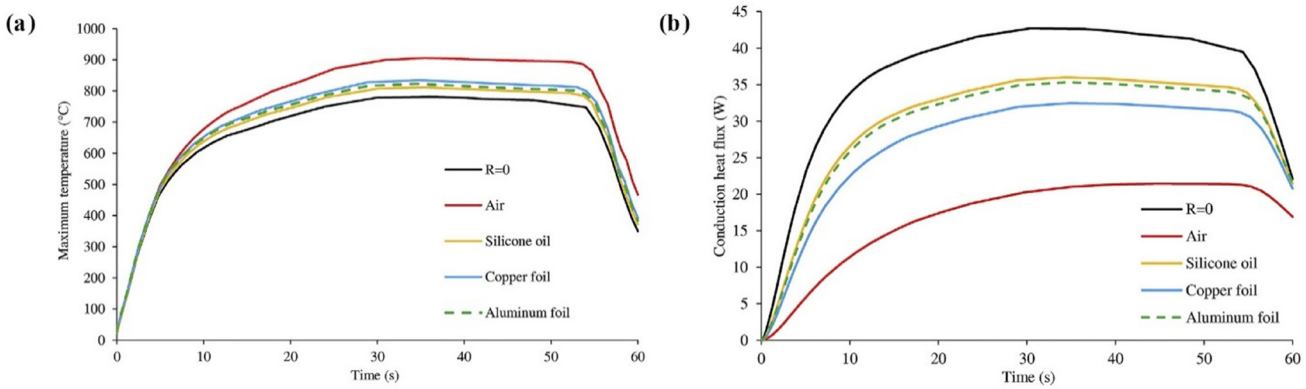

Fig. 16. The effect of different TCRs on the (a) maximum temperature, and (b) heat conduction to the holder and shim. Reproduced with permission [4].

$$U_{RMS} = \sqrt{\frac{1}{P}\int_{t-T}^{t} u^2(\tau)d\tau} \quad (15)$$

where u is the instantaneous voltage, and P is the AC voltage period.

Sakkaki et al. [55] showed that the location of the maximum current density and the maximum temperature are different. The maximum temperature was located at the sample center, while the maximum current density was at the spacer/punch interface due to its minimum area (Fig. 9). The same simulation was performed for TiC [58] and TiB_2 [59]. The results showed that for samples with higher thermal conductivities, a more uniform temperature distribution could be obtained, which has a direct effect on the microstructure of the as-sintered sample.

6. Turbine blades

Gas turbine stator blades experience no centrifugal force and consequent tensile stresses; therefore, ceramics can be good candidates for manufacturing gas turbine stator blades [60]. Sadegh et al. [60] employed Comsol for heat transfer and thermal stress modeling in a gas turbine stator blade made of ZrB_2. Governing equations of heat transfer and stress-strain were considered as equations 1-3. The convective heat transfer coefficient was considered for inner cooling ducts. Since the outer surface encounters hot gases, its effect was considered applying the convective heat transfer coefficient.

The temperature distribution and displacement due to thermal stresses were defined as shown in Fig. 10. The results showed that the ZrB_2-made stator blade acquired considerably lower displacement but higher stress compared to M152 superalloy (Table 2, Fig. 11). Employment of UHTCs like TiB_2 and HfB_2 as the gas turbine stator blades were studied by Vaferi et al. [27] and Nekahi et al. [61], respectively. Vaferi et al. [27] analyzed the thermal stress in a TiB_2 made gas turbine stator blade with Comsol and defined the fatigue possibility of the blade using the Coulomb-Mohr theory. They reported that the blade could tolerate the thermal stresses without failure with the safety factor of 2.4. Nekahi et al. [61] also used Comsol for simulating the heat transfer and calculating the consequent thermal stresses. They compared the temperature and displacement distribution in the blades made of zirconium, titanium, and hafnium diborides (Fig. 12). Employment of HfB_2 as turbine blade material resulted in the lowest displacement and the highest thermal stress values. It was also declared that all three UHTCs could tolerate the applied stresses and no failure predicted based on the Coulomb-Mohr theory.

Table 2.
Comparison of maximum and minimum displacements for turbine blades made of M152 superalloy and ZrB2 UHTC [61].

Material	Maximum displacement (mm)	Minimum displacement (mm)
M152 superalloy	2.27	0.15
ZrB_2 ceramic	1.37	0.13

7. Cutting tools

Ceramics, such as TiB_2 and WC, are widely used as cutting tools due to their excellent hardness [62, 63]. Temperature control and cooling of a cutting device play an essential role in the productivity and quality of the machined surface [63]. Modeling and measuring temperature distribution in cutting tools have attracted much attention lately [4, 64]. Vajdi et al. [62] fabricated a novel TiB_2-based composite using SiC and metallic Ti as reinforcements and measured the thermal properties of fabricated material. Comsol-assisted numerical simulation was applied to determine the temperature distribution in the tool, especially the maximum temperature of the tool tip. They used the heat diffusion equation (Eq. 1) for the solid parts and convection-radiation equation, equations 5 and 6, for heat losses from the walls. The geometry of the cutting tool and the obtained maximum temperature versus time for three different ceramics is demonstrated in Fig. 13. They concluded that the novel TiB_2–SiC–Ti (TST) composite showed better thermal performance than WC made common tools.

Heat transfer in the cutting tools made of different diborides and the effect of SiC addition on the performance of ceramic cutting tools were studied by Sadegh et al. [63]. They conducted a numerical study by Comsol and showed that SiC addition to monolithic ceramics improved their thermal performance. As shown in Fig. 14, the maximum temperature of the cutting tool during a 50-second engagement reduced by adding 20 vol% SiC to the monolithic diborides. The tool transfers the generated heat to the surroundings by radiation, convection, and conduction. To determine the dominant heat transfer mechanism, the authors analyzed each heat transfer mechanism and its portion in the total heat dissipation. The results showed that the most important heat dissipation mechanism was radiation and then conduction to the holder (Fig. 15).

The modeling of the effect of thermal contact resistance (TCR) on the thermal performance of a WC-made cutting tool was performed by Sakkaki et al. [4] employing Comsol Multiphysics. TCR plays an essential role in the heat flow and acts as a barrier; therefore, TCR reduction can ease the heat flow. They showed that an ideal case with no TCR could reduce the maximum temperature considerably, although it was almost impossible due to its high fabrication cost. Moreover, usual methods such as applying silicone or metal foils were proposed, and their effect on heat flow was simulated numerically. In Fig. 16, the effect of different cases on maximum temperature and heat conduction versus

cutting time is shown.

One of the proposed methods to protect the cutting tools from high temperatures is coating their surfaces. Heat transfer and temperature distribution modeling of a coated carbide turning cutting tool was modeled by Ferreira et al. [65]. They used the heat generation at the tool tip according to the results of Brito et al. [64] and obtained the temperature contours in the tool utilizing Comsol Multiphysics. The effect of using TiN and Al_2O_3 as coating materials and their thickness on the thermal performance of the tool was studied. The results showed that Al_2O_3 could protect the WC made cutting tool more than TiN coating as a result of its lower thermal conductivity in comparison with TiN.

8. Summary

Numerical simulations are able to provide the detailed information about the physical behavior of the advanced ceramics in various engineering fields. Comsol Multiphysics, as a numerical simulation pack is a powerful software, which covers a wide range of physical phenomena and provide reliable results. In the present paper, a comprehensive review of numerical studies utilizing Comsol Multiphysics about the heat transfer behavior of some advanced ceramics was carried out. The advantages of advanced ceramics were discussed. Their applications in various fields of engineering products and processes were explained. The performed simulations in laser drilling, heat exchangers, cutting tools, sintering processes, solar systems, and other thermal devices were reviewed. The basic governing equations for each case were given, and some obtained results were depicted. This review article covered the capability of the Comsol Multiphysics to provide reliable results.

REFERENCES

[1] T. Gholizadeh, M. Vajdi, H. Rostamzadeh, A new trigeneration system for power, cooling, and freshwater production driven by a flash-binary geothermal heat source, Renew. Energy. 148 (2020) 31–43. doi:10.1016/j.renene.2019.11.154.

[2] T. Gholizadeh, M. Vajdi, H. Rostamzadeh, Freshwater and cooling production via integration of an ethane ejector expander transcritical refrigeration cycle and a humidification-dehumidification unit, Desalination. 477 (2020) 114259. doi:10.1016/j.desal.2019.114259.

[3] T. Gholizadeh, M. Vajdi, H. Rostamzadeh, Exergoeconomic optimization of a new trigeneration system driven by biogas for power, cooling, and freshwater production, Energy Convers. Manag. 205 (2020) 112417. doi:10.1016/j.enconman.2019.112417.

[4] M. Sakkaki, F. Sadegh Moghanlou, M. Vajdi, F. Pishgar, M. Shokouhimehr, M. Shahedi Asl, The effect of thermal contact resistance on the temperature distribution in a WC made cutting tool, Ceram. Int. 45 (2019) 22196–22202. doi:10.1016/j.ceramint.2019.07.241.

[5] S.K. Yekani, E. Abdi Aghdam, F. Sadegh Moghanlou, Experimental Investigation of The Performance Response of A Spark Ignition Engine to Adding Natural Gas to Gasoline in Lean-Burn Condition, Int. J. Ind. Math. 11 (2019) 307–317.

[6] S.K. Yekani, E. Abdi Aghdam, F. Sadegh Moghanlo, Experimental study and comparison of the exhaust gas emissions response of a spark ignition engine to adding natural gas to gasoline in lean-burn condition, Int. J. Ind. Math. (2020).

[7] F.S. Moghanlou, S. Nekahi, M. Vajdi, Z. Ahmadi, A. Motallebzadeh, A. Shokouhimehr, M. Shokouhimehr, S. Jafargholinejad, M.S. Asl, Effects of graphite nano-flakes on thermal and microstructural properties of TiB2–SiC composites, Ceram. Int. (2020). doi:10.1016/j.ceramint.2020.01.192.

[8] S. Nekahi, F. Sadegh Moghanlou, M. Vajdi, Z. Ahmadi, A. Motallebzadeh, M. Shahedi Asl, Microstructural, thermal and mechanical characterization of TiB2–SiC composites doped with short carbon fibers, Int. J. Refract. Met. Hard Mater. 82 (2019) 129–135. doi:10.1016/j.ijrmhm.2019.04.005.

[9] M. Vajdi, F. Sadegh Moghanlou, Z. Ahmadi, A. Motallebzadeh, M. Shahedi Asl, Thermal diffusivity and microstructure of spark plasma sintered TiB_2/SiC/Ti composite, Ceram. Int. 45 (2019). doi:10.1016/j.ceramint.2019.01.141.

[10] M. Namazizadeh, M. Talebian Gevari, M. Mojaddam, M. Vajdi, Optimization of the Splitter Blade Configuration and Geometry of a Centrifugal Pump Impeller using Design of Experiment, J. Appl. Fluid Mech. 13 (2020) 89–101. doi:10.29252/jafm.13.01.29856.

[11] Z. Hajati, F. Sadegh Moghanlou, M. Vajdi, E. Razavi, S. Matin, Fluid Structure Interaction of blood flow around a vein valve, BioImpacts. (2020).

[12] T. Gholizadeh, M. Vajdi, H. Rostamzadeh, A new biogas-fueled bi-evaporator electricity/cooling cogeneration system: Exergoeconomic optimization, Energy Convers. Manag. 196 (2019) 1193–1207. doi:10.1016/j.enconman.2019.06.053.

[13] T. Gholizadeh, M. Vajdi, F. Mohammadkhani, Thermodynamic and thermoeconomic analysis of basic and modified power generation systems fueled by biogas, Energy Convers. Manag. 181 (2019) 463–475. doi:10.1016/j.enconman.2018.12.011.

[14] T. Gholizadeh, M. Vajdi, H. Rostamzadeh, Energy and exergy evaluation of a new bi-evaporator electricity/cooling cogeneration system fueled by biogas, J. Clean. Prod. 233 (2019) 1494–1509. doi:10.1016/j.jclepro.2019.06.086.

[15] S. Singh, R.S. Kaler, Performance analysis of evanescent wave absorption plasmonic optical sensor with COMSOL FEM method simulation, Procedia Comput. Sci. 125 (2018) 376–381. doi:10.1016/j.procs.2017.12.049.

[16] R.S. Jakati, K.B. Balavalad, B.G. Sheeparamatti, Comparative analysis of different micro-pressure sensors using comsol multiphysics, in: 2016 Int. Conf. Electr. Electron. Commun. Comput. Optim. Tech., IEEE, 2016: pp. 355–360. doi:10.1109/ICEECCOT.2016.7955245.

[17] H. Fu, M. Zhang, J. Ding, J. Wu, Y. Zhu, H. Li, Q. Wang, C. Yang, A high sensitivity D-type surface plasmon resonance optical fiber refractive index sensor with graphene coated silver nano-columns, Opt. Fiber Technol. 48 (2019) 34–39. doi:10.1016/j.yofte.2018.12.017.

[18] M. Sakkaki, F. Sadegh Moghanlou, S. Parvizi, H. Baghbanijavid, A. Babapoor, M. Shahedi Asl, Phase change materials as quenching media for heat treatment of 42CrMo4 steels, J. Cent. South Univ. (2020).

[19] F.S. Moghanlou, A.S. Khorrami, E. Esmaeilzadeh, H. Aminfar, Experimental study on electrohydrodynamically induced heat transfer enhancement in a minichannel, Exp. Therm. Fluid Sci. 59 (2014) 24–31. doi:10.1016/j.expthermflusci.2014.07.019.

[20] A.N. Samant, N.B. Dahotre, Laser machining of structural ceramics—A review, J. Eur. Ceram. Soc. 29 (2009) 969–993. doi:10.1016/j.jeurceramsoc.2008.11.010.

[21] A.S. Kuar, B. Doloi, B. Bhattacharyya, Modelling and analysis of pulsed Nd:YAG laser machining characteristics during micro-drilling of zirconia (ZrO2), Int. J. Mach. Tools Manuf. 46 (2006) 1301–1310. doi:10.1016/j.ijmachtools.2005.10.016.

[22] K. Salonitis, A. Stournaras, G. Tsoukantas, P. Stavropoulos, G. Chryssolouris, A theoretical and experimental investigation on limitations of pulsed laser drilling, J. Mater. Process. Technol. 183 (2007) 96–103. doi:10.1016/j.jmatprotec.2006.09.031.

[23] B.S. Yilbas, C. Karatas, A.F.M. Arif, B.J. Abdul Aleem, Laser control melting of alumina surfaces and thermal stress analysis, Opt. Laser Technol. 43 (2011) 858–865. doi:10.1016/j.optlastec.2010.10.009.

[24] A. Bharatish, H.N. Narasimha Murthy, G. Aditya, B. Anand, B.S. Satyanarayana, M. Krishna, Evaluation of thermal residual stresses in laser drilled alumina ceramics using Micro-Raman spectroscopy and COMSOL Multiphysics, Opt. Laser Technol. 70 (2015) 76–84. doi:10.1016/j.optlastec.2015.01.009.

[25] C. Subramanian, T.S.R.C. Murthy, A.K. Suri, Synthesis and consolidation of titanium diboride, Int. J. Refract. Met. Hard Mater. 25 (2007) 345–350. doi:10.1016/j.ijrmhm.2006.09.003.

[26] A.D. McLEOD, J.S. HAGGERTY, D.R. SADOWAY, Electrical Resistivities of Monocrystalline and Polycrystalline TiB 2, J. Am. Ceram. Soc. 67 (1984) 705–708. doi:10.1111/j.1151-2916.1984.tb19505.x.

[27] K. Vaferi, S. Nekahi, M. Vajdi, F. Sadegh Moghanlou, M. Shokouhimehr, A. Motallebzadeh, J. Sha, M. Shahedi Asl, Heat transfer, thermal stress and failure analyses in a TiB2 gas turbine stator blade, Ceram. Int. 45 (2019) 19331–19339. doi:10.1016/j.ceramint.2019.06.184.

[28] F. Nakamori, Y. Ohishi, H. Muta, K. Kurosaki, K. Fukumoto, S. Yamanaka, Mechanical and thermal properties of bulk ZrB 2, J. Nucl. Mater. 467 (2015) 612–617. doi:10.1016/j.jnucmat.2015.10.024.

[29] M. Le Flem, A. Allemand, S. Urvoy, D. Cédat, C. Rey, Microstructure and thermal conductivity of Mo–TiC cermets processed by hot isostatic pressing, J. Nucl. Mater. 380 (2008) 85–92. doi:10.1016/j.jnucmat.2008.01.033.

[30] E. Zapata-Solvas, D.D. Jayaseelan, H.T. Lin, P. Brown, W.E. Lee, Mechanical properties of ZrB2- and HfB2-based ultra-high temperature ceramics fabricated by spark plasma sintering, J. Eur. Ceram. Soc. 33 (2013) 1373–1386. doi:10.1016/j.jeurceramsoc.2012.12.009.

[31] N. Durlu, Titanium carbide based composites for high temperature applications, J. Eur. Ceram. Soc. 19 (1999) 2415–2419. doi:10.1016/S0955-2219(99)00101-6.

[32] W.S. Williams, The thermal conductivity of metallic ceramics, JOM. 50 (1998) 62–66. doi:10.1007/s11837-998-0131-y.

[33] X. Jia, G. Zhu, Y. Zhang, Y. Chen, H. Wang, P. Shan, K. Aleksei, X. Zhu,

Laser processing of alumina ceramic by spatially and temporally superposing the millisecond pulse and nanosecond pulse train, Opt. Express. 28 (2020) 676. doi:10.1364/OE.381605.

[34] A.N. Samant, N.B. Dahotre, Ab initio Physical Analysis of Single Dimensional Laser Machining of Silicon Nitride, Adv. Eng. Mater. 10 (2008) 978–981. doi:10.1002/adem.200800146.

[35] A.N. Samant, N.B. Dahotre, An integrated computational approach to single-dimensional laser machining of magnesia, Opt. Lasers Eng. 47 (2009) 570–577. doi:10.1016/j.optlaseng.2008.10.001.

[36] A.N. Samant, C. Daniel, R.H. Chand, C.A. Blue, N.B. Dahotre, Computational approach to photonic drilling of silicon carbide, Int. J. Adv. Manuf. Technol. 45 (2009) 704–713. doi:10.1007/s00170-009-2004-0.

[37] H. Wang, H. Lin, C. Wang, L. Zheng, X. Hu, Laser drilling of structural ceramics—A review, J. Eur. Ceram. Soc. 37 (2017) 1157–1173. doi:10.1016/j.jeurceramsoc.2016.10.031.

[38] A. Traverso, A.F. Massardo, R. Scarpellini, Externally Fired micro-Gas Turbine: Modelling and experimental performance, Appl. Therm. Eng. 26 (2006) 1935–1941. doi:10.1016/j.applthermaleng.2006.01.013.

[39] K.M. Deen, M.A. Virk, C.I. Haque, R. Ahmad, I.H. Khan, Failure investigation of heat exchanger plates due to pitting corrosion, Eng. Fail. Anal. 17 (2010) 886–893. doi:10.1016/j.engfailanal.2009.10.023.

[40] M. Fattahi, K. Vaferi, M. Vajdi, F. Sadegh Moghanlou, A. Sabahi Namini, M. Shahedi Asl, Aluminum nitride as an alternative ceramic for fabrication of microchannel heat exchangers: A numerical study, Ceram. Int. (2020). doi:10.1016/j.ceramint.2020.01.195.

[41] O. Smirnova, T. Fend, D. Schöllgen, Numeric modeling of a compact high temperature heat exchanger., in: COMSOL Coference Proc., 2011.

[42] S. Nekahi, M. Vajdi, F. Sadegh Moghanlou, K. Vaferi, A. Motallebzadeh, M. Özen, U. Aydemir, J. Sha, M. Shahedi Asl, TiB2–SiC-based ceramics as alternative efficient micro heat exchangers, Ceram. Int. (2019). doi:10.1016/j.ceramint.2019.06.150.

[43] M. Vajdi, F. Sadegh Moghanlou, E. Ranjbarpour Niari, M. Shahedi Asl, M. Shokouhimehr, Heat transfer and pressure drop in a ZrB2 microchannel heat sink: A numerical approach, Ceram. Int. (2019). doi:10.1016/j.ceramint.2019.09.146.

[44] G. Hansdah, B.K. Sahoo, Pyroelectric Property of Binary Nitrides (AlN, GaN and InN), Int. J. Thermophys. 40 (2019) 20. doi:10.1007/s10765-019-2481-9.

[45] G.A. Slack, R.A. Tanzilli, R.O. Pohl, J.W. Vandersande, The intrinsic thermal conductivity of AIN, J. Phys. Chem. Solids. 48 (1987) 641–647. doi:10.1016/0022-3697(87)90153-3.

[46] F.-D. Börner, M. Schreier, B. Feng, W. Lippmann, H.-P. Martin, A. Michaelis, A. Hurtado, Development of laser-based joining technology for the fabrication of ceramic thermoelectric modules, J. Mater. Res. 29 (2014) 1771–1780. doi:10.1557/jmr.2014.216.

[47] S. Shittu, G. Li, X. Zhao, X. Ma, Y.G. Akhlaghi, E. Ayodele, High performance and thermal stress analysis of a segmented annular thermoelectric generator, Energy Convers. Manag. 184 (2019) 180–193. doi:10.1016/j.enconman.2019.01.064.

[48] Y. Du, W. Tao, Y. Liu, J. Jiang, H. Huang, Heat transfer modeling and temperature experiments of crystalline silicon photovoltaic modules, Sol. Energy. 146 (2017) 257–263. doi:10.1016/j.solener.2017.02.049.

[49] Y. Ren, H. Qi, J. Shi, Q. Chen, Y. Wang, L. Ruan, Thermal Performance Characteristics of Porous Media Receiver Exposed to Concentrated Solar Radiation, J. Energy Eng. 143 (2017) 04017013. doi:10.1061/(ASCE)EY.1943-7897.0000448.

[50] P. Wang, K. Vafai, D.Y. Liu, Analysis of Radiative Effect under Local Thermal Non-Equilibrium Conditions in Porous Media-Application to a Solar Air Receiver, Numer. Heat Transf. Part A Appl. 65 (2014) 931–948. doi:10.1080/10407782.2013.850917.

[51] T. Fend, P. Schwarzbözl, O. Smirnova, D. Schöllgen, C. Jakob, Numerical investigation of flow and heat transfer in a volumetric solar receiver, Renew. Energy. 60 (2013) 655–661. doi:10.1016/j.renene.2013.06.001.

[52] D. Salamon, R. Kalousek, J. Zlámal, K. Maca, Role of conduction and convection heat transfer during rapid crack-free sintering of bulk ceramic with low thermal conductivity, J. Eur. Ceram. Soc. 36 (2016) 2955–2959. doi:10.1016/j.jeurceramsoc.2015.11.034.

[53] X. Wei, C. Back, O. Izhvanov, C. Haines, E. Olevsky, Zirconium Carbide Produced by Spark Plasma Sintering and Hot Pressing: Densification Kinetics, Grain Growth, and Thermal Properties, Materials (Basel). 9 (2016) 577. doi:10.3390/ma9070577.

[54] X. Wei, O. Izhvanov, C. Back, C.D. Haines, D.G. Martin, K.S. Vecchio, E.A. Olevsky, Spark plasma sintering of structure-tailored ultrahigh-temperature components: First step to complex net shaping, J. Am. Ceram. Soc. (2018). doi:10.1111/jace.15752.

[55] M. Sakkaki, F. Sadegh Moghanlou, M. Vajdi, M. Shahedi Asl, M. Mohammadi, M. Shokouhimehr, Numerical simulation of heat transfer during spark plasma sintering of zirconium diboride, Ceram. Int. 46 (2020) 4998–5007. doi:10.1016/j.ceramint.2019.10.240.

[56] A. Pavia, L. Durand, F. Ajustron, V. Bley, G. Chevallier, A. Peigney, C. Estournès, Electro-thermal measurements and finite element method simulations of a spark plasma sintering device, J. Mater. Process. Technol. 213 (2013) 1327–1336. doi:10.1016/j.jmatprotec.2013.02.003.

[57] C. Wang, L. Cheng, Z. Zhao, FEM analysis of the temperature and stress distribution in spark plasma sintering: Modelling and experimental validation, Comput. Mater. Sci. 49 (2010) 351–362. doi:10.1016/j.commatsci.2010.05.021.

[58] S. Mohammad Bagheri, M. Vajdi, F. Sadegh Moghanlou, M. Sakkaki, M. Mohammadi, M. Shokouhimehr, M. Shahedi Asl, Numerical modeling of heat transfer during spark plasma sintering of titanium carbide, Ceram. Int. 46 (2020) 7615–7624. doi:10.1016/j.ceramint.2019.11.262.

[59] M. Fattahi, M. Najafi Ershadi, M. Vajdi, F. Sadegh Moghanlou, A. Sabahi Namini, M. Shahedi Asl, On the simulation of spark plasma sintered TiB2 ultra high temperature ceramics: A numerical approach, Ceram. Int. (2020). doi:10.1016/j.ceramint.2020.03.003.

[60] F. Sadegh Moghanlou, M. Vajdi, A. Motallebzadeh, J. Sha, M. Shokouhimehr, M. Shahedi Asl, Numerical analyses of heat transfer and thermal stress in a ZrB2 gas turbine stator blade, Ceram. Int. 45 (2019) 17742–17750. doi:10.1016/j.ceramint.2019.05.344.

[61] S. Nekahi, K. Vaferi, M. Vajdi, F. Sadegh Moghanlou, M. Shahedi Asl, M. Shokouhimehr, A numerical approach to the heat transfer and thermal stress in a gas turbine stator blade made of HfB2, Ceram. Int. 45 (2019) 24060–24069. doi:10.1016/j.ceramint.2019.08.112.

[62] M. Vajdi, F. Sadegh Moghanlou, Z. Ahmadi, A. Motallebzadeh, M. Shahedi Asl, Thermal diffusivity and microstructure of spark plasma sintered TiB2SiC Ti composite, Ceram. Int. 45 (2019) 8333–8344. doi:10.1016/j.ceramint.2019.01.141.

[63] F. Sadegh Moghanlou, M. Vajdi, J. Sha, A. Motallebzadeh, M. Shokouhimehr, M. Shahedi Asl, A numerical approach to the heat transfer in monolithic and SiC reinforced HfB2, ZrB2 and TiB2 ceramic cutting tools, Ceram. Int. 45 (2019) 15892–15897. doi:10.1016/j.ceramint.2019.05.095.

[64] R.F. Brito, S.R. Carvalho, S.M.M. Lima E Silva, Experimental investigation of thermal aspects in a cutting tool using comsol and inverse problem, Appl. Therm. Eng. 86 (2015) 60–68. doi:10.1016/j.applthermaleng.2015.03.083.

[65] D.C. Ferreira, E. dos S. Magalhães, R.F. Brito, S.M.M. Lima E Silva, Numerical analysis of the influence of coatings on a cutting tool using COMSOL, Int. J. Adv. Manuf. Technol. 97 (2018) 1305–1314. doi:10.1007/s00170-018-1855-7.

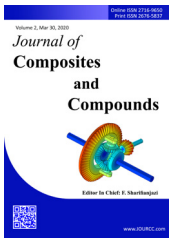

Available online at www.jourcc.com

Journal homepage: www.JOURCC.com

Journal of Composites and Compounds

Production and characterization of PCL (Polycaprolactone) coated TCP/nanoBG composite scaffolds by sponge foam method for orthopedic applications

Jeiran Daraei[a]*

[a] *Materials Engineering Department, Islamic Azad University, Najafabad Branch, Isfahan, Iran*

A B S T R A C T

Bio-ceramics are a set of ceramic materials that possess an important feature called biocompatibility. Bioglass is one of the most applicable ceramic materials contributing to bioactivity improvement due to the presence of Si as an ossification material. Besides, PCL polymer supported by bioglass nanoparticles was used to improve the mechanical properties. In this study, we combined Tricalciumphosphate (TCP) with nano-bioglass (NBG) with four different amounts (10%, 20%, 30%, and 0%) to produce composite scaffolds (lost sponge foam method); then, we coated these composites by Polycaprolactone (PCL) biopolymer, and eventually, evaluated its bioactivity, biodegradability, and mechanical properties. Scanning electron microscopy (SEM) and EDS methods were employed to investigate the morphology and bioactivity of scaffolds. The results of the ion concentration measurement test and SEM and EDS analysis showed the formation of Apatite on the scaffold's surface. The results from SEM indicate that the most bioactivity was observed for composite scaffold containing 20%wt of nano-bioglass presenting it as the preferable sample, in terms of mechanical properties and bioactivity.

Peer review under responsibility of jourcc

A R T I C L E I N F O R M A T I O N

Article history:
Received 15 March 2020
Received in revised form 28 March 2020
Accepted 30 March 2020

Keywords:
Tissue engineering
Tricalcium phosphate
Nanocomposite scaffold
Nanobioglass
Polycaprolactone

1. Introduction

Pathological degeneration, trauma, tumor resection, and congenital deformities are the main factors affecting orthopedic and dental treatments [1, 2]. One of the most effective ways for bone regeneration is bone tissue engineering (BTE) [3, 4]. To overcome the restrictions of damaged tissues or organs and provide biological alternatives, treatment of BTE has been practiced clinically [5, 6]. Using biomaterials for the production of scaffolds is a promising BTE technique. These scaffolds support new tissue growth by the provision of an artificial extracellular matrix [7, 8]. The role of these scaffolds is to provide daily mastication capability like a natural bone in order to build support for the regeneration region and simultaneously undergo gradual degradation with the regeneration of tissue. Acceptable mechanical strength, suitable physicochemical properties, proper surface morphology and porosity, biocompatibility, controllable biodegradability, and osteoconductivity are the most important properties that a well-functioning scaffold should possess [9-11]. Common scaffolds for BTE are currently various bioactive glass, calcium phosphate, and hydroxyapatite (HA) [12, 13]. Tricalcium phosphate (β-TCP) exhibits promising biodegradability, osteoconductivity, and biocompatibility [14]. On the other hand, this bioceramic also has drawbacks; for instance, its degradation rate is higher than bone regeneration [15, 16]. Additionally, because of having a porous structure, the mechanical properties of β-TCP as a support for cell growth is relatively poor [17, 18]. As composites materials provide the opportunity to combine the properties of incorporated components [19, 20], several studies have been focused on the production of composite scaffolds consisting of polymers and β-TCP for improving osteoconductivity and the mechanical properties of the scaffold to overcome these shortcomings. Polymer/ceramic composites have offered promising properties due to benefiting from both materials properties [21-23]. Chitosan and collagen are natural polymers that are used to produce composites [24-26], but these natural polymers do not have sufficient mechanical strength [27]. Polylactic acid and poly-ε-caprolactone (PCL) are synthetic polymers that have been used for overcoming the disadvantages of natural polymers [28, 29]. Owing to biocompatibility, biodegradability, and good mechanical properties, PCL have been widely investigated [23, 30]. Moreover, bioglass materials with different compositions can be integrated with living bone tissue by creating an intimate bond. The bioglasses that are able to form a bond with the bone are called "bioactive". Several studies investigated the production of scaffolds of PCL coated TCP, but no research focused on PCL coated TCP/nanoBG composite scaffolds synthesized via sponge foam method for orthopedic applications to the best of authors' knowledge. Therefore, in this study, we prepared TCP-bioglass composite scaffolds with different compositions. To enhance the mechanical properties of the scaffolds, they were coated by

* *Corresponding author: Jeiran Daraeia; E-mail: jeirandaraei20@gmail.com*
https://doi.org/10.29252/jcc.2.1.6

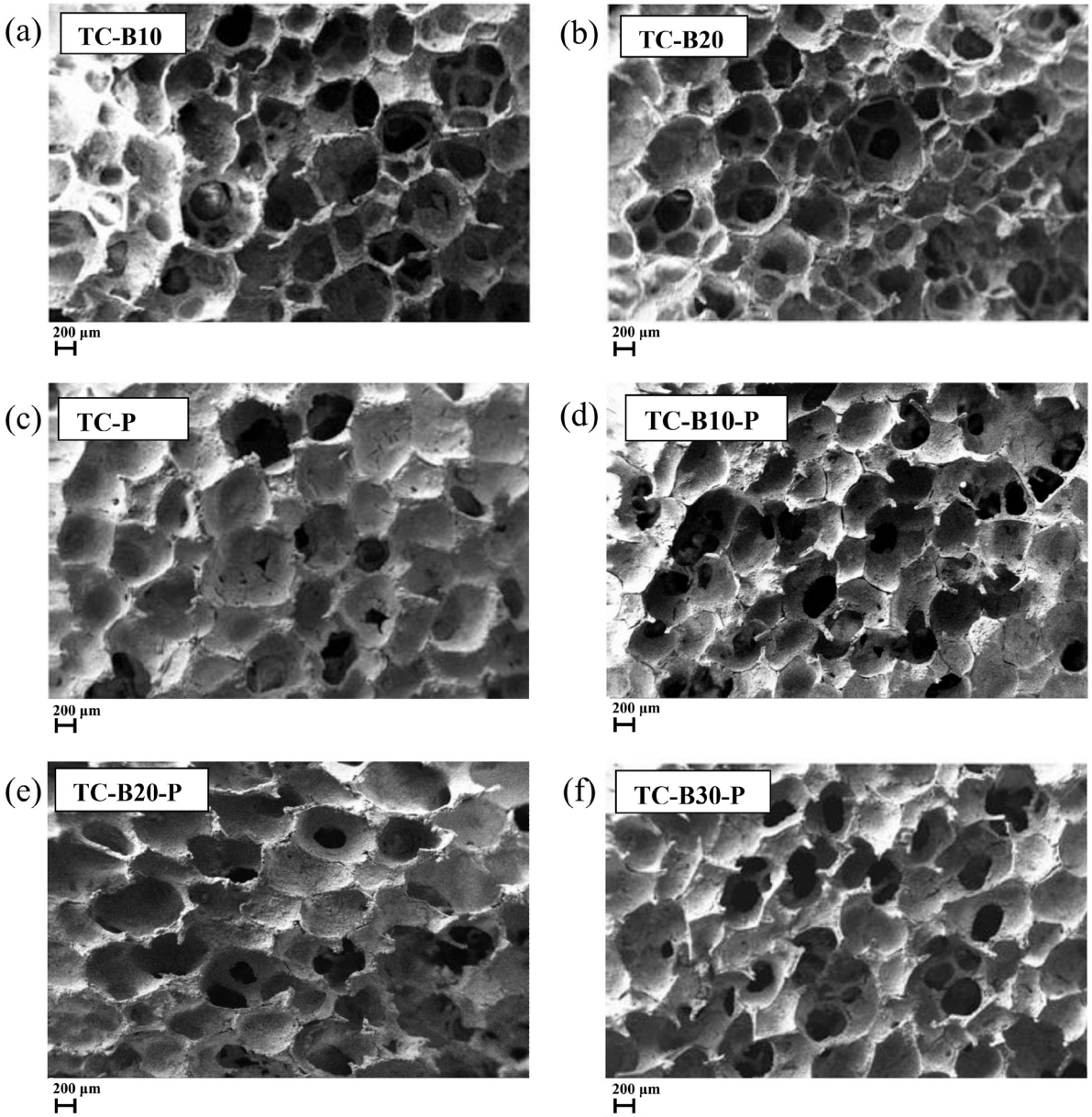

Fig. 1. SEM images TCP/bioglass/PCL composite scaffolds of (a) TC-B10, (b) TC-B20, (c)TC-P, (d) TC-B10-P, (e) TC-B20-P, and (f) TC-B30-P

a polycaprolactone biopolymer, and their mechanical, bioactivity, and biodegradation were evaluated.

2. Experimental

2.1. Materials

In this study, calcium nitrate tetrahydrate ($Ca(NO_3)_2 \cdot 4H_2O$), TEOS ($(C_2H_5O)_4Si$), PCL polymer (molecular weight of 80,000) and tetraethyl phosphate ($(C_2H_5O)_3$ PO) were bought from Aldrich company. Simulated body fluid) SBF), sodium tripolyphosphate solvent, carboxymethyl cellulose powder, nitric acid (63%), and chloroform (99.5%) were obtained from Merck company, Germany.

2.2. Sample preparation

2.2.1. Production of TCP particles

After boiling the cow thigh in water for 2 hours to remove residual tissue, the bone was kept at 60 ° C for 24 hours in an oven to dry. Then, the bone pieces were burnt by fire flame at about 400 ° C for 3 h to degrade the organic components of the bone. The obtained black ash was heated at 900 °C for 2 h to produce hydroxyapatite powder.

2.2.2. Synthesis of bioglass nanoparticles (nanoBG)

For the preparation of bioactive glass, raw materials including calcium nitrate (28 mol. %), TEOS (63 mol. %), and tetraethyl phosphate (9 mol. %) were used. Ethanol and hydrochloric acid were also used as a solvent and a catalyst, respectively. To prepare the sol, the solution of deionized water and hydrochloric acid was stirred by a magnetic stirrer for 30 min. After adding TEOS and ethanol with a molar ratio of 1, the solution was stirred for another 30 minutes following the addition of tetraethyl phosphate and stirring for 20 min. Finally, it was stirred at medium speed for 2 hours with the addition of calcium nitrate. After gelation of the initial solution, the formed gel was dried at 60 °C for 10 h. To eliminate excess gases, the gel was heat-treated for 15 h at 130 °C. Finally, by heating the dried gel at 900 °C for 2 h, bioglass was obtained as the final product of the operation.

2.2.3. Preparation of ceramic slurry and scaffolds

The obtained tricalcium phosphate powders with a mean particle

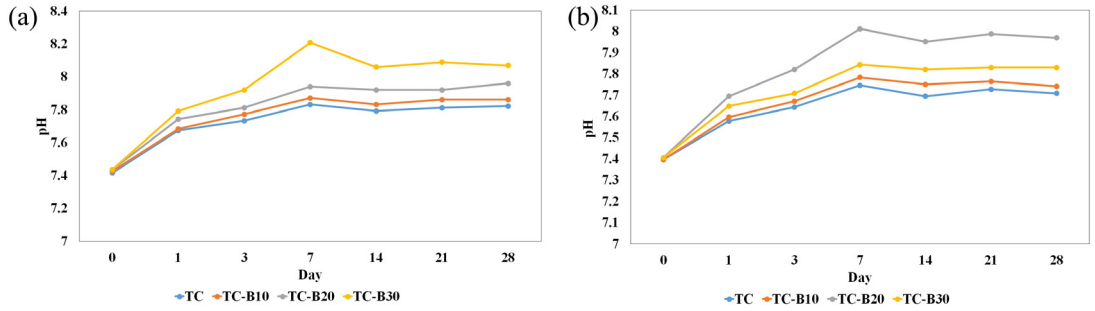

Fig. 2. PH changes in a) uncoated scaffolds and b) coated scaffolds

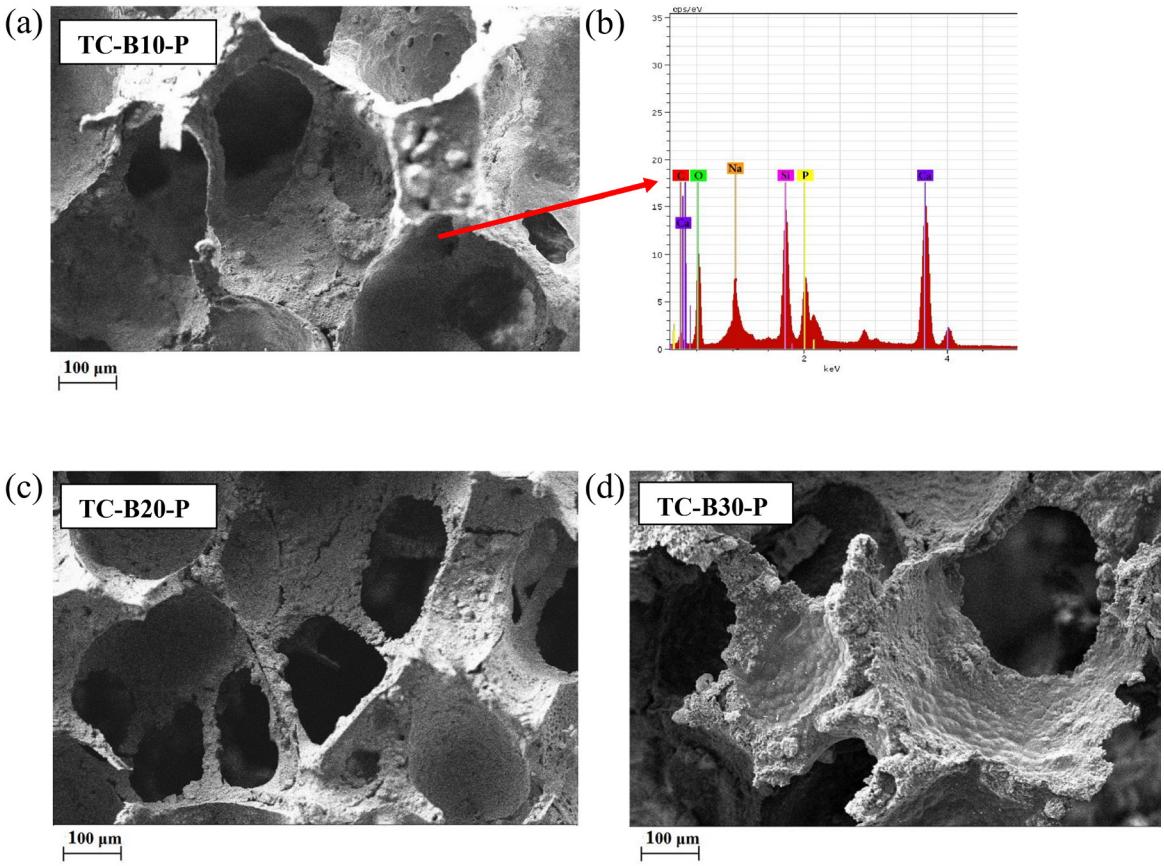

Fig. 3. SEM images of the coated scaffolds of (a) TC-B10-P (b) with its EDX analysis, (c) TC-B20-P, and (d) TC-B30-P after 28 days of immersion in SBF

size of 85 nm were used as the base material to fabricate the scaffold. Hydroxyapatite and nanoBG powders with 0, 10, 20, and 30 wt. % bioglass were added slowly to deionized water. After homogenization of the mixture, 1 wt. % sodium tripolyphosphate (STPP) was used to increase the solid loading on the sponge disks. The slurry was then stirred for 30 min at 300 rpm and then 1 wt. % of carboxymethyl cellulose was added as the binder. Finally, stirring was continued at 60 °C until complete homogenization.

Commercial polyurethane foam was cut into 10×10×10 mm cubes and immersed slowly into the ceramic slurry. Then, the samples were dried in a vacuum for 24 hours to prevent sponge pores from closing. The samples were subjected to heat treatment in the furnace during four stages to prepare the scaffolds: 1) heated at 600 °C for an hour to completely burn the polymer foam (heating rate of 3 °C/min), 2) heating from 600 °C to 1350 °C with a heating rate of 5 °C/min, 3) keeping the samples at 1350 °C for 2 hours, and 4) cooling the samples in the oven to room temperature with a 5 °C/min cooling rate. The uncoated scaffolds containing 10, 20, and 30 wt. % bioglass is noted as TC-B10, TC-B20, and TC-B30, and P denotes the polymer coating in composites scaffolds.

2.2.4. Composite coatings on scaffolds

The PCL polymer (M_w=80000) was dissolved in chloroform (10% (w/v)) and stirred for 30 min. 10 wt. % of nanoBG particles was sonicated in 10 cm^3 chloroform for 15 minutes and then added to the PCL solution. The final solution was then stirred at room temperature for further homogenization for 24 h. After sterilizing the surface of the scaffold with acetone and ethanol, the scaffolds were soaked in the prepared solution for 1 minute. Finally, the scaffolds were dried in an oven for 7 days at 37 °C.

2.3. Characterization

2.3.1. Measurement of scaffold porosity and density

For the calculation of density and porosity of scaffolds, the liquid displacement method was employed. In this study, ethanol 96% was used to diffuse into scaffold porosities. The scaffold density was calcu-

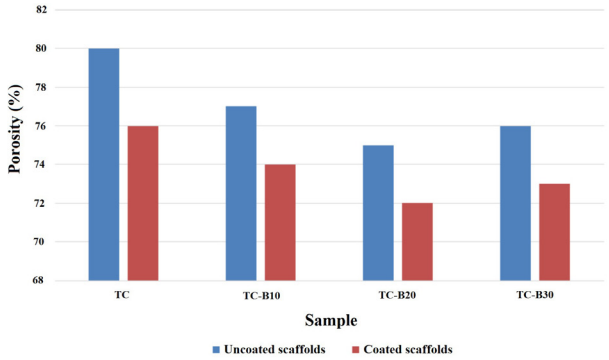

Fig. 4. Porosity percentage of the scaffolds

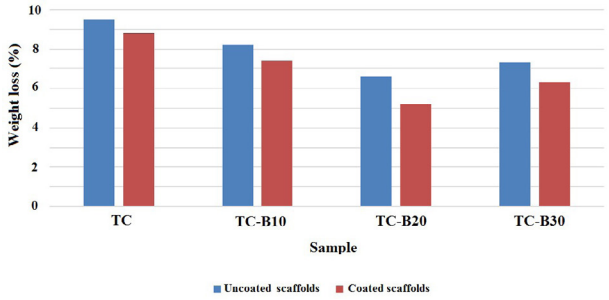

Fig. 6. Weight loss of the scaffolds after 28 days of immersion in SBF

lated from the following equation:

$$\rho = W/(V_2 - V_3) \quad (1)$$

moreover, the amount of open porosity of the scaffold is obtained from the following relationship:

$$\varepsilon = (V_1 - V_3)/(V_2 - V_3) \quad (2)$$

where W, V_1, V_2, and V_3 denote the scaffold weight, the volume of ethanol contained in the cylinder, volume of ethanol after immersion of the scaffold in the cylinder for 5 min, and the volume of ethanol remaining after removal of the scaffold from the cylinder, respectively. The amount of and represent the volume of scaffold and adsorbed ethanol, respectively. Thus, the final volume of the scaffold is calculated through the equation 3.

$$V = (V_1 - V_2)/(V_1 - V_3) \quad (3)$$

2.3.2. SEM and EDS analysis

The microstructure and morphology of the prepared scaffolds were investigated via Zeiss 00947B scanning electron microscope and EDS analysis. Prior to microscopic observations, the surface of the composite scaffolds was gold-coated.

2.3.3. Measurement of pH in SBF solution

After immersion of the scaffolds in the SBF solution, the pH of the solution was measured by Aqbus Model 2000 pH meter after 2, 3, 7, 14, 21, and 28 days of immersion.

2.3.4. Bioactivity assessment

In vitro bioactivity evaluation was performed by immersion in SBF for 28 days. The cubic scaffolds were immersed in SBS solution and incubated at 37 °C and after 1, 7, 14, and 21 days, the composite scaffolds were taken out, washed with water, and dried in a vacuum oven at 60°C and taken for further characterization.

2.3.5. Plasma coupling optical emission spectroscopy (ICP)

ICP method was used to measure the number of ions released from the scaffold immersed in SBF solution. In this study, a Zaies 110394 device was used.

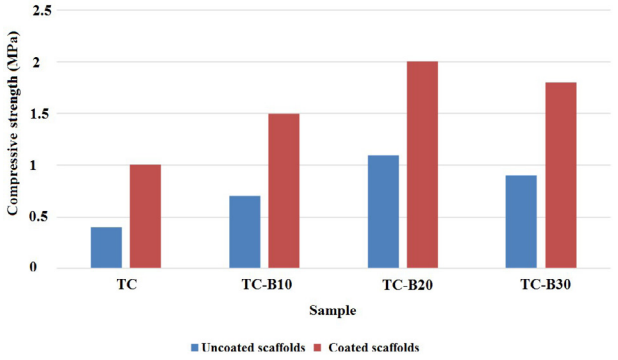

Fig. 5. Compressive strength of the composite scaffolds

3. Results and discussion

3.1. Microstructural study of the composite scaffolds

The SEM images of the TCP/bioglass/PCL scaffolds are shown in Figure 1. As seen in SEM images, the cross-section of the synthesized scaffold shows interconnected porosities. The mean pore size of the scaffolds appears to be about 300-550 µm, which is appropriate for cells to infiltrate into the channels and pores of the scaffold. Ideal scaffolds are required to possess a high volume of open and interconnected pores in order to obtain high cell seeding density in the scaffolds, and to facilitate transporting of oxygen as well as nutrients for cell differentiation and cell proliferation. Scaffolds with porosity dimensions of 100 to 500 microns are considered for cell culture, soft and hard tissue growth, and vascularization. In bone tissue engineering, the pore size larger than 300 microns is required. It should be noted that the increase in porosity size leads to a decrease in the mechanical strength of the scaffold; therefore, the balance between these parameters should be considered. As can be seen in the figure, PCL has been successfully coated on the scaffolds.

3.2. Measurement of pH and Released ions in SBF solution

Figure 2 shows the pH variations of coated and uncoated scaffolds in the SBF solution within 28 days. According to the results, the pH change is between 7.4 and 8, which is acceptable for a physiologic environment to prevent damages to cells and tissues.

SBF solution was analyzed after 28 days to measure the released amount of ions from the scaffolds. The obtained results for uncoated samples are presented in Table 1. As shown in the table, most of the calcium and phosphorus ions were absorbed by the sample surface, and the concentration of theses ions in SBF decreased, showing the apatite formation. The lowest concentration of Ca and P ions is related to the TC-B20 sample, which means the apatite formation is more; in other words, the bioactivity of this scaffold is higher than that of other scaffolds.

As observed in Figure 3, the bright precipitates formed on the surface

Table 1.

The concentration of ions released in SBF

Sample	Ca (ppm)	P (ppm)	Si (ppm)
TC	24	22	0
TC-B10	20	20	50
TC-B20	18	14	40
TC-30	20	19	44
SBF	100	31	0

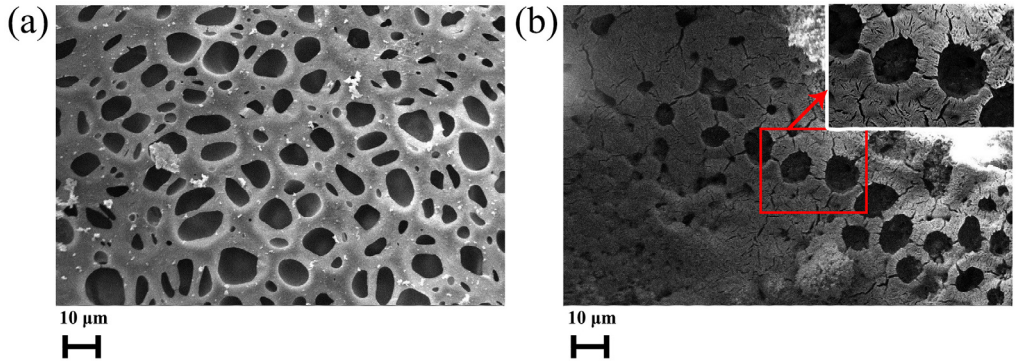

Fig. 7. SEM images of TC-B20-P before and after immersion in SBF for 28 days

of the scaffolds indicate the deposition and formation of apatite particles. In addition, the result of point analysis by EDS on the bright spots of the TC-B10-P scaffold shows the presence of P and Ca, revealing that these precipitates are calcium phosphate. This also indicates the bioactive behavior of this sample.

3.3. Porosity and mechanical properties of the scaffolds

In general, well-functioning implants for tissue engineering are required to have high pore density, good biocompatibility, and sufficient mechanical strength. The porosity percentages of the samples are shown in Figure 4. As shown evidently, polymer coating decreased the porosity of the scaffolds. The porosity of all the prepared samples is in the range of 75-80%, which is in the acceptable range for tissue engineering scaffolds. It can be concluded from the compressive strength results (Figure 5) that the polymer coating inside and on the surface of the porosities caused enhancement of adhesion strength. TC-B20-P shows the highest value of compressive strength. The polymer coating on the surface and inside the pores of the scaffold results in the improvement of the scaffold strength so that in some cases, the strength is multiplied. PCL penetrates the ceramics scaffold, preventing stress concentration and cracking in the scaffold, thus increasing its strength. On the other hand, the highest mechanical strength is related to the sample containing 20 wt. % of bioglass. The bioglass nanoparticles in this sample are homogeneously dispersed in the space between the beta-tricalcium phosphate particles, resulting in higher strength.

3.4. Biodegradation

Weight loss of the scaffolds after soaking in SBF for 28 days is depicted in Figure 6. The sample TC-B20 shows the best performance in terms of biodegradation. In the case of coated specimens, the rate of degradation is relatively lower than that of the coated specimens but similar to the coated specimens, TC-B20-P has the lowest degradation. The SEM images of TC-B20-P before and after degradation are shown in Figure 7.

4. Conclusions

In this research, TCP/nano-bioglass/PCL composite scaffolds with different compositions were produced. Adding 20% bioglass improved the mechanical strength more than 2 times (from 0.4 MPa to 1.1 MPa). The coating of the scaffolds also enhanced the mechanical properties as the strength of the TC-B20 sample increased from 1.1 MPa to 2 MPa. All scaffold samples contain 75-80% porosity, which is acceptable for bone scaffolds. The result of the elemental analysis of ICP showed that the highest bioactivity behavior was related to the TC-B20 sample. Evaluation of elemental analysis results of SBF solution on coated scaffold samples showed the positive effect of coating and improved bioavailability. Finally, the degradation results showed that the degradation improved in TC-B20 and the enhancement was observed by coating.

REFERENCES

[1] S. Rahimi, F. SharifianJazi, A. Esmaeilkhanian, M. Moradi, A.H. Safi Samghabadi, Effect of SiO2 content on Y-TZP/Al2O3 ceramic-nanocomposite properties as potential dental applications, Ceramics International (2020).
[2] E. Jabbarzadeh, T. Starnes, Y.M. Khan, T. Jiang, A.J. Wirtel, M. Deng, Q. Lv, L.S. Nair, S.B. Doty, C.T. Laurencin, Induction of angiogenesis in tissue-engineered scaffolds designed for bone repair: a combined gene therapy–cell transplantation approach, Proceedings of the National Academy of Sciences 105(32) (2008) 11099-11104.
[3] A. Moghanian, A. Ghorbanoghli, M. Kazem-Rostami, A. Pazhouheshgar, E. Salari, M. Saghafi Yazdi, T. Alimardani, H. Jahani, F. Sharifian Jazi, M. Tahriri, Novel antibacterial Cu/Mg-substituted 58S-bioglass: Synthesis, characterization and investigation of in vitro bioactivity, International Journal of Applied Glass Science (2019).
[4] L. Bazli, H. Nargesi khoramabadi, A. Modarresi Chahardehi, H. Arsad, B. Malekpouri, M. Asgari Jazi, N. Azizabadi, Factors influencing the failure of dental implants: A Systematic Review, Composites and Compounds 2(1) (2020).
[5] F. Sharifianjazi, N. Parvin, M. Tahriri, Formation of apatite nano-needles on novel gel derived SiO2-P2O5-CaO-SrO-Ag2O bioactive glasses, Ceramics International 43(17) (2017) 15214-15220.
[6] C. Gao, Y. Deng, P. Feng, Z. Mao, P. Li, B. Yang, J. Deng, Y. Cao, C. Shuai, S. Peng, Current progress in bioactive ceramic scaffolds for bone repair and regeneration, International journal of molecular sciences 15(3) (2014) 4714-4732.
[7] U. Kneser, D.J. Schaefer, E. Polykandriotis, R.E. Horch, Tissue engineering of bone: the reconstructive surgeon's point of view, Journal of cellular and molecular medicine 10(1) (2006) 7-19.
[8] L. Lu, Q. Zhang, D. Wootton, R. Chiou, D. Li, B. Lu, P. Lelkes, J. Zhou, Biocompatibility and biodegradation studies of PCL/β-TCP bone tissue scaffold fabricated by structural porogen method, Journal of Materials Science: Materials in Medicine 23(9) (2012) 2217-2226.
[9] M.S.N. Shahrbabak, F. Sharifianjazi, D. Rahban, A. Salimi, A Comparative Investigation on Bioactivity and Antibacterial Properties of Sol-Gel Derived 58S Bioactive Glass Substituted by Ag and Zn, Silicon 11(6) (2019) 2741-2751.
[10] J.L. Drury, D.J. Mooney, Hydrogels for tissue engineering: scaffold design variables and applications, Biomaterials 24(24) (2003) 4337-4351.
[11] C.-F. Wang, B. Hu, H.-H. Yi, W.-B. Li, The effect of PS porosity on the structure, optical and electrical properties of ZnS/PS, Optics and Spectroscopy 116(3) (2014) 427-430.
[12] F. Sharifianjazi, N. Parvin, M. Tahriri, Synthesis and characteristics of sol-gel bioactive SiO2-P2O5-CaO-Ag2O glasses, Journal of Non-Crystalline Solids 476 (2017) 108-113.
[13] Z. Goudarzi, N. Parvin, F. Sharifianjazi, Formation of hydroxyapatite on surface of SiO2–P2O5–CaO–SrO–ZnO bioactive glass synthesized through sol-gel route, Ceramics International 45(15) (2019) 19323-19330.
[14] A. Esmaeilkhanian, F. Sharifianjazi, A. Abouchenari, A. Rouhani, N. Parvin, M. Irani, Synthesis and characterization of natural nano-hydroxyapatite derived from turkey femur-bone waste, Applied biochemistry and biotechnology 189(3) (2019) 919-932.
[15] B. Liu, D.x. Lun, Current application of β-tricalcium phosphate composites in orthopaedics, Orthopaedic surgery 4(3) (2012) 139-144.
[16] S.H. Kwon, Y.K. Jun, S.H. Hong, I.S. Lee, H.E. Kim, Y.Y. Won, Calcium phosphate bioceramics with various porosities and dissolution rates, Journal of the American Ceramic Society 85(12) (2002) 3129-3131.
[17] S. Bose, J. Darsell, M. Kintner, H. Hosick, A. Bandyopadhyay, Pore size and pore volume effects on alumina and TCP ceramic scaffolds, Materials Science and Engineering: C 23(4) (2003) 479-486.

[18] C. Young, P. Ladd, C. Browning, A. Thompson, J. Bonomo, K. Shockley, C. Hart, Release, biological potency, and biochemical integrity of recombinant human platelet-derived growth factor-BB (rhPDGF-BB) combined with AugmentTM Bone Graft or GEM 21S beta-tricalcium phosphate (β-TCP), Journal of controlled release 140(3) (2009) 250-255.
[19] L. Bazli, M. Siavashi, A. Shiravi, A Review of Carbon Nanotube/TiO2 Composite Prepared via Sol-Gel Method, Composites and Compounds 1(1) (2019).
[20] S. Saadi, B. Nazari, Submission Title: Recent Developments and Applications of Nanocomposites in Solar Cells: a Review, Composites and Compounds 1(1) (2019).
[21] L. Bazli, A. Khavandi, M.A. Boutorabi, M. Karrabi, Correlation between viscoelastic behavior and morphology of nanocomposites based on SR/EPDM blends compatibilized by maleic anhydride, Polymer 113 (2017) 156-166.
[22] L. Bazli, A. Khavandi, M.A. Boutorabi, M. Karrabi, Morphology and viscoelastic behavior of silicone rubber/EPDM/Cloisite 15A nanocomposites based on Maxwell model, Iranian Polymer Journal 25(11) (2016) 907-918.
[23] D. Rohner, D.W. Hutmacher, T.K. Cheng, M. Oberholzer, B. Hammer, In vivo efficacy of bone-marrow-coated polycaprolactone scaffolds for the reconstruction of orbital defects in the pig, Journal of Biomedical Materials Research Part B: Applied Biomaterials: An Official Journal of The Society for Biomaterials, The Japanese Society for Biomaterials, and The Australian Society for Biomaterials and the Korean Society for Biomaterials 66(2) (2003) 574-580.
[24] M.C. Phipps, W.C. Clem, J.M. Grunda, G.A. Clines, S.L. Bellis, Increasing the pore sizes of bone-mimetic electrospun scaffolds comprised of polycaprolactone, collagen I and hydroxyapatite to enhance cell infiltration, Biomaterials 33(2) (2012) 524-534.
[25] S.I. Yoon, Y.K. Lee, K.N. Kim, S. Kim, H. Son, J. Kwak, J. Kim, H. Choi, A comparison of the bone-like apatite formation potency between Hydroxyapatite and β-Tricalcium phosphate in Glass ionomer dental luting cement, Key Engineering Materials, Trans Tech Publ, 2006, pp. 885-890.
[26] A. Ibara, H. Miyaji, B. Fugetsu, E. Nishida, H. Takita, S. Tanaka, T. Sugaya, M. Kawanami, Osteoconductivity and biodegradability of collagen scaffold coated with nano-β-TCP and fibroblast growth factor 2, Journal of Nanomaterials 2013 (2013).
[27] M. Ngiam, S. Liao, A.J. Patil, Z. Cheng, C.K. Chan, S. Ramakrishna, The fabrication of nano-hydroxyapatite on PLGA and PLGA/collagen nanofibrous composite scaffolds and their effects in osteoblastic behavior for bone tissue engineering, Bone 45(1) (2009) 4-16.
[28] Y. Yang, Y. Zhao, G. Tang, H. Li, X. Yuan, Y. Fan, In vitro degradation of porous poly (l-lactide-co-glycolide)/β-tricalcium phosphate (PLGA/β-TCP) scaffolds under dynamic and static conditions, Polymer Degradation and Stability 93(10) (2008) 1838-1845.
[29] W. Xue, A. Bandyopadhyay, S. Bose, Polycaprolactone coated porous tricalcium phosphate scaffolds for controlled release of protein for tissue engineering, Journal of Biomedical Materials Research Part B: Applied Biomaterials: An Official Journal of The Society for Biomaterials, The Japanese Society for Biomaterials, and The Australian Society for Biomaterials and the Korean Society for Biomaterials 91(2) (2009) 831-838.
[30] X. Zhang, W. Chang, P. Lee, Y. Wang, M. Yang, J. Li, S.G. Kumbar, X. Yu, Polymer-ceramic spiral structured scaffolds for bone tissue engineering: effect of hydroxyapatite composition on human fetal osteoblasts, PloS one 9(1) (2014).

Available online at www.jourcc.com

Journal homepage: www.JOURCC.com

Journal of Composites and Compounds

Photosensitive nanocomposites: environmental and biological applications

Ho Won Jangto[a]*, Amir Zareidoost[b], Mostafa Moradi[c], Aliasghar Abuchenari[d], Ameneh Bakhtiarie[e], Rasul Pouriamanesh[f], Behzad Malekpouri[g], Azadeh Jafari Rad[h], Daruosh Rahban[i]

[a] *Department of Materials Science and Engineering, Research Institute of Advanced Materials, Seoul National University, Seoul 08826, Republic of Korea*
[b] *Faculty of Materials & Metallurgical Engineering, Semnan University, Semnan, Iran*
[c] *Department of Materials Science and Engineering, Sharif University of Technology, Azadi Street, Tehran, Iran*
[d] *Materials Engineering, Shahid Bahonar University, Kerman, Iran*
[e] *Department of Biology, Shahid Chamran University, Ahvaz, Iran*
[f] *Mahshahr Pipe Mill Co. (MPM), Iran*
[g] *Department of Materials Science and Engineering, Sharif University of Technology, Tehran, Iran*
[h] *Department of Chemistry Omidiyeh Branch, Islamic Azad University, Omidiyeh, Iran*
[i] *Department of Nanomedicine, School of Advanced MedicalTechnologies, Tehran University of Medical Science, Tehran, Iran*

ABSTRACT

There has been an extensive investigation in the field of optical applications of nanocomposite materials. To prepare photosensitive nanocomposites, an optically functional phase is embedded in a transparent, processable matrix. This provides the opportunity to utilize the optical properties in other forms including fibers and films, which are more technologically important. Due to expansion of optical materials applications, novel transparent materials and optically functional are required. Recent optical nanocomposites and their applications in different areas especially catalysis and drug delivery have been addressed in this paper.

Peer review under responsibility of jourcc

ARTICLE INFORMATION

Article history:
Received 17 March 2020
Received in revised form 27 March 2020
Accepted 29 March 2020

Keywords:
Catalysis
Cancer
Targeted drug delivery
Nanocomposites

Table of contents

1. Introduction 50
2. Light-responsive systems 51
3. Light-responsive nanocomposites 51
4. Application of optical nano-composite 51
4.1 Drug delivery 51
4.2 Purification of water pollutants 55
5. Conclusions and future insights 58

1. Introduction

Incorporation of semiconductor nanoparticles into ceramic, glass, and polymer matrix materials could provide various interesting optical properties such as nonlinearity, luminescence, fluorescence, and absorption [1, 2]. In these nanocomposites, the matrix material acts as a stabilizer for the particles growth and their sizes, while the small particles improve the optical properties. Laser-active composites are produced by incorporation of ceramic nanoparticles of solid-state laser materials into polymer-based matrix leading to the formation of films amplified by solid-state laser, which their preparation was traditionally difficult. To retain the optical properties of polymer and glass matrices, optically functional small molecules and polymers can also be incorporated in these matrix materials. Potential applications of composites with nanostructures have led to development of transparent materials with excellent mechanical properties, magnetic properties, and unusually high RI [3].

* *Corresponding author: Ho Won Jangtoa; E-mail: hwjang@snu.ac.kr*
https://doi.org/10.29252/jcc.2.1.7

2. Light-responsive systems

It is reported the UV light results in several disadvantages such as limited tissue penetration depth, and phototoxicity. This has made scientists to move the research focus onto providing nanoparticle systems that are light responsive in the visible region (400-700 nm), which leads to reduce the phototoxicity. In this regard, the near-infrared light triggered DDSs have become increasingly important for enhancing the tissue penetration depth. Moreover, various studies have been performed about light-based advanced systems for photoacoustic and fluorescent imaging, as well as photothermal and photodynamic therapy [4, 5].

3. Light-responsive nanocomposites

In order to control the loading of guest substances, manage their release and enhance mechanical properties, a combination of inorganic substrates and light-sensitive polymers in one system has been attracted attention in recent years [6-9]. Biocompatible and readily modifiable nanoparticles of SiO_2 with new functionalities are promising for drug delivery applications [10]. Light-responsive nanoparticles of silica with average particle size of 70 nm have been produced by covalent conjugation of amino groups with molecules of photoactive o-nitro benzyl bromide on the particles surface [11]. These groups can be covalently bonded to drugs with hydroxyl, phosphate or carboxylic groups. The o-nitro benzyl bromide molecules transform into o-nitro benzaldehyde after irradiation of the resulting particles at 310 nm. This leads to an irreversible cleavage of the bond between the drug and particle and subsequent release of the drug. The intracellular drug release could be externally controlled as a result of the small size of these particles which enables their penetration into cells. Schematic of an optical nanocomposite [12] is illustrated in Fig. 1.

NIR light exposure results in photothermal effect and an increase in temperature in NIR-responsive systems leading to drug release upon [13-15]. The temperature increase can simultaneously cause cell death called “photothermal treatment” [16, 17]. Other involved mechanisms are upconverting nanoparticles (UCNPs) two- and photon conversion [18]. These mechanisms are illustrated in Fig. 2 [19].

4. Application of optical nano-composite

It is expected that light-sensitive nano-composites attain widespread applications in the industrial and medical fields due to their great potential. The applications of these light-sensitive nano-composites will be discussed in the following section.

4.1. Drug delivery

Intelligent drug delivery systems [20, 21] are able to modulate drug release proportionate to the specific stimuli intensity and can operate in closed or open circuit [22]. By automatic adjusting of the rate of drug release or switching the release on and off, self-regulated or closed-loop systems can detect specific variations in biological variables including concentration of some substances, temperature, or pH through activating or modulating the response. In open-loop systems, the response to particular an external stimulus is carried out by the drug release in a pulsing way. The drug release in these systems is proportional to the intensity and duration of each stimulus. This mode of release is not affected by the biological environment variables resulting in an explicit and precise triggering of the drug release. Upon the development of drug delivery systems responsive to heat, irradiation, magnetic or electrical field, ultrasound or compression, an exponential increase of investigations on polymeric and lipid-based architectures is observed in the last decade. The performance of photo-responsive nanocomposites in DDSs is depicted in Fig. 3 [23].

In a study, Zhang et al. [24] synthesized copper sulfide@polydopamine–folic acid/doxorubicin nanoparticles to produce a novel nanocomposite platform for chemotherapeutic and photothermal tumor-targeting treatment. Compared to CuS/polydopamine, the nanocomposite platform had higher efficiency of photothermal conversion and ultrahigh loading levels.

In another research by Cie et al. [25], the synergistic use of metal organic frameworks (MOFs) and UCNPs for the production of smart nanocomposites was investigated to be applied for photodynamic therapy against hypoxic tumors with high efficiency, which offers novel ways for MOF materials applications in effective cancer treatment. They are of the opinion that their research will provide new opportunities for the production of nanocomposites based on MOFs which integrates both multiple functionalities of encapsulated active parts and the synthetic tunability of MOFs. It is expected that the proposed strategy to reveal the extensive potential of MOFs for address challenges in other disease therapies.

Ghavaminejad et al. [26] proposed that the mussel-inspired nanocomposites they produced had controllable multidrug release and excellent heating properties, which can be offered as promising materials for cancer treatment due to the chemotherapy and photothermal therapy (PTT) synergistic effect. The nanocomposites were composed of a stimuli responsive hydrogel (poly(N-isopropylacrylamide) -co-polyacrylamide) incorporated with dopamine nanoparticles that is an effective photothermal agent. The loading drugs were doxorubicin (DOX) and bortezomib (BTZ).

Wang et al. [27] synthesized a novel photo-responsive nanocomposite composed of indocyanine green (ICG), DOX, and graphene oxide (GO)-polyamidoamine-pluronic F68 (PPF68). The nanocomposite was fabricated by cross-linking of graphene oxide with ICG and DOX and the formation of diselenide bond with PPF68. Contrary to commonly-used nanomaterials, which are responsive to stimuli received from surrounding environmental, this synthesized nanocomposite responds to the reactive oxygen species (ROS) production via NIR by itself. The nanocomposites have the capability of selective accumulation in tumor cells. The lysosomal escape can be occurred due to enhanced ROS level and the high proton sponge effect resulted from polyamidoamine (PAMAM). The production of ROS by ICG can induce the diselenide bond cleavage under NIR laser irradiation, which triggers the decomposition inside tumor cell. As a result, before the drugs flow out by P-glycoprotein (P-gp) of multidrug resistant (MDR) tumor cells, the drug secretion could timely reach the therapeutic level. Finally, DOX nuclear trafficking is achieved in order to kill the MDR tumor cells in an effective way. Furthermore, the overall tumor therapeutic efficacy could be greatly enhanced with combining photothermal therapy and favorable on-demand chemotherapy. These NIR-responsive nanocomposites are shown to be successful in overcoming the MDR of tumor both in-vivo and in vitro, which provide promising novel strategies for clinical MDR cancer therapy.

Based on Nesic et al. [28] research, the nanocomposite based on nanoparticles of TiO_2 as carrier and ruthenium complex with potential anticancer behavior have light controllable release characteristics. The prepared nanocomposite demonstrated biological activity and free radicals were generated. The free radicals are known as efficient tumor cell killers. The transition metal complex was released consistently from the surface demonstrating the controlled drug delivery system. Additionally, Ru-complex secretion from the surface of TiO_2 nanoparticles showed to be dependent on the applied laser (green light) energy. Hence, these properties offer this nanocomposite material as suitable candidates for the photo-responsive chemotherapy. Fig 4 summarizes the results of the

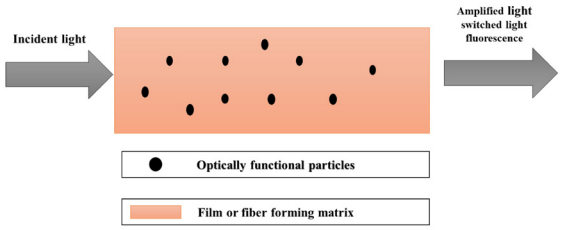

Fig. 1. Schematic of optical nanocomposite.

Hu et al. research [29], in which they developed a novel, low-toxicity, multifunctional QD-rGO nanocomposite to perform as a photothermal cancer-therapy agent in the NIR region and an imaging agent in the region of visible-light.

Chen et al. [30] also manufactured effective nanoplatforms of GO and reduced graphene oxide (rGO) nanomaterials for NIR-based PTT. In addition, many reports have demonstrated successful cancer therapy in-vivo and in-vitro with nanomaterials based on graphene as PTT agents, and also their combination with chemical conjugations, surface modification, ultrasound, imaging-guided, PDT, and chemotherapy to improve the therapeutic efficacy and tune their properties in biological systems [31]. In recent years, there have been novel therapeutic methods/strategies and more functionalized nanocomposite based on graphene to improve the therapeutic efficiency of PTT. For modification of the nanocomposite materials based on graphene with highly efficient drug release, imaging-guided therapy, and multifunctional biological characteristics in a single system with the aim of an efficient PTT and promoted cancer synergistic treatment, different inorganic nanoparticles and functional organic macromolecules have been conjugated on the graphene including magnetic iron oxide nanoparticles (IONPs), silica, Au, and DNA.

Nanocomposite hydrogel prepared by Xu et al [32] showed a homogeneous 3D porous structure with the capability of steady, slow release rate of DOX during one month. The drug release from the prepred hydrogel had pH-responsive property. This behavior was originated from the acid-labile hydrazone bond cleavage between adamantyl group and DOX which occurs in acidic environment. The release of loaded drug from the nanocomposite can be accelerated by NIR irradiation. Graphene nanoribbons (GNRs) photothermal effect causes the collapse of the hydrogel networks and control by the drug release. The excellent photothermal effect and biocompatibility of the prepared hydrogel were confirmed by the in vitro cytotoxicity test. Additionally, the mouse model study revealed that the hydrogel formed in-situ had promising tissue biocompatibility. According to the in vivo antitumor test, nanocomposite hydrogel showed its capacity for synergistic therapy of chemo-photothermal with less adverse effects as a result of efficient photothermal effect and long retention of drug in the tumor site. Thus, this injectable hydrogel that is responsive to NIR and pH could be suggested as a promising material for a long-lasting drug release for chemo-photothermal combined cancer treatment.

Chen et al. [33], developed a mechanically strong and biocompatible nanocomposite hydrogel based on PNIPAM/clay/ carboxymethyl chitosan (CMCTs)/ genipin nanoparticles (GP) using free radical polymerization process with the help of the UV light irradiation, which was responsive to both temperature and pH. To produce the nanocomposites, the natural molecular-genipin and clay were used as the cross-linkers. Under the optimum conditions and high UV light power, the hydrogels demonstrated a high value of tensile strength and the failure strain of about 137.9 kPa and 446.1%, respectively. The synthesized nanocomposite showed high energy absorption in stretching processes. In the first loop at the room temperature, the nanocomposite was able to recover

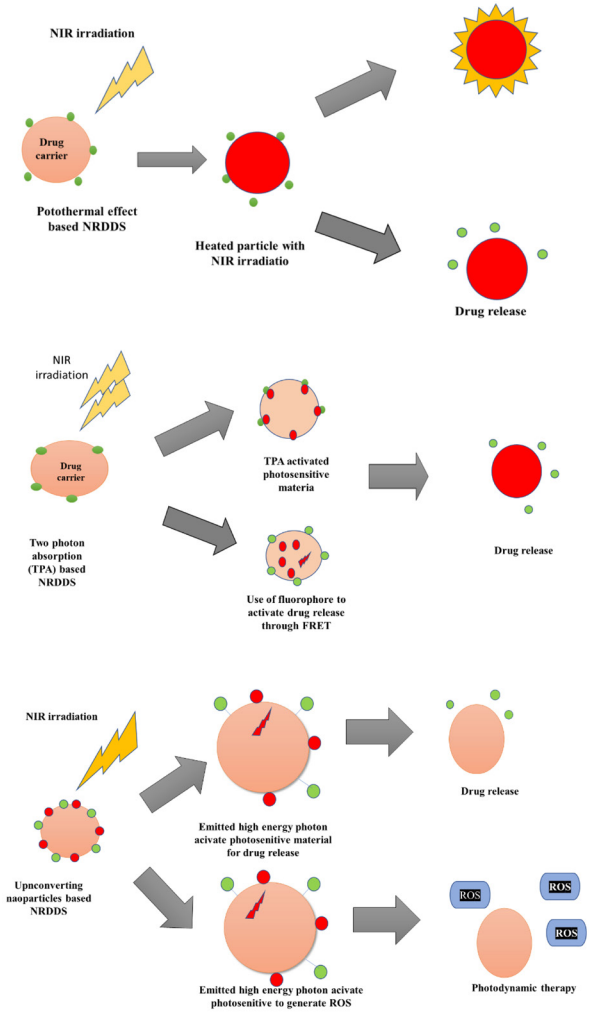

Fig. 2. A scheme of three mechanisms of NIR-responsive drug delivery systems (DDSs).

76.1% of the adsorbed energy in 15 min after the removal of the load. In addition, the swelling/deswelling properties of the obtained nanocomposites was dependent on the content of GP, CMCTs, and clay. Moreover, it was shown that the synthesized hydrogels had a controlled asprin release by regulating the density of crosslinks. According to the results, this promising property suggest theses nanocomposites as proper carriers for controlled drug delivery applications.

A new light-responsive nanocomposite based on GO/Polyhedral oligomeric silsesquioxane (POSS) was synthesized by Teng et al. [34]. The synthesis was based on the reversible host-guest inclusion/exclusion method. Supramolecular assembly/disassembly property was observed upon visible and UV irradiation in graphene oxide nanosheets and POSS nanocage. Furthermore, the GO/POSS nanocomposites demonstrated a significant influence on oxygen permeability and good water dispersion in conventional films coated with polyvinyl alcohol (PVA) under different conditions of light irradiation. This could be helpful for development of smart materials as gas barriers in packaging.

To design tumor-targeted photo-controlled drug delivery, Luo et al. [35] developed a nanocomposite based on mesoporous silica/gold (MSN/Au). In the nanocomposites, gold nanoparticle (AuNP) and MSN acted as indicators and carriers, respectively. Photo-switchable azobenzene (Azo) moieties was employed to immobilize the MSN drug carrier. Poly (ethylene glycol) and a matrix metalloproteinase (MMP) substrate was used to modify the fluorescence-quenched gold nanoparticles. An α, β cyclodextrin dimer bridge connected the two types of nanoparticles. According to in vitro investigations, the specific interaction of the prepared nanocomposite with tumor region was observed overexpressing

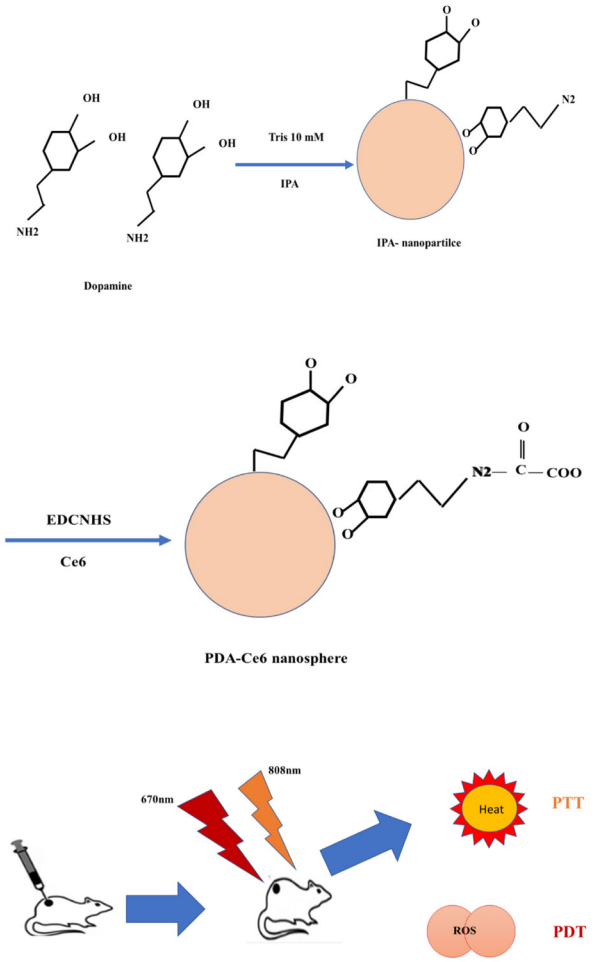

Fig. 3. Illustration of photodynamic therapy (PDT), using a combination of light and chemical photosensitizers (PS).

matrix metalloproteinase-2 (MMP-2) enabling the UV light guidance to release the entrapped drug. The integration of MSN-based drug carrier as well as the Au-based indicator could lead to the precise localization of the released drug to tumor region and significant improvement of therapeutic efficacy.

Shi et al. [36] produced NIR-responsive nanocomposite hydrogels based on poly (N-isopropylacrylamide) (PNIPAM)/GO. To prepare the nanocomposites, they combined physically cross-linked graphene oxide nanosheets with chemically cross-linked small molecules. The excellent NIR response of the prepared hydrogels was originated from combining the polymeric networks of thermoresponsive PNIPAM and GO nanosheets. Incorporation of a low concentration of N,N′-methylenebis(acrylamide) (BIS) molecules for the formation of chemical cross-links in the hydrogels led to the formation of a relatively homogeneous structure with rare dense clusters containing chemical cross-links and flexible long polymer chains and, subsequently, the ultrahigh tensibility. Additionally, a further increase in hydrogel toughness could be achieved by hydrogen bond interactions and physical cross-linking generated among the amide groups existing in PNIPAM chains and oxidized groups of GO nanosheets. This synthesized nanocomposite with ultrahigh tensibility demonstrated fast, repeatable, and reversible NIR response making them remarkably promising candidates for producing artificial muscles, smart actuators, and remote light-controlled devices.

As mentioned, graphene oxide and their nanocomposites are attracting attention in both photothermal therapy and drug delivery due to having high specific surface area as well as high NIR-optical absorption. In this regard, Li et al. [37] integrated (c,c,t-[Pt(NH3)$_2$Cl$_2$(OH)$_2$]) complex and PEGylated nano-graphene oxide (PEG-NGO) and into a single

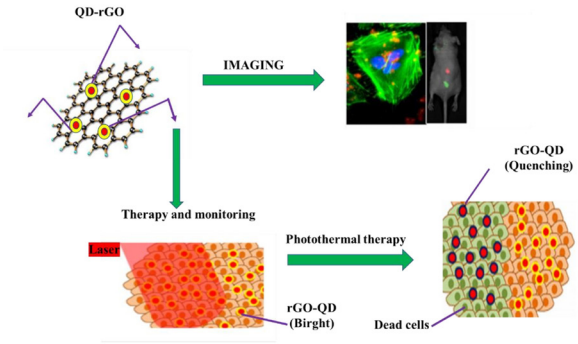

Fig. 4. rGO nanocomposites tagged with quantum dot (left) entered into targeted cancerous cells emit bright fluorescence from the quantum dots, (right) The absorption of NIR radiation by rGO and its convertion into heat, causing fluorescence reduction and cell death (Repriduced with permission [29]).

platform (PEG-NGO-Pt) to produce a multifunctional nanocomposite. The nanocomposite showed capability of synergic photothermal-chemotherapy and targeted drug delivery using NIR laser irradiation, and real-time monitoring with high therapeutic efficacy. The nanocomposite therapeutic influence in cancer therapy was improved by apoptosis and cell death. As a result of the high potential of specific tumor targeting at higher temperatures and the improved cisplatin cytotoxicity, the therapeutic efficacy improvement of the loaded drug accompanied by complete destruction of tumors was indicated. Compared to photothermal or chemotherapy treatment alone, minimal systemic toxicity and no tumor recurrence were observed indicating the beneficial influences of GO and Pt (IV) integration for anticancer therapy.

Using the PEG double acrylates (PEGDA) macromers gelation, Xia et al. [38] constructed porous nanocomposite hydrogels based on silicon. Under NIR irradiation, photosensitysis of porous silicon nanoparticles (PSiNPs) with singlet oxygen was initiated. Sustained drug release with high efficiency, significant photothermal effect, excellent biodegradability, and strong fluorescence of multifunctional PSiNPs/PEGDA hydrogels were indicated. Eventually, NIR light induced the hydrogels in situ growth on tumor cells providing a remarkable localized prevention for the adherence, viability, and tumor cells migration. Hence, they proposed that the fabricated hybrid hydrogels could be potential material for local cancer treatment in clinical practice in the future.

Yang et al. [39] grafted lactose acid (LA) onto polydopamine (PDA)@cobalt phytate (CoPA) to produce a novel multifunctional nanocomposite for photothermal therapy and photothermal imaging of cancers. The role of PDA core was to provide a template for the CoPA formation. The dual photo-responsive abilities of CoPA shell included induction of singlet oxygen formation as well as in-situ production of O_2 through catalyzing intracellular water-splitting, which enhanced photodynamic therapy influence on cancer cells under laser irradiation. Moreover, the LA grafting provide the synthesized nanocomposites with the targeting ability to determine particular targeted cancer treatment. The excellent synergistic PDT and PTT effect of PDA@CoPA-LA nanoparticles demonstrated their potential in the clinic cancer therapy applications.

Using facile and scalable solvothermal method, Ma et al. [40] synthesized CdS/rGO nanocomposites for efficient anticancer treatment. According to morphological analysis, CdS/rGO nanoflakes were formed by firm attachment of the spherical CdS nanoparticles on the rGO thin sheets. The cell survival cytocompatibility of the CdS/rGO nanomaterials obtained from the live-dead assay method was indicated to be above 95% revealing that they are appropriate for the cancer treatment. The improvement of CdS/rGO nanoflakes temperature profile under the NIR

radiation accelerated the cancer cell death. It was suggested that the proposed nanocomposites with anticancer activity could provide opportunities in biomedicine research to produce efficient materials for clinical applications.

In another study, Gorgizadeh et al. [41] synthesized $MnFe_2O_4$/C nanocomposite with uniform spherical particles and cracked surface with the average particle size of 221.6 ± 22 nm. Saturation magnetization, coercivity, and magnetic moment of $MnFe_2O_4$/C nanocomposite were 13.250 emu g−1, 13.204 G, and 0.55, respectively. Cubic spinel $MnFe_2O_4$ dots with the diameter of 2.1 ± 0.6 nm were embedded in carbon entity. The nanocomposite acted as a new absorbing agent of both ultrasound (US) wave and 808 nm laser light in treatment of mice with melanoma tumor and C540 cancer cells. $MnFe_2O_4$/C nanocomposite can also be used in magnetic resonance imaging as a contrast agent. Although $MnFe_2O_4$/C showed relative biocompatibility, their effect on the tumor cells was negligible at US waves of 1.0 MHz and 808 nm laser light. The activation of nanocomposites to kill the C540 cancer cells occurred at US waves and the laser light at power densities of 1.0 and 0.5 W cm^{-2}. At these power densities, cell viability upon irradiation of both US and the laser light in the presence of 25 μg mL−1 nanocomposite reached 4.6% and 21.5, respectively. Moreover, intratumoral injection of the nanocomposite accompanied by US and laser light irradiations indicated via histological analyses resulted in a deep tumor tissue necrosis. Its potential theranostic effect in nanomedicine is apparent due to its SDT and PTT efficacies as well as a highly contrast induction in MRI.

Liu et al. [42] fabricated rGO-hybridized PEG smart hydrogel and optimized their pH and NIR-responsive drug release properties for cancer therapy. The reason for selecting rGO was to improve photothermal property of the hydrogel [43, 44]. The results of study performed by Tan et al. [45] demonstrated that the injectable Dox/celecoxib (Cel)/MOFs@Gel nanocomposite showed remarkable biological abilities such as enhanced biocompatibility, antitumor efficacy, and pH-responsiveness suggesting this nanocomposite as an appropriate carrier for local oral cancer therapy.

Using NIR-responsive polymers (HAMAFA-b-DDACMM) coating on the nanoparticles of hollow mesoporous SiO_2, which was modified by octadecyltrimethoxysilane (C18) (HMS@C18) through self-assembly, Lin et al. [46] fabricated novel multifunctional nanovehicles for cell

Table. 1. Optical nano-composite applied in the field of drug delivery

Author	Optical nano-composite	Application	Ref.
Wang et al.	AuNR@SiO_2/Ce@polydopamine@aptamer nano-composite	Enhancing treatment of non-small cell lung cancer	[55]
Zhang et al.	Se@SiO_2–FA–CuS nanocomposites	Chemo-Photothermal Cancer Therapy	[24]
Cai et al.	UCNPs/MB@ zeolitic imidazolate framework (ZIF-8)@catalase smart nanocomposite with core-shell structure	Efficient H_2O_2/NIR -responsive PDT agent for hypoxic tumor cells treatment	[25]
Ghavami Nejad et al.	Nanocomposite Hydrogel	Chemo-Photothermal Cancer Therapy	[26]
Yu et al.	Rattle-type gold nanorods@void@porous-SiO_2 (GVPSPR)-DOX/tetradecanol (TD) nanocomposites	Chemo-Photothermal Cancer Therapy	[56]
Wang et al.	ICG/DOX/GO-PPF68 NIR-responsive nanocomposite	Clinical treatment of MDR cancer	[27]
Nešić et al.	Nanocomposite system made of colloidal TiO_2	Potential controlled metallo-drug delivery	[28]
Niu et al.	Polydimethylsiloxane (PDMS)/GNPs nanocomposites	drug-delivery, microswitches , and soft robotics	[57]
Chen et al.	Graphene-derived nanocomposites	Photothermal therapy of tumor treatment	[30]
Xu et al.	(NIPAm-co- methacrylated poly-β-cyclodextrin (MPCD))/GNRs nanocomposite	Chemophotothermal synergistic cancer therapy	[32]
Chen et al.	Nanocomposite double network PNIPAM/clay/CMCTs/GP	Controlled drug release of asprin	[33]
Teng et al.	GO-POSS nanocomposites	Host-guest inclusion Oxygen permeability	[58]
Luo et al.	Mesoporous silica/gold (MSN/Au) nanocomposite	Controlled drug delivery system	[35]
Shi et al.	PNIPAM-GO nanocomposite	Artificial muscles, smart actuators, and remote light-controlled devices	[36]
Li et al.	Pt(IV) complexes/PEGylated GO sheets multifunctional nanocomposite	A synergistic effect in the therapeutic efficacy improvent of Pt drug using combined chemo-therapy photothermal treatment	[37]

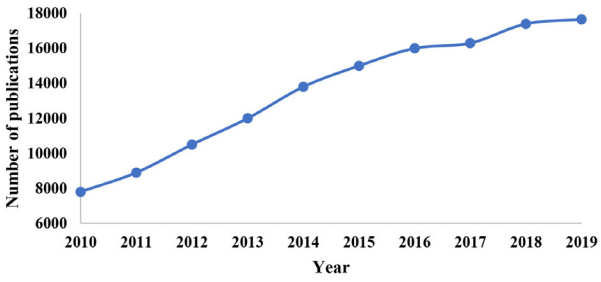

Fig. 5. Research reports focusing on optical nano-composite for purification of waste water based on scholar-google database.

imaging and tumor treatment. HMS@C18 was selected as the core due to enhancement of biological stability and the drug loading capacity; the loading efficiency of which was higher than 70%. As a result of the light-responsive copolymers degradation under NIR light excitation at 800 nm, the pre-loaded nanocomposites could release the drug. The correlation of the release efficiency with the light power and irradiation time was also indicated. Based on in vitro investigations, the cancer cells over-expressing FA receptor (FR (+)) like KB cells by endocytosis were easily targeted by the prepared nanocomposites. Additionally, strong fluorescence of the copolymer provided the ability to track the drug delivery process.

Wang et al. [47], integrated stimuli-responsive release property and magnetic targeting by the synthesis of a new smart core-shell drug delivery system using magnetic mesoporous SiO_2, which was coated by light-responsive azobenzene derivatives with covalent grafting. The loaded molecule release in the mesopores was triggered by visible light irradiation.

In another research, Jiang et al. [48], synthesized composite nanoparticles of Au/mesoporous SiO_2/rhodamine B isothiocyanate. These nanoparticles with well-defined mesoporous structure were shown to be suitable for drug loading and had strong absorption of infrared surface plasmon for light-controlled drug delivery as well as photothermal cancer treatment and could be functionalized for fluorescence imaging. This new nanomaterial can open an avenue in chemotherapy of cancer by synergistic use of hyperthermia and cell imaging.

According to Dong et al. [49], core/shell nanoparticles of superparamagnetic Fe_3O_4/Au with tunable optical properties and sizes were developed by a facile seed-mediated growth method. For the synthesis of the nanoparticles, gold seed were formed and attached on the surface of the core by Au-S covalent bonding, which were created in a simultaneous reaction in the one-pot operation. This synthesized nanocomposite was proposed to deliver a high capability of localized photothermal tumor treatment and MRI under NIR laser radiation.

In a study performed by Zhang et al. [50], DOX was loaded into nanospheres composed of UCNPs@mSiO_2-poly(N-isopropylacrylamide-comethacrylic acid) (NIPAm-co-MAA). The prepared composite drug delivery system showed a significant improved drug release at low pH values and high temperature, which exhibited an apparent pH/thermo controlled drug release. These hybrid nanospheres could also be employed as biomonitors and bioimaging agents for tracking the drug release extent. Simultaneous stimuli-responsive drug delivery and imaging suggest these materials as a novel and reliable multifunctional nanocarriers.

Zhu et al. [51], synthesized a photo-responsive nanocomposite hydrogel based on PNIPAM/GO by in situ polymerization using γ-irradiation. Different levels of GO doping in the hydrogel led to the change in colors and phase-transition temperatures. The prepared hydrogel showed great photothermal properties as a result of the high value of optical absorbance of the GO. It was possible to control phase transitions by irradiation of NIR laser. The rate of NIR-induced temperature increase with GO loading amount and the temperature could be adjusted effectively by the duration of irradiation. It was proposed that the prepared nanocomposite with its excellent photothermal properties could be used in the biomedical applications, particularly as microfluidic devices and the easy synthetic method could be employed to synthesize other nanocomposites.

A novel Au nanorod (AuNRs)/NGO core/shell nanostructure was developed by Xu et al. [52] as an efficient agent for chemophotothermal cancer therapy. The role of NGO shells was to reduce the toxicity of AuNRs coated with surfactant and create anchor sites for conjugating of hyaluronic acid. Higher photothermal efficiency and the potential of targeting hepatoma Huh-7 cancer cells was achieved for the HA-conjugated nanocomposites (NGOHA-AuNRs) compared with AuNRs. DOX-loaded NGOHA-AuNR exhibited pH-responsive and triggered the drug-release with near-infrared light irradiation. In comparison with single photothermal therapy and chemotherapy, combined chemo-photothermal therapy showed higher rates of cancer cell death, with biosafety to nontargeting cells.

The PEG-GO/CuS nanocomposites synthesized by Bai et al. [53] showed excellent biocompatibility with high photothermal conversion efficiency, high anticancer DOX storage capacity, and capability of the tumor ablation. The DOX-loaded nanocomposites demonstrated higher toxicity compared to pure nanocomposites and free DOX under NIR laser irradiation, due to both cytotoxicity of DOX release triggered by light and photothermal ablation mediated by PEG-GO/CuS. According to mouse models investigation, the chemo-photothermal influence of DOX-loaded nanocomposites led to significant inhibition of mouse cervical tumor growth and an effective tumor cell reduction. In general, the synergetic therapy demonstrated higher therapeutic efficacy in comparison with photothermal and chemotherapy treatment alone.

A DNA cross-linked polymer was coated on Au–Ag nanorods by Kang et al. [54] for a NRI-responsive drug delivery system. In order for gel scaffold to encapsulate anticancer drugs, DNA has been cross-linked for development of a sol–gel transition system based on polyacrylamide. By functionalization with targeting moieties like aptamers, nanohydrogel could specifically recognize tumor cells. The photothermal effect induced by NIR irradiation made the temperature of the surrounding gel increase rapidly, which led to the quick and controlled drug release with spatial/temporal resolution.

4.2 Purification of water pollutants

Due to increasing pace of industrialization, there are serious concerns about water pollution which creates major damages to human beings and microorganisms [59-61]. Several industries produce textile and other industrial dyes which can be combined with fresh water. Moreover, due to containing highly toxic organic substances, these industrial dyes are considered as major water pollutants [62, 63]. Thus, researchers in worldwide consider the removal of industrial organic contaminants as the most urgent action. One of the green approaches for complete elimination of organic contaminants is semiconductor photocatalysis. In these photocatalysts, solar energy sources can be used without creating any secondary pollution [64-66]. Metal oxides especially ZnO and TiO_2 are commonly utilized photocatalysts for purification of waste-water due to their strong photo-stability, non-toxicity, low-cost, and more availability [67]. Fig. 5 depicts the volume of research conducted in water purification field over the past decade.

Shi et al. [68], produced novel carbon nanotubes (CNTs) photocatalysts loaded with Ag/AgX (X = I, Br, and Cl) composite using a facile deposition–precipitation route with ultrasound. According to the results, the direct interfacial contact between CNTs and Ag/AgX nanoparticles was observed exhibiting superior visible light absorbance because of

the Ag surface plasmon resonance (SPR). These produced composite photocatalysts were able to eliminate 2, 4, 6-tribromophenol (TBP) in aqueous phase. In comparison with pure CNTs or AgX, the nanocomposites showed a significant improvement in visible light photocatalytic degradation efficiency because they effectively transfer electron from plasmon-excited Ag (0) and photoexcited AgX nanoparticles to CNTs. As a result, a prolonged photoholes lifetime and enhancement of the degradation efficiency could be achieved due to effective reduction of electron–hole recombination.

Using a hydrothermal process, Yue et al. [69] produced a visible-light-sensitive heterojunction photocatalyst with the formula of Bi_2MoO_6–BiOCl. The as-prepared composite showed an irregular multi-plate structure composed of BiOCl and Bi_2MoO_6 nanoplates over each other. Compared to pure Bi_2MoO_6 and BiOCl, the synthesized photocatalyst showed higher photocatalytic activity. 30% Bi_2MoO_6 content was found to be optimal for the photocatalytic activity of the composites. The O_2 and OH^- had the main roles in rhodamine B (RhB) degradation through the Bi_2MoO_6–BiOCl composite.

In another study, Hamid et al. [70] synthesized a UV-visible light-responsive nanophotocatalyst composed of TiO_2 and multiwalled carbon nanotube (MWCNT). The nanocomposites were produced via a modified sol-gel technique by functionalized MWCNTs and titanium isopropoxide as the initiating precursors. It was indicated that the surface of the MWCNTs were coated by TiO_2 nanoparticles with a diameter of 10–20 nm. MWCNT/TiO_2 Pure and TiO_2 nanoparticles had the specific surface areas of 181 and 80 m^2/ g, respectively. Therefore, photocatalytic performance of MWCNT/TiO_2 was better compared to pure TiO_2 due to higher surface area leading to functioning as enhanced electron acceptors and electron-hole pair recombination inhibitors. Other reports have also highlighted the CNT/TiO_2 nanocomposites [71].

Photocatalytic performance under visible light radiation for the degradation of RhB by g-C_3N_4–Fe_3O_4 nanocomposites synthesized by Kumar et al. [72], exhibited remarkabe improvement. Based on the obtained results, the nanocatalysts could be magnetically recovered and exhibited good recyclability while keeping their photocatalytic activity after six cycles. The high photocatalysts activity of the nanocomposite is because of improved charge-separation properties, high visible-light-absorption efficiency, and the large surface-exposure area. Additionally, the nanocomposites possessed superparamagnetic properties suggesting them as promising candidates for bionanotechnology and lithium storage capacity applications.

Research investigation on Cu-doped ZnO/carbon nanotube nanocomposites by Ahmad et al. [73] showed effective MO bleaching out which was the indicator of a significant photocatalytic improvement over ZnO, ZnO/CNTs, and Cu-doped ZnO nanoparticles. Based on the results, the organic molecules were completely destroyed with color disappearance and the significant reduction in chemical oxygen demand of the treated effluent. The large surface area and excellent electrical properties of CNTs caused increased charge/separation efficiency, extended light absorbing capability, and higher dyes adsorptivity and, eventually, dramatic improvement of nanocomposite photoactivity.

Another visible-light-induced photocatalyst fabricated by a simple solution method is Ag_2O/GO nanocomposite. During Ag_2O/GO nanocomposite formation, negatively charged GO sheets interact electrostatically with positively charged Ag+. The synthesized nanocomposites demonstrated promoted photocatalytic activity compared to Ag_2O nanoparticles because of the enhanced electron–hole pair separation, smaller sizes of the Ag_2O nanoparticles, and the enhanced adsorption capacity. The obtained results open new avenues to design photocatalysts with high efficiency for eliminating organic contaminants from water [73].

Tongon et al. [74] incorporated Ag-doped TiO_2 into mesostructured silica (MCM-41) by a microwave assisted sol–gel route for the preparation of a nanocomposite film with visible light responsive property. High photocatalytic properties and adsorbability of the TiO_2 photocatalyst improved by MCM-41 and Ag were observed. Ag/Ti/Si with the composition of 0.1/1/2 showed methylene blue (MB) decolorization efficiency equal to 30% under visible light, and 81% under UV light.

Ong et al. [74] prepared solvent exfoliated graphene (SEG)/ZnO photocatalysts using a simple chemical deposition-calcination method. The Reactive Black 5 (RB5) degradation of prepared nanocomposites were 97% and their rate constant was 0.0199 min–1 under an energy-saving light bulb which was indicated to be more than that of ZnO and SEG. The ZnO content of 69.0 wt. % in the nanocomposite showed a significant improvement after graphene hybridization comparwd to pure ZnO. The enhancement was reported to be due to electron–hole recombination retardation and effective dye sensitization by SEG as electron storage.

The CdS/$La_2Ti_2O_7$ photocatalyst nanocomposite was produced using a sonochemical coupled technique. This nanocomposite demonstrated a strong photocatalytic decomposition of methyl orange (MO) under visible light and UV radiation. The highest photocatalytic activity was obtained for the sample with La to Cd ratio of 1:3. The improved photocatalytic property of this nanocomposite was proposed to be related to the matched band potential of the two semiconductors and the layered structure of the nanocomposite [75].

Zhu et al. [76] used GO nanosheets to enwrap Ag/AgX (X = Cl, Br) nanocomposites using a water/oil system. The prepared hybrid nanocomposites had the potential to be employed as a stable plasmonic photocatalyst for degradation of MO by visible-light radiation. Ag/AgX/GO nanocomposites displayed improved photocatalytic activities in comparison with the Ag/AgX nanocomposites. Incorporation of GO nanosheets caused the retarded electron–hole pairs recombination, the facilitated charge transfer, the smaller Ag/AgX nanoparticles, and the nice adsorptive capacity to MO molecules leading to promotion of photocatalytic performance of Ag/AgX/GO. Based on these obtained results, developing graphene oxide-based plasmonic photocatalysts with high efficiency and stability would be possible.

In another research, nanocomposites of SnS_2/SnO_2 consisting of different SnO_2 contents were produced by in situ hydrothermal oxidation of tin sulfide nanoparticles. According to the results, the synthesized nanocomposites with optimum amount of SnO_2 showed remarkable photocatalytic stability as well as higher photocatalytic activity in comparison with SnS_2 nanoparticles and the physical mixture of SnO_2 and SnS_2 nanoparticles. The high photocatalytic performances of SnS_2/SnO_2 nanocomposites relates to bonding of SnO_2 to SnS_2 particles through which electron transfer at the interface could be facilitated and the self-agglomeration of the particles could be reduced [77].

Dong et al. [78] used an in situ photoactivated method to fabricate AgBr/Ag nanocomposites in which Ag nanoparticles deposited evenly on the AgBr surface. Exposing to the irradiation of direct sunlight or cool daylight fluorescent lamp, the prepared nanocomposites revealed superior visible light photocatalytic performance against organic pollutant decomposition even under the diffuse indoor daylight. Moreover, the nanocomposites showed higher stability.

TiO_2/(TiO_2–V_2O_5)/polypyrrole (PPy) nanocomposites were synthesized by Piewnuan et al. [79] using in situ polymerization. According to the results, the absorbance of the nanocomposites was higher than those of neat TiO_2 and TiO_2/PPy due to the reduction in the band gap energy of the materials. The nanocomposite catalytic activity was also continued in the dark. The mentioned behaviors are caused by capability of the polymer to act as a binder in the system and the energy storage ability of V_2O_5.

Gu et al. [80] incorporated reduced graphene oxide in N-doped TiO_2 (N–TiO_2) as well as V co-doped TiO_2 (N, V–TiO_2) using a hydrothermal method. Both nanocomposite exhibited superior visible light photocatalytic performance compared to N,V–TiO_2 and N–TiO_2. The

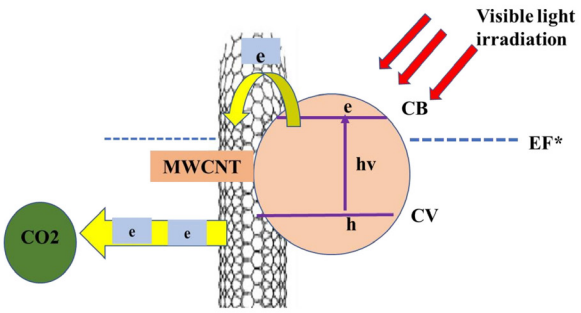

Fig. 6. MWCNT/TiO_2 core–shell nanocomposites.

reasons for such enhancement included minimizing the photoinduced electrons and holes recombination, high light absorption intensity, more excited states, and improvement of pollutants adsorption under visible light irradiation.

Pakula et al. [81] synthesized metal/ poly(methylmethacrylate) (PMMA) nanocomposites with light-controlled conductance switching property. The nanocomposites preparation was carried out by physical vapor deposition of Pt and Au clusters on azo-dye doped poly(methylmethacrylate) thin film. Functionalizing the azo groups with branches and tails caused high dye concentrations, which enhanced solubility. Under alternating irradiation of blue light and UV, a complete reversible optical switching of the absorption bands of the nanocomposites was observed.

Graphene quantum dots (GQDs) [82], functionalized by polyethylenimine (GQD–PEIs) nanocomposites were produced by Liu et al. [83] using hydrothermal method. Subsequently, by the amidation reaction of the PEI moieties with isobutyric anhydride, isobutyric amide (IBAm) groups were anchored on the functionalized GQD. The prepared nanocomposites was responsive to temperature, pH, loaded organic guests, and inorganic salts. The modulation of cloud point temperature (Tcp) of the composites in aqueous solutions was reported to be done by altering the the inorganic salts type, pH, the inorganic salts concentration, loaded organic guests, and the number of IBAm units in the nanocomposites. It was indicated that the nanocomposites were photoluminescent, and outside stimuli did not influence their maximum emission wavelengths. A negligibly influence of polar aspirin guest, pH, and traditional salting-out anions such as SO42− and Cl− on emission intensities were observed. It was also verified that the aspirin guest with relative polarity was absorbed by PEI–IBAm shell, while, the PBA guest with relative hydrophobicity was adsorbed by the GOD core. The guest release rate varied below and above Tcp.

Ren et al. [84] developed a graphene (GR)–CdS nanocomposite using a hydrothermal route in which the GR scaffold closely enwrapped CdS ingredients. They reported that incorporation of two-dimensional GR scaffolds to CdS microspheres had significant influence on hybrid nanocomposites properties including morphology, electronic and optical nature of the nanocomposite. The selective organic transformation results showed that the synthesized nanocomposite could be used as a visible-light-activated photocatalyst for efficient benzyl alcohol oxidation to benzaldehyde at ambient temperature. The combined influence of high electron conductivity and improved light absorption intensity of GR incorporated to remarkably improve the photocatalytic activity of the nanocomposites. These factors increased the lifetime of electron–hole pairs generated by light irradiation and facilitated charge separation. The research could provide the information for production of narrow band-gap semiconductor or GR hybrid nanocomposites applicable for a wide range of photocatalysis.

In a study conducted by Fernández et al. [85], Au nanorods (NRs) were coated by thermoresponsive poly(N-isopropylacrylamide) microgel shells. The investigations by optical extinction measurements and simultaneous laser-heating revealed that the Au cores could be simultaneously utilized for sensitive optical reporting of the microgel state and fast optothermal manipulating (switching) with the possibility of external control in a reversible manner.

Kong et al. [86] functionalized TiO_2 nanoparticles with antifouling ethylene glycol dimethacrylate and biocidal 2-(tert-butylamino)ethyl methacrylate containing nontoxic secondary amine. Compared to pure TiO_2 nanoparticles, core/shell nanoparticles showed higher photocatalytic antibacterial characteristics due to the synergetic antibacterial activity of light-driven biocidal polymer shell as well as TiO_2 core. The prepared nanocomposites showed high antimicrobial efficiency of 95.7% for gram-positive S. aureus in the dark condition. Moreover, in comparison with pristine TiO_2 nanoparticles, the nanocomposite demonstrated enhanced inhibition of bacterial growth during UV irradiation.

Woo et al. [87] reported the improved photoluminescence of layered nanocomposites consisting of Sr_2SiO_4:Eu green phosphor core, multishell of CdSe/CdS/CdZnS/ZnS red quantum dots, and thermo-curable resin. Two kinds of mixed and layered composite were produced, and the layered structure was found to be more effective compared to the mixed structure in terms of thermal loss, PL decay, and PL intensity. Moreover, by using the layered nanocomposite for preparing white light emitting diodes, the value of color rendering index increased to 88.4 and brightness enhanced by 37% in comparison with the mixed one.

Choi et al. [88], fabricated a dual-responsive nanocomposite including two noble metal nanoparticles and two polymer brushes and reported that they exhibited a significant improvement in selectivity for determining various liquids in comparison with a single-responsive LSPR sensor. Two hydrophilic and hydrophobic polymer brushes provided the dual-responsive LSPR sensor, which showed different response according to the interaction degree among the surrounding liquids and the polymer brushes. Additionally, the accurate estimation of the mixing ratio of two solvents, suggesting the dual-nanocomposite LSPR sensor as in situ process monitoring platform.

Chaengchawi et al. [89] synthesized a visible-light responsive nanocomposite of CdS/ZnO as a photocatalyst. The obtained results demonstrated that the ZnO to CdS ratio had a significant effect on photocatalytic activity among which the highest photocatalytic performance was related to the mole ratio of 1:4 exhibiting higher activity compared to pure ZnO and CdS. A novel ZnO-TiO_2 nanocomposite was also proposed by Haghighatzadeh et al. [90].

Nanocomposites with the composition of $TiO_{2-x}N_y$/Ag–$PbMoO_4$ were produced using sonochemical technique. In comparison with Ag–$PbMoO_4$ and $TiO_{2-x}N_y$, photoinactivation of green tide (Tetraselmis suecica) of the synthesized nanocomposites was improved under simulated solar light. The nanocomposites were able to remove 100% of Tetraselmis suecica after 25 minutes. By inhibition of electron–hole recombination, the charge transfer was facilitated leading to enhancement of the nanocomposite photocatalytic activity [91].

In a study carried out by Pirhashemi et al. [92], the ZnO/Ag/Ag-$_2WO_4$ nanocomposites exhibited good photocatalytic activity for RhB degradation. This enhancement was due to the heterojunctions formation among the counterparts and the surface plasmon resonance effect of Ag, which resulted in effective suppression of photogenerated charge carriers' recombination.

A novel nanocomposite for photocatalytic degradation of organic pollutants composed of Ag/CeO_2 was produced by Saravanakumar et al. [93] using hydrothermal method. The nanocomposite showed superior activity with the ability to degrade the RhB dye in 70 minutes, under visible light irradiation. Due to producing a large amount of OH radicals, the photocatalytic degradation enhanced. As a result of the lower

charge carriers' recombination, the nanocomposite efficacy was much higher compared to pure CeO_2. The surface plasmon resonance effect of Ag nanoparticles is a reason for the high photocatalytic activity of nanocomposites.

According to Ahmad et al. [94] study, the incorporation of GO in CdO/GO nanocomposites improved the organic dyes photocatalytic degradation due to provision of more active sites available in high surface area. Highest MB degradation of 95% was achieved for the composition of 3.3% GO after 35 minutes irridation in comparison with CdO and other compositions. GO inhibits the electron–hole pair recombination, extends the light absorption range, and increase the adsorbability of the catalysts, which leads to photocatalytic efficiency improvement of CdO/GO nanocomposite. It was proposed that these nanomaterials have the potential to be employed for organic pollutants degradations from wastewater.

Hybrid nanocomposite photocatalysts of $CuO(x)/SmFeO_3$ were prepared by Behzadifaed et al. [95]. Because of larger separation efficiency of photoinduced electron-hole pair, the CuO(10 wt%)/$SmFeO_3$ electrode showed the photocurrent of approximately 2 times more than that of the CuO and $SmFeO_3$. The highest photocatalytic efficiency of 65% and the photocatalytic activity of 100% were achieved under visible light radiation for RhB dye degradation exhibiting the existence of both photocatalytic mechanisms and Fenton-like oxidation. Due to being highly active and stable, they suggested the prepared hybrid photocatalyst as a potential material for industrial water treatment.

According to a study by Gan et al. [96], $CoFe_2O_4$ incorporated Ag_3PO_4 nanocomposites with core-shell structure were synthesized using a precipitation method. According to the results, the $CoFe_2O_4$ nanoparticles incorporation narrowed the Ag_3PO_4 band gap. The core-shelled structured nanocomposites showed superior efficiency of dyes degradation under the tungsten halogen lamp light in comparison with pristine Ag_3PO_4. Additionally, the nanocomposites exhibited good recycling stability for the dyes photocatalysis degradation and were magnetically separable. Overall, this research offers a new nanocomposite with the capability of photocatalytic degradation of organic contaminants present in wastewater, while does not introduce secondary pollutant into the system.

Using ultrasonic-irradiation echnique, Mousavi et al. [97] fabricated g-C_3N_4/Fe_3O_4/Ag_3PO_4/ AgCl nanocomposites which had promising photocatalytic activity under visible-light irradiation. This nanocomposite demonstrated higher photocatalytic performance in degradation of RhB than that of g-C_3N_4. Because of significant saturation magnetization of 8.78 emu.g−1, it was possible to easily separate the photocatalyst from the solution after treatment by an external magnetic field. It was found that driving the degradation reaction is caused mostly by holes as main active species.

The $NiFe_2O_4$/MWCNTs/ZnO nanocomposite was also fabricated with solar radiation driven photocatalic activity. Upon solar radiation, the prepared nanocomposite showed a significant enhancement in photocatalytic activity in comparison with ZnO and $NiFe_2O_4$ for degradation of MB dye in aqueous solutions. Recombination retardation of electron–hole pairs caused higher charge separation efficiency leading to improved photocatalytic activity. They reported that the apparent rate constant (kapp) of the MB degradation in 300 minutes using ZnO, $NiFe_2O_4$, and $NiFe_2O_4$/MWCNTs/ZnO were 0.002, 4.12857E-4, and 0.00438 min−1, respectively. The magnetic properties of the nanocomposite provide the possibility of its separation and re-usability after degradation experiments. It was suggested that the prepared nanocomposite can be utilized as a solar radiation driven photocatalyst [98].

Ebrahimi et al. [99] reported that by using Mn-doped ZnO_2/graphene nanocomposite 66.2% of 2,4-D could be degraded photocatalytically under LED radiation at pH 5.

Paul et al. [100] reported the preparation of a $MnMoO_4$/$NiFe_2O_4$ nanocomposite using co- hydrothermal and precipitation routes. The synthesized photocatalyst exhibited 95% Basic Fuchsin removal efficiency and superior photocatalytic activity with 96% efficiency for different dyes including Methyl Violet (MV), RhB, and MB degradation in aqueous medium under visible light radiation. Increased agglomerated forms of the synthesized $MnMoO_4$/$NiFe_2O_4$ nanocomposites were observed in the spent photocatalyst.

Nickel tungstate/tin phthalocyanine (NiWO4/SnPc) nanocomposite produced by the solvent evaporation technique showed the enhancement of NiWO4 photocatalytic property for Rhodamine blue degradation [101].

Core–shell nanocomposites consisted of MWCNT/TiO_2 demonstrated that their photoactivity in the visible light was remarkably improved with extension of absorption edge to the region related to visible light. These nanocomposites showed continuous transformation of CO_2 into methane at atmospheric pressure and under the irradiation of low power visible light. After 6 hours of irradiation, the maximum methane production of ca. 0.17 μmol/g-catalyst/h was achieved. Fig 6 depicts the model used in this article [102].

5. Conclusions and future insights

Using light-sensitivity as an attractive property for preparation of advanced DDS that can modulate the rate and site externally. In order to optimize the therapeutic efficiency and reproducible release profiles of the light responsive materials various approaches is currently investigated. In order to use the light-sensitive DDS for clinical practices, considerable additional efforts are required regarding specific aspects including: (1) In vivo analysis of newly developed delivery systems. In order to make progress toward clinical applications, supplementary in vivo studies must be carried out in addition to in vitro investigations. (2) Specialized equipment to provide sufficient irradiation intensity for targeting specific region while does not alter surrounding tissues. Because the human body is to relatively impermeable to the light, applicability of the visible light⁄ UV-sensitive DDS is limited to treatments of the skin surface layers. Feasible alternatives to light⁄ UV-sensitive DDS appear to be NIR-sensitive light materials and NIR lasers. (3) Design and fabrication of new biocompatible materials for extending the range of light-sensitive polymers and lipids which meet the needs for developing safe products. For example, azobenzene groups are considered as toxic materials by the FDA which constrains the application of such DDS [103].

It is expected that novel nanocomposites with various chemical designs will offer an attractive and insightful approaches to overcome the problems of both ingestion and identification, enhance intertumoral accumulation and decrease the drugs toxicity to produce high-sensitive materials with high efficiency.

REFERENCES

[1] S. Ravi, F. Winfred Shashikanth, Magnetic properties of Mo-doped TiO_2 nanoparticles: A candidate for dilute magnetic semiconductors, Materials Letters 264 (2020) 127331.

[2] S. Ananthakumar, J. Ramkumar, S.M. Babu, Semiconductor nanoparticles sensitized TiO_2 nanotubes for high efficiency solar cell devices, Renewable and Sustainable Energy Reviews 57 (2016) 1307-1321.

[3] L.L. Beecroft, C.K. Ober, Nanocomposite materials for optical applications, Chemistry of materials 9(6) (1997) 1302-1317.

[4] H. Chen, Y. Zhao, Applications of Light-Responsive Systems for Cancer Theranostics, ACS Applied Materials & Interfaces 10(25) (2018) 21021-21034.

[5] R. Bisht, J.K. Jaiswal, I.D. Rupenthal, Nanoparticle-loaded biodegradable light-responsive in situ forming injectable implants for effective peptide delivery to the posterior segment of the eye, Medical Hypotheses 103 (2017) 5-9.

[6] K. Haraguchi, Nanocomposite hydrogels, Current Opinion in Solid State and Materials Science 11(3-4) (2007) 47-54.

[7] S. Sortino, Nanostructured molecular films and nanoparticles with photoactivable functionalities, Photochemical & Photobiological Sciences 7(8) (2008) 911-924.
[8] E. Johansson, E. Choi, S. Angelos, M. Liong, J.I. Zink, Light-activated functional mesostructured silica, Journal of sol-gel science and technology 46(3) (2008) 313-322.
[9] A.K. Agegnehu, C.-J. Pan, M.-C. Tsai, J. Rick, W.-N. Su, J.-F. Lee, B.-J. Hwang, Visible light responsive noble metal-free nanocomposite of V-doped TiO_2 nanorod with highly reduced graphene oxide for enhanced solar H_2 production, International Journal of Hydrogen Energy 41(16) (2016) 6752-6762.
[10] I.I. Slowing, B.G. Trewyn, S. Giri, V.Y. Lin, Mesoporous silica nanoparticles for drug delivery and biosensing applications, Advanced Functional Materials 17(8) (2007) 1225-1236.
[11] D.Y. Wu, S. Meure, D. Solomon, Self-healing polymeric materials: a review of recent developments, Progress in polymer science 33(5) (2008) 479-522.
[12] R.M. Abozaid, Z.Ž. Lazarević, I. Radović, M. Gilić, D. Šević, M.S. Rabasović, V. Radojević, Optical properties and fluorescence of quantum dots CdSe/ZnS-PMMA composite films with interface modifications, Optical Materials 92 (2019) 405-410.
[13] H.U. Kim, Y.H. Roh, M.S. Shim, K.W. Bong, Microfluidic fabrication of fatty alcohol-based microparticles for NIR light-triggered drug release, Journal of Industrial and Engineering Chemistry 80 (2019) 778-783.
[14] L.-t. Liu, M.-j. Chen, H.-l. Yang, Z.-j. Huang, Q. Tang, C.-f. Chow, C.-b. Gong, M.-h. Zu, B. Xiao, An NIR-light-responsive surface molecularly imprinted polymer for photoregulated drug release in aqueous solution through porcine tissue, Materials Science and Engineering: C 106 (2020) 110253.
[15] Z. Liu, J. Shi, Y. Wang, Y. Gan, P. Wan, Facile preparation of pyrenemethyl ester-based nanovalve on mesoporous silica coated upconversion nanoparticle for NIR light-triggered drug release with potential monitoring capability, Colloids and Surfaces A: Physicochemical and Engineering Aspects 568 (2019) 436-444.
[16] M.S. Noh, S. Lee, H. Kang, J.-K. Yang, H. Lee, D. Hwang, J.W. Lee, S. Jeong, Y. Jang, B.-H. Jun, Target-specific near-IR induced drug release and photothermal therapy with accumulated Au/Ag hollow nanoshells on pulmonary cancer cell membranes, Biomaterials 45 (2015) 81-92.
[17] J. Wang, Y. Liu, Y. Ma, C. Sun, W. Tao, Y. Wang, X. Yang, J. Wang, NIR-Activated Supersensitive Drug Release Using Nanoparticles with a Flow Core, Advanced Functional Materials 26(41) (2016) 7516-7525.
[18] G. Yang, J. Liu, Y. Wu, L. Feng, Z. Liu, Near-infrared-light responsive nanoscale drug delivery systems for cancer treatment, Coordination Chemistry Reviews 320 (2016) 100-117.
[19] A. Raza, U. Hayat, T. Rasheed, M. Bilal, H.M.N. Iqbal, "Smart" materials-based near-infrared light-responsive drug delivery systems for cancer treatment: A review, Journal of Materials Research and Technology 8(1) (2019) 1497-1509.
[20] X. Li, D. Liu, Y. Wang, S. Xu, H. Liu, Water dispersive upconversion nanoparticles for intelligent drug delivery system, Colloids and Surfaces A: Physicochemical and Engineering Aspects 555 (2018) 55-62.
[21] H.M. Lin, W.K. Wang, P.A. Hsiung, S.G. Shyu, Light-sensitive intelligent drug delivery systems of coumarin-modified mesoporous bioactive glass, Acta Biomaterialia 6(8) (2010) 3256-3263.
[22] S. Sershen, J. West, Implantable, polymeric systems for modulated drug delivery, Advanced drug delivery reviews 54(9) (2002) 1225-1235.
[23] D. Zhang, M. Wu, Y. Zeng, L. Wu, Q. Wang, X. Han, X. Liu, J. Liu, Chlorin e6 conjugated poly (dopamine) nanospheres as PDT/PTT dual-modal therapeutic agents for enhanced cancer therapy, ACS applied materials & interfaces 7(15) (2015) 8176-8187.
[24] W. Chen, S. Zhang, X. Liu, Q.-X. Sun, O. Johnson, T. Yang, M.-L. Chen, J.-H. Wang, CuS@ PDA–FA Nanocomposites: A Dual Stimuli-responsive DOX Delivery Vehicle with Ultrahigh Loading Level for Synergistic Photothermal-chemotherapies on Breast Cancer, Journal of Materials Chemistry B (2020).
[25] H.-J. Cai, T.-T. Shen, J. Zhang, C.-F. Shan, J.-G. Jia, X. Li, W.-S. Liu, Y. Tang, A core–shell metal–organic-framework (MOF)-based smart nanocomposite for efficient NIR/H2O2-responsive photodynamic therapy against hypoxic tumor cells, Journal of Materials Chemistry B 5(13) (2017) 2390-2394.
[26] A. GhavamiNejad, M. SamariKhalaj, L.E. Aguilar, C.H. Park, C.S. Kim, pH/NIR light-controlled multidrug release via a mussel-inspired nanocomposite hydrogel for chemo-photothermal cancer therapy, Scientific reports 6(1) (2016) 1-12.
[27] M. Wang, J. Wu, Y. Li, F. Li, X. Hu, G. Wang, M. Han, D. Ling, J. Gao, A tumor targeted near-infrared light-controlled nanocomposite to combat with multidrug resistance of cancer, Journal of Controlled Release 288 (2018) 34-44.
[28] M. Nešić, I. Popović, A. Leskovac, Z. Šaponjić, M. Radoičić, M. Stepić, M. Petković, Testing the photo-sensitive nanocomposite system for potential controlled metallo-drug delivery, Optical and Quantum Electronics 48(2) (2016) 119.
[29] S.H. Hu, Y.W. Chen, W.T. Hung, I.W. Chen, S.Y. Chen, Quantum-dot-tagged reduced graphene oxide nanocomposites for bright fluorescence bioimaging and photothermal therapy monitored in situ, Advanced materials 24(13) (2012) 1748-1754.
[30] Y.-W. Chen, Y.-L. Su, S.-H. Hu, S.-Y. Chen, Functionalized graphene nanocomposites for enhancing photothermal therapy in tumor treatment, Advanced drug delivery reviews 105 (2016) 190-204.
[31] A. Kazemzadeh, M.A. Meshkat, H. Kazemzadeh, M. Moradi, R. Bahrami, R. Pouriamanesh, Submission Title: Preparation of Graphene Nanolayers through Surfactant-assisted Pure Shear Milling Method, Composites and Compounds 1(1) (2019).
[32] X. Xu, Z. Huang, Z. Huang, X. Zhang, S. He, X. Sun, Y. Shen, M. Yan, C. Zhao, Injectable, NIR/pH-responsive nanocomposite hydrogel as long-acting implant for chemophotothermal synergistic cancer therapy, ACS applied materials & interfaces 9(24) (2017) 20361-20375.
[33] Y. Chen, G. Song, J. Yu, Y. Wang, J. Zhu, Z. Hu, Mechanically strong dual responsive nanocomposite double network hydrogel for controlled drug release of asprin, Journal of the mechanical behavior of biomedical materials 82 (2018) 61-69.
[34] Z. Teng, B. Wang, Y. Hu, D. Xu, Light-responsive nanocomposites combining graphene oxide with POSS based on host-guest chemistry, Chinese Chemical Letters 30(3) (2019) 717-720.
[35] G. Luo, W. Chen, H. Jia, Y. Sun, H. Cheng, R. Zhuo, X. Zhang, An indicator-guided photo-controlled drug delivery system based on mesoporous silica/gold nanocomposites, Nano Research 8(6) (2015) 1893-1905.
[36] K. Shi, Z. Liu, Y.-Y. Wei, W. Wang, X.-J. Ju, R. Xie, L.-Y. Chu, Near-infrared light-responsive poly (N-isopropylacrylamide)/graphene oxide nanocomposite hydrogels with ultrahigh tensibility, ACS applied materials & interfaces 7(49) (2015) 27289-27298.
[37] J. Li, Z. Lyv, Y. Li, H. Liu, J. Wang, W. Zhan, H. Chen, H. Chen, X. Li, A theranostic prodrug delivery system based on Pt (IV) conjugated nano-graphene oxide with synergistic effect to enhance the therapeutic efficacy of Pt drug, Biomaterials 51 (2015) 12-21.
[38] B. Xia, W. Zhang, J. Shi, J. Li, Z. Chen, Q. Zhang, NIR light-triggered gelling in situ of porous silicon nanoparticles/PEGDA hybrid hydrogels for localized combinatorial therapy of cancer cells, Journal of Applied Polymer Science 136(17) (2019) 47443.
[39] Z. Yang, X. Liu, X. Wang, P. Wang, S. Ruan, A. Xie, Y. Shen, M. Zhu, 4-in-1 Phototheranostics: PDA@ CoPA-LA Nanocomposite for Photothermal Imaging/Photothermal/In-situ O2 Generartion/Photodynamic Combination Therapy, Chemical Engineering Journal (2020) 124113.
[40] Y. Ma, F. Yan, L. Liu, W. Wei, Z. Zhao, J. Sun, The enhanced photo-thermal therapy of Surface improved photoactive cadmium sulfide (CdS) quantum dots entrenched graphene oxide nanoflakes in tumor treatment, Journal of Photochemistry and Photobiology B: Biology 192 (2019) 34-39.
[41] M. Gorgizadeh, N. Behzadpour, F. Salehi, F. Daneshvar, R.D. Vais, R. Nazari-Vanani, N. Azarpira, M. Lotfi, N. Sattarahmady, A MnFe2O4/C nanocomposite as a novel theranostic agent in MRI, sonodynamic therapy and photothermal therapy of a melanoma cancer model, Journal of Alloys and Compounds 816 (2020) 152597.
[42] W. Liu, X. Zhang, L. Zhou, L. Shang, Z. Su, Reduced graphene oxide (rGO) hybridized hydrogel as a near-infrared (NIR)/pH dual-responsive platform for combined chemo-photothermal therapy, Journal of colloid and interface science 536 (2019) 160-170.
[43] R. Klajn, Spiropyran-based dynamic materials, Chemical Society Reviews 43(1) (2014) 148-184.
[44] W. Wu, A.D. Li, Optically switchable nanoparticles for biological imaging, (2007).
[45] G. Tan, Y. Zhong, L. Yang, F. Ren, Metal-Organic Frameworks@ Thermosensitive Hydrogel as Injectable Implant for Dual Drug Synergistic Oral Cancer Therapy, Available at SSRN 3458140.
[46] Q. Lin, C. Bao, S. Cheng, Y. Yang, W. Ji, L. Zhu, Target-activated coumarin phototriggers specifically switch on fluorescence and photocleavage upon bonding to thiol-bearing protein, Journal of the American Chemical Society 134(11) (2012) 5052-5055.
[47] Y. Wang, B. Li, L. Zhang, H. Song, L. Zhang, Targeted delivery system based on magnetic mesoporous silica nanocomposites with light-controlled release character, ACS applied materials & interfaces 5(1) (2013) 11-15.
[48] Z. Jiang, B. Dong, B. Chen, J. Wang, L. Xu, S. Zhang, H. Song, Multifunctional Au@ $mSiO_2$/rhodamine B isothiocyanate nanocomposites: cell imaging, photocontrolled drug release, and photothermal therapy for cancer cells, small 9(4)

(2013) 604-612.
[49] W. Dong, Y. Li, D. Niu, Z. Ma, J. Gu, Y. Chen, W. Zhao, X. Liu, C. Liu, J. Shi, Facile synthesis of monodisperse superparamagnetic Fe3O4 core@ hybrid@ Au shell nanocomposite for bimodal imaging and photothermal therapy, Advanced materials 23(45) (2011) 5392-5397.
[50] X. Zhang, P. Yang, Y. Dai, P.a. Ma, X. Li, Z. Cheng, Z. Hou, X. Kang, C. Li, J. Lin, Multifunctional Up-converting nanocomposites with smart polymer brushes gated mesopores for cell imaging and thermo/pH dual-responsive drug controlled release, Advanced Functional Materials 23(33) (2013) 4067-4078.
[51] C.H. Zhu, Y. Lu, J. Peng, J.F. Chen, S.H. Yu, Photothermally sensitive poly (N-isopropylacrylamide)/graphene oxide nanocomposite hydrogels as remote light-controlled liquid microvalves, Advanced Functional Materials 22(19) (2012) 4017-4022.
[52] C. Xu, D. Yang, L. Mei, Q. Li, H. Zhu, T. Wang, Targeting chemophotothermal therapy of hepatoma by gold nanorods/graphene oxide core/shell nanocomposites, ACS applied materials & interfaces 5(24) (2013) 12911-12920.
[53] J. Bai, Y. Liu, X. Jiang, Multifunctional PEG-GO/CuS nanocomposites for near-infrared chemo-photothermal therapy, Biomaterials 35(22) (2014) 5805-5813.
[54] H. Kang, A.C. Trondoli, G. Zhu, Y. Chen, Y.-J. Chang, H. Liu, Y.-F. Huang, X. Zhang, W. Tan, Near-infrared light-responsive core–shell nanogels for targeted drug delivery, ACS nano 5(6) (2011) 5094-5099.
[55] Y. Wang, L. Wang, L. Guo, M. Yan, L. Feng, S. Dong, J. Hao, Photo-responsive magnetic mesoporous silica nanocomposites for magnetic targeted cancer therapy, New Journal of Chemistry 43(12) (2019) 4908-4918.
[56] Y. Yu, M. Zhou, W. Zhang, L. Huang, D. Miao, H. Zhu, G. Su, Rattle-type gold nanorods/porous-SiO_2 nanocomposites as near-infrared light-activated drug delivery systems for cancer combined chemo–photothermal therapy, Molecular pharmaceutics 16(5) (2019) 1929-1938.
[57] D. Niu, W. Jiang, H. Liu, T. Zhao, B. Lei, Y. Li, L. Yin, Y. Shi, B. Chen, B. Lu, Reversible bending behaviors of photomechanical soft actuators based on graphene nanocomposites, Scientific reports 6 (2016) 27366.
[58] S. Tang, B. Xuan, X. Ye, Z. Huang, Z. Qian, A modular vaccine development platform based on sortase-mediated site-specific tagging of antigens onto virus-like particles, Scientific reports 6(1) (2016) 1-9.
[59] H. Wang, L. Zhang, Z. Chen, J. Hu, S. Li, Z. Wang, J. Liu, X. Wang, Semiconductor heterojunction photocatalysts: design, construction, and photocatalytic performances, Chemical Society Reviews 43(15) (2014) 5234-5244.
[60] F. Correia, M. Calheiros, J. Marques, J. Ribeiro, C. Tavares, Synthesis of Bi_2O_3/TiO_2 nanostructured films for photocatalytic applications, Ceramics International 44(18) (2018) 22638-22644.
[61] T. Jayaraman, A.P. Murthy, V. Elakkiya, S. Chandrasekaran, P. Nithyadharseni, Z. Khan, R.A. Senthil, R. Shanker, M. Raghavender, P. Kuppusami, Recent development on carbon based heterostructures for their applications in energy and environment: A review, Journal of Industrial and Engineering Chemistry 64 (2018) 16-59.
[62] H. Li, Y. Zhou, W. Tu, J. Ye, Z. Zou, State-of-the-art progress in diverse heterostructured photocatalysts toward promoting photocatalytic performance, Advanced Functional Materials 25(7) (2015) 998-1013.
[63] C. Chang, L. Zhu, S. Wang, X. Chu, L. Yue, Novel mesoporous graphite carbon nitride/BiOI heterojunction for enhancing photocatalytic performance under visible-light irradiation, ACS applied materials & interfaces 6(7) (2014) 5083-5093.
[64] F. Soleimani, M. Salehi, A. Gholizadeh, Comparison of visible light photocatalytic degradation of different pollutants by $(Zn, Mg)_xCu_{1-x}Bi_2O_4$ nanoparticles, Ceramics International 45(7) (2019) 8926-8939.
[65] B. Pant, M. Park, S.-J. Park, H.-Y. Kim, One-pot synthesis of CdS sensitized TiO2 decorated reduced graphene oxide nanosheets for the hydrolysis of ammonia-borane and the effective removal of organic pollutant from water, Ceramics International 42(14) (2016) 15247-15252.
[66] T. Jayaraman, S.A. Raja, A. Priya, M. Jagannathan, M. Ashokkumar, Synthesis of a visible-light active V_2O_5–gC_3N_4 heterojunction as an efficient photocatalytic and photoelectrochemical material, New Journal of Chemistry 39(2) (2015) 1367-1374.
[67] R.A. Senthil, S. Osman, J. Pan, Y. Sun, T.R. Kumar, A. Manikandan, A facile hydrothermal synthesis of visible-light responsive $BiFeWO_6/MoS_2$ composite as superior photocatalyst for degradation of organic pollutants, Ceramics International 45(15) (2019) 18683-18690.
[68] H. Shi, J. Chen, G. Li, X. Nie, H. Zhao, P.-K. Wong, T. An, Synthesis and characterization of novel plasmonic Ag/AgX-CNTs (X= Cl, Br, I) nanocomposite photocatalysts and synergetic degradation of organic pollutant under visible light, ACS applied materials & interfaces 5(15) (2013) 6959-6967.
[69] D. Yue, D. Chen, Z. Wang, H. Ding, R. Zong, Y. Zhu, Enhancement of visible photocatalytic performances of a Bi_2MoO_6–BiOCl nanocomposite with plate-on-plate heterojunction structure, Physical Chemistry Chemical Physics 16(47) (2014) 26314-26321.
[70] S.B.A. Hamid, T.L. Tan, C.W. Lai, E.M. Samsudin, Multiwalled carbon nanotube/TiO2 nanocomposite as a highly active photocatalyst for photodegradation of Reactive Black 5 dye, Chinese Journal of Catalysis 35(12) (2014) 2014-2019.
[71] L. Bazli, M. Siavashi, A. Shiravi, A Review of Carbon Nanotube/TiO_2 Composite Prepared via Sol-Gel Method, Composites and Compounds 1(1) (2019).
[72] S. Kumar, B. Kumar, A. Baruah, V. Shanker, Synthesis of magnetically separable and recyclable g-C_3N_4–Fe_3O_4 hybrid nanocomposites with enhanced photocatalytic performance under visible-light irradiation, The Journal of Physical Chemistry C 117(49) (2013) 26135-26143.
[73] M. Ahmad, E. Ahmed, Z.L. Hong, X.L. Jiao, T. Abbas, N.R. Khalid, Enhancement in visible light-responsive photocatalytic activity by embedding Cu-doped ZnO nanoparticles on multi-walled carbon nanotubes, Applied Surface Science 285 (2013) 702-712.
[74] W. Tongon, C. Chawengkijwanich, S. Chiarakorn, Visible light responsive Ag/TiO_2/MCM-41 nanocomposite films synthesized by a microwave assisted sol–gel technique, Superlattices and Microstructures 69 (2014) 108-121.
[75] R. Wang, D. Xu, J. Liu, K. Li, H. Wang, Preparation and photocatalytic properties of CdS/$La_2Ti_2O_7$ nanocomposites under visible light, Chemical Engineering Journal 168(1) (2011) 455-460.
[76] M. Zhu, P. Chen, M. Liu, Graphene oxide enwrapped Ag/AgX (X= Br, Cl) nanocomposite as a highly efficient visible-light plasmonic photocatalyst, Acs Nano 5(6) (2011) 4529-4536.
[77] Y.C. Zhang, Z.N. Du, K.W. Li, M. Zhang, D.D. Dionysiou, High-performance visible-light-driven SnS_2/SnO_2 nanocomposite photocatalyst prepared via in situ hydrothermal oxidation of SnS2 nanoparticles, ACS applied materials & interfaces 3(5) (2011) 1528-1537.
[78] L. Dong, S. Tang, J. Zhu, P. Zhan, L. Zhang, F. Tong, Photoactivated route and new bromine source for AgBr/Ag nanocomposites with enhanced visible light photocatalytic activity, Materials Letters 91 (2013) 245-248.
[79] C. Piewnuan, J. Wootthikanokkhan, P. Ngaotrakanwiwat, V. Meeyoo, S. Chiarakorn, Preparation of TiO_2/(TiO_2–V_2O_5)/polypyrrole nanocomposites and a study on catalytic activities of the hybrid materials under UV/Visible light and in the dark, Superlattices and Microstructures 75 (2014) 105-117.
[80] Y. Gu, M. Xing, J. Zhang, Synthesis and photocatalytic activity of graphene based doped TiO2 nanocomposites, Applied Surface Science 319 (2014) 8-15.
[81] C. Pakula, V. Zaporojtchenko, T. Strunskus, D. Zargarani, R. Herges, F. Faupel, Reversible light-controlled conductance switching of azobenzene-based metal/polymer nanocomposites, Nanotechnology 21(46) (2010) 465201.
[82] E. Asadi, A. Fassadi Chimeh, S. Hosseini, S. Rahimi, B. Sarkhosh, L. Bazli, R. Bashiri, A.H. Vakili Tahmorsati, A Review of Clinical Applications of Graphene Quantum Dot-based Composites, Composites and Compounds 1(1) (2019).
[83] X. Liu, H.-J. Liu, F. Cheng, Y. Chen, Preparation and characterization of multi stimuli-responsive photoluminescent nanocomposites of graphene quantum dots with hyperbranched polyethylenimine derivatives, Nanoscale 6(13) (2014) 7453-7460.
[84] Z. Ren, J. Zhang, F.-X. Xiao, G. Xiao, Revisiting the construction of graphene–CdS nanocomposites as efficient visible-light-driven photocatalysts for selective organic transformation, Journal of Materials Chemistry A 2(15) (2014) 5330-5339.
[85] J. Rodríguez-Fernández, M. Fedoruk, C. Hrelescu, A.A. Lutich, J. Feldmann, Triggering the volume phase transition of core–shell Au nanorod–microgel nanocomposites with light, Nanotechnology 22(24) (2011) 245708.
[86] H. Kong, J. Song, J. Jang, Photocatalytic antibacterial capabilities of TiO2−biocidal polymer nanocomposites synthesized by a surface-initiated photopolymerization, Environmental science & technology 44(14) (2010) 5672-5676.
[87] J.Y. Woo, K. Kim, S. Jeong, C.-S. Han, Enhanced photoluminance of layered quantum dot–phosphor nanocomposites as converting materials for light emitting diodes, The Journal of Physical Chemistry C 115(43) (2011) 20945-20952.
[88] J. Choi, M.-J. Choi, J.-K. Yoo, W.I. Park, J.H. Lee, J.Y. Lee, Y.S. Jung, Localized surface plasmon-enhanced nanosensor platform using dual-responsive polymer nanocomposites, Nanoscale 5(16) (2013) 7403-7409.
[89] P. Chaengchawi, K. Serivalsatit, P. Sujaridworakun, Synthesis of visible-light responsive CdS/ZnO nanocomposite photocatalysts via simple precipitation method, Key Engineering Materials, Trans Tech Publ, 2014, pp. 224-229.
[90] A. Haghighatzadeh, M. Hosseini, B. Mazinani, M. Shokouhimehr, Improved photocatalytic activity of ZnO-TiO_2 nanocomposite catalysts by modulating TiO2 thickness, Materials Research Express 6(11) (2019) 115060.
[91] T.-H. Kim, Y.-H. Jo, G. Gyawali, R. Adhikari, T. Sekino, S.-W. Lee, Synthesis

of $TiO_{2-x}N_y$/Ag–$PbMoO_4$ nanocomposites: An effective approach for photoinactivation of green tide under simulated solar light, Materials Letters 101 (2013) 99-102.

[92] M. Pirhashemi, A. Habibi-Yangjeh, Ultrasonic-assisted preparation of plasmonic ZnO/Ag/Ag_2WO_4 nanocomposites with high visible-light photocatalytic performance for degradation of organic pollutants, Journal of colloid and interface science 491 (2017) 216-229.

[93] K. Saravanakumar, M.M. Ramjan, P. Suresh, V. Muthuraj, Fabrication of highly efficient visible light driven Ag/CeO_2 photocatalyst for degradation of organic pollutants, Journal of Alloys and Compounds 664 (2016) 149-160.

[94] J. Ahmad, K. Majid, Enhanced visible light driven photocatalytic activity of CdO–graphene oxide heterostructures for the degradation of organic pollutants, New Journal of Chemistry 42(5) (2018) 3246-3259.

[95] Z. Behzadifard, Z. Shariatinia, M. Jourshabani, Novel visible light driven CuO/$SmFeO_3$ nanocomposite photocatalysts with enhanced photocatalytic activities for degradation of organic pollutants, Journal of Molecular Liquids 262 (2018) 533-548.

[96] L. Gan, L. Xu, K. Qian, Preparation of core-shell structured $CoFe_2O_4$ incorporated Ag_3PO_4 nanocomposites for photocatalytic degradation of organic dyes, Materials & Design 109 (2016) 354-360.

[97] M. Mousavi, A. Habibi-Yangjeh, M. Abitorabi, Fabrication of novel magnetically separable nanocomposites using graphitic carbon nitride, silver phosphate and silver chloride and their applications in photocatalytic removal of different pollutants using visible-light irradiation, Journal of colloid and interface science 480 (2016) 218-231.

[98] F.A. Hezam, O. Nur, M.A. Mustafa, Synthesis, structural, optical and magnetic properties of $NiFe_2O_4$/MWCNTs/ZnO hybrid nanocomposite for solar radiation driven photocatalytic degradation and magnetic separation, Colloids and Surfaces A: Physicochemical and Engineering Aspects 592 (2020) 124586.

[99] R. Ebrahimi, M. Mohammadi, A. Maleki, A. Jafari, B. Shahmoradi, R. Rezaee, M. Safari, H. Daraei, O. Giahi, K. Yetilmezsoy, Photocatalytic degradation of 2, 4-dichlorophenoxyacetic acid in aqueous solution using Mn-doped ZnO/graphene nanocomposite under LED radiation, Journal of Inorganic and Organometallic Polymers and Materials 30(3) (2020) 923-934.

[100] A. Paul, S.S. Dhar, Construction of hierarchical $MnMoO_4$/$NiFe_2O_4$ nanocomposite: Highly efficient visible light driven photocatalyst in the degradation of different polluting dyes in aqueous medium, Colloids and Surfaces A: Physicochemical and Engineering Aspects 585 (2020) 124090.

[101] H. Hitha, A. Jose, M. John, T. Varghese, Structural and optical modification of $NiWO_4$ – Formation of $NiWO_4$/SnPc nanocomposite for improved photocatalytic activity, Materials Chemistry and Physics 239 (2020) 122080.

[102] M.M. Gui, S.-P. Chai, B.-Q. Xu, A.R. Mohamed, Enhanced visible light responsive MWCNT/TiO_2 core–shell nanocomposites as the potential photocatalyst for reduction of CO_2 into methane, Solar Energy Materials and Solar Cells 122 (2014) 183-189.

[103] C. Alvarez-Lorenzo, L. Bromberg, A. Concheiro, Light-sensitive intelligent drug delivery systems, Photochemistry and photobiology 85(4) (2009) 848-860.